Deciphering the trajectory of iPSC-derived hepatic stellate cells in physiology and disease

Raquel Adela Martinez Garcia de la Torre

Deciphering the trajectory of iPSC-derived hepatic stellate cells in physiology and disease

Doctoral thesis dissertation presented by *Raquel Adela Martinez Garcia de la Torre* to apply for the degree of doctor at the University of Barcelona.

Directed by:

Pau Sancho-Bru (University of Barcelona and Fundació de Recerca Clínic Barcelona-Institut d'Investigacions Biomèdiques August Pi i Sunyer (IDIBAPS))

The tutor:

Pere Ginès Gibert (University of Barcelona and Hospital Clinic de Barcelona)

Doctoral Program in Medicine and Translational Research.
School of Medicine and Health Sciences. University of Barcelona.
September 2024

Acknowledgements

Funding

This research was funded by the Instituto de Salud Carlos III (ISCIII) through the personal grant “FI18/00215” awarded to the candidate, as well as by the Asociación Española para el Estudio del Hígado, through the 2023 Nuevas Tecnologías grant for the candidate's International Internship. Additional support came from ISCIII grants “FIS PI20/00765” and “DTS22/00032”, AGAUR grants “2019 PROD 00055” and “2021 PROD 00035”, and co-funding from the European Union’s “HORIZON-HLTH-2022-STAYHLTH-02-01” initiative. We sincerely thank these institutions for their crucial financial support, which made this PhD research possible.

INDEX

Glossary

3D: three dimensional

ALT: Alanine transaminase

AP: Phosphatase alkaline

AST: Aspartate transaminase

ATP: Adenosine Triphosphate

BDL: Bile duct ligation

CAFs: Cancer Associated Fibroblasts

CCl_4: Carbon Tetrachloride

CDE: Choline-deficient, ethionine-supplemented

cyHSCs: cytokine producing HSCs

DDC: 3,5-Diethoxycarbonyl-1,4-Dihydrocollidine Diet

DE: Definitive Endoderm

DEGs: Differentially Expressed Genes

diHSCs: Differentiated Hepatic Stellate Cells

Doxy: Doxycyline

ECM: Extracellular Matrix

ESCs: Embryonic Stem Cells

FGFs: Fibroblast Growth Factors

GO: gene Ontology

GSEA: Gene Set Enrichment Analysis

HCC: Hepatcellularcarcinoma

HDBR: Human Developmental Biology Resource

HGF: Hepatic Growth Factor

HSCs: Hepatic Stellate Cells

IP: Intraperitoneal

iPSC-RORA-/- : iPSCs cell line Homozygous Knockout for RORA

iPSC-RORA+/- : iPSCs cell line Heterozygous Knockout for RORA

iPSCs: Induced Pluripotent Stem Cells

ISO: Isoproterenol-induced Cardiac Hypertrophy Model

KCs: Kupffer Cells

KO: Knockout

LDH: Lactate dehydrogenase

LSECs: Liver Sinusoidal Endothelial Cells

MASLD: Metabolic Dysfunction-Associated Steatotic Liver Disease

myHSCs: myofibroblastic HSCs

OSM: Oncostatin M

OXPHOS: Oxidative Phosphorylation

PCA: Principal Component Analysis

PDAC: Pancreatic Ductal Adenocarcinoma

PDGF: Platelet-Derived Growth Factor

PFs: Portal Fibroblasts

PSCs: Pancreatic Stellate Cells

RA: Retinoic Acid

RORA: Retinoic Acid Receptor-Related Orphan Receptor A

RT: Room temperature

SAMes: Scar- Associated Mesenchymes

scRNA-seq: Single Cell RNA sequencing

sg/sg: staggerer mice

STM: Septum Transversum Mesenchyme

TALENs: Transcription Activator-like Effector Nucleases

TFs: Transcription Factors

TGFb: Transforming Growth Factor-Beta

UUO: Unilateral Ureteral Obstruction

WT: Wild-type

ZFNs: Zinc-Finger Nucleases

Thesis in classic format with 1 article annexed and 1 article in revision.

The thesis consists of 3 objectives and 1 article:

Objectives

1. Standardize the production, preservation, storage and use of hepatic stellate cells derived from iPSCs (diHSCs).
2. Characterize the differentiation trajectory of diHSCs and investigate the functional consequences of diverging trajectories in liver fibrosis.
3. Define the heterogeneity and differentiation potential of cell populations generated during diHSC differentiation.

Published article

Martínez García de la Torre RA, Vallverdú J, Mannaerts I, Verhulst S, Smout A, Coll M, Ariño S, Rubio-Tomás T, Aguilar-Bravo B, Martínez-Sánchez C, Blaya D, Verfaillie CM, van Grunsven LA, Sancho-Bru P. Directed differentiation of human induced pluripotent stem cells to hepatic stellate cells. Nature Protocols. 2020; 16(5):2542-2563. doi: 10.1038/s41596-021-00509-1. PMID: 33864055. Impact Factor: 13.491. Quartil 1. Area: Biochemistry, Genetics and Molecular Biology.

The published article is cited in the objective 1 of this thesis.

RESUM

Les cèl·lules estrellades hepàtiques (HSCs) són les principals responsables de la fibrosi hepàtica, una característica comuna en totes les malalties hepàtiques, independentment de la seva etiologia, i que actualment no té tractament. A més, la fibrosi es correlaciona directament amb el pronòstic i la supervivència dels pacients amb malalties hepàtiques cròniques. Per aquest motiu, comprendre la fisiologia i patofisiologia d'aquestes cèl·lules és fonamental pel desenvolupament de nous tractaments antifibrogènics. Aquesta tesi doctoral es centra en l'estudi de la diferenciació de cèl·lules estrellades hepàtiques (diHSCs) derivades de cèl·lules mare pluripotents induïdes (iPSCs), amb l'objectiu d'entendre la patofisiologia de la fibrosis hepàtica.

Al llarg d'aquest treball, s'han abordat els aspectes clau per la producció, caracterització i aplicació a gran escala de les diHSCs. S'ha demostrat que les diHSCs poden ser passades i criopreservades sense perdre el fenotip de cèl·lules estrallada així com preservar la seva capacitat de resposta a estímuls profibròtics, convertint-les en models valuosos per a l'estudi de la fibrogènesi i per a assajos de cribratge de fàrmacs a gran escala. A més, l'estudi del perfil proteòmic i genòmic d'aquestes cèl·lules al llarg de la trajectòria de diferenciació ha revelat que la diferenciació es produeix en tres fases, recapitulant parcialment els fenotips embrionaris associats a la diferenciació de les cèl·lules estrellades hepàtiques.

Un dels descobriments clau d'aquesta tesi és el paper del factor de transcripció RORA (Retinoic Acid Receptor-Related Orphan Receptor A) en la regulació metabòlica durant la diferenciació i l'activació de les diHSCs. La modulació adequada de RORA és essencial per guiar la transició de les cèl·lules cap al mesoderma i mantenir el perfil de quiescència de les diHSCs. Per contra, la seva desregulació exacerba la fibrosi hepàtica, tant en models humans in vitro com en models animals in vivo. A més, l'ús d'un agonista de RORA ha demostrat tenir potencial terapèutic, no només per al tractament de la fibrosi hepàtica, sinó també en models de fibrosi extrahepàtica, suggerint que l'estudi d'aquest receptor podria ser clau per al tractament de malalties fibròtiques en general.

Aquesta tesi també reflecteix que el protocol de diferenciació desenvolupat reproduïx parcialment la heterogeneïtat del teixit hepàtic, cosa que permetria l'estudi de la manipulació del comportament cel·lular de les HSCs amb fins terapèutics. A més, s'han estudiat les diferències entre les cèl·lules estrellades hepàtiques i pancreàtiques, demostrant que presenten marcadors específics segons el teixit, subratllant així la influència de les senyals ambientals en el desenvolupament d'aquests òrgans. Finalment, aquesta tesi ha demostrat que les interaccions entre cèl·lules epitelials i mesenquimals durant la diferenciació són essencials per la modulació de la trajectòria de diferenciació de les cèl·lules i l'adquisició de característiques específiques dels òrgans. A més, els estudis de scRNA-seq validen l'ús de models *in vitro* per a l'estudi d'aquests processos de desenvolupament i diferenciació.

INTRODUCTION

1. Fundamentals and applications of pluripotent stem cells.

1.1. Induced pluripotent stem cells.

Embryonic stem cells (ESCs) are pluripotent stem cells derived from the inner cell mass of a blastocyst, an early-stage pre-implantation embryo and are distinguished by their ability to differentiate into any embryonic cell type and by their ability to self-renew. The first isolation of ESCs was in 1981 by the British biologist Martin Evans and Mathew Kauffman as well as the American Gail Martin. In 1988 James Thompson did it for human ESCs. These cells were used as a reference for the reprogramming of somatic cells in the following years (1).

In 2006, Shinya Yamanaka and Kazutoshi Takahashi described for the first time the reprogramming of adult mice fibroblast into pluripotent stem cells. By the induction of the well-known Yamanaka factors, which include OCT4, SOX2, KLF4 and C-MYC, Yamanaka and colleagues reported the generation of induced pluripotent stem cells (iPSCs) that behaved similarly to ESCs, avoiding the ethical concerns associated with ESCs(2,3). Human iPSCs were stablished similarly one year later by Yamanaka(3). Since that, the field of iPSC technology has advanced remarkably over the past eighteen years and Yamanaka and Thompson were recognized for their discoveries with the 2012 Nobel Prize in Physiology or Medicine (4).

The iPSCs, like ESCs, present self-renewal capacity and can be differentiated into any cell type of the body, but with reduced ethical concerns. Moreover, iPSCs can be generated from patients, allowing personalized medicine approaches for treating a range variety of diseases, from degenerative disorders to mechanical injuries, holding the potential to redefine the future of medicine, as they can be differentiated into cell types otherwise inaccessible (5). These cells also serve as valuable source for physiology and disease modeling *in vitro*, which will be the main use of the iPSCs within this PhD. Additionally, iPSCs exhibit unique epigenetic states and metabolic profiles that distinguish them from differentiated cells. The capacity to differentiate to any cell type allow us to obtain any cell of interest to integrate them in complex *in vitro* models, *in vitro* screening systems or to study its differentiation trajectory, enhancing our comprehension of normal development but also providing insights into aberrant processes associated with diseases (1). (Figure 1).

Moreover, iPSCs derived from patients with genetic disorders or complex diseases enable to understand the underlying mechanisms of these conditions, screen potential drug candidates, and develop targeted therapies. The possibility to use iPSCs derived from patients allow also to perform population studies taking into account polymorphisms associated with diseases, as well as to perform drug screening assays from a more personalized point of view. Given the human origin of iPSCs and the capacity to create patient-specific iPSCs with a genetic background relevant to the disease, modeling human biology with iPSCs and iPSC-derived cells is particularly appealing. Additionally, the generation of complex human-like tissues, such as organoids, that comprise a variety of cell types, have architecture like that of primitive human tissue, and allow for the modeling of higher order cell-cell interactions has been made possible by the ever-increasing complexity of iPSC-based cellular models (6).

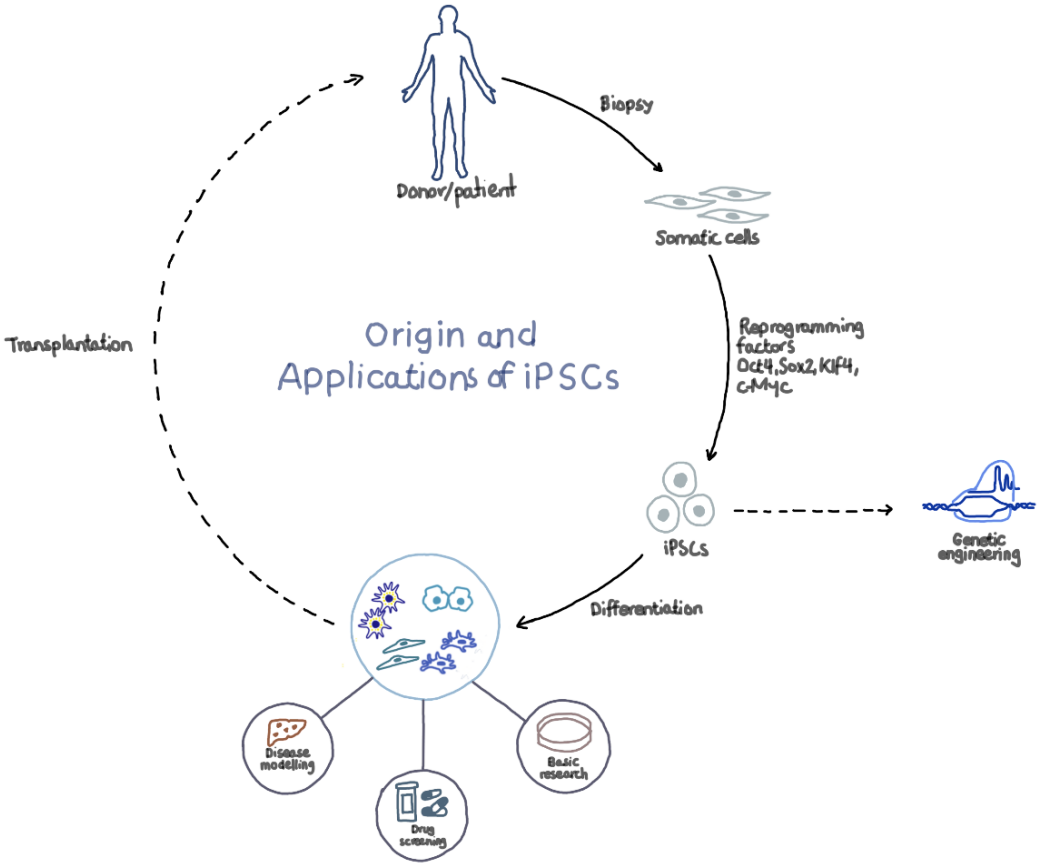

Figure 1. Schematic representation of the origin and applications of the induced pluripotent stem cells (iPSCs). iPSCs can be obtained from somatic cells of patients by reprogramming them using the Yamanaka Factors *OCT4*, *SOX2*, *KLF4* and *c-MYC*. Moreover, iPSCs can be easily genetic engineered. Potentially, they have the capacity to differentiate into any cell type that can be used for disease modelling, drug screening and basic research. Moreover, they can be used in regenerative medicine strategies as a source of cells to transplant again to patients.

Furthermore, it is easy to genetically modify iPSCs utilizing a variety of methods; the most widely utilized method in the field is based on the CRISPR-Cas9 system, which can be used for the insertion, removal, or correction of genes within these cells. Other genetic techniques that have been widely used to modify iPSCs cells including transcription activator-like effector nucleases (TALENs) and Zinc-finger nucleases (ZFNs) that similarly to CRISPR-Cas9, allow precise genome editing, correcting mutations or inserting therapeutic genes. Additionally, site-specific integration systems, like PiggyBac transposons, further improve the stability and predictability of genetic modifications (7). The capacity to alter genes in the *in vitro* models based on iPSCs makes it easier to model genetic illnesses, study how genes work, and create possible treatments. In this PhD, we have used CRISPR-Cas9 gene editing strategies to elucidate the physiological role of the target gene in the differentiation and pathology of stellate cells.

iPSC-based systems are unique tools for exploring human cell trajectories, offering insights into the dynamic paths that cells follow throughout their lifespan. These trajectories include processes such as differentiation, maturation, specialization, and disease progression (8). Regarding development, understanding the differentiation trajectories is fundamental to unraveling the complexities of tissue and organ development as well as the pathogenic processes in multicellular organisms. By tracking the developmental journey of cells, it is possible to identify critical checkpoints, master regulators, and key signaling events that influence cellular fate and specification.

On the other hand, in the context of disease modeling, differentiating iPSCs into disease-relevant cell types allows us to study how cellular trajectories deviate from the "healthy path," providing critical insights into the onset and progression of disorders. This approach enables the identification of molecular and genetic aberrations that drive disease states, facilitating the development of targeted therapies and personalized medicine. Additionally, iPSC-derived models can be used to screen potential therapeutic compounds, assess their efficacy, and understand their mechanisms of action in a controlled and patient-specific context.

1.2. Cell reprogramming during iPSCs differentiation

The reprogramming from iPSCs to differentiated cells involves reversing the pluripotent state and guiding the cells through specific developmental pathways to generate specialized cell types. This transition is governed, among other processes by the activation of lineage-specific transcription factors (TFs), which play a crucial role in ensuring the fidelity of differentiation, as they bind to specific sequences in the genome to alter gene expression and specify cell states (9,10). Overexpression of single TFs can drive profound changes in cell fate. These TFs drive the expression of genes necessary for the development of specific cell types while simultaneously silencing pluripotency-associated genes (9,10). For example, during the differentiation of iPSCs into mesodermal cells, some of the TFs that guide the transition to specialized cells arising from mesoderm are Brachyury (T), MESP1, GATA4 and EOMES are essential for this process. The correct regulation of the key TFs is such an important process that some strategies to improve the differentiation of iPSCs towards specific cell types go through the upregulation genetically of the expression of those TFs. Concurrently, the overexpression of some of them such as T, increased the number of FLK1-positive mesoderm cells (11). The expression of cell lineage specific TFs actively represses pluripotency-associated genes, such as *OCT4*, *SOX2*, and *NANOG*, to ensure that the iPSCs commit to the mesodermal lineage. The silencing of these pluripotency genes is critical to prevent the cells from retaining their undifferentiated state or deviating into other germ layers, such as ectoderm or endoderm.

Therefore, understanding the intricate network of transcription factors during this reprogramming process is key to optimizing differentiation protocols and ensuring the success of iPSC-based therapies in regenerative medicine and disease modeling.

Retinoic Acid-Related Orphan Receptor Alpha (RORα) is a TF with an important role in regulating circadian rhythm, inflammation, metabolism, and cellular development. RORA is expressed in several tissues in which it activates the transcription of specific genes. In situ hybridization has revealed RORα expression in the adult brain in cerebellar Purkinje cells, inferior olive, olfactory bulb, hippocampus, thalamus, cortex, suprachiasmatic nuclei of the hypothalamus, and retinal ganglion cells. Outside the central nervous system, RORα mRNA have been detected in thymus, skeletal muscle,

skin, heart, vessels, liver, lung, gut, kidney tubules, whisker follicles, and pancreas. In the liver, regulates various target genes related to lipid metabolism. In this PhD, we have explored the role of RORA in diHSCs trajectory.

1.3. Metabolic plasticity during iPSCs differentiation protocols

Metabolic plasticity refers to the adaptability of cellular metabolic processes in response to changing environmental conditions or cellular demands. Cells have the ability to adjust their metabolic pathways to maintain energy homeostasis and support various cellular functions. This adaptability is crucial for the survival and functionality of diverse cell types in different tissues and organs. Metabolic plasticity is intricately linked to cellular signaling pathways, transcriptional regulation, and post-translational modifications that collectively orchestrate metabolic responses (12).

The concept of metabolic plasticity is particularly evident in the context of induced iPSCs and their differentiation into specialized cell types. iPSCs exhibit a highly flexible metabolic profile resembling that of ESCs(13). iPSCs primarily rely on glycolysis for energy production, even in the presence of oxygen, what is known as aerobic glycolysis or Warburg effect. Similar to cancer cells, this metabolic strategy supports rapid cell proliferation and biomass production, which are essential for maintaining their pluripotent state and high proliferative capacity. The preference for glycolysis over oxidative phosphorylation (OXPHOS) enables iPSCs to generate ATP quickly and provide the necessary metabolic intermediates for biosynthetic processes (14,15).

Moreover, iPSCs have very low number of mitochondria, are less mature and exhibit a fragmented network compared to differentiated cells. This mitochondrial morphology and function are indicative of a metabolic state optimized for stem cell maintenance and proliferation rather than efficient energy production through OXPHOS. As iPSCs undergo differentiation, their metabolic profile shifts, with an increase in mitochondrial biogenesis, maturation, and a transition towards oxidative phosphorylation, which supports the energy demands of specialized cell functions(16).

However, when they start to differentiate, they change their energetic sources, based on the cell type to differentiate(17,18). When mesoderm differentiation starts, there is a significant metabolic shift towards increased OXPHOS. This transition allows efficient ATP production, which is essential to meet the heightened energy demands associated with differentiation. Concurrently, the mitochondria undergo substantial changes: they

become more numerous, larger, and develop more complex cristae structures. These changes are indicative of increased mitochondrial biogenesis and enhanced functionality, which are necessary to support the energy-intensive process of OXPHOS. In addition to these mitochondrial adaptations, there is a marked increase in fatty acid oxidation during mesoderm differentiation via MYC activity(19). This metabolic shift provides an additional energy source, ensuring that the high ATP demands of the differentiating cells are met. Fatty acid oxidation not only supplements ATP production but also generates metabolic intermediates that are crucial for various biosynthetic pathways. The coordinated upregulation of OXPHOS and fatty acid oxidation highlights the dynamic metabolic reprogramming that occurs, optimizing their metabolic state to support the development and function of specialized cell types (19). In this thesis, we explored the metabolic shifts during stellate cell differentiation and how to improve differentiation capacity by affecting this metabolic shift towards mesoderm. (Figure 2).

On the other hand, ectoderm differentiation retains high glycolytic activity but also shows increased oxidative phosphorylation, although to a lesser extent than mesoderm differentiation. Ectoderm differentiation shown a slight maturation of mitochondria as well, with increased mitochondrial activity compared to iPSCs but less pronounced than in mesoderm differentiation and increased synthesis of membrane lipids to support neural differentiation and the formation of complex neural structures(20) (Figure 2).

Endoderm differentiation metabolic adaptations are more complex. Similar to mesoderm, there is a shift towards increased oxidative phosphorylation, similar to mesoderm differentiation but with variations depending on the specific endodermal lineage (21). As a consequence, there is a significant mitochondrial biogenesis and maturation to support OXPHOS and an enhanced lipid metabolism, particularly in the liver where lipid synthesis and oxidation are crucial for hepatocyte function (Figure 2).

Therefore, each germ layer adapts its metabolic pathways to support specific biosynthetic and energy needs, with variations in glycolytic, and lipid metabolism.

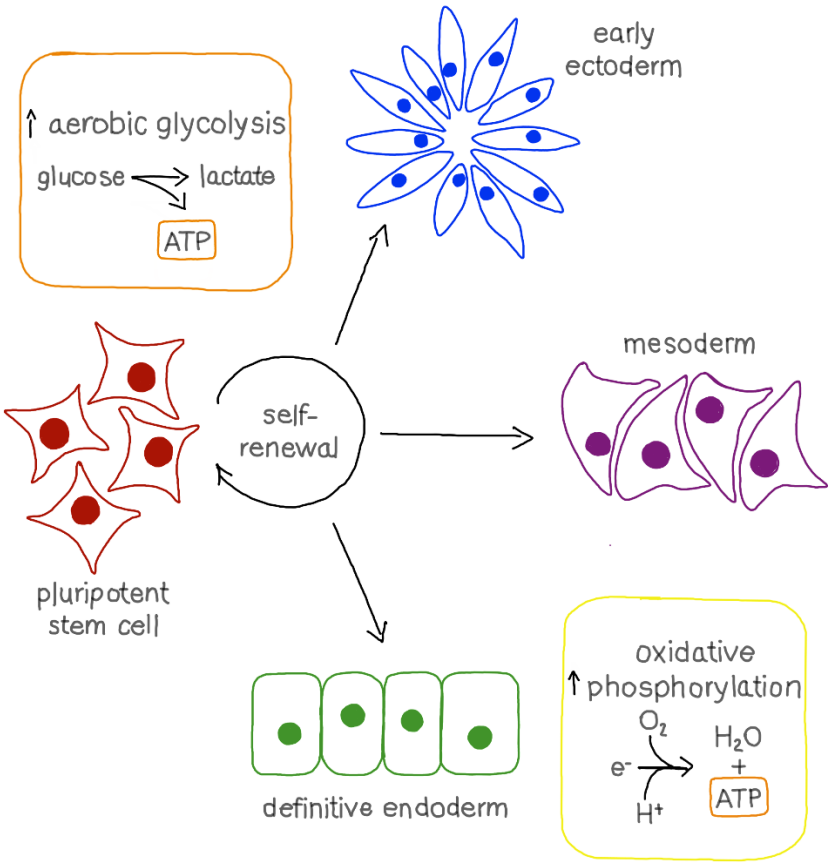

Figure 2. Schematic representation of the metabolic process involved in the maintenance of the pluripotency state and the acquisition of germ-layers phenotypes. Self-renewal and early ectoderm is characterized by higher levels of aerobic glycolysis whereas mesoderm and definitive endoderm are characterized by an impair towards oxidative phosphorylation.

Understanding these metabolic changes during differentiation is important not only for unraveling the details of embryonic development but also for advancing strategies in regenerative medicine and tissue engineering, as it can improve the differentiation capacity of the stem cells.

2. Basic principles of liver and pancreas embryo development

By closely studying the molecular cues and signaling pathways that guide cells during embryogenesis, we can replicate these conditions *in vitro*, directing iPSCs to follow precise differentiation trajectories. This capability not only facilitates the generation of diverse cell types for research and therapeutic purposes but also highlights the importance of unraveling the details of embryonic development to fully exploit the potentiality of the iPSCs. To provide a comprehensive understanding of the differentiation protocols developed and utilized in this thesis, it is essential to first

discuss the embryonic development of two key digestive organs: the liver and the pancreas.

Although the liver and pancreas exhibit distinct physical characteristics and macroscopic appearances, they share notable similarities, particularly in their developmental origins, as both organs arise from adjacent regions of the foregut endoderm during embryogenesis (22–24). The liver develops from an epithelial bud that emerges on the ventral side of the foregut endoderm (25). In contrast, the pancreas originates from two separate buds—the ventral and dorsal pancreatic buds—located on opposite sides of the foregut endoderm. These buds later fuse to form the mature pancreas (26). Also, the specification of these cells is influenced according to the signaling cues that the cells received, mainly secreted by surrounding mesenchymal cells, suggesting that even within similar cell populations, mesenchymal cells undergo as well their own specification within tissues, contributing to the diversity of outcomes during development. Although similar cells, mesenchymal specification within the tissues also occurs (27,28). There is then a co-differentiation process alongside the endoderm and this coordinated development between the endoderm and its associated mesenchyme is critical for the proper formation of tissues and organs(29). For instance, in the liver, several authors had explored this concept. Takebe et al. 2013, Berger et al. 2015, Goulart et al. 2019 and Raggi et al. 2022 have demonstrated that the interaction of the hepatoblast with non-parenchymal cells is necessary to increase the maturation of them(30–33). In the pancreas, Cozzitorto et al. demonstrated that a specialized mesenchymal niche promotes endocrine differentiation (34). Disruptions in this interaction can lead to significant pathological implications, as unsuitable mesenchymal signaling or miscommunication between the endoderm and mesenchyme can result in developmental abnormalities and contribute to the onset of various diseases (35). This concept has also been examined in the third objective of this PhD, where we investigated the mesenchymal specification of stellate cells into hepatic or pancreatic phenotypes as well as this mesenchymal specification may play a crucial role in influencing the differentiation of endodermal cells in an iPSC-based system.

2.1. Liver embryo development.

Around the third week of human gestation, the liver primordium begins to develop as a hepatic diverticulum, which is essentially a bud that emerges from the posterior foregut

endoderm (36) . This initial formation of the liver is a crucial step in its development, and it is guided by a complex interplay of signaling molecules. Fibroblast growth factors (FGFs) from the adjacent cardiac mesoderm and bone morphogenetic proteins (BMPs) from the septum transversum mesenchyme, which play pivotal roles in liver specification. These signaling molecules stimulate the expression of key liver-specific transcription factors, including Hepatocyte Nuclear Factor 4 Alpha (HNF4α) and GATA4, within the foregut endoderm (37). The activation of these transcription factors marks the beginning of hepatic lineage specification, where the endodermal cells commit to a liver developmental fate (36).

As liver specification progresses, the foregut endodermal cells differentiate into hepatoblasts, which are bipotential progenitor cells capable of giving rise to both hepatocytes (the primary functional cells of the liver) and biliary epithelial cells (which line the bile ducts)(38). These hepatoblasts proliferate extensively and undergo differentiation to form the liver's parenchymal cell population (39). Concurrently, the hepatic bud invades the septum transversum mesenchyme (STM), a mesodermal structure situated between the developing liver and the diaphragm (40). During this interaction, mesodermal cells migrate into the developing liver and differentiate into hepatic stellate cells (HSCs) and endothelial cells, which will establish the hepatic sinusoids, a network of specialized blood vessels essential for liver function. HSCs contribute to the formation of the extracellular matrix during development that will provide structural support for developing hepatocytes and vascular structures (41).

The lineage tracing studies conducted by Asahina and colleagues have provided crucial insights into the embryonic development of HSCs(42,43). Specifically, these studies demonstrated that mesodermal cells expressing the MESP1 gene play a significant role in forming the STM, characterized by the expression of various markers including FOXF1, ALCAM, LHX2, GATA4, HAND1, HLX, and WT1. In particular, Asahina et al. (2011) identified that STM cells which differentiate into mesothelial cells are those expressing ALCAM and WT1 (44). These cells secrete PTN and HGF to induce proliferation of the progenitor hepatic cells. Mesothelial cells give rise to submesothelial cells, which start to express some classical HSC markers such as p75NTR, DES and PDGFRA. Apparently are those mesothelial and submesothelial population of cells positive for WT1, ALCAM, DES, p75NTR and PDGFRA that migrates from the liver surface to generate HSCs and

perivascular mesenchymal cells(42)(45). This suggests that submesothelial cells serve as an intermediate stage between mesothelial cells and fully differentiated HSCs. Once HSCs have migrated into the developing liver bud, they actively participate in hepatic morphogenesis. They interact with hepatoblasts and contribute to the formation of the liver's vasculature and connective tissue framework. Additionally, HSCs are involved in regulating the balance between hepatocyte proliferation and apoptosis, thereby influencing liver growth and differentiation (Figure 4) (46). Through paracrine signaling and extracellular matrix remodeling, HSCs create a microenvironment favorable to hepatic development, ensuring proper tissue organization and function. Furthermore, emerging evidence suggests that HSCs may also influence the fate determination of hepatic progenitor cells (47). As hepatocytes mature, they organize into the liver's characteristic lobular structure, which will be described in greater detail in the following chapter of this PhD introduction.

2.2. Pancreas embryo development

On the other hand, the pancreas originates from dorsal and ventral pancreatic buds, from the posterior foregut endoderm (26). Pancreatic specification is regulated by signaling pathways, including retinoic acid from the mesoderm, FGF, and BMP inhibitors. Key transcription factors like PDX1, SOX9, and PTF1A are crucial for pancreatic progenitor cell specification (24) (Figure 3). Pancreatic progenitor cells proliferate and the buds undergo branching morphogenesis, forming a ductal network. The dorsal and ventral buds eventually fuse, contributing to the formation of the head, body, and tail of the pancreas. Pancreatic progenitors differentiate into endocrine and exocrine lineages. Endocrine progenitors give rise to the islets of Langerhans, containing insulin-producing β-cells, glucagon-producing α-cells, and other hormone-secreting cell types. Exocrine progenitors form acinar cells, which produce digestive enzymes, and ductal cells, which form the ductal tree for enzyme transport (48) (Figure 7). Similar to the liver, the pancreas bud is also influenced by the surrounding mesenchymal cells including Pancreatic Stellate Cells (PSCs). The mesenchymal phenotype is different according to the endoderm fraction where they are close by (49). This differential mesenchymal environment not only influences the development and specialization of these two pancreatic fractions but may also have implications for diseases like diabetes and pancreatic cancer, where the mesenchyme plays a role in pathogenesis.

During embryogenesis, PSCs secrete extracellular matrix (ECM) components, such as collagen and fibronectin, which provide a scaffold for the developing pancreatic architecture and facilitate the proper organization of pancreatic cells into ducts, acini, and islets. They also release growth factors and cytokines, including fibroblast growth factors (FGFs) and transforming growth factor-beta (TGF-β), that influence the proliferation, differentiation, and migration of pancreatic progenitor cells. Furthermore, PSCs support the formation of blood vessels by producing pro-angiogenic factors, ensuring adequate vascularization and nutrient supply to the growing pancreatic tissue (50).

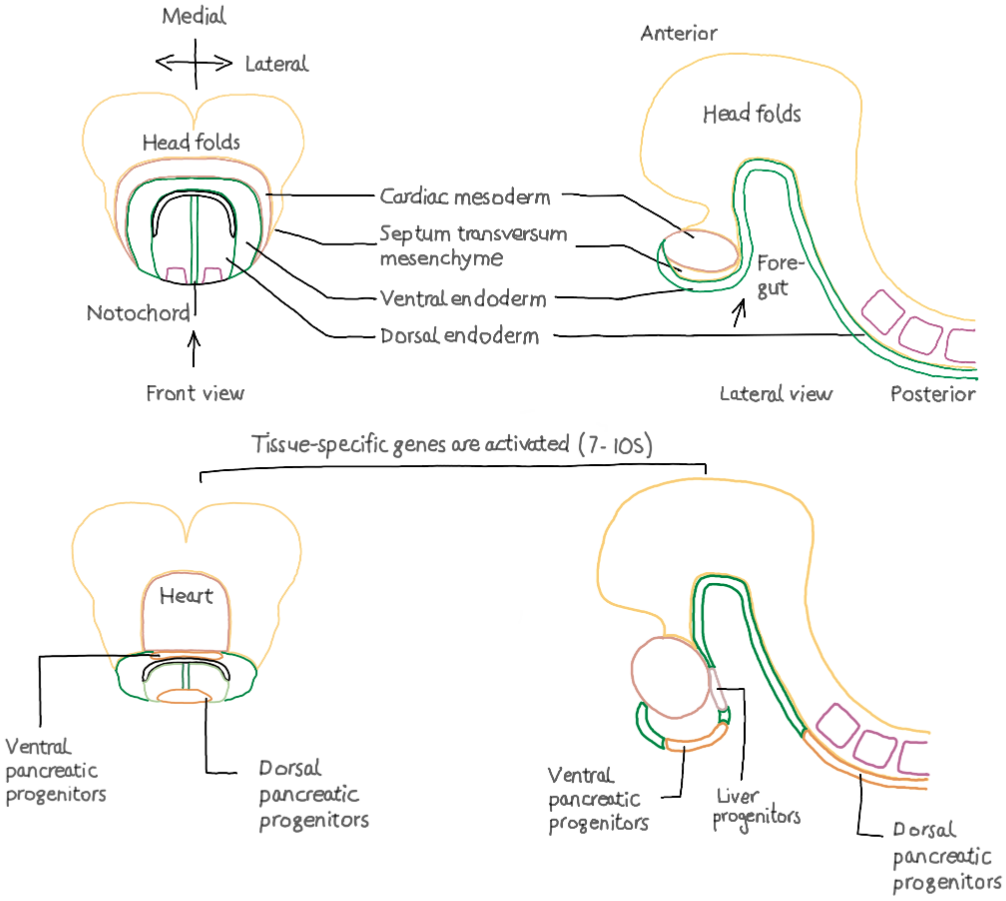

Figure 3. Developmental origin of the liver and the pancreas. Fate map of liver and pancreatic progenitor domains in the mouse. According to fate-mapping studies, the pancreatic progenitors (orange) reside in paired lateral domains of endoderm (the ventral pancreas) and a medial dorsal domain (the dorsal pancreas), while the liver progenitors (purple) reside in paired lateral domains of endoderm and a medial ventral domain of endoderm. Both endoderm are influenced by the mesoderm surrounding tissues.

In the third objective of this PhD, we aim to investigate the differences between hepatic and pancreatic stellate cells and explore how these cells are influenced by their respective organ-specific endoderm.

2.3. Differentiation of iPSCs towards hepatic and pancreatic endoderm

The differentiation of iPSCs into both hepatic and pancreatic lineages follows a shared foundation that reflects early embryonic development. Both processes begin with the formation of definitive endoderm (DE), a critical germ layer that gives rise to organs such as the liver or the pancreas and is crucial, as the efficiency and purity of DE directly influence the success of subsequent steps towards specific lineages.

The induction of DE from iPSCs is typically achieved through the activation of the Nodal signaling pathway, often by using high concentrations of Activin A. Activin A, a member of the TGF-β superfamily, mimics the role of Nodal in early embryogenesis, promoting the expression of DE markers such as SOX17 and FOXA2. The standard protocol involves culturing iPSCs in a medium supplemented with Activin A for 3-5 days, often alongside low serum conditions to enhance the specificity of differentiation. Wnt signaling modulators, such as CHIR99021, a GSK-3β inhibitor, are sometimes added to further promote DE formation by enhancing mesendoderm specification.

After the formation of definitive endoderm, the differentiation towards hepatic and pancreatic lineage involves the acquisition of the posterior foregut endoderm. The differentiation of DE to posterior foregut endoderm is guided by modulating key signaling pathways, particularly Wnt, FGF, and BMP signaling. Wnt signaling plays a crucial role in posteriorizing the endoderm. In the context of posterior foregut specification, activation of Wnt signaling through small molecules such as CHIR99021 (a GSK3β inhibitor) helps to posteriorize the definitive endoderm, promoting the formation of posterior foregut tissues. Wnt signaling activation should be balanced, as excessive Wnt signaling can push cells toward more posterior endodermal fates, such as midgut or hindgut, rather than foregut. In addition to Wnt activation, BMP and FGF signaling pathways are also crucial in specifying posterior foregut endoderm. BMP4 and FGF4 are often used in combination to promote the posterior foregut identity. These signals help in inducing the expression of transcription factors such as HNF4α and PDX1, which are critical for posterior foregut development. Once posterior foregut phenotype is acquired, cells should transition into hepatic or pancreatic progenitors (51). The hepatic

phenotype is achieved by exposing the cells to FGF2 and BMP4. FGF2 and BMP4 are crucial during early liver development, where they help induce the expression of hepatic markers such as HNF4α and AFP. Following hepatic specification, the cells are subjected to further maturation signals to promote their differentiation into hepatocyte-like cells. Hepatocyte growth factor (HGF) and oncostatin M (OSM) are commonly used at this stage. HGF promotes cell growth and morphogenesis, while OSM helps in the final maturation towards functional hepatocytes. During this stage, cells begin to express mature hepatic markers such as ALB, CK18, and CYP450 enzymes, which are indicative of liver function (52). To enhance hepatic differentiation and function, some protocols incorporate three-dimensional (3D) culture systems, which better mimic the liver's structural environment. Additionally, co-culturing iPSC-derived hepatic cells with endothelial cells or mesenchymal cells can further improve maturation and functionality by providing necessary paracrine signals and supporting the complex liver microenvironment.

The differentiation of iPSCs into pancreatic endoderm follows a distinct pathway after the induction of the posterior foregut endoderm. Concurrently, retinoic acid (RA) is introduced to the culture medium, a crucial factor in driving the formation of pancreatic progenitors. This stage is characterized by the expression of early pancreatic markers such as PDX1, a transcription factor essential for pancreatic development(53). After the specification to pancreatic progenitors, factors like FGF10 and Noggin are used to promote the expansion and further differentiation of these progenitors. FGF10 plays a critical role in the expansion of pancreatic progenitor cells, while Noggin inhibits BMP signaling to favor pancreatic lineage over other possible fates. During this stage, the cells begin to express additional pancreatic markers such as NKX6.1 and SOX9. The final differentiation step focuses on generating functional pancreatic cells, particularly endocrine cells like insulin-producing β-cells as currently (54), no effective differentiation protocol towards exocrine lineage is accepted (55). While both hepatic and pancreatic differentiation protocols share a common starting point with the induction of definitive endoderm and the posterior foregut specification, they diverge significantly in subsequent stages to recapitulate organ-specific development, that may be influence by specific niche cells such as mesenchymal cells.

3. Chronic liver diseases and fibrosis.

3.1. Exploration of liver architecture and cellular organization

The liver is a vital organ with a complex architecture that enables it to perform its essential functions in maintaining homeostasis and metabolism within the body. Comprising approximately 2% of the total body weight, the liver is characterized by a distinctive lobular structure. Hepatocytes are grouped into hexagonal plates and radiate outward from a central vein to form each liver lobule. These functional units are separated by sinusoids, which are capillary-like vessels facilitating the exchange of nutrients, metabolites, and waste products between the hepatocytes and the bloodstream. Additionally, hepatic portal triads, composed of a bile duct, hepatic artery, and portal vein, are strategically positioned at the periphery of lobules, ensuring a coordinated supply of oxygen, nutrients, and hormones to the hepatocytes(56) (Figure 4).

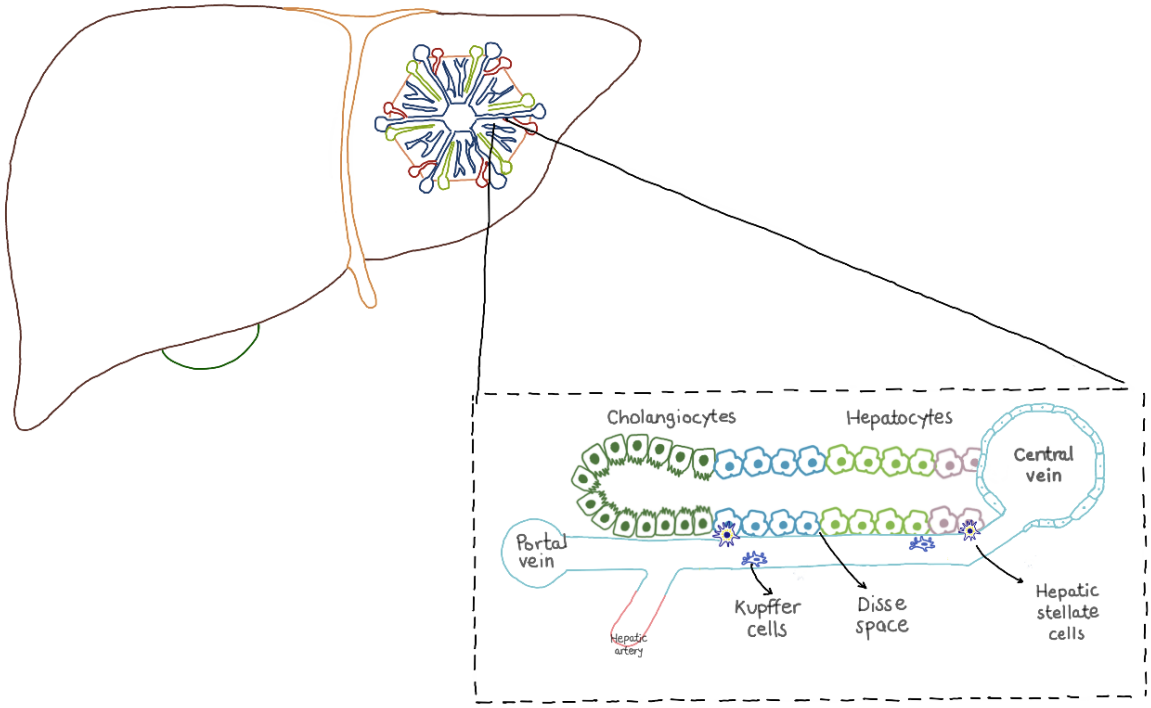

Figure 4. Schematic representation of the liver architecture. The liver is organized into hepatic lobules, which include the portal triad, central vein and hepatic sinusoids. The diagram also shows the different cell types along the hepatic lobule.

At cellular level, the liver is composed by parenchymal and non-parenchymal cells. The hepatocytes, the main parenchymal cell type within the organ, are crucial for protein synthesis, metabolism, and liver detoxification on a cellular level in a healthy liver. They represent a highly specialized cells, which functions varies according to their localization

within the hepatic lobule. Although they represent an heterogenous population, they are characterized by the expression of specific markers such as *ALB*, a major protein produced by hepatocytes, critical for maintaining plasma oncotic pressure and transporting substances; CYP450 enzymes, *HNF4A*, a transcription factor essential for hepatocyte differentiation and *AFP*, typically expressed during liver development and re-expressed in some liver diseases (56). Hepatocytes proximal to the portal triads, termed periportal or zone 1 hepatocytes, engage prominently in gluconeogenesis, glycolysis, and detoxification processes. In contrast, hepatocytes closer to the central vein, referred to as pericentral or zone 3 hepatocytes, are primarily involved in processes such as fatty acid oxidation, urea synthesis, and drug metabolism. Zone 2 hepatocytes are located between both regions and exhibit a metabolic profile that reflects a balance between the functions of both adjacent regions, as they participate in processes such as intermediary metabolism, including the synthesis of proteins and lipids. They contribute to the regulation of glucose homeostasis, amino acid metabolism, and lipid storage. The hepatocytes in this zone play a role in integrating signals from both the portal blood supply, carrying nutrients absorbed from the gastrointestinal tract, and the central vein, which drains blood from the lobule. The differential expression of enzymes and transporters across these zones enables efficient and coordinated responses to the heterogeneous demands on the liver (57). The other parenchymal cell type within the liver are the cholangiocytes, epithelial cells organized into tubular structures, forming the bile ducts and playing play a central role in the formation and transport of bile. They control the regulation of bile acid flow and alkalinity by secreting bicarbonate and water and have the capacity to reabsorb circulating compounds such as glucose. They also play a role in sensing changes in bile composition and can respond to injury or inflammation, participating in the liver's adaptive responses. Cholangiocytes express CK7, CK19, EPCAM and SOX9, an important transcription factor for cholangiocyte differentiation and function (58).

Although they are not directly implicated in the metabolic functions of the organ, the non-parenchymal liver cell types are also responsible for the maintenance of the organ's homeostasis. These cells include Kupffer cells (KCs), HSCs, portal fibroblast (PFs) and liver sinusoidal endothelial cells (LSECs). KCs, residing within the sinusoids, are the liver’s resident macrophages(56,59). They play a fundamental role in the organ's immune

defense by phagocytosing pathogens, cellular debris, and aged red blood cells, thereby maintaining a clean and functional hepatic environment. They also contribute to immune surveillance and response by secreting cytokines and chemokines, which modulate local and systemic immune responses. KCs are positive for *CD68*, a common macrophage marker but they express specific markers such as *MARCO*(60). HSCs, located in the space of Disse between sinusoidal endothelial cells and hepatocytes, represent the main storage cell of vitamin A and have a pivotal role in liver fibrosis and wound healing through their activation into myofibroblast-like cells (61). LSECs line the inner surface of the liver sinusoids and are specialized for facilitating the exchange of nutrients, oxygen, and waste products between the bloodstream and hepatocytes. LSECs have unique characteristics, including a fenestrated structure that enhances their ability to filter blood and interact with circulating particles and cells. They play a critical role in maintaining the hepatic microenvironment by regulating blood flow and supporting hepatocyte function and are positive for common endothelial markers such as *CD31* and *CD32b* but characterized by the expression of *LYVE1*, *STAB1* and *STAB2* (62). Finally, PFs are located in the portal tracts of the liver, primarily associated with the fibrotic response in conditions such as biliary fibrosis and chronic liver disease playing a critical role in the fibrogenic process, particularly in cholestatic liver diseases. Those mesenchymal cells are characterized by the expression of Thy-1 (CD90) and Elastin(63). The dynamic interactions among non-parenchymal cells and parenchymal cells of the organ, highlights their crucial role in preserving liver homeostasis and adapting to different physiological stresses(59,64).

3.2. Chronic liver diseases and liver fibrosis

Upon acute liver injury, the regenerative process in the liver involves both parenchymal and non-parenchymal liver cells. Parenchymal cells, mount a critical response aimed at restoring liver function and maintaining tissue integrity. Hepatocytes enter a state of rapid proliferation to compensate for cell loss. This regenerative response is driven by the activation of growth factors such as HGF and EGF, as well as cytokines like IL-6. These signals activate pathways including the STAT3, MAPK, and PI3K/AKT pathways, which promote cell survival, proliferation, and tissue repair. Additionally, hepatocytes upregulate the expression of stress response genes, to protect against oxidative stress and further damage. On the other hand, cholangiocytes also respond to injury,

particularly when the bile ducts are damaged or obstructed. They proliferate and engage in ductular reaction. This response is mediated by factors like TGF-β and Notch signaling, which promote cholangiocyte proliferation and differentiation. Cholangiocytes also secrete various cytokines and chemokines, contributing to the inflammatory response and interacting with other liver cell types to coordinate the repair process.

In parallel, non-parenchymal cells become activated, playing a critical role in mediating the inflammatory response and orchestrating the repair process (65). KCs are among the first responders, releasing pro-inflammatory cytokines like TNF-α and IL-6, which activate other immune cells and promote inflammation. These cytokines, along with TGF-β, also stimulate HSCs to transdifferentiate into myofibroblasts, a key event in liver fibrosis. Activated HSCs express genes such as *ACTA2* (encoding α-SMA), *COL1A1*, and *TIMP1*, leading to extracellular matrix deposition and scarring. Additionally, LSECs, which normally maintain a quiescent state, lose their fenestrations and contribute to the capillarization of the sinusoids, exacerbating the fibrotic response.

Upon chronic liver injury the response of liver cells, becomes more complex and maladaptive, leading to progressive liver damage and fibrosis, which is the common outcome of the bast majority of liver diseases, independently on the etiology (65). Activated HSCs are the main culprits of liver fibrosis. They contribute to the inflammatory environment by producing cytokines, growth factors, and other signaling molecules that recruit and activate additional immune cells to the site of injury. They also secrete matrix metalloproteinases MMPs, and proteoglycans that are involved in the remodeling of the ECM and the wound healing process(66,67). Key features of activated HSCs include enhanced contractility and chemotaxis abilities, which enable them to move to and exert force on the injury site, facilitating tissue repair, upon acute damage. Additionally, there is an increase in the expression of cytoskeleton proteins, which supports the structural changes required for their new functions. Activated HSCs also upregulate cytokine receptors and inflammatory mediators, which allows them to respond more effectively to local and systemic inflammatory signals(68). This transformation into a myofibroblast-like phenotype is crucial for the wound healing process in an acute phase but can also contribute to pathological fibrosis if the activation is excessive or prolonged due to chronic damage on the organ (69). (Figure 5).

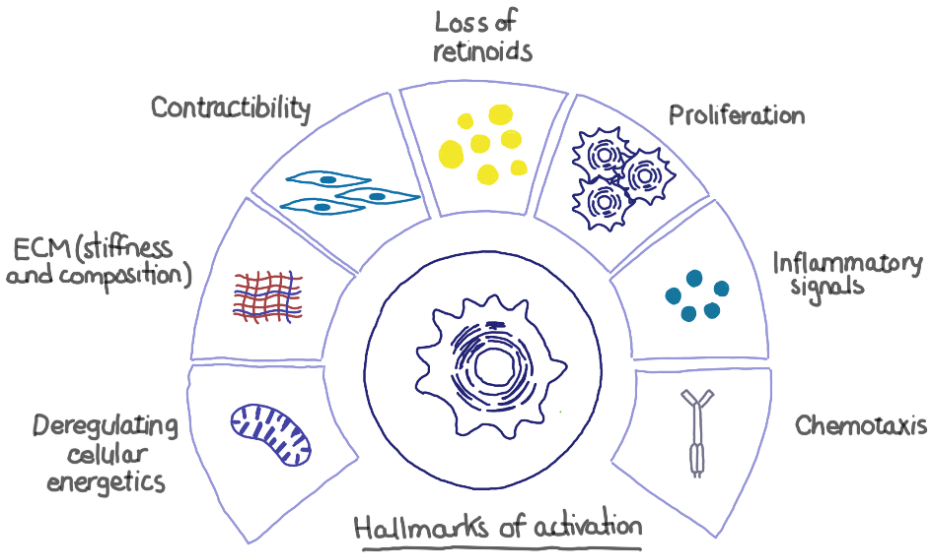

Figure 5. Hallmarks of Stellate Cell activation. When there is a continuous damage within the liver, HSCs achieve a myofibroblastic phenotype characterized by changes in stiffness and composition of the ECM, contractibility, proliferation, secretion of inflammatory and chemoattractant signals, loss of retinoids from cytoplasm and deregulation of cellular energetics.

Liver diseases include a broad spectrum of pathological conditions that affect the liver's structure and function, with fibrosis being a common response to chronic liver injury (70). Liver fibrosis is characterized by the excessive accumulation of extracellular matrix proteins, particularly collagen (71). The liver is susceptible to various insults such as viral infections, alcohol abuse, metabolic dysfunction-associated steatotic liver disease (MASLD), and autoimmune disorders. Chronic liver diseases represent a significant global health issue with high incidence, prevalence, and mortality rates, accounting for up to 2 million deaths annually. The burden of these diseases is expected to rise in the future, largely driven by the increasing prevalence of obesity and diabetes, which are key risk factors for the progression of liver pathology(72). Persistent liver injury triggers an aberrant wound healing response characterized by the continuous activation of HSCs and the subsequent deposition of collagen-rich scar tissue. This process leads to progressive liver fibrosis, which can eventually advance to cirrhosis, a severe and irreversible scarring of the liver that compromises its functionality (73). Cirrhosis is associated with a range of serious complications, including portal hypertension, which can cause life-threatening gastrointestinal bleeding and ascites; liver failure, which impairs the liver's ability to perform vital functions; and hepatocellular carcinoma, a liver cancer that often develops in the context of chronic liver disease (74). Given these risks,

early detection and intervention are critical. Monitoring the progression of fibrosis and diagnosing it in its early stages allow for timely implementation of therapeutic strategies aimed at halting or reversing liver damage. Understanding the molecular mechanisms that drive liver fibrosis is crucial for developing effective treatments. Despite the significant clinical need, there are currently no approved therapies specifically targeting liver fibrosis (75). Research into the pathways and cellular processes involved in fibrosis is essential for identifying novel drug targets and designing therapies that can address the underlying causes of the disease. To extend our understanding of liver fibrosis, we must also expand our knowledge of stellate cell physiology and pathophysiology.

3.3. *In vitro* modeling of liver fibrosis

Historically, primary HSCs or immortalized cell lines have been the primary tools for in vitro liver fibrosis modeling. These cells are activated through passage or by profibrogenic cytokines like TGF-β to mimic fibrosis. While valuable, these simplified systems do not fully replicate the liver's cellular complexity (76,77). Recently, advanced models such as liver-on-a-chip and liver organoids have emerged, combining different liver cell types in co-culture (77). These systems offer a more physiologically relevant environment, improving the study of HSC activation and fibrogenesis mechanisms.

4. Stellate cells: physiology and pathophysiology

HSCs under normal physiological conditions, are quiescent and reside in the perisinusoidal space of Disse in the liver (Figure 4). They represent the 10% of the total cellular components of the liver (61,78). Although they are characterized by the expression of some genes related to retinol metabolism, such as *LRAT*, they do not express unique markers, making it difficult to distinguish them from other mesenchymal cells in the organ such as vascular smooth muscle cells or portal fibroblast. However, the characteristic that makes them unique and allows their isolation and distinction within the tissue is their capacity to store vitamin A (78).

4.1. Physiology of the hepatic stellate cells in hepatic homeostasis

During embryo development as described previously, HSCs play crucial roles in the formation of the extracellular matrix during development that will provide structural

support for developing hepatocytes and vascular structures (41) and they actively participate in hepatic morphogenesis. They interact with hepatoblasts and contribute to the formation of the liver's vasculature and connective tissue framework.

In an adult healthy liver, HSCs are multifunctional quiescent cells that contribute to the maintenance of liver homeostasis under normal physiological conditions. HSCs in their quiescent state represent the primary storage of retinoids of the body. In their cytoplasm, they store retinyl esters and represent a crucial role for maintaining systemic vitamin A homeostasis (78). They also regulate the ECM dynamics of the organ, as they are producers of ECM proteins such as collagens (type IV and VI) that give structural support to the organ. They also contribute to the regulation of the hepatic blood flow, as they are specialized liver pericytes in close contact to the liver sinusoidal endothelial cells and to the immune modulation, as it has been described that these cells present antigen presenting capacities(61). More importantly, they are also involved in liver regeneration, like its role during liver embryo development, the paracrine signaling secreted by stellate cells may promote the differentiation and proliferation of liver progenitor cells during the regenerative response (47).

4.2. Pathophysiology of the hepatic stellate cells

However, in response to chronic liver injury, HSCs undergo a complete transformation from a quiescent to a permanent activated state, becoming the primary source of extracellular matrix (ECM) proteins, particularly collagen (type I and III) and fibronectin, which contributes to the fibrotic scarring observed in all chronic liver diseases. The activation of HSCs is a complex process involving various signaling pathways and molecular mechanisms (66). One key mediator of HSC activation is mediated by cytokines such as TGF-β. TGF-β is released in response to liver injury by different cell types of the liver including damaged hepatocytes, acting as a potent profibrogenetic cytokine, triggering the SMAD signaling pathway. This leads to the transcription of genes associated with fibrogenesis, including *COL1A1*, *TIMP1* and *ACTA2*, stimulating the production and deposition of these ECM components (79). Other signaling molecules, such as platelet-derived growth factor (PDGF), also contribute to HSC activation by promoting cell proliferation and migration, activating downstream signaling pathways such as PI3K/AKT, MAPK/ERK, and JAK/STAT contributing to the transdifferentiation of quiescent HSCs into myofibroblast-like cells (80). Other key molecular events for HSCs

activation include oxidative stress, immune cell interactions, changes in the ECM and autocrine and paracrine signaling, which maintain their activated state reinforcing the fibrogenic response (66).

As mentioned, during activation, HSCs undergo a phenotypic shift, characterized by increased synthesis of ECM proteins and a transition from a lipid-storing phenotype to a myofibroblast-like phenotype that can be divided in two stages: initiation and perpetuation. In the initial states of activation, HSCs acquire profibrogenic and proinflammatory capacities to amplify the accumulation of ECM generating tissue scarring, inducing the progression of the injury. Those initial states of the activation of HSCs are amplified by signaling from other cell types such as hepatocytes, endothelial cells, and inflammatory cells(81,82). During the perpetuation phase, activated HSCs acquire contractile and proliferative properties and contribute to the contractile forces that drive the alteration of liver architecture in fibrotic conditions (82) (Figure 5). The myofibroblast phenotype is a high-demanding energetic state and HSCs dysregulate their cellular energetic balance, increasing glycolysis, lipid droplet mobilization, beta oxidation, and glutaminolysis, as well as activation of cell-intrinsic stress pathways such as the UPR and ER stress, similar to the Warburg effect in cancer cells(83,84). In addition to cytokines and growth factors, the extracellular microenvironment also plays a crucial role in HSC activation and fibrosis. The interaction between HSCs and components of the ECM, such as collagen and fibronectin, provides signals that perpetuate the activation process.

Understanding the signaling pathways and molecular events that govern HSC activation is essential for developing therapeutic interventions. In this PhD, we have explored the possibility to target the metabolic adaptations that stellate cells suffer to acquire the myofibroblast phenotype as an intervention to disrupt the fibrotic cascade.

4.3. Metabolic plasticity during HSCs activation

In the context of diseases, metabolic plasticity plays a crucial role in cellular adaptation to pathological conditions. Cancer cells, for instance, frequently display altered metabolic profiles to sustain their rapid proliferation. The Warburg effect, characterized by increased glycolysis even in the presence of oxygen, is a classic example of metabolic plasticity observed in cancer cells. Additionally, many cancer cells exhibit enhanced nutrient uptake and utilization to support their energy and biomass requirements. On

the contrary, certain neurodegenerative diseases, such as Alzheimer's and Parkinson's, are associated with impaired metabolic plasticity, leading to dysfunctional energy metabolism and mitochondrial defects, and becoming a target as well for treatment of pathological conditions(85).

Metabolic plasticity plays also significant role in the context of liver fibrosis (84). Hepatocytes, experience a shift in glucose metabolism, with a decrease in oxidative phosphorylation and an increase in glycolysis. This shift is associated with the need to support hepatocyte proliferation during regenerative attempts, but it can also lead to lactate accumulation, fueling further fibrogenesis. KCs adapt their metabolism to a more glycolytic state as they become activated and secrete pro-inflammatory cytokines that promote HSC activation and fibrosis. The altered lipid metabolism in hepatocytes also impacts KCs. LSECs contribute to fibrosis by undergoing capillarization, a process linked to changes in their metabolic state, which reduces nitric oxide production and exacerbates the hypoxic environment of the fibrotic liver. HSCs suffer a shift towards a pro-fibrotic metabolic profile (Figure 6), increasing glycolysis, lipid droplet mobilization, beta oxidation, and glutaminolysis which provides not only energy for their enhanced synthetic activities but also contributes to the production of profibrotic molecules(86–88).

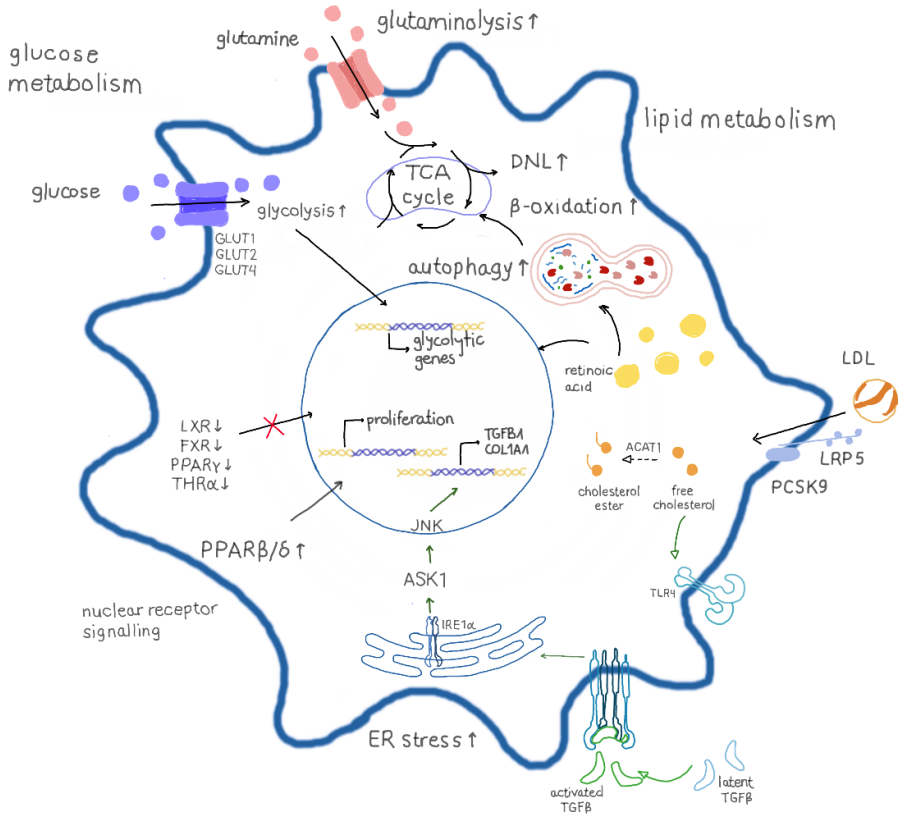

Figure 6. Metabolic plasticity adaptions from activated stellate cells. Hepatic stellate cells (HSCs) experience a marked phenotypic shift upon activation, including increased substrate availability to supply building blocks and energy including changes in glucose, gultaminolysis and lipid metabolism; ER stress and nuclear receptors signalling.

Additionally, there is evidence of altered lipid metabolism, with a release of vitamin A lipid droplets, the main characteristic of quiescent stellate cells and an increase in fatty acid synthesis (89). Liver fibrosis and HSC activation are also highly dependent on mitochondrial biogenesis and increased rates of OXPHOS, by increasing mitochondrial number and respiratory capacity (87). Activated HSCs also complement their high energetic demands through glutaminolysis, a process where glutamine is metabolized to a-ketoglutarate, which feeds into the citrate cycle to generate ATP. The activation of HSCs is accompanied by a sustained cellular stress response, including increased oxidative stress, activation of the UPR, subsequent ER stress, and autophagy. All these metabolic changes are linked to the activation of signaling pathways such as TGF-β. Furthermore, the interaction between different cell types within the fibrotic microenvironment, including immune cells, and epithelial cells, involves a dynamic interplay of metabolic adaptations. This complex crosstalk contributes to the

perpetuation of fibrotic processes and highlights the importance of understanding metabolic plasticity in the context of fibrosis.

4.4. Multiorgan fibrosis

Fibrosis can affect any organ, including the liver, lungs, kidneys, and heart, and is responsible for up to 45% of all deaths in the industrialized world. This process is typically driven by the activation of specific cell types, such as fibroblasts, myofibroblasts, and HSCs in the liver, and is recognized as a highly dynamic process(90). A promising strategy to address this challenge is to target the shared mechanisms and core pathways that play a central role in the development of fibrosis across different organs. While the factors that influence susceptibility and initiation of fibrotic diseases vary, with each organ having its unique risk factors, triggers, and sites of initial injury, a common feature is the activation of fibrotic cell types, primarily fibroblasts, myofibroblasts, or specialized resident cells like HSCs (91). By focusing on this activation process, there is potential to develop effective antifibrogenic therapies. Therefore, studying the pathophysiological progression of these cells toward their activated state can offer valuable insights for the development of treatments aimed at combating multiorgan fibrosis.

Fibrogenic cell types undergo common metabolic adaptations that support their activation and sustained fibrotic activity, making these adaptations attractive targets for antifibrogenic therapies. One key adaptation is the shift from OXPHOS to glycolysis, even in the presence of oxygen. Additionally, increased glutaminolysis and altered lipid metabolism are often observed, supplying critical building blocks for collagen synthesis and cellular proliferation. The heightened demand for nutrients and energy in these activated cells is also linked to the dysregulation of mitochondrial function and enhanced ROS production, which further promotes fibrotic signaling pathways (92). Targeting these metabolic pathways, offers a promising therapeutic approach to disrupt the activation and persistence of fibrogenic cells to reverse fibrosis across multiple organs.

4.5. The good, the ugly and the bad: Hepatic stellate cell heterogeneity

Until recently, HSCs and myofibroblast were considered homogenous cell types but in the recent years and thanks to the single cell RNA sequencing era, have uncovered transcriptional heterogeneities among HSCs populations and zonation, similar to the

parenchymal cells (93). Even in healthy conditions, the liver may contain at least two types of stellate cells that differ in retinoid storing capacity and the expression of activation-associated genes(94). The identification of different phenotypes, among them the “good”, which maintain the liver physiology in a healthy tissue; the “bad” that appear upon fibrosis and the “ugly”, which even promote hepatocellularcarcinoma (HCC), may be of interest to target particular phenotypes as potential treatments of chronic liver injuries. Payen et al. described that although stellate cells are located in the space of Disse, they are distributed throughout the liver lobule and according to their localization, we can distinguish the portal and central vein concentrated GPC3+ HSCs, which are involved in the regulation of glycosaminoglycans metabolisms and have a more active role in ECM turnover and the perisinusoidally DBH+ HSCs, that may have as well, different functionalities and responses to stimuli and have antigen presenting capacities (95). Similarly, Andrews et al described three subtypes of stellate cells in a healthy context that may respond to different functionalities as well: stellate 1 may be involved in vitamin A metabolism; stellate 2 may have regenerative properties as they express HGF and stellate 3 population that have an enriched signature in inflammatory and fibrin-clot associated genes, with potential antigen presenting properties and immune modulators (93). The heterogeneity of stellate cells has been extensively studied in the context of liver disease, with much of the research conducted using animal models. These studies have provided valuable insights into the activation, localization, and functional diversity of stellate cells. However, in this thesis, I will focus specifically on the studies performed with human samples to better understand the heterogeneity of stellate cells in the human liver.

Ramachandran et al. 2019, identified that in cirrhotic tissue, there were scar-associated mesenchymes (SAMes) that transdifferentiate from resting stellate cells, losing the expression of PGS5 and IGFBP5 and increasing the expression of ECM proteins such as COL3A1 and COL1A1. SAMes were further divided into SAMesA and SAMesB (96). He and colleagues identified 2 HSCs sub-clusters, resting HSCs and activated HSCs that changed their expression profile upon transition from NAFLD to NASH, changing the proportion of cells, increasing in NASH the cell numbers of aHSCs observing as well that there was an enrichment in immune response related pathways(97). Finally, from the Friedman research group we could learn that NASH associated HSCs were increased in

cell matrix adhesion and integrin signaling as well as an elevated paracrine and autocrine communication between HSCs and endothelial and immune cells in the liver(98). Taking into account that some chronic liver diseases evolve to HCC, Schwabe group explore the heterogeneity of HSCs and CAFs (Cancer Associated Fibroblasts) within this context identifying two different stellate cell populations: cytokine producing HSCs (cyHSCs), which secrete HGF and gradually decrease in number during fibrosis progression, and myofibroblastic HSCs (myHSCs), which are enriched in ECM proteins and increase in number during fibrosis progression. Patients with a higher prevalence of myHSC over cyHSC were more prone to HCC development (99). A summary table of the various stellate cell populations identified to date is depicted in Table 1.

Functional validation of HSCs subpopulations and their characteristic markers is crucial for understanding their roles in liver physiology and pathology. While transcriptional profiling provides valuable insights into gene expression patterns, it cannot reliably predict protein expression, which ultimately determines cellular function. Therefore, it is essential to complement transcriptional analyses with protein-level validation. Additionally, obtaining these distinct stellate cell populations in vitro would provide valuable models to study various aspects of stellate cell physiology. Therefore, the third objective of this PhD research is to elucidate the heterogeneity present in the differentiation protocol of iPSCs into HSCs and to determine whether this observed heterogeneity mirrors that found in human tissue.

5. The stellate cell system

HSCs are considered specialized liver pericytes but other stellate cells have been described in other organs, which functions can vary depending on the organ but all of them are characterized by a star-shaped or stellate appearance and are often involved in tissue structure, function, and repair. Also, their main phenotypic trait is the capacity to store vitamin A as retinyl sters in their cytoplasm (100). Similar to HSCs in the liver, PSCs are found in the pancreas. In response to pancreatic injury or inflammation, PSCs can become activated and contribute to the fibrotic response seen in chronic pancreatitis and some forms of pancreatic cancer. The differential characteristic of stellate cells in comparison to other fibroblast and myofibroblast is their capacity to

store retinyl sters of vitamin A in their cytoplasm. It is important to note that while stellate cells in various organs may share a similar morphological appearance, their functions and responses can differ significantly depending on the specific tissue and its unique physiological requirements. Understanding the behavior of stellate cells in different organs is crucial for elucidating their roles in health and disease and for developing targeted therapeutic strategies.

5.1. Pancreatic stellate cells

Pancreatic stellate cells are found in the exocrine pancreas, around the acinar cells and within the interlobular connective tissue as well as around blood capillaries and pancreatic ducts (Figure 7) and are estimated to constitute about 4–7%.

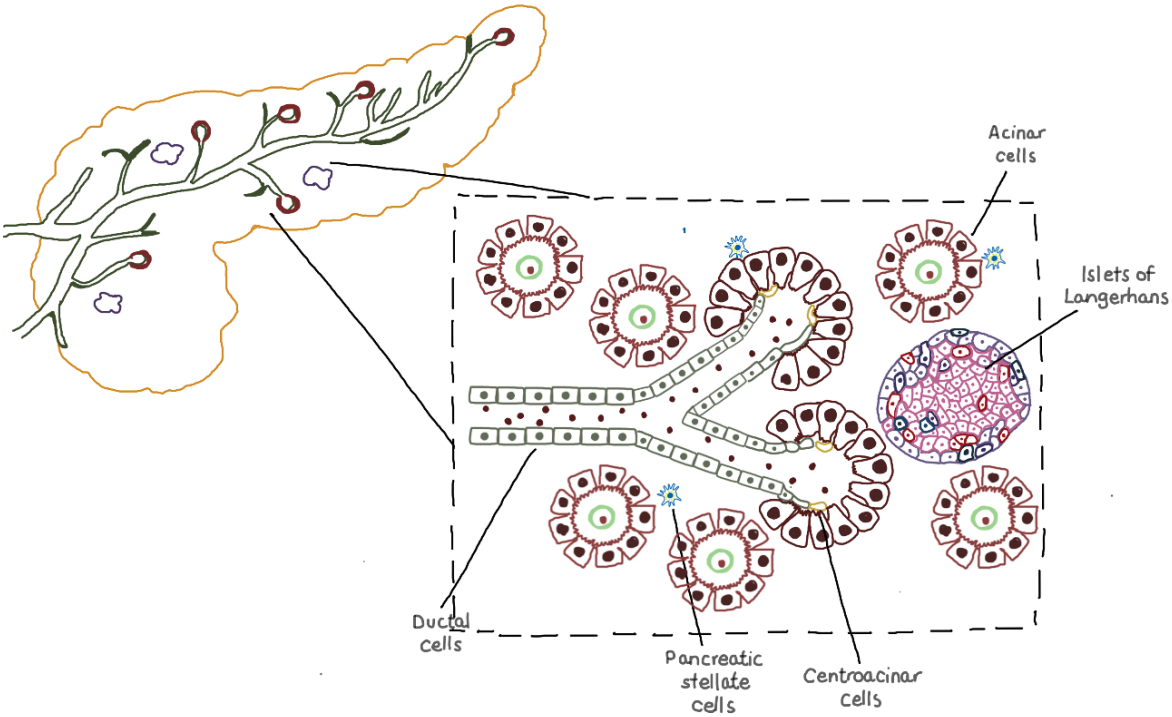

Figure 7. Schematic illustration of pancreatic cellular architecture. Pancreatic tissue is organized between endocrine (Islets of Langerhans) and exocrine (Acinar and Ductal Cells) portions of the organ. Pancreatic Stellate Cells reside around exocrine portion of the organ.

Table 1. Sum up table reflecting the heterogeneity of human hepatic stellate cells populations.

Reference	Stellate cell population	Disease state	Markers	Functional roles	Localization	Characteristics
Payen et al. 2021	Portal and central GPC3+	Healthy	GPC3, DPT, FBLN1, CCL2, RBP1, COLEC10, IGFBP3	ECM turnover, regulation of glycosaminoglycan metabolism.	Portal vein area	Involved in glycosaminoglycans metabolism, active in ECM turnover.
	Perisinusoidal DBH+	Healthy	SPARC, QSOX1, PTN, MYL9, CXCL12, COLEC11, DCN, IGFBP7	Antigen presentation, varied responses to liver stimuli.	Perisinusoidal space	May have antigen-presenting capacities, possibly different functional responses to stimuli.
Andrews et al 2022	Stellate 1	Healthy	PDE3B, RBP1, LRAT	Vitamin A metabolism	Throughout the liver	Involved in vitamin A metabolism
	Stellate 2	Healthy	HGF	Liver regeneration, HGF secretion	Throughout the liver	Associated with regenerative properties, express HGF.
	Stellate 3	Healthy	PLIN2, CLIP1, TAPBP, CD74	Immune modulation, antigen presentation, inflammation response	Throughout the liver	Enriched in inflammatory and fibrin-clot associated genes, potential antigen-presenting properties and immune modulation.
Ramachandran et al. 2019	SAMesA	Cirrhosis	PDGFRBA, TIMP1, COL1A1, COL3A1, COL1A2,	ECM production	Scar tissue in cirrhotic livers	Transdifferentiated from resting stellate cells during cirrhosis,

			CCL2, IGF1, LOXL1			increased ECM protein expression with loss of LGR5 and IGFBP5.
	SAMesB	Cirrhosis	RBP1, IGFBP3, ENDRB, COLEC11, OGN, CRABP2, OCR1, ELN, FBLN2, CTHRC1	Fibrosis progression		
He at al. 2022	rHSCs	NAFLD	RGS5, MYH11, SERPIN1, FOXS1, NOTH3, PLN, PGF, RCAN2, NET1	Storage of vitamin A, maintenance of normal liver architecture	Throughout the liver	Maintain quiescent state in healthy liver, with potential to activate during liver injury.
	aHSCs	NASH	LUM, COL3A1, MIF, COL1A1, LGALS3, SPON2, VCAN, COLEC10, PODN, PCOLCE.	ECM production, fibrogenesis and interaction with immune cells		Increased in number during NASH, enriched in immune response-related pathways, undergo activation during liver injury.
Wang et al 2023	NASH-associated	NASH	PDGFRB, ACTA2, COL1A1, COL3A2, MMP2, TIMP1, TIMP2	Fibrosis, autocrine and paracrine signaling	Liver tissue in NASH	Increased cell-matrix adhesion, integrin signaling and elevated paracrine/autocrine communication with endothelial and immune cells
Fillol et al 2022	cyHSCs	HCC	RGS5, COLEC11, ANGPTL6, TMEM56, ECM1, IFITM1, FCNA,	Cytokine production, tissue homeostasis		Secretes HGF, decreases in number during fibrosis progression, possible

			LRAT, COLEC10, RELN, HGF		protective against excessive fibrosis.
	myHSCs	HCC	SPP1, MGP, S100A6, TIMP1, SERPINE2, PTN, COL15A1, COL1A1, ELN, LPL	ECM production, higher prevalence associated with higher risk of HCC	Enriched in ECM proteins, increase in number during fibrosis progression and associated with higher HCC development risk.

Similar to HSCs, in their quiescent state, PSCs store vitamin A and help maintaining normal ECM homeostasis in the pancreas. During embryo development, as their hepatic counterparts, PSCs contribute to the organogenesis of the tissue as they are involved in the formation of the extracellular matrix (ECM), which provides structural support for developing acinar cells and ductal cells (101). Due to their similarities, it has been proposed a common embryonic origin for both cell types and although the mesenchymal origin of HSCs it has been already prove it by lineage tracing experiments, these studies are still missing for the PSCs (41). Similar to their hepatic counterparts, when there is a damage in the pancreas, PSCs acquire a myofibroblast phenotype, associated with the same hallmarks of activation as the HSCs (Figure 5). Importantly, PSCs have been shown to regulate inflammation, angiogenesis and cancer cell biology via secretion of cytokines and growth factors(102).

The main risk factors for hepatic and pancreatic fibrosis are very similar. Chronic inflammation, often driven by persistent infections such as hepatitis viruses in the liver or recurrent pancreatitis, is a key underlying mechanism. Metabolic disturbances, including obesity, insulin resistance, and MAFLD, are critical in both conditions, promoting fibrotic processes through the activation of hepatic stellate cells and pancreatic stellate cells, respectively. Additionally, excessive alcohol consumption is a well-established risk factor that exacerbates oxidative stress and inflammation in both organs, accelerating fibrosis. Genetic predispositions also play a crucial role, with specific polymorphisms influencing susceptibility to fibrogenesis in both the liver and pancreas. Taking into account all these similarities, there is relatively little known about their direct comparison, particularly in terms of their similarities and differences. While both cell types are central to the fibrotic processes in their respective organs, the details of their embryonic origins and the mechanisms underlying their tissue-specific differentiation remain poorly understood. The extent to which their developmental pathways converge or diverge is not well characterized, leaving gaps in our understanding of how these cells acquire their specialized functions within the liver and pancreas.

5.2. Differentiation of iPSCs towards stellate cells

The first stepwise differentiation protocol aimed at generating hepatic stellate cells (HSCs) was published by our group (Coll et al., 2018; Martinez&Vallverdú et al., 2021; Martinez et al. 2023)(103–105). It is a 12-day protocol based on the sequential addition of growth factors related to liver embryonic development of this cell type. First, we induce the acquisition of mesoderm phenotype by culturing cells with BMP4 during the first 4 days, expressed in the STM (106,107). Then, we add FGF1 and FGF3 as FGFs family member that will induce proliferation and expansion of mesenchymal/mesothelial cells (108). Finally, the cells are incubated with palmitic acid and RA to promote the differentiation and maturation of HSCs (109) (Figure 8). The final population (diHSCs) is phenotypically, transcriptomically, and functionally similar to primary HSCs, exhibiting an intermediate phenotype between the activation and quiescence states, with the ability to respond to acute and chronic fibrogenic stimuli.

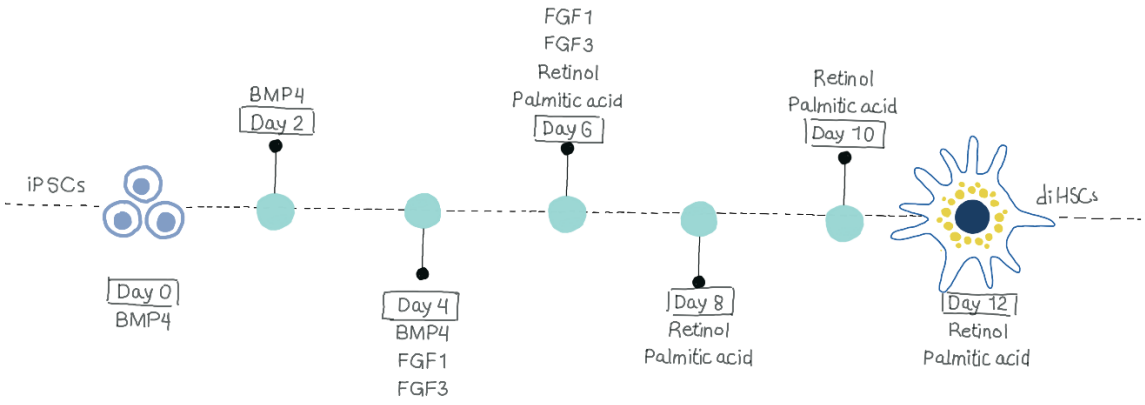

Figure 8. Schematic overview of the differentiation protocol from iPSCs towards diHSCs*. Differentiation workflow from day 0 to day 12 of iPSCs towards diHSCs, including each media change. iPSCs=induced pluripotent Stem Cells and diHSCs= Hepatic stellate cells differentiated from iPSCs.*

Additionally, they can be co-cultured with hepatocytes to form hepatic spheroids that maintain the capacity to respond to fibrogenic and toxicological agents. This differentiation protocol has been used in various scientific publications focused on generating complex *in vitro* models. diHSCs can be co-cultured with hepatoblasts, endothelial cells, and macrophages derived from iPSCs to model steatohepatitis and hepatic fibrosis (110), and they can also be incorporated into automated devices for large-scale production of iPSC-derived hepatic spheroids for disease modeling and drug

screening (111,112). In addition to this differentiation protocol, other alternative strategies for generating HSCs from iPSCs have been published. Miyoshi et al. (2019) described a 6-day protocol based on culturing iPSCs with cytokines such as BMP4, bFGF, CHIR99012, B-27, and N-2 supplement. These iPSC-derived cells were capable of accumulating Vitamin A, activating in response to fibrogenic stimuli, and maturing the parenchymal cell phenotype in co-culture (113). On the other hand, Koui et al. (2017) described the generation of HSCs from iPSCs by differentiating them into an ALCAM-positive mesodermal progenitor. The progenitor population could be expanded and differentiated into mature HSCs through exposure to Y27632 (a Rhodopsin, Rho inhibitor), which induced hepatocyte maturation in a co-culture setup (114). Using the co-differentiation strategy, Ouchi et al. (2019) obtained organoids composed of both parenchymal and non-parenchymal cells, identifying a population with HSC-like characteristics(115). These iPSC -derived organoids have the potential to model steatohepatitis *in vitro*, and can be used for drug toxicology studies.

Currently, there are no established protocols for differentiating induced pluripotent stem cells (iPSCs) specifically into pancreatic stellate cells (PSCs), a gap that may be attributed to the incomplete understanding of their embryonic origins and development. The challenge in developing such protocols lies in the complex developmental pathways that lead to PSCs, which are not yet fully characterized. However, recent studies have explored innovative approaches to address this gap. For instance, Takeuchi et al. (2023) and Kometani et al. (2023) have adapted hepatic stellate cell (HSC) differentiation protocols to derive pancreatic-like stellate cells. These modified protocols rely on the similarities between hepatic and pancreatic stellate cells, incorporating growth factors and signaling molecules known to influence stellate cell biology. To further enhance the relevance of these cells for pancreatic cancer research, these pancreatic-like stellate cells are co-cultured with pancreatic tumor organoids. This co-culture system aims to replicate the pancreatic ductal adenocarcinoma (PDAC) microenvironment, providing a valuable model for studying the interactions between stellate cells and pancreatic tumors. By simulating the stroma of pancreatic cancer, this approach offers insights into the role of PSCs in tumor progression and fibrosis. Despite

these advances, more research is needed to refine these protocols and fully understand the functional characteristics and developmental origins of PSCs.

6. Strategies for the treatment of liver fibrosis

Currently, there is no established treatment for liver fibrosis. Given the severity of advanced liver fibrosis and the limitations of liver transplantation, significant research has focused on developing therapeutic strategies to stop or reverse the fibrotic process (116,117). These strategies can be broadly classified into several categories: Reduce the fibrogenic activity of HSCs, induce the reversion of activated HSCs to a quiescent state, or eliminate myofibroblasts through apoptosis or cell death processes.

Efforts to develop antifibrotic drugs have primarily focused on targeting the cellular and molecular mechanisms that drive fibrosis. Current strategies include:

- **Angiotensin II Receptor Blockers (ARBs) and ACE Inhibitors:** Angiotensin II is a pro-fibrotic molecule, and drugs that block its effects, such as losartan (an ARB) or enalapril (an ACE inhibitor), have shown potential in reducing fibrosis by inhibiting HSC activation and collagen synthesis(118).
- **Peroxisome Proliferator-Activated Receptor (PPAR) Agonists:** PPARs are nuclear receptors that regulate lipid metabolism and inflammation. PPAR-γ agonists, such as Elafibranor, have been investigated for their ability to reduce HSC activation and fibrosis, particularly in patients with NAFLD-related fibrosis(119,120).
- **Metabolic Modulators:** Using metabolism regulators as antifibrogenic drugs represents a novel and promising approach for treating fibrosis. By targeting metabolic pathways, such as glycolysis, oxidative phosphorylation, or lipid metabolism, regulators can disrupt this metabolic shift, reducing the activation and survival of fibrogenic cells. Several compounds that modulate key metabolic enzymes or pathways have shown antifibrogenic potential in preclinical studies such as ACC inhibitors (GS834356) or GLS1 inhibitors (GS-836644) (121,122).
- **Matrix Metalloproteinases/Tissue Inhibitors of Metalloproteinase:** Matrix metalloproteinases/TIMPs are important enzymes that regulate the deposition and degradation of ECM. MMPs are the main ECM-degrading enzyme in the liver and their endogenous inhibitors are TIMPs. With liver injury, MMPs are inhibited

by TIMPs, which are high expressed. This causes the break of the balance between deposition and degradation of ECM, which leads to excessive deposition of ECM and eventually leads to liver fibrosis. The use of some small molecules, such as Halofuginone, has demonstrated the relevance of the downregulation of TMPS to alleviate liver fibrosis(117).

- **Antioxidants and Anti-inflammatory Agents:** Since oxidative stress and inflammation play key roles in fibrosis progression, agents that reduce oxidative stress (GS060093 – Sphingosine kinase inhibitors) or inflammation (e.g., corticosteroids, pentoxifylline) are being studied as potential antifibrotic treatments (117).

Specific signaling pathways are crucial in the initiation and progression of liver fibrosis. Targeting these pathways has emerged as a promising approach:

- **TGF-β Signaling Inhibitors:** Transforming growth factor-beta (TGF-β) is a potent fibrogenic cytokine that drives HSC activation and ECM production. Small molecule inhibitors of TGF-β signaling, such as SB52334, an ALK5 inhibitor, have shown potential in preclinical and early clinical trials by reducing fibrosis (123).
- **Wnt/β-Catenin Pathway Inhibitors:** The Wnt/β-catenin pathway is involved in tissue repair and fibrosis. Inhibitors of this pathway, like SB-216763, a blocking agent of GSK-3β, are being investigated for their ability to limit fibrosis by reducing the activation of HSCs (124).
- **The Rho/MRTF signaling pathway**: It regulates the transcription of profibrotic genes that promote this fibrotic response. By inhibiting this pathway, using inhibitors such as CCG-203971, it is possible to reduce HSC activation and prevent the production of fibrogenic proteins. Preclinical research has shown that targeting the Rho/MRTF axis can effectively slow down or even reverse the progression of liver fibrosis, offering a promising strategy for therapeutic intervention in chronic liver diseases (125).
- **Inhibition of CTGF:** Connective tissue growth factor is an important pro-fibrotic factor in the process of fibrosis and is induced by TGF-β1. It has been reported that pioglitazone inhibited the development of liver fibrosis by inhibiting the expression of CTGF and type III collagen in HSCs and preventing the

morphological changes of HSCs induced by TGF-β1 in a dose-dependent manner(126).

In addition, interfering with the action of other liver cells, such as hepatocytes or immune cells, could be considered to change the fibrogenic environment by reducing fiber accumulation and oxidative stress, and to some extent, reverse liver fibrosis.

Despite significant efforts in the development of antifibrogenic therapies, no treatment has yet been successfully translated into routine clinical practice. Challenges such as incomplete efficacy, off-target effects, and the need for long-term safety data have delayed the transition of these therapies from the lab to the clinic. As a result, liver fibrosis remains an unmet medical need, highlighting the importance of continued research and innovation in this field.

Understanding stellate cell paths in differentiation and activation is essential to delineate how cells acquire their phenotype and how this is lost during disease, thereby providing pathophysiological insights for the development of novel anti-fibrogenic treatments. Although cell trajectory upon disease can be studied using animal models, the translation to human samples is sometimes complex, and differentiation trajectories during embryo development are difficult to study.

This thesis seeks to harness the potential of iPSC technology to generate hepatic stellate cells in a controlled and reproducible manner, facilitating the development of more physiologically relevant in vitro models for liver fibrosis.

HYPOTHESIS

The hypothesis of this PhD thesis is that examining the differentiation trajectory of hepatic stellate cells using an iPSCs-based model will yield critical insights into their physiological functions and pathological roles in liver fibrosis. We propose that characterizing the molecular mechanisms driving the differentiation of induced hepatic stellate cells (diHSCs) will identify key regulators and signaling pathways that influence either the maintenance of diHSCs in a quiescent state or their activation into profibrogenic myofibroblasts. Additionally, we hypothesize that interventions targeting molecular drivers of diHSCs differentiation in chronic liver diseases can be good therapeutic strategies to prevent the activation of HSCs and to reduce fibrosis. Moreover, we postulate that the interaction between the endoderm and mesenchyme can influence the differentiation path of diHSCs, potentially directing their fate. Specifically, contact with organ-specific endoderm, such as that from the pancreas, may alter the differentiation trajectory of these cells, leading them to differentiate into pancreatic-like stellate cells.

OBJECTIVES

1. **Standardize the production, preservation, storage and use of diHSCs:**
    - Scale-up the production of diHSCs from iPSCs.
    - Develop and implement guidelines for cryopreservation and long-term storage of diHSCs to maintain their viability, functionality, and reproducibility in experimental assays.
2. **Characterize the differentiation trajectory of diHSCs and investigate the functional consequences of diverging trajectories in liver fibrosis:**
    - Profile gene expression and proteomic changes during differentiation.
    - Identify key molecular regulators and signaling pathways governing the differentiation of diHSCs from their quiescent state to activated myofibroblast.
    - Construct a comprehensive map of the differentiation trajectory of diHSCs, defining the sequential changes in cellular identity and functional properties.
    - Explore the impact of dysregulated differentiation trajectories of diHSCs on the development and progression of liver fibrosis using human in vitro and *in vivo* murine models.
3. **Define the heterogeneity and differentiation potential of cell populations generated during diHSC differentiation:**
    - Elucidate the molecular mechanisms underlying distinct cellular states and functional phenotypes.
    - Identify distinct subpopulations of diHSCs along differentiation and validate them in human samples.
    - Investigate how environmental factors, such as cytokines, growth factors, and other cell types, influence the heterogeneity and specification of stellate-cell populations.

MATERIALS AND METHODS

EXPERIMENTAL MODELS

1. *In vitro* cell cultures

1.1. Induced Pluripotent Stem Cells: The study utilized several iPSC lines for various experimental purposes, each selected based on its relevance to the specific goals of the research:

- **KULi003-A:** This iPSC line was derived from human fibroblasts (ATCC® CRL-2522™) and generated in the laboratory of Catherine Verfaillie at the Stem Cell Institute, KU Leuven, Belgium. It has been used as the primary cell line for the differentiation into hepatic stellate cells (HSCs), including the generation of constitutive knockouts for the RORA gene. This line was also crucial in characterizing the differentiation protocol to HSCs, as documented in the studies by Martinez & Vallverdú et al. (104)(105).
- **KOLF2J.1**: Acquired from The Jackson Laboratory, this iPSC line was used as a reference in collaborative studies (127). The differentiation of KOLF2J.1 into diHSCs helped validate the robustness and reproducibility of the differentiation protocol developed by the group. Additionally, this line was used to obtain hepatoblast-like cells for comparative studies.
- **XM001 BIHi043-A:** Employed during an internship in Professor Spagnoli's lab at King's College London, this cell line was utilized to differentiate into hepatoblasts and pancreatic progenitors, facilitating cross-laboratory comparisons and enhancing the versatility of the iPSC differentiation protocols.
- **dCas9-FL-BCL:** Obtained from the Banco Nacional de Líneas Celulares (BNCL), this cell line was used to generate an inducible knockout of RORA. This inducible system allowed for temporal control of RORA gene expression during the differentiation of iPSCs into diHSCs, following the established protocol.

1.2. iPSC culture conditions: All iPSC lines were cultured in Stem Flex medium, within 6-well plates coated with 1% vitronectin diluted in DPBS-/-. The medium was refreshed every 48 hours, maintaining the cells until they reached approximately 80% confluence. For expansion, cells were detached using 50 µM EDTA for 5-10 minutes at room temperature, with a standard split ratio of 1:6 to ensure consistent growth and maintenance of the cultures.

1.3. Gene editing strategies used in iPSCs:

- **Generation of a Constitutive Knockout for RORA**: The study employed CRISPR-Cas9 gene editing to create a heterozygous knockout of the RORA gene in iPSCs. The specific sgRNA sequence used was "5'-ATCTGTGGAGACAAATCATCAGG-3'", designed using the CRISPR tool at CNB-CSIC. The iPSCs were prepared for nucleofection by pre-treatment with 10mM Rock inhibitor (Y-27632) for 3 hours. The CRISPR-Cas9 RNP complex was formed by incubating 100 pmol of Cas9 Nuclease with 120 pmol of sgRNA at 25ºC for 10 minutes. A total of 200,000 cells were nucleofected using the 4-D Nucleofector System (Lonza) with program CA-137. Post-nucleofection, cells were cultured in mTSR1 medium supplemented with Y-27632 for 72 hours. Single-cell colonies were generated, followed by genotyping via PCR and Sanger sequencing to confirm the knockout. This process was repeated to ensure clonal purity.
- **Generation of an Inducible Knockout for RORA**: To create an inducible RORA knockout, the same sgRNAs were cloned into a lentiviral vector. Virus production involved co-transfecting HEK293T cells with the gRORA plasmid, packaging plasmids (psPAX2), and PEI. After 24 hours of incubation and subsequent media changes, the viral supernatant was collected, concentrated by ultracentrifugation, and stored at -80ºC. iPSCs (iCas9-FL-BCL) (128) were then infected with the virus and selected with hygromycin for one week to ensure stable integration.
- **Induction of RORA Guide in iCas9-FL-BCL Cell Line**: To induce the knockout, cells were treated with doxycycline (1 µg/mL) to activate the Cas9.

2. Differentiation protocols

All differentiation medias used within this PhD are collected in table 3.

a) **Differentiation Towards Stellate Cells**: The differentiation of iPSCs into diHSCs followed a multi-step protocol, optimized to produce high-quality diHSCs that closely resemble primary HSCs:

   i. **Initial Plating**: iPSCs were detached using 50 µM EDTA and seeded at a density of 15,000 cells/cm² on plates coated with 2% Matrigel Growth Factor Reduced in DMEM.

ii. Differentiation Process:

- Day 0 to Day 4: When cells achieved 70% confluence, they were cultured in liver differentiation medium (LDM) supplemented with BMP4 (20 ng/mL). This phase induced mesodermal commitment.
- Day 4 to Day 6: BMP4, FGF1 (20 ng/mL), and FGF3 (20 ng/mL) were added to promote further mesodermal differentiation towards a mesothelial/mesenchymal phenotype.
- Day 6 to Day 8: The medium was supplemented with FGF1, FGF3, retinol (5 mM), and palmitic acid (100 mM) to initiate early stellate cell differentiation.
- Day 8 to Day 12: Cells were maintained in LDM with retinol and palmitic acid to mature the stellate cell phenotype.

  Differentiated cells were either used immediately for functional assays, subcultured, or cryopreserved for future studies.

b) **Expansion of diHSCs:** To expand diHSCs while minimizing activation, cells were cultured on Matrigel pre-coated plates and detached using trypsin 0.25% EDTA. Post-detachment, cells were filtered to remove excess ECM and seeded at a density of 73,000 cells/cm² with Revitacell during the first 24h to enhance viability.

c) **Cryopreservation of diHSCs:** Cells were prepared for cryopreservation following the same detachment protocol. Approximately 2 million cells were stored per cryovial for future use. Different cryopreservation medias were used both commercial and non-commercial.

- BB: Bambanker cryopreservation media
- CSCS10: CryoStor CS10
- GRCFM: Gibco Recovery Cell Culture Freezing Media
- FBS: 80% FBS + 20% DMSO
- KoSR: 80% Knockout Serum + 20% DMSO

d) **Fibrosis modeling using diHSCs:** Two fibrogenic models were used:

- Model 1: diHSCs were passaged at day 12 for expansion, mimicking early activation.

- Model 2: Cells at day 12 were treated with TGFβ (5 ng/mL) for either 24 hours or 7 days to simulate acute and chronic fibrosis, respectively.

e) ***In vitro* screening of antifibrogenic drugs:** diHSCs were activated by passage and when 90% confluence was achieved, they were treated with different potential antifibrogenic drugs (Table 2) during 24 hours. Samples were then collected for subsequent analysis.

Table 2: Potential antifibrogenic drugs tested in Objective 1.

Drug	Target	Concentration
Elafibranor	PPAR agonist	
GS-490470 (SB525334)	TGFβ receptor I (ALK5)	250nM
GS834356	ACC inhibitor	10nM
GS1052649 ((CCG-203971)	Rho/MRTF/SRF pathway inhibitor	10uM
GS1066192	ROCK2 inhibitor	5uM
GS060093	Sphingosine kinase inhibitor (SKI-II)	4uM
GS-836644	GLS inhibitor	26nM

f) ***In vitro* modulation of RORA activity with commercial agonist and antagonist:** On day 2 of the differentiation protocol, cells were treated with synthetic agonists (SR1078, Merck, Cat#557352) or antagonists (SR1001, MCE, Cat#HY-13421) targeting RORA and RORG, at concentrations of 0.1 mM and 85 nM, respectively. The treatment was refreshed every two days, and samples were collected on day 12 for further analysis. To modulate RORA after passage, differentiated cells at day 12 were passaged as described previously. Once the cells reached 70% confluence, they were treated with SR1001 (85 nM) and SR1078 (3 mM) for 24 hours. Samples were then collected for subsequent analysis.

g) ***In vitro* modulation of Notch signalling:** On day 8 of the differentiation protocol, cells were treated with recombinant DLK1 (Enzo Life Sciences, Cat# 50-200-7986) at 100ng/mL or Jagged-1 (MedChem, Cat#HY-P1846A) at 20μM targeting NOTCH signalling. The treatment was refreshed at day 10 of the differentiation and samples were collected at day 12 for further analysis.

h) **Non-directed mesoderm differentiation:** iPSCs were washed with DPBS-/-, detached using Accutase (5-7 minutes at 37°C), and resuspended in Stem Flex medium. After centrifugation at 1200 rpm for 3 minutes, cells were counted and plated at 1x10^4 cells per well in a 96-well non-adherent round-bottom plate with 150 µL SF medium supplemented with Revitacell (1:100). The plate was centrifuged at 800g for 5 minutes and incubated for 24 hours to allow EB formation, followed by an additional 24-hour incubation. EBs were then transferred to non-adherent plates and cultured in StemFlex for 2 days. Subsequently, EBs were transferred to Matrigel-coated slide flasks (1:40) and cultured in mesoderm differentiation medium (EBm + 0.5 mM Ascorbic Acid) for 2-3 weeks, with medium changes every 2-3 days. EBm medium consisted of KO-DMEM, Glutamax, NEAA, 2-Mercaptoethanol, 10% FBS-HyClone (KOSR), and Penicillin-Streptomycin.

i) **Differentiation towards hepatic and pancreatic progenitors:** Endoderm progenitor differentiation followed a protocol modified from established islet differentiation methods (54), which consist of different stages of differentiation:
   - Stage 1: Definitive endoderm was induced using CHIR99021 (from 3 to 0.3 uM) and Activin A (100 ng/mL) with daily media changes.
   - Stage 2: Cells were cultured with Vitamin C (0.25mM) and FGF7 (50ng/mL) over three days.
   - Stage 3: Posterior foregut endoderm was formed using SANT1 (0.625mM), Retinoic Acid (2.5mM), LDN-192189 (0.25mM), TPB (0.5mM), and continued cultivation in FGF7 and Vitamin C.
   - Stage 4 – Pancreatic progenitors: Pancreatic progenitors were formed using SANT1, Retinoic Acid, LDN-192189, TPB, Y-27632 (10uM), followed by continued cultivation in FGF7(2ng/mL), EGF (100ng/mL), Activin A(10ng/mL), and nicotinamide (10mM).

- Stage 4 – Hepatoblast: Cells were cultured in BMP4 (5uL/mL) and FGF1 (2uL/mL) to guide cells towards a hepatoblast-like phenotype. After four days, cells were harvested for co-culture experiments with stellate cells.

3. **Co-cultures**

Three co-culture systems were established during this PhD:

- **System 1**: HepG2 cells (epithelial) were co-cultured with stellate cells, with direct cell-cell contact.
- **System 2**: Hepatoblasts or pancreatic progenitors were co-cultured with stellate cells, with direct cell-cell contact.
- **System 3**: Conditioned media from hepatoblasts or pancreatic progenitors was diluted to 50% with differentiation media from stellate cells, starting from day 8 of the stellate cell differentiation and doing one media refreshment at day 10.

For both direct co-culture systems, cells were detached, counted, and mixed in a 2:1 epithelial to mesenchymal ratio. Cells were plated at a density of 10,000 cells/well in 96-well U-bottom plates under non-adherent conditions. Aggregates were formed by centrifuging the plates at 200g for 3 min, and regular medium changes were performed carefully to maintain the integrity of the co-culture system.

Table 3: Media and growth factors used in the in vitro models listed.

Cell culture	Basal medium	Supplements/Cytokines
iPSCs expansion and culture	Stem Flex	Commercial supplement
diHSCs differentiation (Day 0-4)	Liver differentiation media (LdM): 57% DMEM, Low Glucose, Pyruvate; 40% MCDB 201 medium; 1% L-Ascorbic Acid; 0.25% Insulin-Transferrin-Selenium (ITS-G); 0.25% LA-BSA; 0.1% 2-Mercaptoethanol (50 mM); 0.4% Dexamethasone; 1% Penicillin-Streptomycin Mixture (P/S)	BMP4 (20 ng/mL)
diHSCs differentiation (Day 4-6)	LdM	BMP4 (20 ng/mL), FGF1 (20 ng/mL), FGF3 (20 ng/mL)
diHSCs differentiation (Day 6-8)	LdM	FGF1 (20 ng/mL), FGF3 (20 ng/mL), Retinol (5 mM), Palmitic Acid (100 mM)

diHSCs differentiation (Day 8-12)	LdM	Retinol (5 mM), Palmitic Acid (100 mM)
Exapnsion and thawing of diHSCs	DMEM glutamax 10% FBS, 1% P/S	Revitacell (1:100) during the first 24h
Mesoderm differentiation	KO DMEM	1% Glutamax, Glutamax, 1% NEAA, 2-Mercaptoethanol, 10% FBS-HyClone (KOSR), 1% P/S, Ascorbic acid 0.5M
Hepatic and pancreatic progenitor differentiation (Stage 1)	Stage 1 basal medium: MCDB131, GlutaMAX (10 mM), Glucose (1.5 g/L), $NaHCO_3$ (2.5 g), BSA (0.5%)	Activin A (100 ng/mL), CHIR99021 (3uM; 0.3μM)
Hepatic and pancreatic progenitor differentiation (Stage 2)	Stage 1 basal medium	FGF7 (50ng/mL) and Ascorbic acid (0.25mM)
Hepatic and pancreatic progenitor differentiation (Stage 3)	Stage 3 basal medium: MCDB131, GlutaMAX (10 mM), Glucose (2.5 g/L), $NaHCO_3$ (10 g), ITS-X (0.5X), BSA (2%)	SANT1(0.625mM), Retinoic Acid(2.5mM), LDN-192189(0.25mM), TPB(0.5mM), FGF7 (50ng/mL) and Ascorbic Acid (0.25mM)
Hepatic differentiation (Stage 4)	Stage 3 basal medium	FGF1 (2μL/mL) and BMP4 (4μL/mL)
Pancreatic differentiation (Stage 4)	Stage 3 basal medium	SANT1 (0.625mM), Retinoic Acid(0.25mM), LDN-192189(0.5mM), TPB(0.25mM), FGF7 (2ng/mL), Ascorbic Acid(0.25mM), EGF(100ng/mL), Activin A (10ng/mL), nicotinamide (10mM), Y-27632 (10μM)

4. Animal models

In this thesis the use of animal models was strictly limited to cases where validation of *in vitro* findings derived from iPSCs systems needed physiological relevance confirmation *in vivo* or to answer reviewer comments in the revision process of an article. All animal experiments were approved by the Ethics Committee of Animal Experimentation of the University of Barcelona and were conducted in accordance with the National Institute of Health Guide for the Care and Use of Laboratory Animals.

a) **Hepatic Fibrotic Model (CCl_4):** The carbon tetrachloride (CCl_4) model is a well-established experimental approach for inducing liver fibrosis in rodents,

providing a valuable system for investigating fibrogenesis mechanisms and evaluating potential therapeutic interventions. CCl_4 is a potent hepatotoxin that undergoes biotransformation in the liver by cytochrome P450 enzymes, predominantly CYP2E1. This biotransformation produces highly reactive free radicals, including trichloromethyl (CCl3•) and trichloromethylperoxy (CCl3OO•) radicals. These radicals cause oxidative stress, lipid peroxidation, and hepatocellular damage, triggering inflammation and the activation of HSCs. Chronic administration of CCl4 leads to sustained liver injury and progressive fibrosis, with the severity of fibrosis being modifiable through variations in dosage, frequency, and duration of exposure.

b) Wildtype Animals: Fourteen C57BL/6J mice were used in this study. Mice were administered CCl4 at a dose of 0.5 mL/kg (diluted in 25% corn oil) via intraperitoneal (I.P.) injection twice weekly for a total of four weeks. In the final two weeks of the experiment, mice were divided into two groups:

- SR1078-treated Group: Mice received I.P. injections of SR1078 at a dose of 10 mg/kg twice weekly. SR1078 was prepared in 5% DMSO, resulting in a final concentration of 2 mg/mL.
- Vehicle-treated Group: Mice received I.P. injections of vehicle solution (5% DMSO) twice weekly.

c) Staggerer Animals: To assess the physiological role of RORA in liver fibrosis, a carbon tetrachloride (CCl_4) model was established using 14 staggerer mice and their wildtype counterparts. Mice were injected I.P. with 0.5 mL/kg of CCl_4 (diluted in corn oil) twice a week for four weeks. Blood and liver tissues were collected post-sacrifice for subsequent analysis.

d) RORA Knockout (KO) HSC-Specific Animals: To investigate the effects of RORA knockout specifically in HSCs within the context of liver fibrosis, a new animal strain was created. This was achieved by crossing RORA floxed (fl/fl) mice with Lrat-Cre. The presence of the floxed allele and the Cre transgene in offspring was confirmed by PCR. 10 Rora fl/wt mice, including Cre- and Cre+ were used to stablish a CCl_4 model of 4 weeks. Mice were injected I.P. with 0.5 mL/kg of CCl_4 (diluted in corn oil) twice a week.

e) **Heart fibrotic model (ISO model):** To induce cardiac fibrosis, ten C57BL/6J mice were administered isoproterenol (ISO) (Sigma Aldrich, Cat#SLC62971) via continuous infusion at a dose of 60 mg/kg/day using minipumps (Model 1007D, Alzet). Mice were divided into two treatment groups:

- SR1078-treated Group: Mice received SR1078 at a dose of 10 mg/kg every 48 hours.
- Vehicle-treated Group: Mice were administered a vehicle solution (same as SR1078 preparation) every 48 hours.

Animals were sacrificed after one week of treatment for further analysis.

f) **Kidney fibrotic model (UUO model):** For kidney fibrosis induction, nineteen C57BL/6J mice underwent unilateral ureteral obstruction (UUO). Post-surgery, mice were divided into two groups:

- SR1078-treated Group: Mice received SR1078 at a dose of 10 mg/kg starting from day 3 after surgery until the end of the study.
- Vehicle-treated Group: Mice were administered a vehicle solution (as used for SR1078) starting from day 3 after surgery and continued for 15 days.

Blood, as well as kidney tissues, were collected for analysis following sacrifice.

5. Human samples

a) **Adult liver human samples**: Liver biopsies from patients diagnosed with liver diseases or controls from liver resections of metastic tumors who were admitted to the Liver Unit at the Hospital Clinic of Barcelona were utilized for this study. Prior to participation, all patients provided signed informed consent, ensuring their voluntary involvement and understanding of the study's purpose. The study protocol adhered to ethical standards and was rigorously reviewed and approved by the Ethics Committee of the Hospital Clinic, ensuring compliance with both institutional and international ethical guidelines for research involving human subjects.

b) **Adult pancreatic human samples**: Pancreatic adult tissue samples were obtained from the Clinic Biobank following approval from the Ethics Committee. These samples were collected from patients undergoing surgical resection for duodenal tumors. Importantly, the tissue sections provided for the study were histologically normal and deemed healthy by pathologists. The acquisition and

use of these samples adhered to ethical guidelines, ensuring that all procedures were conducted with informed consent from the patients and in compliance with regulatory standards set by the Ethics Committee.

c) **Fetal liver and pancreas human samples**: During my internship in Professor Spagnoli's lab, human embryo samples were utilized as part of the research. These samples were provided by the Human Developmental Biology Resource (HDBR) consortium, which is dedicated to advancing our understanding of human development. All research activities involving these samples were conducted in full compliance with ethical guidelines and were approved by the relevant Ethics Committees. The use of these human embryo samples adhered to the highest ethical standards, ensuring that all procedures respected the principles of informed consent and responsible research practices.

MOLECULAR ANALYSIS

1. **Protein analysis**

   a) **Proteomics**: This analysis was conducted in collaboration with the proteomics platform at CICBiogune, with only the initial cell processing performed in our laboratory. diHSCs were collected at days 0, 2, 4, 6, 8, 10, and 12 of differentiation. Human primary HSCs isolated from liver samples were used as a positive control. Cells were washed once with DPBS -/- and lysed with 500 µL of a buffer containing 7M urea, 2M thiourea, and 4% CHAPS. Protein extraction and processing followed the filter-aided sample preparation (FASP) protocol with slight modifications. Proteins were digested overnight at 37°C with trypsin at a 1:50 enzyme-to-protein ratio. After digestion, the samples were dried using a RVC2 speedvac concentrator (Christ) and reconstituted in 0.1% formic acid. Peptide desalting was carried out using C18 stage tips (Millipore), and the samples were then analyzed using a timsTOF Pro mass spectrometer (Bruker Daltonics) coupled to a nanoElute liquid chromatography system (Bruker). A 200-ng aliquot of each sample was injected onto a 15 cm Bruker FIFTEEN C18 analytical column and separated over a 30-minute gradient at a flow rate of 400 nL/min, with the column maintained at 50°C.

Protein identification and quantification were conducted using MaxQuant software with default settings, searching against a human protein database from Uniprot/Swissprot. Precursor and fragment mass tolerances were set to 20 ppm and 0.05 Da, respectively. Only proteins identified with at least two peptides at a false discovery rate (FDR) of <1% were included in the downstream analysis. The resulting label-free quantification (LFQ) intensities were processed using the Perseus software platform, where data were log2-transformed and imputed. Protein abundance data were normalized to the day 0 samples for each experiment to facilitate comparative analysis across time points.

b) **Immunoflourescence:** This technique was used for both in vitro systems and tissues.

- For cells: Cells were first fixed with 4% Neutral Buffered Formalin for 15 minutes at room temperature (RT). After fixation, the cells were washed with DPBS to remove excess fixative. Permeabilization was carried out using 0.2% Triton X-100 in PBS for 30 minutes at RT. To block nonspecific antibody binding, the cells were incubated with 3% donkey serum at RT. Following the blocking step, cells were incubated overnight at 4°C with primary antibodies diluted in DAKO REAL™ Antibody Diluent. After overnight incubation, cells were washed to remove unbound primary antibodies and incubated with secondary antibodies conjugated to fluorophores, diluted 1:700, for 30 minutes at RT. Finally, the samples were mounted with a mounting medium containing DAPI to visualize the nuclei (Vectashield mounting media).
- For tissues: Paraffin-embedded liver sections (3 µm thick) from both human and mouse samples were deparaffinized and subjected to antigen retrieval using Target Retrieval Solution. For antigen retrieval, the sections were either heated in a pressure cooker in citrate buffer for 20 minutes or treated with EnVision Flex Target Retrieval Solution (Low or High pH) in a Dako PT Link system. After antigen retrieval, tissue sections were blocked for 30 minutes and incubated overnight with primary antibodies. The following day, sections were incubated with secondary

antibodies conjugated to fluorophores in a 1:700 dilution. Finally, the sections were mounted with a mounting medium containing DAPI for nuclear visualization (Vectashield mounting media).

Table 4: Antibodies used for immunofluorescence.

Reactivity	Host	Dilution	Brand
RELN	Rabbit	1:100	*Thermo Scientific*
RSPO3	Rabbit	1:50	*Thermo Scientific*
VIPR1	Rabbit	1:100	*Thermo Scientific*
LUM	Rabbit	1:100	*LifeSpan BioScience*
OCT4	Mouse	1:100	*STEMCELLS*
aSMA	Rabbit	1:100	*Abcam*
COLLAGEN	Rabbit	1:100	*Biodesign International*
EOMES	Mouse	1:100	*R&D Systems*
VIM	Mouse	1:100	*Leica*
GATA4	Rabbit	1:40	*Invitrogen*
ALCAM	Rabbit	1:100	*Abcam*
SMOC2	Sheep	1:100	*R&D Systems*
SOX17	Goat	1:200	*Biotechne*
PDX1	Rabbit	1:500	*Abcam*
HNF4A	Mouse	1:500	*Abcam*
NKX6.1	Mouse	1:500	*Hybridoma Bank*
ALB	Rabbit	1:600	*Dako*

c) **Immunohistochemistry:** For immunohistochemistry, deparaffinized tissue sections using the above-mentioned antigen retrieval systems were incubated with primary antibodies at 4ºC overnight. Following primary antibody incubation, sections were washed to remove unbound antibodies and subsequently incubated with peroxidase blocking solution for 10 min and secondary antibodies conjugated to horseradish peroxidase (HRP) for 30 min at room temperature. After incubation with secondary antibodies, the sections were treated with a chromogenic substrate, diaminobenzidine (DAB), to develop the color signal. To enhance visualization, the sections were counterstained with

hematoxylin to provide contrast between the stained antigen and the surrounding tissue. Finally, the slides were dehydrated through graded alcohols, cleared in xylene, and coverslipped using a permanent mounting medium for microscopic examination (DPX).

Table 5. List of primary antibodies used in paraffin embedded samples.

Reactivity	Host	Dilution	Retrieval	Brand
Anti-h/ms-KI67	Rabbit	1:50	Citrate Ph6 - pressure cooker	*Abcam*
Anti-ms-CD3	Goat	1:50		*BioRad*
Anti-h/ms-alphaSMA	Rabbit	1:200		*Abcam*
Anti-h-RORalpha	Rabbit	1:100		*Abcam*
Anti-h-EPCAM	Mouse	1:100	Low PH – DAKO PT LINK	*Dako*
Anti-ms-F4/80	Rat	1:50		*BioRad*
Anti-ms-CD177	Rabbit	1:50		*Abcam*
Anti-ms-EPCAM	Rabbit	1:200		*Abcam*
Anti-h/ms-MPO	Rabbit	1:50	High PH – DAKO PT LINK	*Abcam*

h, human; ms, mouse

Table 6. List of secondary antibodies used for histology analysis.

Reactivity	Host	Dilution	Brand
anti-rabbit Cy3	Donkey	1:200	*Jackson ImmunoResearch*
anti-goat Cy3	Donkey	1:200	*Jackson ImmunoResearch*
anti-rabbit Alexa Fluor 488	Donkey	1:200	*Jackson ImmunoResearch*
anti-mouse Alexa Fluor 488	Goat	1:400	*Invitrogen*
biotinylated anti-rat IgG H+L	Rabbit	1:200	*Vector Laboratories*

2. **Gene expression analysis**

   a) **Bulk RNA Sequencing**: For bulk RNA sequencing, the quality of extracted RNA was assessed using Agilent RNA 6000 Nano Chips (Agilent Technologies, Santa Clara, CA, USA). Sequencing libraries were prepared using the TruSeq Stranded mRNA Sample Preparation kit, starting with 125 ng of total RNA per sample. The libraries were sequenced on a HiSeq2500 instrument (Illumina Inc., San Diego, CA, USA), generating at least 30 million 51-nucleotide single-end reads per sample. To identify differentially expressed genes (DEGs) from the transcriptomic data, raw

sequencing reads were first processed using standard quality control and alignment procedures. The reads were mapped to the reference human genome and the resulting expression counts were normalized to account for library size and other technical variables. DEGs were then determined by comparing expression levels between experimental conditions using DESeq2 with significance thresholds set to a false discovery rate (FDR) of <0.05. To further interpret the functional implications of these DEGs, gene ontology (GO) biological processes, KEGG pathways, and Reactome pathways analyses were performed using EnrichR. Additionally, gene set enrichment analysis (GSEA) was conducted using the GSEA database to identify enriched biological pathways and processes associated with the DEGs.

b) **Single-Cell RNA Sequencing of diHSCs**: For single-cell RNA sequencing (scRNA-seq) of iPSC differentiation into HSCs, cells were collected at days 0, 4, 6, 8, and 12 of differentiation. Cell dissociation followed a standard protocol, and the resulting cell pellets were resuspended in 100 µL of FACS Buffer, with a 1:1000 dilution of the Live/Dead viability antibody (Thermo Fisher Scientific). After 20 minutes of incubation at 4°C, the cells were centrifuged at 300g for 5 minutes and resuspended in PBS with 0.05% BSA. Live cells were sorted to obtain approximately 100,000 cells per differentiation point. The samples were filtered twice using 40 µm filters (pluriSelect) to remove aggregates, and cell concentration and viability were assessed using the TC20™ Automated Cell Counter (Bio-Rad Laboratories, S.A.). The single-cell suspensions were processed using Gel Bead-in-Emulsion (GEM) to capture approximately 6,000 total cells per sample. cDNA sequencing libraries were prepared using the Chromium Next GEM Single Cell 3’ v3.1 kit (10X Genomics). cDNA amplification involved 12 cycles, and the resulting products were quantified using an Agilent Bioanalyzer High Sensitivity chip (Agilent Technologies). For library preparation, 100 ng of cDNA was used, and indexing was performed by PCR using the PN-220103 Chromium i7 Sample Index Plate. The distribution and concentration of the 3' cDNA libraries were verified

using the Agilent Bioanalyzer High Sensitivity chip. Sequencing was conducted on an Illumina NovaSeq 6000 platform, yielding approximately 40,000 reads per cell. Data processing was performed using CellRanger 5.0.0 (10X Genomics) and aligned to the GRCh38 Ensembl 98 reference genome. Cells expressing fewer than 200 genes or more than 20% mitochondrial content were filtered out. Data analysis and normalization were carried out using Seurat 4.0.3, with data integration performed using the NormalizeData and ScaleData functions. Samples from different timepoints were integrated using Harmony, in order to correct batch effects. Visualization was achieved through Uniform Manifold Approximation and Projection (UMAP) within RStudio.

c) **Analysis of Public Single-Cell Data**: Public single-cell RNA sequencing datasets were downloaded from the GEO repository (Table XX) and processed using Seurat. Quality control measures were implemented to remove low-quality cells based on mitochondrial gene content and the number of expressed genes. Data normalization was then performed, followed by dimensionality reduction to identify cell clusters. Cell annotation was conducted using reference datasets from PanglaoDB and DescartesDB.

d) **Gene expression analysis:** RNA extraction from cells was carried out using the Quick RNA-Microprep Kit (Zymo, Cat#R1050) according to the manufacturer's instructions. For 3D cultures, total RNA was extracted from 6 pooled spheroids using the same kit. Additionally, total RNA was extracted from mouse whole liver tissue using Trizol (Life Technologies, Carlsbad, CA, Cat#15596026). The quality of the extracted RNA was assessed using the Bioanalyzer 2100 (Agilent Technologies, Santa Clara, CA), and RNA concentrations were quantified using the Nanodrop 1000 (ThermoFisher). Subsequently, cDNA synthesis was performed using the MultiScribe Reverse Transcriptase (Applied Biosystems, Cat#4368813) followed by quantitative reverse transcription polymerase chain reaction (qRT-PCR) on an ABI 7900HT cycler (Applied Biosystems) using SYBR green master mix (Life Technologies, Cat#11733046). Gene expression

levels were normalized to GAPDH for in vitro systems and Actb for *in vivo* experiments, and expression values were calculated using the ΔΔCt method.

Table 7: List of primers used for gene expression analysis in human and mice samples.

Gene	SOURCE	IDENTIFIER	Specie
LRAT	Integrated DNA Technologies (IDT)	Hs.PT.58.39384980	Human
RELN		Hs.PT.58.761851	Human
COL1A1		Hs.PT.58.15517795	Human
ACTA2		Hs.PT.56a.2542642	Human
GAPDH		Hs.PT.39a.22214836	Human
LOX		Hs.PT.58.1471308	Human
LHX2		Hs.PT.58.19323386	Human
RORA		Hs.PT.58.27208579	Human
SOX2		Hs.PT.58.237897.g	Human
NANOG		Hs.PT.58.21480849	Human
GLI2		Hs.PT.58.3039554	Human
ALDOB		Hs.PT.56a.948966	Human
ACACA		Hs.PT.56a.513712.g	Human
VIM		Hs.PT.58.38906895	Human
EOMES		Hs.PT.58.27752441	Human
GS6P		Hs.PT.58.46489349	Human
SMOC2		Hs.PT.58.20763253	Human
BACH2		Hs.PT.58.2653742	Human
HGF		Hs.PT.58.4192354	Human
VIPR1		Hs.PT.58.22279020	Human
IGF2		Hs.PT.58.39913403	Human
SLIT2		Hs.PT.58.3815432	Human
LHFP		Hs.PT.58.27833950	Human
AFP		Hs.PT.56a.571602	Human
ALB		Hs.PT.56a.1501965	Human
HNF4A		Hs.PT.58.22303533	Human
PDX1		Hs.PT.58.2295117	Human
NKX6.1		Hs.PT.58.25073618	Human
CPA1		Hs.PT.58.39705861	Human

CYP3A4		Hs.PT.58.1272782	Human
Actb		Mm.PT.39a.22214843.g	Mouse
Acta2		Mm.PT.58.16320644	Mouse
Col1a1		Mm.PT.58.7562513	Mouse
Col1a2		Mm.PT.58.5206680	Mouse
Col3a1	Integrated DNA Technologies (IDT)	Mm.PT.58.13848686	Mouse
Timp1		Mm.PT.58.30682575	Mouse
Fn1		Mm.PT.58.8135568	Mouse
Mpo		Mm.PT.58.5251395	Mouse
F4/80		Mm.PT.58.11087779	Mouse
CD3e		Mm.PT.58.41689106	Mouse
Il1β		Mm.PT.58.41616450	Mouse
Tnfα		Mm.PT.58.12575861	Mouse
Tgfβ		Mm.PT.58.8169936	Mouse
Rora		Mm.PT.58.32675621	Mouse
Mmp2		Mm.PT.58.9606100	Mouse
Mmp9		Mm.PT.58.10100097	Mouse
Mmp12		Mm.PT.58.31615472	Mouse
Il6		Mm.PT.58.10005566	Mouse
Nppa		Mm.PT.58.12973594.g	Mouse
Pdk4		Mm.PT.58.9453460	Mouse

Hs=Human; Mm= Mouse.

e) **Lipidomics:** The lipidomics assay was performed in collaboration with Olobion. In our lab, only the cell culture part was performed. Briefly, cells were harvested using trypsin and washed it with PBS, to remove residual media and contaminants. A volume of 275 µL of methanol was put directly on the cells with a milling ball. After homogenization (1 min), 1 mL of MTBE was added. Then this mixture was shaken and centrifuged. For the lipidomic profiling, 100 µL of the upper organic phase was collected, evaporated, and resuspended using 100 µL methanol with an internal standard, shaken, centrifuged, and used for LC-MS analysis. The lipids were separated on an ACQUITY UPLC BEH C18 column maintained at 65°C and coupled to a ZenoTOF 7600 system (SCIEX). The sample was

injected at 4 µL in ESI positive and negative mode. The lipidomics data were processed by oloMAP 2.0.

FUNCTIONAL ANALYSIS

1. **Intracellular Glucose Level Testing**: Intracellular glucose levels were measured using the Glucose-Glo™ Assay (Promega, Cat#TM494) following the manufacturer's instructions. The assay was performed on cells from day 4 of differentiation and diHSCs that had been passaged. Cells were cultured in 96-well plates, and the media was removed prior to testing. Each well was washed with 100 µL of DPBS. Glucose uptake was initiated by adding 50 µL of 2DG in DPBS. After the glucose absorption period, the assay was completed according to the manufacturer's protocol. The intensity of the luminescent signal is directly proportional to the intracellular glucose levels.
2. **XF24 extracellular flux**: The Seahorse XF Cell Mito Stress Test (Agilent, Santa Clara, CA, US) was utilized to measure the oxygen consumption rate (OCR) in iPSC-RORA +/- and their wild-type (WT) counterparts. According to the manufacturer's protocol, cells were sequentially treated with 1 µM oligomycin, 2 µM carbonyl cyanide m-chlorophenyl hydrazone (CCCP), and a mixture of 1 µM rotenone and antimycin A. On day 4 of differentiation, cells were exposed to the RORA agonist SR1078 at a concentration of 0.1 mM, both with and without treatment. The experimental data were analyzed using Agilent's Seahorse XFe Wave Software. Additionally, RORA agonist and/or TGFβ were administered to the cells for a full day post-passage. Total protein content for normalization and quantification was determined using the BCA Protein Assay Kit (ThermoFisher, Cat# 23225).
3. **Collagen tissue determination:** The hydroxyproline content in liver tissues from staggerer mice and UUO model animals was assessed using a Hydroxyproline Assay Kit (Abcam, Cat#MAK008-1KT), following the manufacturer's guidelines. First, tissue samples are homogenized to prepare a solution for analysis. The samples undergo acid hydrolysis to convert hydroxyproline into a detectable form. Following hydrolysis, the samples are mixed with the assay reagents provided in the kit, which form a colorimetric complex specifically with hydroxyproline. Absorbance was measured at 540 nm using a BMG LABTECH FLUOstar OPTIMA FL reader.

4. **Biochemical determination by Echevarne laboratories (Barcelona, Spain)**: Blood from mice included in the experimental studies was collected and analyzed for alanine transaminase (ALT), aspartate transaminase (AST), phosphatase alkaline (AP) and lactate dehydrogenase (LDH) values.

STATISTICAL ANALYSIS

GraphPad Prism v8.0 was used for the statistical analyses. The D'Agostino-Pearson omnibus normality test, Anderson-Darling test and Shapiro-Wilk normality test were performed to assess data distribution. For statistical analysis of parametric data, the two-tailed unpaired Student's t test was used for groups of two; one-way ANOVA followed by Sidak multiple comparison posthoc tests were used for comparison of more than two groups. For non-parametric data, the Mann-Whitney U test was used for groups of two while the Kruskal-Wallis test followed by Dunn multiple comparison posthoc test was used for comparison of more than two groups.

RESULTS

Objective 1: Standardize the production, preservation, storage and use of diHSCs.

The first objective of this doctoral thesis was to scale up the production of diHSCs. Additionally, we developed guidelines for the cryopreservation and long-term storage of diHSCs, with a focus on maintaining their viability, functionality, and reproducibility for experimental assays.

1. **Scale up the production of diHSCs.**

Initially, differentiation of iPSCs towards HSCs was performed in 12-well plates, each providing a 3.6 cm^2 surface area for cell culture. This approach produced approximately 500,000 cells per well. However, the heterogeneous morphologies observed under brightfield microscopy within the final cell populations across different wells were pronounced, leading to inconsistencies in the differentiation process. Due to the variability between wells, the detachment process resulted in significant cell loss, reducing the overall number of cells obtained from an expected 6 million cells to 4 million cells, primarily due to cell mortality in the detaching process.

During my PhD work, I successfully scaled up the differentiation process to a 75 cm^2 culture surface in cell culture flask, which significantly improved cell production, obtaining up to 8 million cells per plate. The larger culture surface reduced heterogeneity within the differentiation, resulting in a more uniform cell population. This homogeneity not only facilitated the detachment process but also decreased cell mortality, thereby enhancing the overall success rate of the experiments (Figure 9A).

To validate the effectiveness of the scale-up, differentiated cells from the 75 cm^2 flask were characterized and compared to those obtained from the 12-well plates. Three independent differentiations were performed in both formats, and PDGFRβ expression was assessed by flow cytometry at the end of the differentiation (Figure 9B). Additionally, the gene expression levels of HSC markers, including *LRAT, PCDH7, RELN, ACTA2*, and *COL1A1*, were analyzed. The results showed no significant differences between the two differentiation modalities (Figure 9C). However, the larger surface area provided lower variability and heterogeneity in the differentiation process, leading to a higher number of viable cells at the endpoint. This improvement was due to the reduced mortality associated with cell detachment from the more homogeneous culture environment of the 75 cm^2 flask.

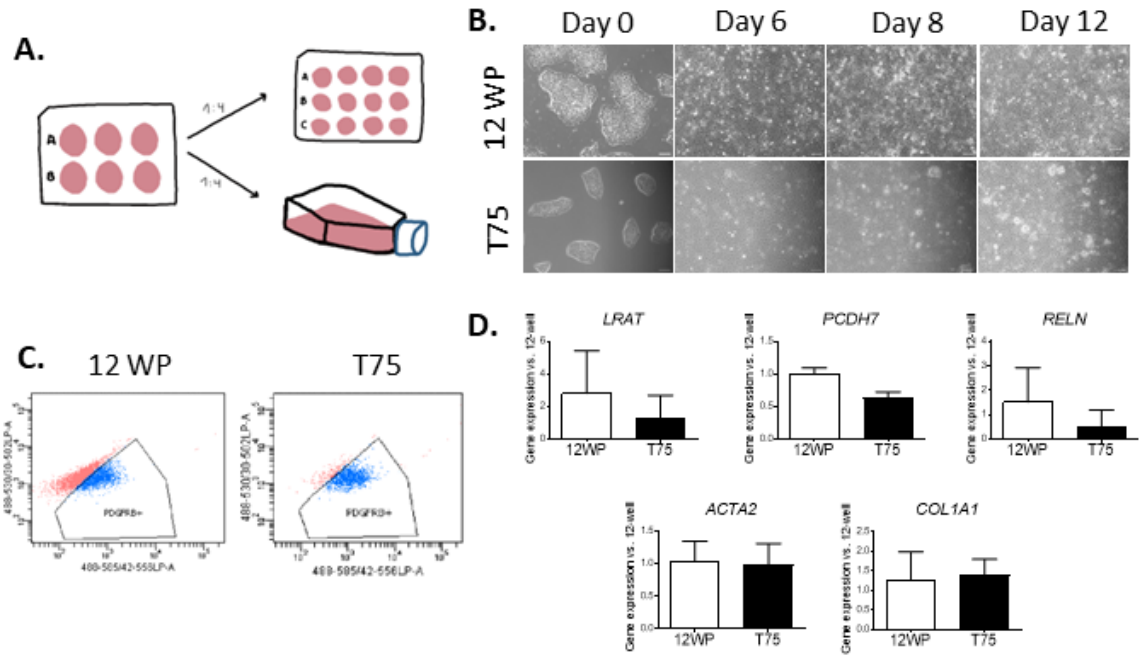

Figure 9. Scaling up diHSC production*. (A) Schematic representation illustrating the seeding strategy employed to scale up the production of diHSCs. (B) Representative microscope images showing different stages of diHSC differentiation in 12-well plates versus T75 flasks, highlighting increased heterogeneity in the 12-well plate conditions. Scale bars = 100µm. (C) Flow cytometry analysis of PDGFRβ expression comparing diHSCs differentiated in 12-well plates and T75 flasks. (D) Gene expression analysis of quiescent markers (LRAT, PCDH7, RELN) and activation markers (ACTA2, COL1A1) in diHSCs derived from 12-well plates and T75 flasks. diHSCs = differentiated hepatic stellate cells; 12WP=12-well plates; T75= Flask of 75cm². Data is presented as mean ± SEM, with statistical significance assessed by t-test between 12WP and T75, **p < 0.01, n=3.*

2. Expansion and cryopreservation of diHSCs

We then assessed whether at the end of the differentiation protocol, diHSCs could be expanded or frozen for future *in vitro* assays. The passage of diHSCs was optimized at a 73000 cells/cm^2 cell density in Expansion Media. On the other hand, differentiated cells could be frozen and the freezing media was optimized compering both commercial and non-commercial medias. Thawing of the cells is recommended in a cell density of 145000 cells/cm^2. (Figure 10A). We observed that cell viability did not significantly change between different cryopreservation medias (Figure 10B) and neither changes in gene expression of HSCs markers (*ACTA2*, *COL1A1*, *LRAT*, *PCDH7 and RELN*) were observed (Figure 10C). Altogether, we conclude that diHSCs can be cryopreserved with several commercial and non-commercial media showing similar expression and viability of HSC markers. However, due to their lowest price and highest viability, FBS and KoSR will be chosen as the preferred conditions. For both passage and thawed cells is

recommended to supplement the Expansion Medium for the first 24H with Revitacell, as less mortality was observed (Figure 10D).

Next, we evaluated the gene expression of some HSC markers in comparison to freshly differentiated cells. Passaged and thawed cells show a significant increase in *PCDH7* expression with respect to day 12 cells but the expression of other markers characteristic of HSCs such as *PDGFRβ* and *COL1A1* was maintained. On the other hand, the expression of the quiescence gene *LRAT* was lower in thawed and expanded cells, whereas the expression of activation markers such as *ACTA2* and *LOX* was higher, showing a significantly increase in passage cells (Figure 10E). On the other hand, protein expression of HSC markers such as RELN, RSP03 and VIPR1, were similar in diHSCs at day 12 and expanded cells at day 1 (Figure 10F). However, the immunofluorescence of both cell cultures indicated the existence of positive cells with different levels of marker expression, as well as cells negative for these markers.

In summary, we conclude that diHSCs can be successfully passaged and cryopreserved while maintaining the heterogeneous phenotype observed on day 12 of the differentiation protocol. This heterogeneity may be related to the cells' differentiation stage or maturity. Additionally, the observed increase in activation markers after passage or thawing suggests that these processes may induce a more activated phenotype, indicating that passaging could itself serve as an activation assay for diHSCs.

3. Functional assessment of passaged and cryopreserved diHSCs

In order to evaluate the response capacity of passaged and thawed cells, diHSCs were exposed to both pro-fibrogenic and pro-inflammatory cytokines. Cells were cultured in expansion media and were stimulated when they reached 70% confluency with TGFβ as a pro-fibrogenic cytokine and LPS as a pro-inflammatory cytokine (Figure 11A).

Both passaged and thawed cells exposed to acute and chronic TGFβ stimuli (5ng/mL) acquired an activated phenotype as noted by the increment of *COL1A1*, *ACTA2* and *LOX* (Figure XB). However, when cells were exposed to proinflammatory acute stimuli (LPS 100ng/mL), diHSCs increased the expression of *IL-6* and although no significant, an increase in *MCP1* and *CCL20* (Figure 11B). Altogether, these results suggest that passaged and cryopreserved diHSCs maintain the capacity to response to pro-fibrogenic stimuli and even though they could respond to pro-inflammatory stimuli, the response of expanded and thawed diHSCs was limited.

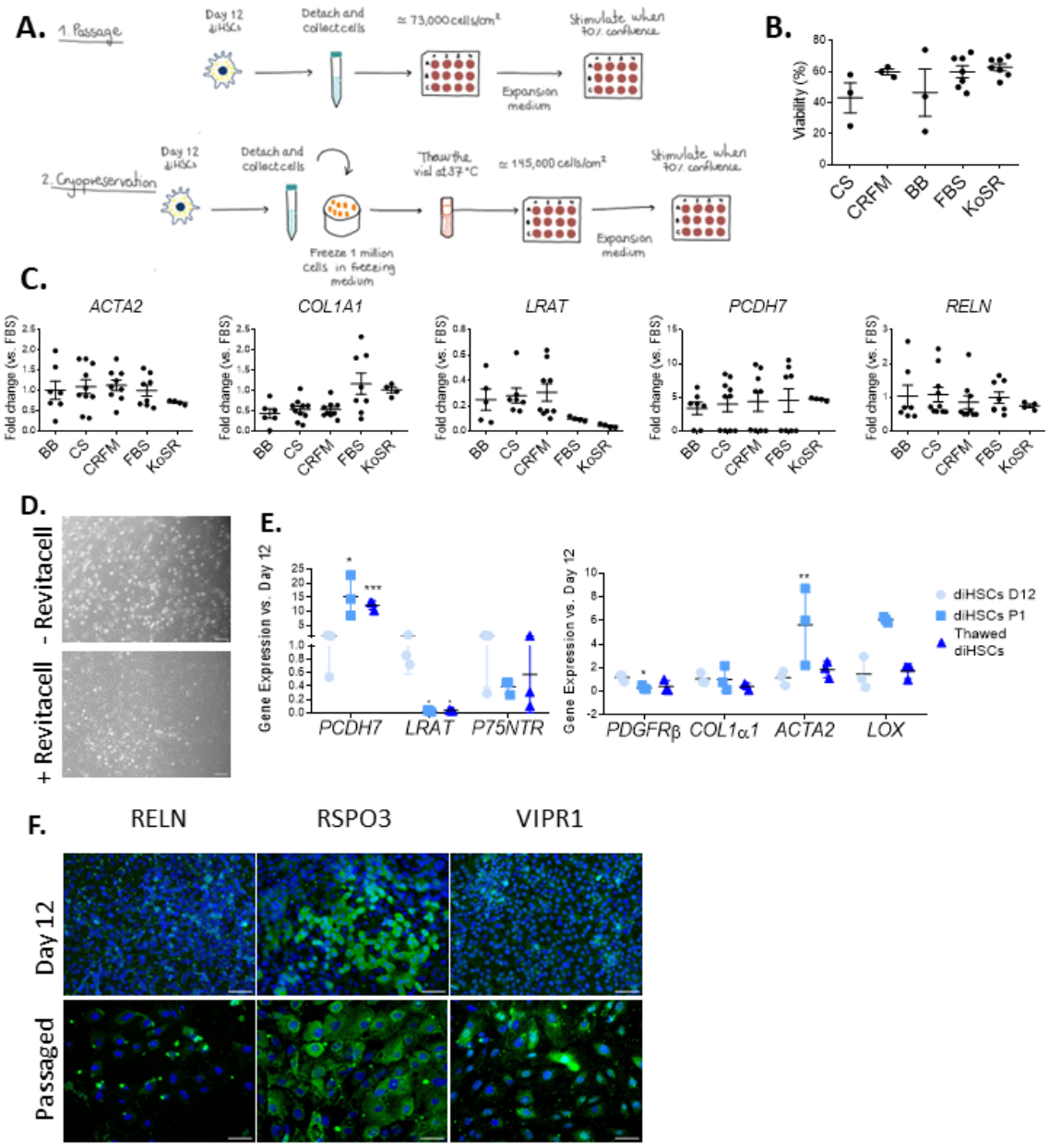

Figure 10. Expansion and Cryopreservation of diHSCs*. (A) Schematic representation of the strategies for cell passage and cryopreservation of diHSCs. (B) Assessment of diHSC viability using various cryopreservation media, including commercial (CS, CRFM, BB) and non-commercial (FBS, KoSR) options. (C) Gene expression analysis of activation markers (ACTA2, COL1A1) and quiescent markers (LRAT, PCDH7, RELN) across different cryopreservation media. (D) Viability of diHSCs without (-Revitacell) and with (+Revitacell) supplementation following passage. Scale bars = 100µm. (E) Comparison of gene expression levels for activation markers (ACTA2, COL1A1) and quiescent markers (LRAT, PCDH7, RELN) in diHSCs at day 12, post-passage, and after thawing. (F) Immunofluorescence staining for HSC markers (RELN, RSPO3, VIPR1) in differentiated cells at day 12 and after passage, highlighting cell heterogeneity. Scale bars = 100µm. Data are presented as mean ± SEM, with statistical significance assessed by 2-way ANOVA for the different cryopreservation media and 1-way ANOVA for the comparison of day 12, passage and thawed cells, **p < 0.01, n=3.*

We also evaluated the potential of diHSCs to perform drug screening assays by evaluating their response against three potential anti-fibrogenic drugs in clinical trials. diHSCs were treated with Elafibranor (20uM), an agonist of PPARα and PPARδ, for 24h.

Treated cells showed a significant reduction in the expression of *COL1A1*, *ACTA2* and *LOX* (Figure 11C). We also tested the antifibrogenic capacity of GS834356 in diHSCs. This compound, an Acetyil-CoA carboxylase (ACC) inhibitor, induced a clear reduction of *ACTA2* while there were no significant changed in the expression of *COL1A1* and *LOX* (Figure 11D). Finally, an inhibitor of glutaminase (GLS1) was also tested in diHSCs, observing a significant increase in *LOX* but showing no effect on the expression of *COL1A1* and *ACTA2* (Figure 11D). Altogether, these results indicated the potential to use diHSCs as a source of cells for drug screening of potential antifibrogenic drugs and have allowed us to establish Elafibranor as a systematic positive control of anti-fibrogenic action in our cells, to be used as a reference in future studies.

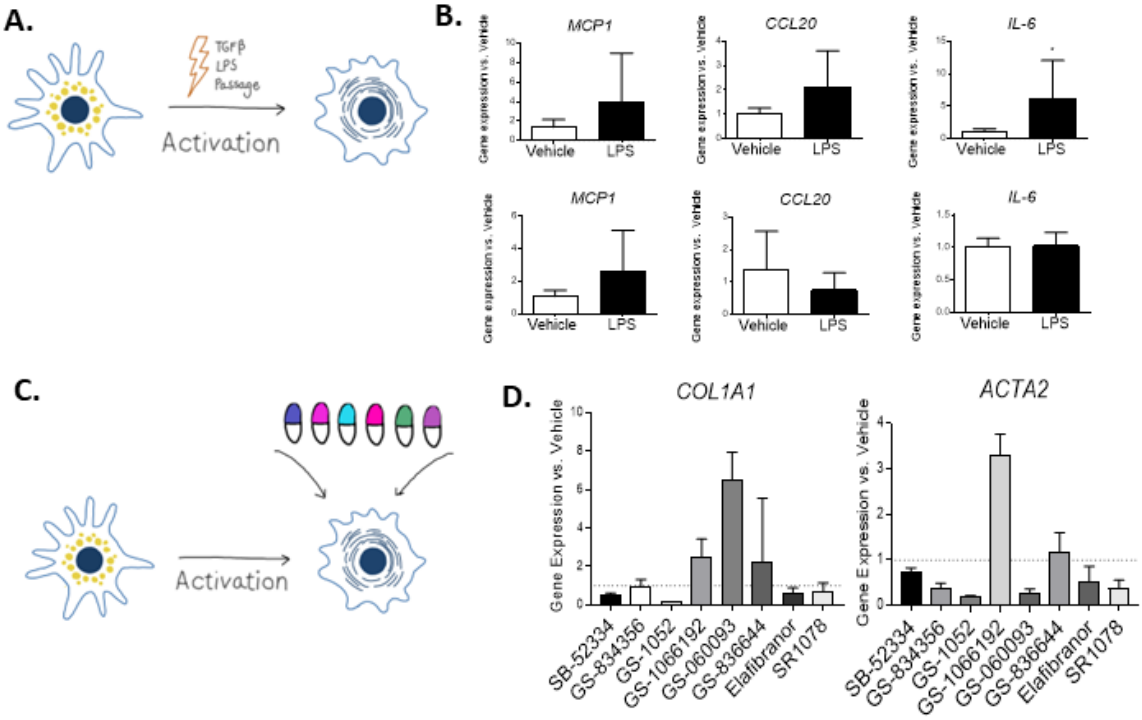

Figure 11. Functional Assessment of Passaged and Cryopreserved diHSCs*. (A) Schematic diagram illustrating the activation approaches that can be used in fresh and cryopreserved diHSCs. (B) Gene expression analysis of inflammatory markers (MCP1, CCL20, and IL6) in passaged and thawed diHSCs treated with LPS (20 ng/mL). (C) Schematic representation of the strategy for evaluating diHSCs' response to antifibrogenic drugs. (D) Gene expression analysis of activation markers (COL1A1 and ACTA2) following a 24-hour treatment with antifibrogenic drugs. Data are presented as mean ± SEM. Statistical significance between treated and untreated cells, as well as between passage and thawed cells, was determined using a t-test, *p < 0.05, n=3.*

The results from the first objective of this PhD, published in *Nature Protocols* and *Methods in Molecular Biology*, show that diHSCs can be successfully expanded and cryopreserved while retaining their profile and ability to respond to pro-fibrogenic stimuli. Additionally, this PhD research has demonstrated that these cells are suitable for drug screening assays and in vitro disease modeling.

Objective 2: Characterize the differentiation trajectory of hepatic stellate cells (diHSCs) and investigate the functional consequences of aberrant diHSCs differentiation in liver fibrosis.

The second objective of this doctoral thesis involved employing proteomic and transcriptomic methodologies to profile the alterations in gene expression and protein composition throughout the differentiation process. By doing so, we aimed to identify the crucial molecular regulators and signaling pathways orchestrating the differentiation process to quiescent diHSCs and the transition into activated myofibroblasts. Furthermore, we constructed a detailed proteomic roadmap of diHSC differentiation, elucidating the sequential shifts in protein expression and cellular characteristics along differentiation. Additionally, this study aimed to investigate how aberrant differentiation trajectories based on the alteration of expression of the TF of RORA during diHSCs differentiation and in the quiescent phenotype, contributed to the onset and advancement of liver fibrosis, using both human *in vitro* systems and *in vivo* murine models to explore these dynamics.

1. **Proteomic characterization of diHSCs differentiation and comparison with primary human HSCs.**

To achieve a comprehensive understanding of the diHSCs differentiation process with temporal resolution, we collected samples at seven timepoints throughout the differentiation protocol: days 0, 2, 4, 6, 8, 10, and 12. Mass spectrometry (MS)-based profiling was employed to analyze these samples across four independent differentiation experiments (Figure 12A). Four samples of human primary HSCs (pHSCs) obtained from healthy patients were included as positive controls as well. Through this approach, we constructed a detailed proteomic roadmap of the transition from iPSCs to diHSCs, identifying 3.064 proteins, of which 2.475 were reliably quantified.

As expected, proteins associated with pluripotency, such as RIF1, POU5F1 (OCT4), DPPA4, KPNA2, and DNMT3B, showed a marked decrease as differentiation progressed. In contrast, markers characteristic of HSCs, including DCN, LUM, PTN, MMP2, PCOLCE, LAMA5, IGFBP3, LGALS1, IGFBP5, and various collagens, exhibited a significant increase (Figures 12B-C). The proteomic profile of day 0 cells was predominantly linked to gene ontologies (GOs) related to pluripotency, translation, cell division, and the proliferation

of undifferentiated cells (Figure 12B). By day 12, the proteome profile of the cells had shifted, showing an enrichment in proteins involved in ECM organization, collagen metabolism, wound healing, and TGF-β signaling, hallmarks of the differentiated HSC phenotype (Figure 12B).

GSEA comparing the diHSCs proteome to human liver cell types(129) revealed that the diHSCs exhibited a proteome profile highly enriched in HSC-specific markers, closely reflecting the pHSCs phenotype (Figure 12D). Additionally, we identified five distinct expression clusters based on dynamic proteomic changes: matrisome-enriched, metabolic, proliferation and pluripotency, and basal-proteins (Figure 12E-I). These clusters offer insights into the key proteins driving the differentiation process and provide a structured proteomic roadmap for understanding the transition from iPSCs to diHSCs.

Notably, when comparing the proteome of diHSCs to that of pHSCs derived from liver donors, we found that over 80% of their proteomic profiles were shared (Figure 12J). Differential protein expression involved in the activation phenotype of the HSCs are enriched in the pHSCs such as EHD2, TIMP3, THY1, TIMP1, MYL9, and FBLN2 exhibit characteristics typical of an activated phenotype (Figure 12J). EHD2, involved in membrane trafficking and endocytosis, suggests heightened cellular activity, a hallmark of activated HSCs. The enrichment of TIMP3 and TIMP1, both inhibitors of metalloproteinases, points to a critical role in ECM preservation and the prevention of excessive ECM degradation, processes integral to fibrosis. THY1, a surface glycoprotein associated with cell adhesion and migration, is upregulated in the activated state, further supporting the fibrogenic potential of these cells. MYL9, linked to cytoskeletal organization and cell contraction, indicates the contractile function that contributes to tissue stiffness during fibrosis. Finally, FBLN2, an ECM protein involved in matrix production and remodeling, underscores the active ECM synthesis characteristic of HSC activation. Together, these markers strongly suggest that primary HSCs present a higher activated state than diHSCs. On the contrary, differential proteins expressed by diHSCs indicated a proliferative state, characterized by increased cell division, chromatin remodeling, and gene regulation, characteristics of cells derived from iPSCs (Figure 12J).

However, both cell types shared proteins related to extracellular matrix remodeling, such as FSTL1, MMP14, SFRP2, PALLD, LOXL2, and RAB13 (Figure 12J).

During differentiation, diHSCs exhibited pathways reported in bibliography (130) associated with quiescence, activation, and a broad stellate cell phenotype (Figure 12K-M). This finding underscores the progressive acquisition of the stellate cell phenotype by iPSCs differentiation, validating diHSCs as a robust model for studying stellate cell biology and their role in cellular commitment. The similarities in proteomic profiles between diHSCs and pHSCs further support the use of diHSCs as a relevant model for future research in liver fibrosis and related pathologies.

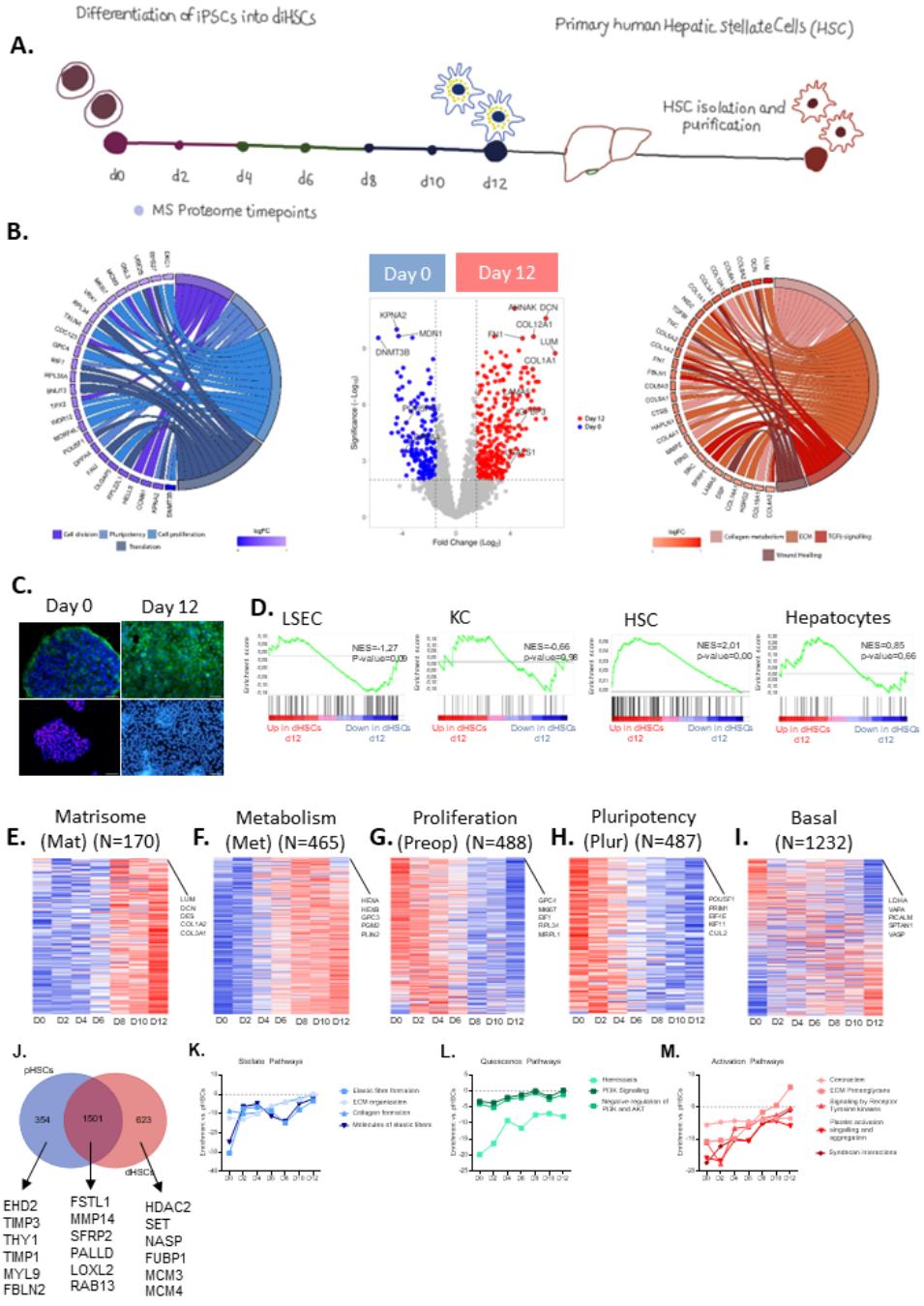

Figure 12. Overview and functional proteome analysis of cell differentiation from Day 0 to Day 12*. (A) Schematic diagram illustrating the experimental design used to characterize the differentiation process at the proteome level and compare it to primary HSCs. (B) Circular chord diagram showing the Gene Ontology (GO) terms enriched at day 0 and day 12, along with a volcano plot depicting the differentially expressed proteins between these timepoints. (C) Representative immunofluorescence images of LUM and OCT4 at day 0 and day 12. Scale bars represent 200 µm at day 0 and 100 µm at day 12. (D) Gene Set Enrichment Analysis (GSEA) of reported proteomic signatures from various human liver cell types: LSEC (Liver Sinusoidal Endothelial Cells), KC (Kupffer Cells), HSC (Hepatic Stellate Cells), and HEP (Hepatocytes). (E-I) Protein profiles of the five identified clusters throughout the differentiation process. In the graphics, D0 indicates day 0, D2 represents day 2, D4 is day 4, D6 is day 6, D8 is day 8, D10 is day 10, and D12 is day 12. (J) Venn Diagram showing that both cell types share a similar proteome profile. (K-M) diHSCs acquired the expression of pathways associated with quiescence and activation, as well as pathways common to stellate cells.*

2. Identification of RORA as a driver of diHSCs differentiation trajectory

The differentiation profile of diHSCs was analyzed using Principal Component Analysis (PCA), which demonstrated that the samples distributed along the differentiation in a time-dependent manner (Figure 13A). The first principal component (PC1) captured the progression of stellate cell commitment, revealing a gradual acquisition of proteins associated with collagen metabolism, ECM organization, and wound healing processes as differentiation advanced. This suggests that the differentiation process involves a systematic gain of ECM remodelling properties, characteristic of HSCs. When primary HSCs are included in this PCA analysis, diHSCs are very similar in terms of the PC1 but are totally contrary in terms of PC2 (Figure 13B).

To further dissect the differentiation progression, Pearson's correlation analysis divided the proteome data into three distinct phases of differentiation (Figure 13C). Phase 1 (days 0 to 2) was marked by the expression of pluripotency-associated proteins (RIF1, POU5F1) and early mesodermal markers (NID2, MFGE8 and CALB1), reflecting the initial commitment away from the pluripotent state (Figure 13D). Phase 2 (days 4 to 6) represented a transitional period where cells began expressing mesenchymal and intermediate differentiation markers (VIM, FN1, KRT18, ALCAM), indicating the onset of mesothelial commitment (Figure 13D). Finally, Phase 3 (days 8 to 12) was characterized by the emergence of a mature population of diHSCs, with a proteome enriched in collagen synthesis and ECM organization proteins (NES, MMP2, MMP14, DES, DCN, and several collagens), hallmarks of fully differentiated hepatic stellate cells (Figure 13D).

The differential expression profiles between Phase 1 and Phase 2 revealed proteins linked to mesenchymal and mesothelial characteristics, such as those involved in desmosome and tight junction formation. This indicates that during the transition from Phase 1 to Phase 2, cells undergo significant structural changes, acquiring traits

necessary for mesenchymal differentiation. In contrast, the transition from Phase 2 to Phase 3 was dominated by the expression of proteins related to collagen production and ECM organization, stressing the final maturation into a stellate cell phenotype. The transition between differentiation phases reveals a progression from a pluripotent state to a more specialized cell type, recapitulating key aspects of the embryonic development such as the differentiation into mesoderm-like cells initially, the acquisition of mesothelial markers in the intermediate phase of differentiation to finally acquire specific mature HSCs markers.

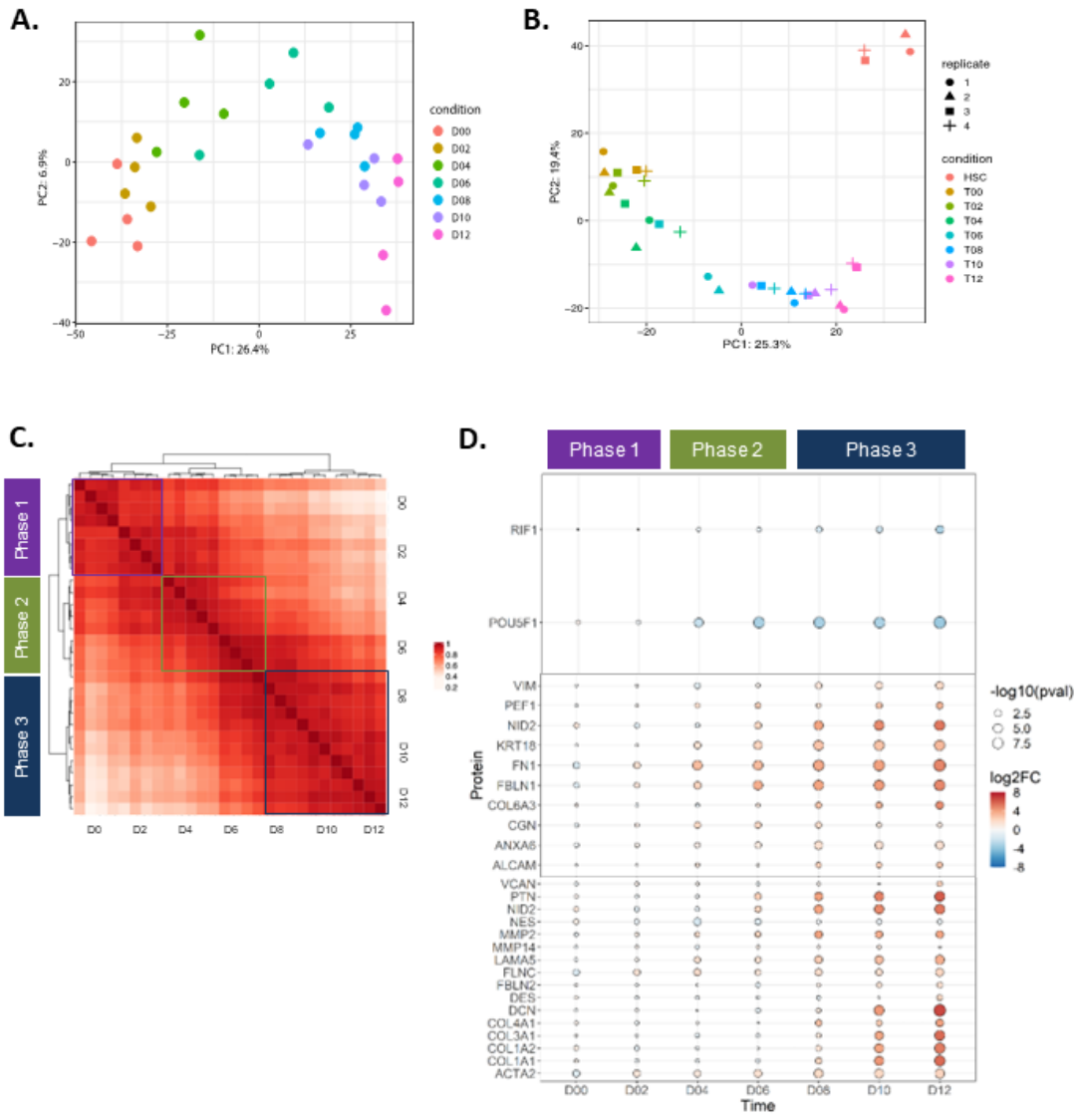

Figure 13. Time-course proteomic characterization of diHSC differentiation*. (A) Principal Component Analysis (PCA) of the proteomic data across the time course reveals a clear time-dependent separation, illustrating distinct differentiation stages. (B) PCA comparing the differentiation protocol to primary HSCs (HSC) highlighting the clustering of replicates (1 to 4) across different time points, emphasizing the consistency, reproducibility of the differentiation process and the differences with HSCs. (C) Pearson correlation analysis identifies three phases of differentiation: Phase 1 (days 0-4), Phase 2 (days 4-8), and Phase 3 (days 8-12). (D) Dot plot depicting the log2 fold change (log2FC) and*

statistical significance (-log 10 pval) of various proteins across Phase 1, Phase 2, and Phase 3, highlighting key markers of differentiation and their dynamic regulation over time.

To elucidate the transcriptional regulation underlying the differentiation transitions, we used the DAVID bioinformatics tool to identify key TFs associated with each phase. By comparing differential protein expression between differentiation phases, our analysis revealed that *RORA* (Retinoic Acid Receptor-Related Orphan Receptor A) was the most significant TF regulating the transition from Phase 1 to Phase 2 (Figure 14A). This finding highlights *RORA*'s critical role in guiding the early stages of mesodermal differentiation, suggesting it is involved in initiating the transition from a pluripotent state to a more specialized mesodermal phenotype.

In contrast, *MEIS1* (Meis Homeobox 1) was identified as a key regulator of the transition from Phase 2 to Phase 3 (Figure 14B). This indicates MEIS1's crucial role in orchestrating the final maturation of diHSCs, suggesting its involvement in the progression from a mesodermal state to the mature, fully differentiated HSC phenotype, emphasizing its function in acquiring ECM remodeling properties of the cells in the differentiation process during the later stages.

Further analysis comparing Phase 3 diHSCs with pHSCs revealed that *RORA* was also involved in regulating the differences between both phenotypes (Figure 14C). Checking transcriptomic data previously generated in the laboratory, (GSE90525 & GSE67664) it revealed that RORA was consistently upregulated in both quiescent and activated pHSCs (Figure 14D). This consistent upregulation suggests that *RORA* may play a central role in establishing and maintaining the HSC phenotype. The persistent presence of RORA in both quiescent and activated states highlights its potential as a master regulator of HSC identity, making it a promising target for further studies aimed at understanding and manipulating HSC behavior and function.

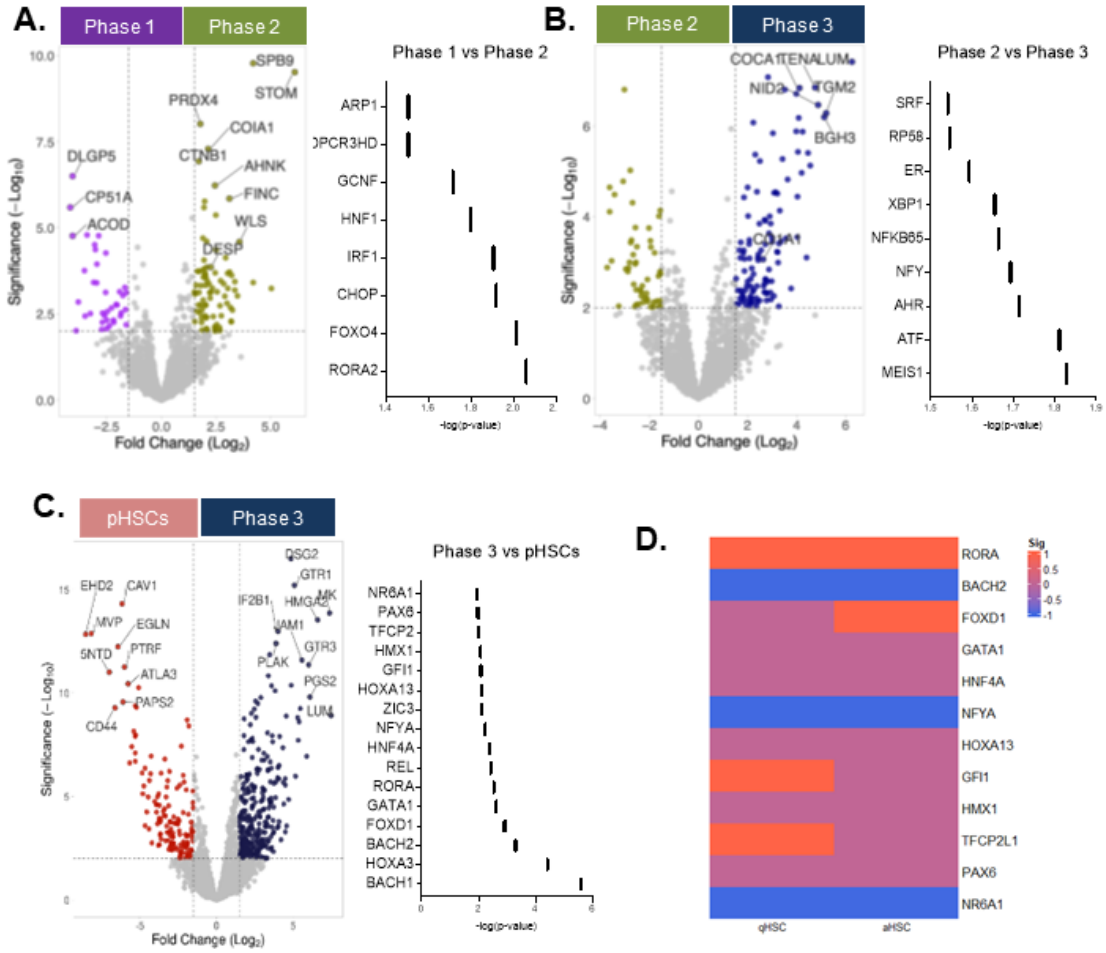

Figure 14. RORA as a potential regulator of hepatic stellate cell differentiation*. (A) A volcano plot comparing Phase 1 to Phase 2 highlights the enrichment of mesothelial markers (e.g., DESP, DSG2, PRDX4, WLS) and identifies in silico predicted transcription factors (TFs) associated with the early differentiation transition. (B) A comparison between Phase 2 and Phase 3 reveals a significant increase in collagen and extracellular matrix (ECM) proteins (e.g., COL5A1, LUM, TNC, TGFBI, NID2), along with TFs predicted to be involved in this progression. (C) A volcano plot contrasting Phase 3 diHSCs with primary HSCs shows differential protein expression, pinpointing TFs that may contribute to the adult stellate cell phenotype. (D) Transcriptomic analysis comparing primary activated and quiescent stellate cells to diHSCs identifies TFs predicted to modulate the adult stellate cell phenotype.*

3. Functional role of RORA along diHSCs differentiation.

RORA is a member of the steroid/thyroid hormone receptor superfamily and is known for its involvement in various aspects of hepatocyte metabolism, including lipid, cholesterol, and glucose metabolism. Beyond these metabolic roles, RORA plays a crucial part in the development and differentiation of multiple tissue types, including cerebellar development, smooth muscle cells differentiation as well as skeletal muscle differentiation (131). However, its specific functions in HSCs have not been fully elucidated.

During the differentiation of two different iPSC lines into diHSCs, KULi003-A and KOLF2J.1 (127), *RORA* gene expression was notably high at day 4 but showed a decline at days 6, 8, and 10, with reduced expression levels observed by day 12 (Figure 15A). To investigate the impact of RORA on diHSCs differentiation, we employed the RORA agonist SR1078 from day 2 until the end of the differentiation process, as depicted in the scheme from Figure 15B. While RORA agonism did not alter the morphology of diHSCs, it significantly increased the expression of mature HSC markers, including *PCDH7*, *LRAT*, *LHX2*, and *RELN* (Figure 15C).

The GSEA analysis of quiescent, stellate and activated profile of pHSCs (130)reveled that RORA activation by means of the synthetic agonist SR1078 promoted the quiescent phenotype profile of the diHSCs (Figure 15D) while preserving their responsiveness to TGF-β, as indicated by the sustained expression of *COL1A1* and *ACTA2*. Additionally, at the protein level, exposure to SR1078 resulted in reduced expression of αSMA and collagen suggesting a modulation of the contractile phenotype of diHSCs (Figure 15E).

Transcriptomic analysis of diHSCs treated with the RORA agonist revealed significant changes in gene expression, highlighting the enrichment of biological processes and markers associated with mesoderm development and mesenchyme differentiation (Figure 15F-H). Conversely, there was a reduction in biological processes related to cell proliferation (Figure 15F). Functional analysis of the transcriptomic data identified enriched Reactome pathways, such as FGF signaling, while pathways related to beta-oxidation, the tricarboxylic acid cycle, and the mitotic cycle were reduced (Figure 15I). Overall, our results indicate that RORA plays a significant role in directing the differentiation of iPSC-derived HSCs and highlight its potential as a regulator of HSC maturation and function of diHSCs.

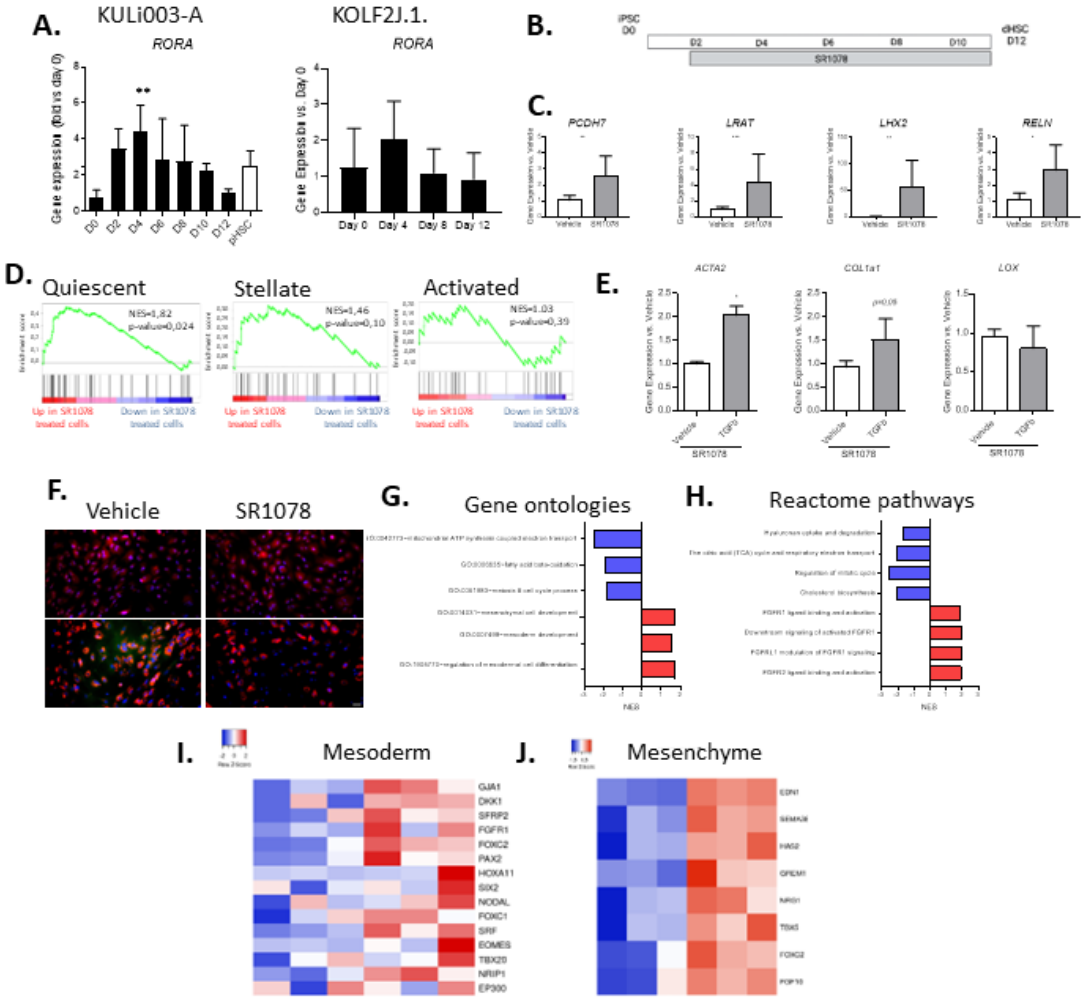

Figure 15. RAR-related orphan receptor A (RORA) as a regulator of diHSC phenotype, enhancing mesoderm commitment and modulating activation state*. (A) RORA gene expression across differentiation stages in two iPSC lines, KULi003-A and KOLF2J.1, compared to primary HSCs (pHSCs). The experiment was conducted with three independent differentiations and three pHSC replicates. (B) Schematic representation of the experimental design for SR1078 treatment. Cells were treated with 0.1 mM of the RORA agonist SR1078 from day 2 onward. (C) Gene expression analysis of stellate cell markers (PCDH7, LRAT, LHX2, and RELN) in SR1078-treated cells versus vehicle-treated controls, n=3 (D) Gene Set Enrichment Analyses (GSEA) of reported gene signatures for quiescent, pan-activated, and activated stellate cells. (E) Gene and protein expression analysis of activated markers (ACTA2, COL1A1, and LOX) in diHSCs treated with SR1078 during differentiation and subsequently exposed to 10 ng/mL TGF-β for 24 hours, n=3. (F) Immunoflourescence of αSMA and COLLAGEN in vehicle and treated cells with RORA agonist SR1078. (G) Gene Ontology (GO) terms upregulated (red) and downregulated (blue) in SR1078-treated cells, n=3. (H) Reactome pathways upregulated (red) and downregulated (blue) in SR1078-treated cells, n=3. (I) Heatmap of mesoderm markers in treated and untreated cells across differentiation stages with SR1078, n=3. (J) Heatmap of mesenchymal markers in treated and untreated cells during differentiation with SR1078, n=3. Data is presented as mean ± SEM, with statistical significance assessed by t-test, **p < 0.01, n=3.*

We then established three clones of RORA +/- iPSCs (Het-1, Het-2 and Het-3) using Cas9 technology to investigate the role of RORA in the differentiation of diHSCs (Figure 16A). All clones exhibited a reduction in RORA protein expression while preserving pluripotency markers (Figure 16B-C) and maintaining a normal karyotype, indicating genome stability in the newly generated cell lines (Figure 16D). However, generating a

homozygous RORA KO clone (Figure 16E-F) was extremely challenging, with a notably low efficiency, as only one clone was obtained out of more than 80 clones tested (RORA$^{-/-}$). During the attempts to differentiate homozygous RORA KO clones, the resulting cells exhibited no expression of characteristic stellate cell markers, such as LHX2, *LRAT* and *RELN* (Figure 16G). This absence of stellate cell markers strongly suggests that RORA is essential for the differentiation of iPSCs into diHSCs. Moreover, the failure to obtain mature stellate cells from these homozygous clones highlights RORA's critical role in guiding the differentiation process and maintaining the stellate cell phenotype. The difficulty in obtaining RORA-null clones suggests that RORA may be critical for cell survival or function, implying that its absence could be detrimental to the differentiation process. For these reasons, the following experiments to determine the role of RORA in diHSCs physiology were performed using the RORA$^{+/-}$ clones and for visualization purposes, the results of only one clone are shown.

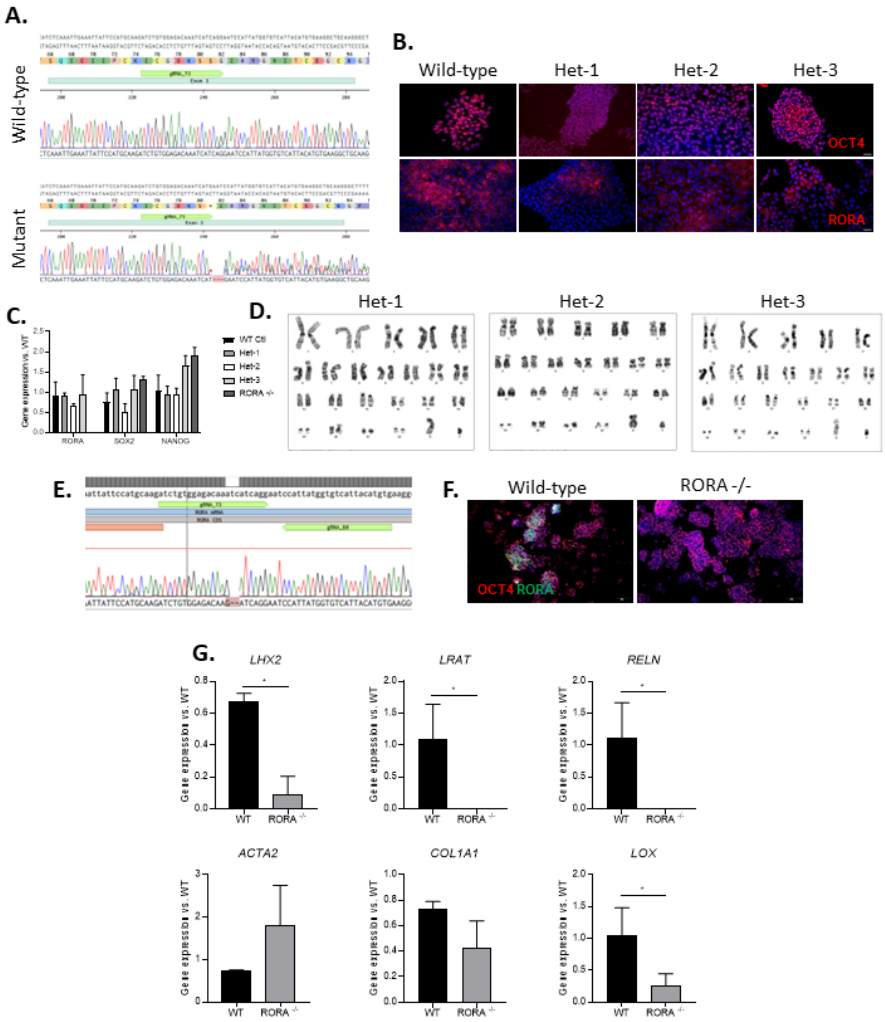

Figure 16. Generation of RORA knockout iPSC lines*. (A) Sanger sequencing confirming heterozygous RORA knockout in iPSCs (iPSC-RORA+/−). (B) Immunofluorescence analysis of the pluripotency marker OCT4 and RORA in three iPSC-RORA+/− clones compared to wild-type (WT) iPSCs. (C) Gene expression analysis of pluripotency markers in three iPSC-RORA+/− clones (Het-1, Het-2 and Het-3) and the full RORA knockout (iPSC-RORA−/−) and WT iPSCs. (D) Karyotype analysis of the three iPSC-RORA+/− (Het-1, Het-2, Het-3) clones. (E) Sanger sequencing confirming full RORA knockout in iPSCs (iPSC-RORA−/−). (F) Immunofluorescence analysis of OCT4 and RORA in a full RORA knockout (iPSC-RORA−/−) clone compared to WT iPSCs. (G) Gene expression analysis of PCDH7, LRAT, RELN, ACTA2, COL1A1, and LOX in three independent differentiations from the iPSC-RORA−/− clone. Scale bars = 100µm. Data are presented as mean ± SEM, n=3.*

During differentiation of the three heterozygous clones, nearly 80% of the cells died by day 4 (Figure 17A). The surviving cells exhibited lower expression of mature HSC markers (*LRAT, LHX2 and RELN*) and an increase in activation genes (*ACTA2*), indicating a compromised differentiation process (Figure 17B). To address cell mortality, we used the RORA agonist SR1078 from day 2 through the end of differentiation in the heterozygous cell lines. The treatment rescued cell viability and partially restored the diHSCs phenotype, as evidenced by the expression of mature HSC markers such as *LRAT*, *LHX2* and *RELN* (Figure 17A-B). Moreover, constitutive RORA$^{+/-}$ iPSC clones exhibited an enhanced activation phenotype upon passage, as evidenced by changes in cell morphology and increased expression of activation markers *ACTA2*, *COL1A1* and *LOX* (Figure 17C-D).

In order to avoid the lethality of RORA at the initial stages of differentiation, we also stablished an inducible (iCas9) system to generate a downregulation of RORA, once mesoderm phase is achieved. As reported previously, the correct induction of the Cas9 is after 72h of doxycycline exposure at 2ug/mL. In order to start expressing Cas9 at the beginning of stage 3 of the differentiation (day 8), once stellate cell phenotype is achieved, we incubated the cells with doxy (doxycycline from day 4. Doxy stimulation was refreshed with every change of media of the differentiation. By day 12, differentiated cells exhibited a robust increase in CAS9 expression, which was accompanied by a significant upregulation of key stellate cell activation markers, specifically *ACTA2* and *COL1A1* (Figure 17E). Conversely, we observed a marked downregulation of *LRAT*, *RELN*, and *LHX2* (Figure 17E), indicating a shift away from quiescent HSCs characteristics, when compared to the cells not exposed to Doxy.

The results were further validated by inhibiting RORA activity from day 2 until the end of the differentiation of wild-type iPSCs using SR1001, a chemical antagonist of RORA. Cells treated with SR1001 displayed a notable shift in morphology, adopting a spindle-

like shape that is characteristic of activated, rather than quiescent HSCs (Figure 17F). At the functional level, SR1001-treated cells showed a significant increase in ECM production by the end of the differentiation process, as shown by a Sirius red staining *in vitro*, which is typically associated with a more fibrotic and activated state of stellate cells (Figure 17F).

In terms of gene expression, SR1001-treated cells, similarly to the gene edited cell lines, exhibited a marked reduction in the expression of key HSC markers, such as *RELN* and *LHX2* (Figure 17G). Their downregulation in the presence of the RORA antagonist suggests a disruption in the differentiation process. Conversely, the SR1001-treated cells showed increased expression of *ACTA2* and *COL1A1*, both of which are markers of an activated stellate cell phenotype (Figure 17G). Additionally, there was a corresponding increase in collagen deposition, further indicating that RORA inhibition drives the cells towards a more activated, fibrotic state rather than maintaining or achieving quiescence.

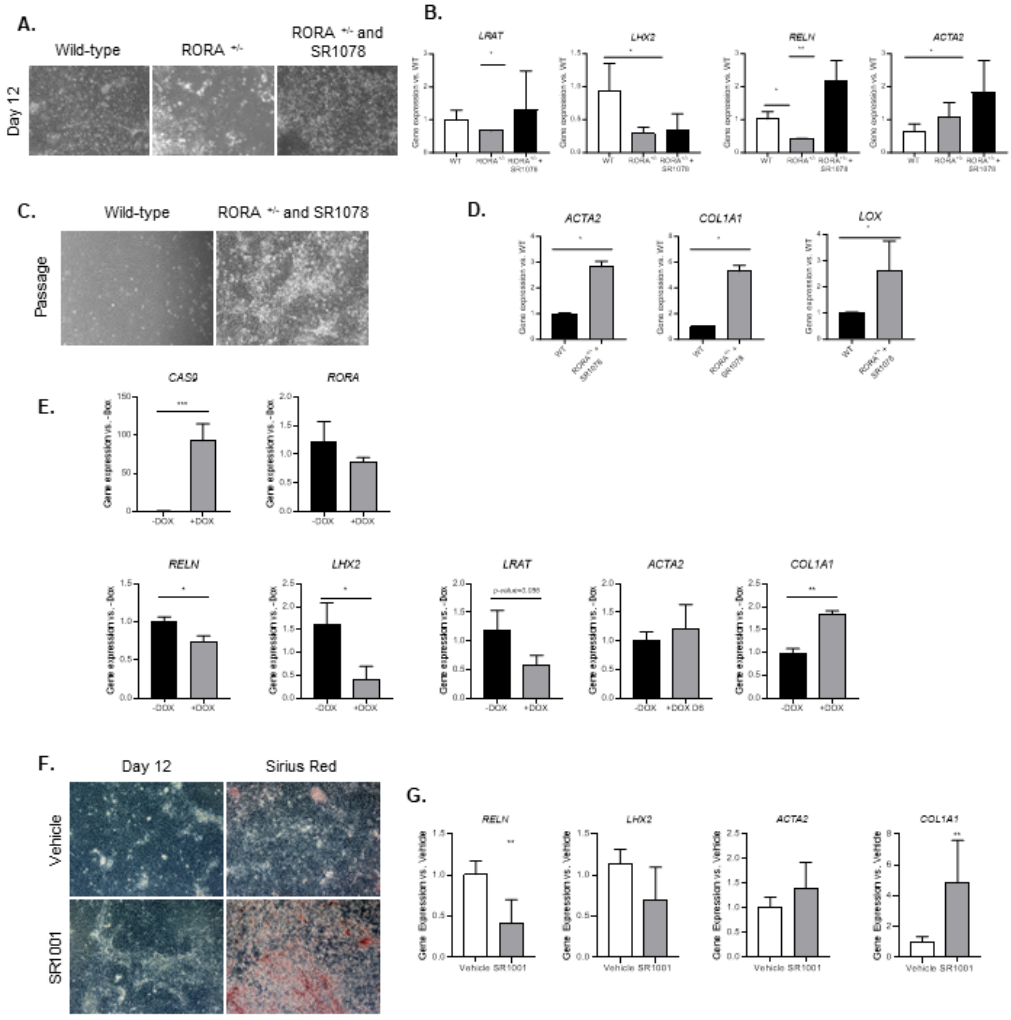

Figure 17. RAR-related orphan receptor A (RORA) as a regulator of diHSC phenotype, enhancing mesoderm commitment and modulating activation state*. (A) Representative microscopy images of diHSCs at day 12 from wild-type (WT), iPSC-RORA+/−, and iPSC-RORA+/− cells treated with the RORA agonist (rescue condition). Scale bar: 100 µm. (B) Gene expression analysis of stellate cell markers (LRAT, LHX2, RELN, and ACTA2) in WT, iPSC-RORA+/−, and iPSC-RORA+/− cells treated with the RORA agonist at day 12. (C) Representative microscopy images of passaged (P1) diHSCs from WT and iPSC-RORA+/− cells treated with SR1078. Scale bar: 100 µm. (D) Gene expression analysis of activated stellate cell markers (ACTA2, COL1A1, and LOX) in WT and iPSC-RORA+/− cells after SR1078 treatment. (E) Gene expression of activation markers (ACTA2 and COL1A1) and quiescent markers in diHSCs differentiated from iPSCs-iCas9, Doxycycline treatment induced from day 4 of the differentiation. Doxy= Doxycycline. (F) Representative Sirius Red staining images of cell cultures at day 12, comparing untreated (Vehicle) and SR1001-treated cells across differentiation. (G) Gene expression analysis of quiescent markers (LHX2, RELN) and activation markers (ACTA2, COL1A1) following SR1001 treatment. Scale bars = 100µm. Data is presented as mean ± SEM with statistical significance assessed by t-test, n=3.*

These findings support the role of RORA as a transcriptional regulator in the differentiation of iPSCs into HSCs. Specifically, RORA appears to be essential for mesoderm and mesenchymal specification, as well as for the acquisition of a quiescent stellate cell phenotype. The inability to obtain stellate cells from RORA homozygous knockout lines underscores the crucial role of RORA in the proper differentiation and maturation of HSCs. Together, these results suggest that RORA not only guides early mesodermal differentiation but also ensures the proper transition of these cells into a quiescent HSC state, maintaining the balance between activation and quiescence that is crucial for liver homeostasis.

4. Functional role of RORA in diHSCs activation.

To further investigate the role of RORA in diHSCs activation, we employed two distinct *in vitro* models: one based on mechanical activation through cell passage and the other on cytokine-driven activation using TGF-β. We have observed distinct molecular pathways activated in diHSCs depending on whether they were subjected to mechanical activation via passage or cytokine-based activation using TGF-β.

During mechanical passaging, diHSCs undergo several significant changes, including increased contractility and ECM remodeling, heightened stress responses, and the activation of signaling pathways related to proliferation, migration, and oxidative stress defense. Notably, there is enhanced regulation of NF-kappaB signaling and reorganization of the cytoskeleton, reflecting the cells' adaptive and stress-responsive nature during passaging (Figure 18A). In contrast, HSCs activated by TGF-β show enrichment in GO terms related to carbohydrate and glycolytic processes, indicating a metabolic shift to support increased energy demands. Additionally, the upregulation of TGF-β signaling and apoptotic regulation pathways suggests that TGF-β treatment drives

a pro-fibrotic and activated state, potentially affecting cellular survival and immune responses (Figure 18B). These models allowed us to explore both major pathways of HSC activation and assess the impact of RORA modulation in these contexts.

In the passage-based activation model, the treatment with the RORA agonist SR1078 effectively prevented this activation, as evidenced by a significant decrease in the expression of classic activation markers *ACTA2* and *COL1A1* while enhancing the expression of markers associated with the quiescent HSC phenotype, including *LRAT* and *LHX2* (Figure 18C)**.** Transcriptomic analysis of treated cells revealed a reduction in GO terms related to de novo lipogenesis and mitochondrial beta-oxidation of fatty acids (Figure 18D). This suggests that the metabolic state of diHSCs is significantly remodeled during activation, potentially linking RORA's role in metabolism with its ability to modulate HSC activation.

Conversely, cells treated with the RORA antagonist SR1001 after passage exhibited an increased activation profile, characterized by elevated expression of activation markers *ACTA2*, *COL1A1* and *LOX* (Figure 18E). This indicates that inhibiting RORA promotes HSC activation, further emphasizing RORA's role in maintaining quiescence.

The TGF-β-based activation model involved treating diHSCs with TGF-β for either 24 hours or 7 days, mimicking cytokine-induced activation. In this model, SR1078 was administered during the last 24 hours of TGF-β treatment. Remarkably, SR1078 reduced both short-term and long-term TGF-β-induced activation. This was demonstrated by a significant decrease in the expression of *ACTA2*, *COL1A1*, and *LOX* (Figure 18G). Moreover, aSMA staining decreased as well after the treatment with SR1078 for the last 24 hours (Figure 18H).

To extend these findings to a more physiologically relevant context, we used 3D liver spheroids composed of HepG2 cells, a hepatocyte well-stablished cell line, and diHSCs. In this complex model, SR1078 treatment after TGFβ stimuli, similarly reduced the expression of *ACTA2*, *COL1A1* and *LOX*, (Figure 18I) at 24h and 7 days stimuli (Figure 18J), further confirming RORA's role in inhibiting fibrogenesis within a three-dimensional liver microenvironment.

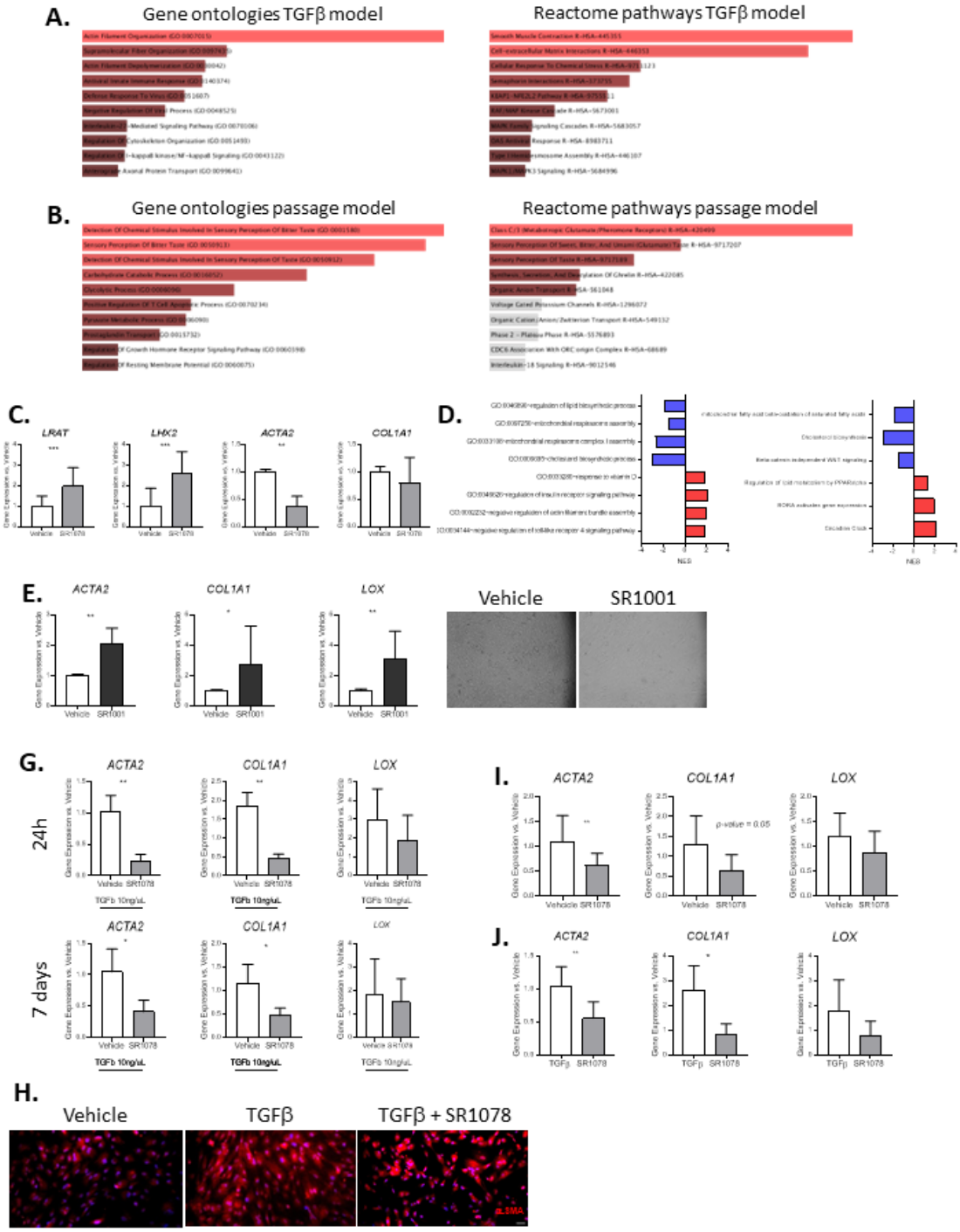

Figure 18. Role of RORA in Regulating Hepatic Stellate Cell Activation. *(A) Gene Ontology (GO) and Reactome pathways enriched in the mechanical activation model of passaged diHSCs. (B) GO and Reactome pathways upregulated in diHSCs activated by TGF-β stimulation (10 ng/mL) for 24 hours. (C) Gene expression of quiescent markers (LRAT, LHX2) and activated markers (ACTA2, COL1A1) in diHSCs treated with the RORA agonist during passaging. (D) GO terms upregulated (red) and downregulated (blue) in diHSCs treated with the RORA agonist during passaging. (E) Reactome pathways upregulated (red) and downregulated (blue) in diHSCs treated with the RORA agonist during passaging. (F) Representative images of passaged diHSCs treated with the RORA agonist SR1001 for 24 hours. (G) Gene expression of activation markers (COL1A1, ACTA2, LOX) in diHSCs treated with the RORA antagonist SR1001 during passaging for 24 hours. Significant differences are indicated as *p < 0.05. (H) Gene expression of activated markers (ACTA2, COL1A1, LOX) in liver spheroids after treatment with the RORA agonist SR1078 (3 mM) for 24 hours. (I) Gene expression of activated markers (ACTA2, COL1A1, LOX) in liver spheroids after TGF-β stimulation (10*

ng/mL) for 24 hours, followed by SR1078 (3 mM) treatment for an additional 24 hours. Data is presented as mean ± SEM with statistical significance assessed by t-test, n=3.

Overall, these results suggest that RORA plays a critical role in the deactivation of diHSCs and in maintaining the quiescent phenotype of these cells**.** The ability of RORA to modulate both mechanical and cytokine-driven activation pathways, potentially through the inhibition of metabolic adaptations required for diHSC activation, underscores its importance as a key regulator of HSC physiology and a potential target for therapeutic intervention in liver fibrosis.

5. Regulation of cell metabolism mediated by RORA in diHSCs.

To further understand RORA's role in metabolic regulation along the diHSC differentiation trajectory, we conducted a detailed analysis of iPSC-RORA+/- cells during various stages of differentiation and activation. At day 4 of differentiation, iPSC-RORA+/- cells demonstrated a notable increase in mitochondrial respiration, indicated by higher OXPHOS activity. This was accompanied by an increase in ATP production from glycolysis, suggesting that these cells were relying on both glycolytic and mitochondrial pathways to meet their energy demands (Figure 19A-C). Additionally, intracellular glucose levels were elevated (Figure 19D), pointing to increased glucose uptake and utilization, which is characteristic of a metabolic profile that resembles undifferentiated or less committed cells.

Further supporting this result, gene expression of *ALDOB* and *G6SP* revealed higher levels of glycolytic genes, indicating a robust glycolytic flux (Figure 19E). At the same time, the expression of *ACACA*, a key enzyme involved in fatty acid synthesis, was decreased, suggesting that lipid biosynthesis pathways were downregulated in these cells (Figure 19E). Interestingly, the gene and protein expression of mesodermal marker *EOMES* and mesenchymal marker *VIM* was also reduced in iPSC-RORA+/- cells at day 4 of differentiation compared to wild-type iPSCs (Figure 19F), indicating a delayed or impaired transition to the mesodermal lineage. This reduction in commitment to a mesodermal phenotype was further corroborated by experiments showing that iPSC-RORA+/- cells exhibited diminished differentiation potential when subjected to undirected differentiation conditions, showing a reduction in the double staining of GATA4 and αSMA (Figure 19G). To explore whether RORA agonism could modulate

these metabolic characteristics, we treated iPSC-RORA+/- cells with the RORA agonist SR1078 from day 2 of differentiation onward. Remarkably, treatment with SR1078 resulted in a significant metabolic shift of the cells at day 4. Intracellular glucose levels and glycolysis-dependent ATP production were markedly reduced, indicating a suppression of glycolytic activity (Figure 19A). Furthermore, the expression of glycolytic genes (*ALDOB* and *GS6P*) and glucose consumption from the media were both decreased, suggesting a metabolic reprogramming that favored a less glycolytic and more quiescent metabolic state (Figure 19B-E). SR1078 treatment also led to a reduction in mitochondrial respiration and OXPHOS-dependent ATP production, highlighting its role in downregulating both mitochondrial and glycolytic pathways (Figure 19B).

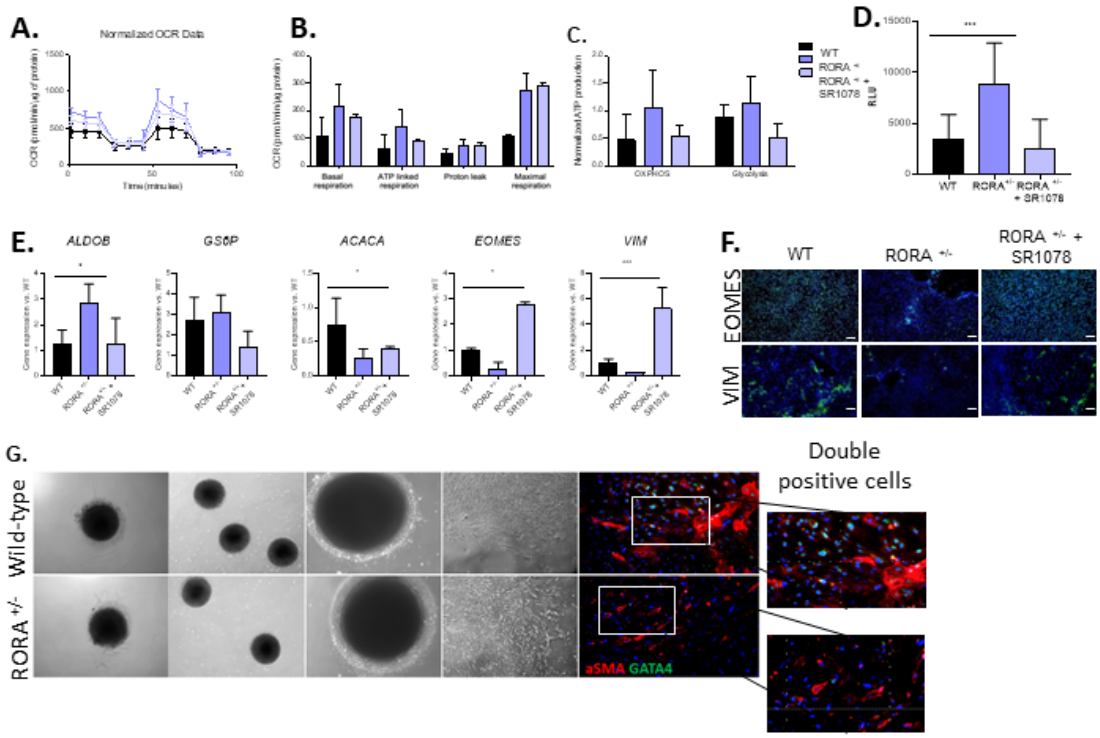

Figure 19. RORA Regulation of Metabolic Pathways During Mesoderm Differentiation*. (A) Oxygen consumption rate (OCR) analysis on day 4 of wild-type (WT) iPSCs and iPSC RORA+/- cells, comparing treated and untreated conditions from day 2. (B) OCR parameters for day 4 WT and RORA+/- iPSCs, highlighting differences between treated and untreated conditions from day 2. (C) Normalized ATP production from oxidative phosphorylation (OXPHOS) and glycolysis in day 4 WT and RORA+/- iPSCs, comparing treated and untreated conditions from day 2. (D) Glucose consumption measurement at day 4 of WT and RORA+/- iPSC differentiations, comparing treated and untreated conditions from day 2. (E) Gene expression analysis of key glycolytic (ALDOB, GS6P), lipid synthesis (ACACA), and mesodermal/mesenchymal markers (EOMES, VIM) in day 4 WT and RORA+/- iPSCs. (F) Immunofluorescence staining for mesodermal (EOMES) and mesenchymal (VIM) markers on day 4 of differentiated cells from WT, RORA+/- and RORA+/- treated with the RORA agonist from day 2. Scale bars represent 100 µm. (G) Immunofluorescence analysis of undirected mesodermal differentiation in WT and RORA+/- cells, showing a reduced number of double-positive cells for mesodermal markers (αSMA and GATA4) in the RORA knockout (KO) cell line. Scale bars represent 100 µm. Data is presented as mean ± SEM with statistical significance assessed by t-test, n=3.*

Upon activation of diHSCs by passage, the treatment with the RORA agonist reduced the expression of genes associated with glycolysis and lipid synthesis, which were otherwise elevated during diHSC activation, as shown by transcriptomic analysis (Figure 20A). Furthermore, the metabolic profile of activated cells, characterized by elevated OXPHOS and glycolysis, was significantly reduced following treatment with the RORA agonist (Figure 20B-D). Intracellular levels of glucose were also reduced (Figure 20E). Moreover, in the cytokine mediated activation model, the reduction of OXPHOS and glycoslysis (Figure 20F-H) as well as the intracellular glucose was also observed (Figure 20I). The gene expression of glycolytic genes (*ALDOB*, *GS6P* and *ACACA)* was also reduced (Figure 20J). These changes suggest that RORA not only modulates energy metabolism but also impacts lipid biosynthetic pathways, reinforcing its role as a metabolic regulator in diHSCs.

To further validate RORA's role in diHSC activation and quiescence and the impact on lipid metabolism, we employed a lipidomic approach by treating differentiated and passaged (mechanically activated) diHSCs with SR1078 for 24 hours. Lipidomic analysis, conducted on samples from four independent replicates, revealed a significant shift in the lipid profile of treated cells. Specifically, the data indicated a reversion toward a quiescent-like lipidomic phenotype upon treatment, aligning with the lipidomic signatures previously reported by Milenaar et al. (J Biol Chem, 2023) (132). According to Milenaar et al., early HSC activation is marked by a decrease in phosphatidylcholines (PCs) and sphingomyelins with saturated or monounsaturated fatty acids, while later stages of activation show an increase in PCs and dihexosylceramide (Hex2Cer) (132). In our study, SR1078 treatment led to a downregulation of PCs and triglycerides (TG), consistent with a move away from an activated state (Figure 20K). Although we did not observe a significant reduction in HexCer levels, likely due to the short-term nature of the activation period in our experiments, the overall lipidomic shift still supported the idea that RORA agonism promotes a quiescent-like phenotype. In treated differentiated cells, lipidomic changes were particularly evident in PC2, driven by alterations in PCs and sphingomyelins, which shifted toward less unsaturated and shorter fatty acid chains (Figure 20L-M). This suggests that SR1078 treatment also impacts lipid metabolism,

reinforcing the quiescent state of diHSCs and reducing the lipidomic hallmarks of activation.

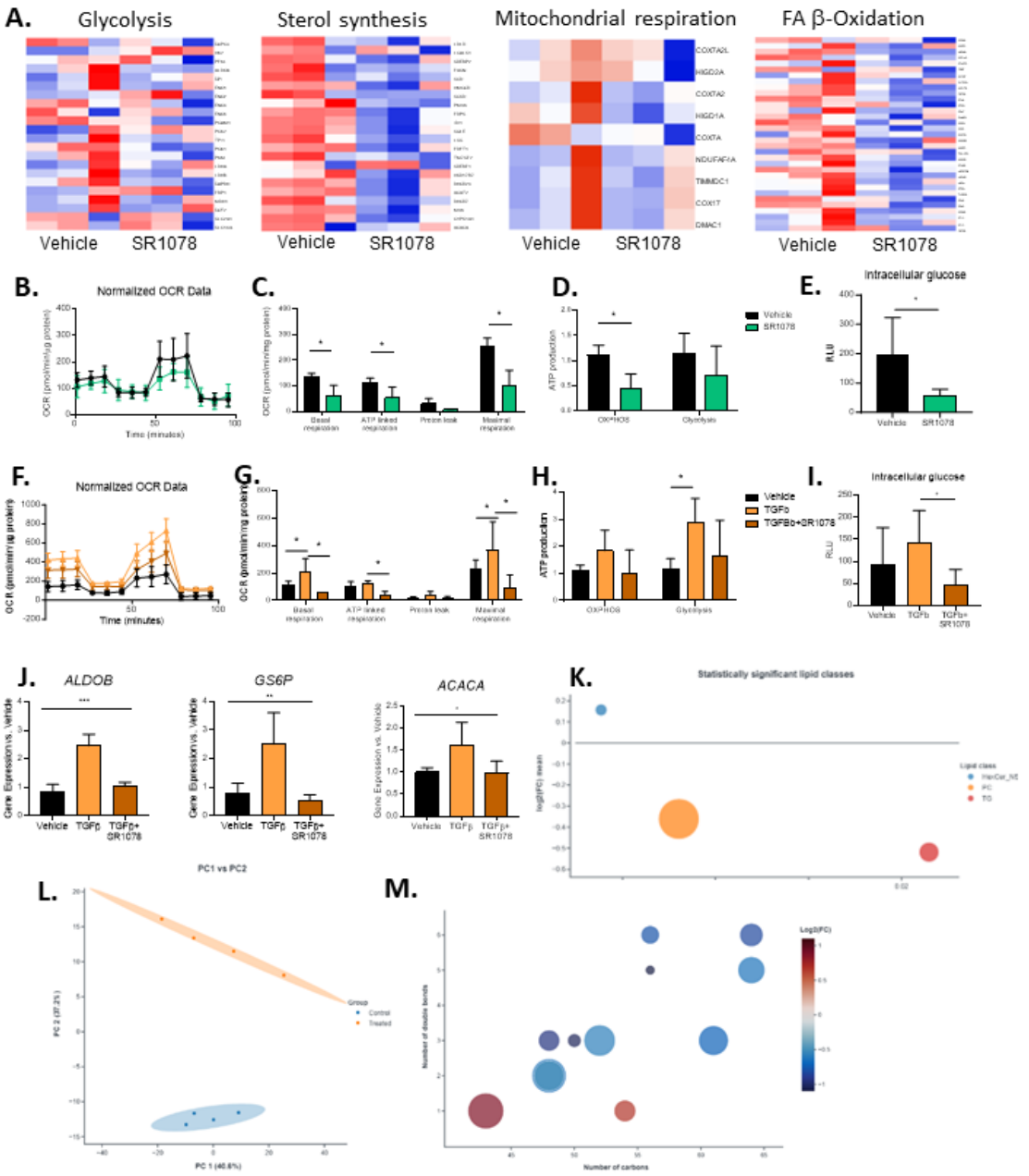

Figure 20. RORA Regulation of Metabolic Pathways During diHSC Activation. *(A) Heatmap showing changes in glycolytic activity, sterol synthesis, mitochondrial respiration, and fatty acid beta-oxidation in passaged diHSCs treated with or without the RORA agonist for 24 hours. (B) Oxygen consumption rate (OCR) measurements of passaged diHSCs treated with the RORA agonist for 24 hours. (C) OCR parameters of passaged diHSCs treated with the RORA agonist for 24 hours. (D) Normalized ATP production from oxidative phosphorylation (OXPHOS) and glycolysis in passaged diHSCs treated with or without the RORA agonist for 24 hours. (E) Glucose consumption in passaged diHSCs treated with or without the RORA agonist for 24 hours. (F) OCR of passaged diHSCs treated with TGF-β (10 ng/mL) for 24 hours, followed by rescue treatment with the RORA agonist for an additional 24 hours. (G) OCR parameters of passaged diHSCs treated with TGF-β (10 ng/mL) for 24 hours and rescued with the RORA agonist for an additional 24 hours. (H) Normalized ATP production from OXPHOS and glycolysis in the TGF-β activation model, rescued with the RORA agonist for 24 hours. (I) Intracellular glucose levels in the TGF-β activation model, rescued with the RORA agonist for 24 hours. (J) Gene expression analysis of key glycolytic and lipid synthesis markers (ALDOB, GS6P, ACACA) in the TGF-β activation model, rescued with the RORA agonist for 24 hours. Significant differences are indicated as *p < 0.05.*

(K) Principal Component Analysis (PCA) of the lipidomic profile of diHSCs treated or untreated with the RORA agonist SR1078 for 24 hours. (L) Lipid expression analysis showing reduced levels of phosphatidylcholines (PC) and triglycerides (TAG) in cells treated with SR1078 RORA agonist for 24 hours, with no significant change in dihexosylceramide (Hex2Cer). (M) Lipidomic profile of cells treated with SR1078 RORA agonist for 24 hours, indicating a shift towards less unsaturated and shorter fatty acid chains. Data is presented as mean ± SEM with statistical significance assessed by t-test or ANOVA 1-way, n=3.

Collectively, these results demonstrate that RORA acts as a crucial regulator of both energetic and lipidomic pathways in diHSCs. By modulating glucose metabolism and lipid synthesis, RORA plays a pivotal role in the differentiation trajectory of diHSCs and their transition from mesoderm phenotype as well as in the transition between quiescent to activated state, demonstrating the importance of RORA in maintaining the physiological balance required for proper HSC function and provides new insights into the metabolic and lipidomic mechanisms governing HSC quiescence and activation.

6. RORA is implicated in fibrogenic response *in vivo* and its agonist mitigates multiorgan fibrosis models

To validate our *in vitro* findings, we assessed the role of RORA in *in vivo* HSC activation and liver fibrosis models. First, we evaluated the expression of Rora in various animal models that cause liver fibrosis including the 3,5-Diethoxycarbonyl-1,4-Dihydrocollidine Diet (DDC), Bile duct ligation (BDL), choline-deficient, ethionine-supplemented (CDE) and carbon tetrachloride (CCl_4). All models shown a reduction in *Rora* expression in the presence of fibrosis as depicted by Sirius Red staining (Figure 21A).

Staggerer (sg/sg) mice is a spontaneous RORA-deficient mice. In them we observed no difference in baseline fibrosis levels assessed by hydroxyproline content (Figure 21B). However, we observed a slight increase in activation markers, such as *Acta2* and *Timp1*, in the RORA-deficient mice (Figure 21C). To further investigate the fibrogenic response, we employed a CCl_4-induced liver fibrosis model over 4 weeks (Figure 21D). Livers from sg/sg mice exhibited increased fibrotic content and enhanced αSMA staining compared to WT controls (Figure 21E). Additionally, sg/sg mice showed more significant tissue damage in pericentral hepatocytes and elevated levels of liver enzymes including ALT, AST, AP and LDH (Figure 21F). Gene expression analysis revealed significantly higher levels of fibrogenic markers such as *Acta2*, *Col1a1*, *Col1a2*, *Timp1*, and *Fn1* (Figure 20G) in the mutant group, with increased neutrophil content (Mpo) but no notable differences in macrophage (F4/80) or lymphocyte (Cd3b) populations (Figure 21E).

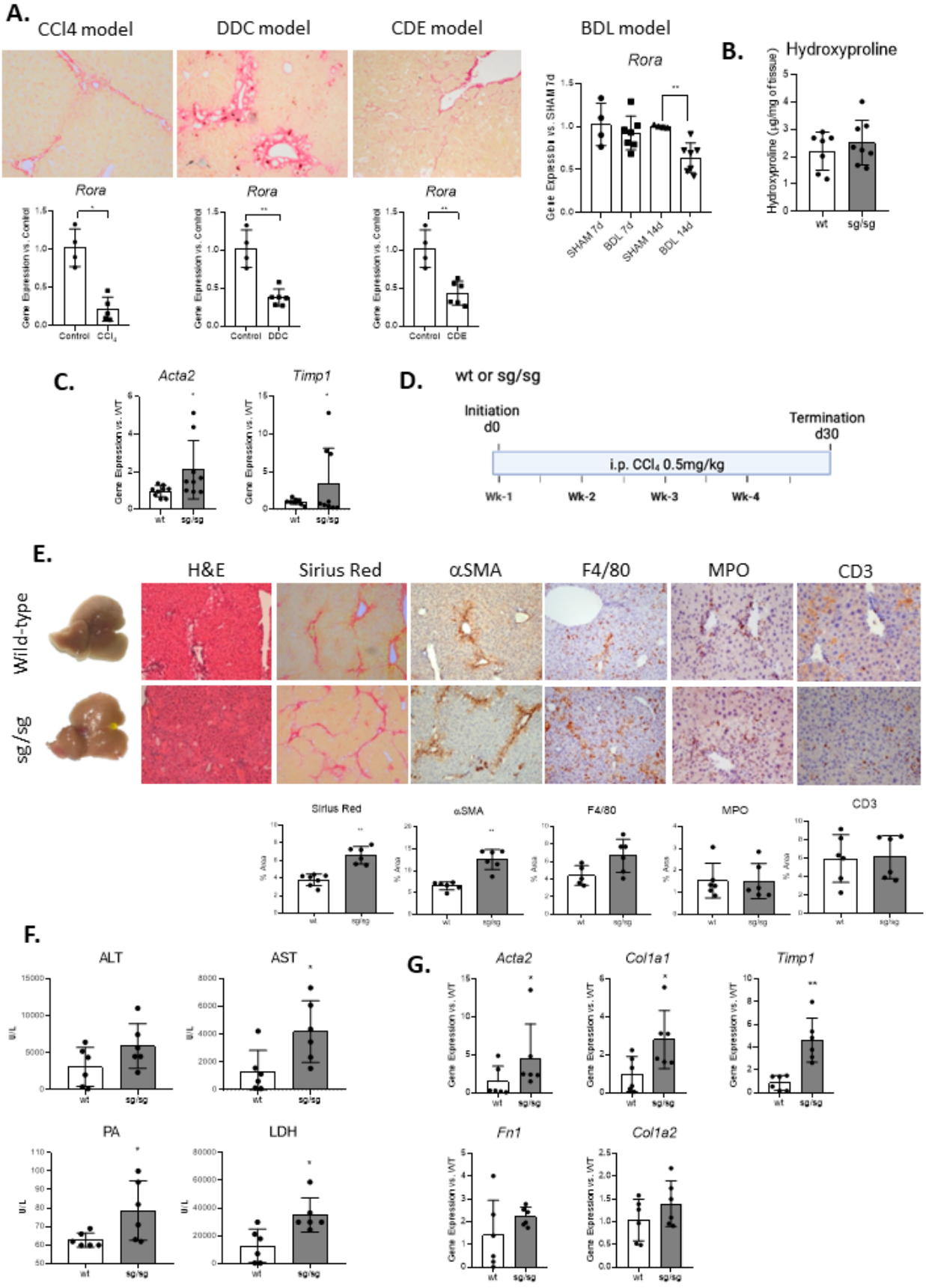

Figure 21. RORA regulates HSC activation and contributes to liver fibrosis development. *(A) Comparative analysis of liver fibrosis models: DDC, BDL, CDE, and CCl4. (3,5-Diethoxycarbonyl-1,4-Dihydrocollidine= DDC, Bile duct ligationB*

=BDL, choline-deficient, ethionine-supplemented =CDE and carbon tetrachloride =CCl4) The CCl4 model was selected for subsequent experiments. (B) Hydroxyproline content in basal livers of sg/sg (Staggerer; n=8) and WT (Wildtype; n=7) mice. (C) Basal liver gene expression levels of Acta2 and Timp1 in sg/sg (n=8) and WT mice(n=7). (D) Schematic overview of the CCl4-induced liver fibrosis model in sg/sg mice. (E) Representative liver images after 4 weeks of CCl4 treatment in sg/sg and WT mice, including H&E staining, Sirius Red staining, αSMA, F4/80, Mpo and CD3 immunohistochemistry and quantification. Scale bars = 100 µm. (F) Serum levels of ALT, AST, LDH, and AP in sg/sg and WT mice following 4 weeks of CCl4 treatment; n=6. (G) Gene expression analysis of fibrogenic and HSC activation markers (Acta2, Col1a1, Timp1, Fn1, and Col1a2) in 7 sg/sg and 7 WT mice after CCl4 treatment. Data is presented as mean ± SEM with statistical significance assessed by t-test, n=6.

In vivo KO studies using LRAT Cre mice, which specifically targeted RORA in HSCs (133) revealed a reduction in total *Rora* gene expression in the liver, accompanied by a trend towards an increased fibrogenic response in heterozygous KO mice as depicted by an increase hydroxyproline content (Figure 22A). While no differences were observed in the liver-to-body weight ratio (Figure 22B), elevated expression levels of *Acta2*, *Col1a1*, *Fn1*, and *Mmp2* were detected, along with a reduction in *Lhx2* as well as in *Rora* expression (Figure 22C). Additionally, there was an increase in collagen deposition marked by an increased Sirirus Red staining and αSMA levels, though no significant changes were noted in parenchymal cell proliferation (Mki67) or immune infiltration (F4/80 and Mpo) (Figure 22D). These findings align with *in vitro* results, further supporting RORA's involvement in fibrogenic responses.

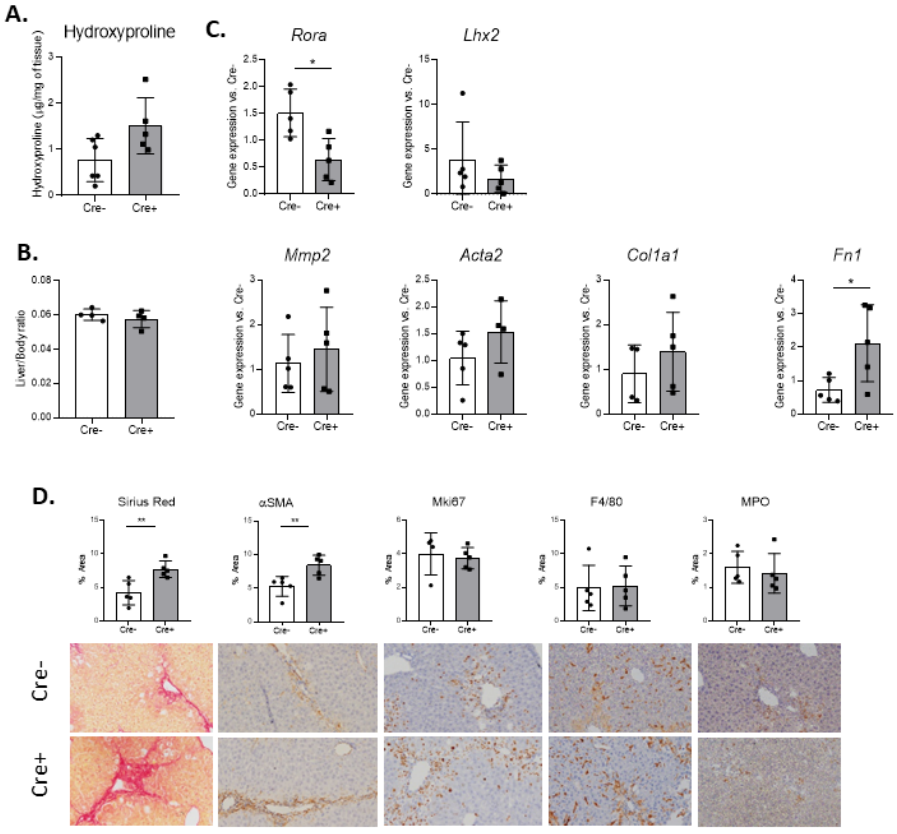

Figure 22. RORA deletion in stellate cells enhances fibrogenic responses in vivo. *(A) Liver-to-body weight ratios remained unchanged between wildtype and heterozygous KO mice. (C) Rora gene expression in the heterozygous KO (knockout) Lrat-Cre. (D) Gene expression analysis revealed elevated levels of fibrogenic markers (Acta2, Col1a1, Fn1, and Mmp2) and decreased expression of Lhx2 in 5 heterozygous KO Cre+ mice and 5 Cre negative mice. Significant differences are indicated by *p < 0.05. (D) Histological assessment showed increased collagen deposition by Sirirus Red and αSMA levels in heterozygous KO livers, with no significant differences in parenchymal cell proliferation, as depicted by Mki67 and immune response assessed by F4/80 (macrophages) and Mpo (neutrophils). Scale bars = 100 µm. Data is presented as mean ± SEM with statistical significance assessed by t-test, n=3.*

To evaluate the translational relevance of these findings, we established three *in vivo* fibrogenic models treated with the RORA agonist SR1078. In CCl4-treated mice (Figure 22A), administration of SR1078 led to increased *Rora* gene expression and reduced tissue damage, collagen deposition, and αSMA staining (Figure 23B). Additionally, there was a decrease in gene expression of fibrogenic and HSC activation markers, including *Acta2, Col1a1*, *Timp1*, *Fn1, Col1a2, Pparg, Mmp2, Mmp9, Mmp12, and Timp1* (Figure 23C). Immunohistochemical analysis showed a non-significant reduction in inflammatory cell populations (neutrophils – Mpo, macrophages – F4/80 and lymphocytes – Cd3b) with SR1078 treatment (Figure 23D).

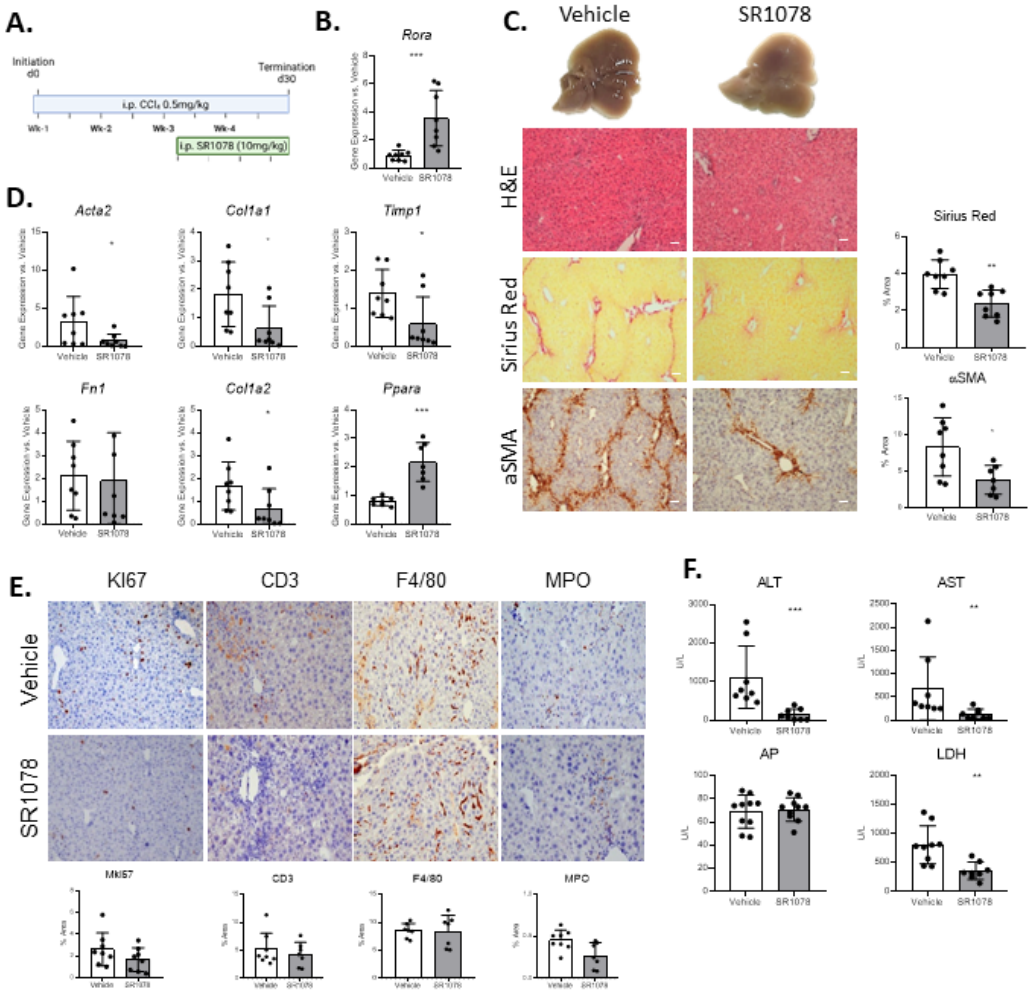

Figure 23. RORA agonist SR1078 attenuates liver fibrosis in a CCl4-induced model. *(A) Schematic representation of the experimental design for CCl4-induced liver fibrosis followed by SR1078 treatment. (B) Gene expression of Rora in the CCl4 model comparing untreated (vehicle) and treated with RORA agonist (SR1078); n=14. (C) Representative liver images following CCl4 treatment with or without SR1078, including H&E staining, Sirius Red staining, and αSMA immunohistochemistry in vehicle (untreated) and SR1078-treated groups. Scale bars = 200 µm. (D) Gene expression analysis of fibrogenic and HSC activation markers (Acta2, Col1a1, Col1a2, Timp1, and Fn1) in 7 vehicle-treated and 7 SR1078-treated mice. Significant differences are indicated by *p < 0.05 after t-test; n=14. (E) Immunofluorescence analysis of macrophages (F4/80), neutrophils (MPO), lymphocytes (CD3), and proliferating cells (Ki67) in the CCl4-induced fibrosis model after 2 weeks of SR1078 treatment. (F) Serum levels of ALT, AST, LDH, and AP in sg/sg and WT mice following 4 weeks of CCl4 treatment; n=6. Data is presented as mean ± SEM with statistical significance assessed by t-test.*

In extrahepatic wound healing response models, we tested the RORA agonist in an isoproterenol-induced cardiac hypertrophy model (ISO) as depicted in Figure 24A. This model showed increased cardiac fibrosis and a reduction in cardiac *Rora* expression (Figure 24B). Treatment with SR1078 promoted *Rora* gene expression, reduced cardiac fibrogenic gene expression of *Col3a1* and *Acta2*, and diminished extracellular matrix (ECM) deposition as assessed by Masson's trichrome and Sirius Red (Figure 24B-D). However, echocardiography revealed no significant differences in cardiac structure or function between the treated and control groups (Table 7). In the UUO model, a kidney fibrogenic model (Figure 24E), the RORA agonist-treated group demonstrated reduced hydroxyproline content (Figure 24F), indicating decreased collagen deposition, though αSMA expression was only minimally affected (Figure 24G). Gene expression analysis revealed a non-significant reduction in *Acta2* and *Col1a1*, accompanied by increased *Rora* expression (Figure 24H). These results suggest that enhancing RORA activity could be a promising strategy for mitigating multiorgan fibrogenesis.

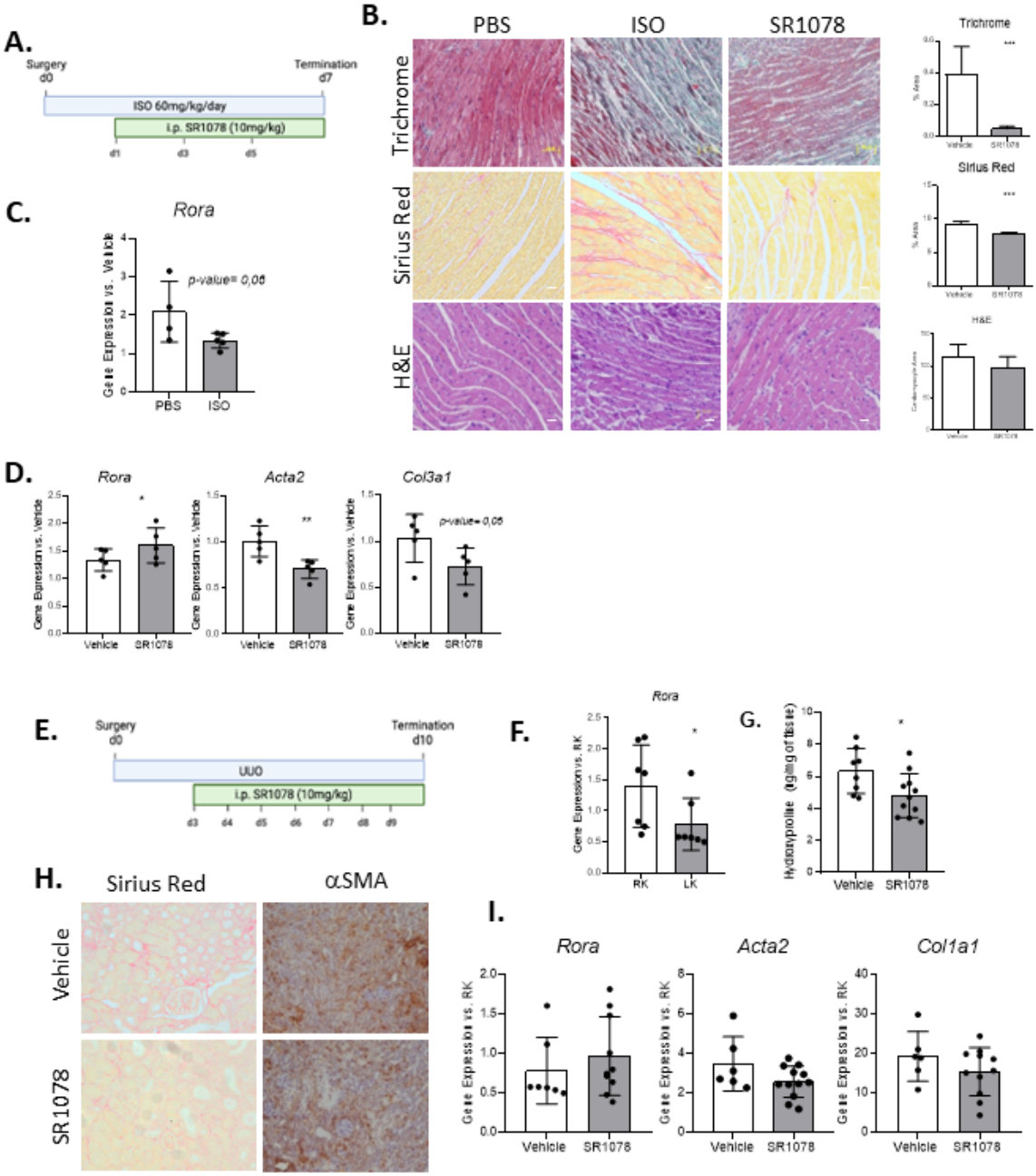

Figure 24. RORA agonist reduces fibrosis in multi-organ injury models. *(A) Schematic representation of the experimental design for the isoproterenol (ISO)-induced cardiac injury model. (B) Representative heart images from vehicle-treated, ISO-treated, and ISO + RORA agonist-treated groups, showing Masson's trichrome, Sirius Red, and H&E staining. Scale bars = 100 µm. (C) Rora gene expression in the hearts of vehicle and ISO-treated groups. (D) Gene expression analysis of Rora, fibrogenic markers (Acta2 and Col3a1), and the hypertrophy marker Acta1 in ISO-treated and ISO + RORA agonist-treated hearts. (E) Schematic representation of the unilateral ureteral obstruction (UUO) model. (F) Rora gene expression in the damaged kidney (left kidney, LK) compared to the control kidney (right kidney, RK) in the UUO model. (G) Representative images of Sirius Red and αSMA staining in left kidneys from vehicle-treated and SR1078-treated groups. (H) Gene expression analysis of Rora, Acta2, and Col1a1 in the left kidneys of vehicle-treated and SR1078-treated groups. Data is presented as mean ± SEM with statistical significance assessed by t-test*

I.

Table 7. Echocardiographic data from wildtype animals treated with RORA agonist (SR1078) after isoproterenol-induced hypertrophy.

	PBS (n=5)		ISO (n=5)				ISO + SR1078 (n=5)					One-Way ANOVA	
	Mean	SEM	Mean	SEM	vs PBS	Sign.	Mean	SEM	vs PBS	vs ISO	Sign.	p-value	Sign.
Weight (g)	27,00	0,3324214	27,06	0,9064215	0,9981	n.s.	**29,54**	**0,7865113**	**0,0672**	**0,0744**	**+, &**	0,0449	*
HW/TL (mg/mm)	7,33	0,2170275	8,60	0,4770525	0,0368	*	8,42	0,2165247	0,0861	0,9206	*	0,0368	*
HW/BW (mg/g)	4,51	0,177757	5,35	0,1742112	0,0045	**	5,11	0,0602953	0,0350	0,5047	*	0,0049	**
IVSd (mm)	0,72	0,0568859	1,09	0,0209603	<0,0001	****	1,09	0,0184511	<0,0001	>0,9999	****	<0,0001	****
LVPWd (mm)	0,78	0,0724983	1,06	0,0474225	0,0137	*	1,01	0,0521898	0,0406	0,8199	*	0,012	*
LVIDd (mm)	4,11	0,0513225	3,71	0,0605677	0,0212	*	3,76	0,1336978	0,0427	0,9186	*	0,0165	*
IVSs (mm)	1,06	0,0730479	1,66	0,0556677	<0,0001	****	1,67	0,0600518	<0,0001	0,9932	****	<0,0001	****
LVPWs (mm)	1,05	0,0490419	1,60	0,0473216	<0,0001	****	1,63	0,0748287	<0,0001	0,9303	****	<0,0001	****
LVIDs (mm)	3,06	0,0895272	2,41	0,1333642	0,0252	*	2,26	0,2054183	0,0071	0,7655	**	0,0063	**
EF (%)	57,33	2,8867513	70,60	4,0570926	0,1154	n.s.	**75,33**	**5,4272973**	**0,0281**	0,718	*****	0,0292	*
FS (%)	26,00	1,6227549	35,20	3,0177254	0,1647	n.s.	**39,67**	**4,6163959**	**0,0324**	0,6192	*****	0,0367	*
EDV (mm3)	74,81	2,211089	58,78	2,2516137	0,0162	*	60,95	5,0470108	0,0361	0,8969	*	0,0128	*
ESV (mm3)	36,90	2,7288016	20,75	2,7616187	0,0121	*	18,30	4,1936443	0,0047	0,8607	**	0,0035	**
H/R	0,36	0,0373045	0,58	0,0404951	0,0019	**	0,53	0,0234068	0,0117	0,5768	*	0,0018	**
SI	2,06	0,0247133	1,85	0,480944	0,8599	n.s.	2,12	0,0677217	0,9875	0,7793	n.s.	0,7790	n.s.
LVm (%)	100,00	8,33937	139,38	6,574084	0,0199	*	137,75	8,9609471	0,0154	0,9887	*	0,0070	**
Heart rate M-Mode (bpm)	470,33	27,154564	459,00	22,209107	0,9639	n.s.	448,47	32,204486	0,8703	0,9575	n.s.	0,8793	n.s.
Aortic peak (m/s)	0,84	0,0413805	0,92	0,0396008	0,3752	n.s.	0,89	0,030991	0,6657	0,819	n.s.	0,4066	n.s.
VTI (cm)	3,96	0,1281396	4,57	0,3096593	0,4143	n.s.	**5,18**	**0,313156**	**0,0582**	0,319	**+**	0,0665	+
E peak (m/s)	0,81	0,0525404	0,77	0,0415478	0,8924	n.s.	0,78	0,0679918	0,9377	0,9905	n.s.	0,8994	n.s.
Mitral deceleration (m/s)	38,50	8,3338889	44,07	7,6240846	0,8890	n.s.	40,87	7,4629455	0,9787	0,9492	n.s.	0,8925	n.s.

Aortic diameter (mm)	1,50	0,011547	1,61	0,0254864	0,0951	+	**1,72**	**0,0370885**	**0,0022**	**0,0529**	****, &**	0,0027	**
SV (uL)	34,91	0,9204472	38,03	2,2564999	0,7970	n.s.	42,65	4,0387606	0,2859	0,5298	n.s.	0,2907	n.s.
CO (mL/min)	152,70	2,1157387	169,44	9,4564099	0,5370	n.s.	165,39	11,289067	0,6928	0,9498	n.s.	0,5577	n.s.

LVIDd, Left ventricular internal diameter during diastole; LVIDs, Left ventricular internal diameter during systole; IVSd, internal ventricular septum diameter during diastole; IVSs, internal ventricular septum diameter during systole; LVPWd, Left ventricular posterior wall thickness diameter during diastole; LVPWs, Left ventricular posterior wall thickness diameter during systole. EDV, end-diastolic volume; ESV, end-systolic volume; EF, ejection fraction; FS, fractional shortening; H/R, ventricular thickness/radius; IE, sphericity index; LVm, left ventricular mass; VTI, Velocity time integral; SV, stroke volume; CO, cardiac output

7. Human liver fibrosis and RORA gene expression have a negative correlation.

To conclude the second objective of this PhD thesis, we conducted an extensive evaluation of RORA expression in a cohort of liver disease patients(134). Our analysis revealed a notable reduction in both RORA protein and gene expression in liver tissues from cirrhotic patients compared to control individuals (Figure 25A). Additionally, we also compared the gene expression of *RORA* from HSCs isolated from these cirrhotic patients with the control group showing a loss of it during HSCs activation and fibrogenesis process (Figure 25B).

We further investigated the relationship between RORA expression and fibrosis by examining patients across different stages of chronic liver disease. We observed a progressive decrease in RORA gene expression from Metavir F1 to F4 stages and a significant negative correlation with the FIB4 fibrosis score (Figure 25D-E). Moreover, RORA expression inversely correlated with HSC activation and the levels of fibrogenic markers, including *ACTA2, COL1A1, LOXL2, TIMP1, VEGFC and TAGLN,* reinforcing the role of RORA in modulating the fibrogenic response in HSCs (Figure 25F). These findings underscore the potential of RORA as a valuable target for therapeutic intervention in chronic liver disorders.

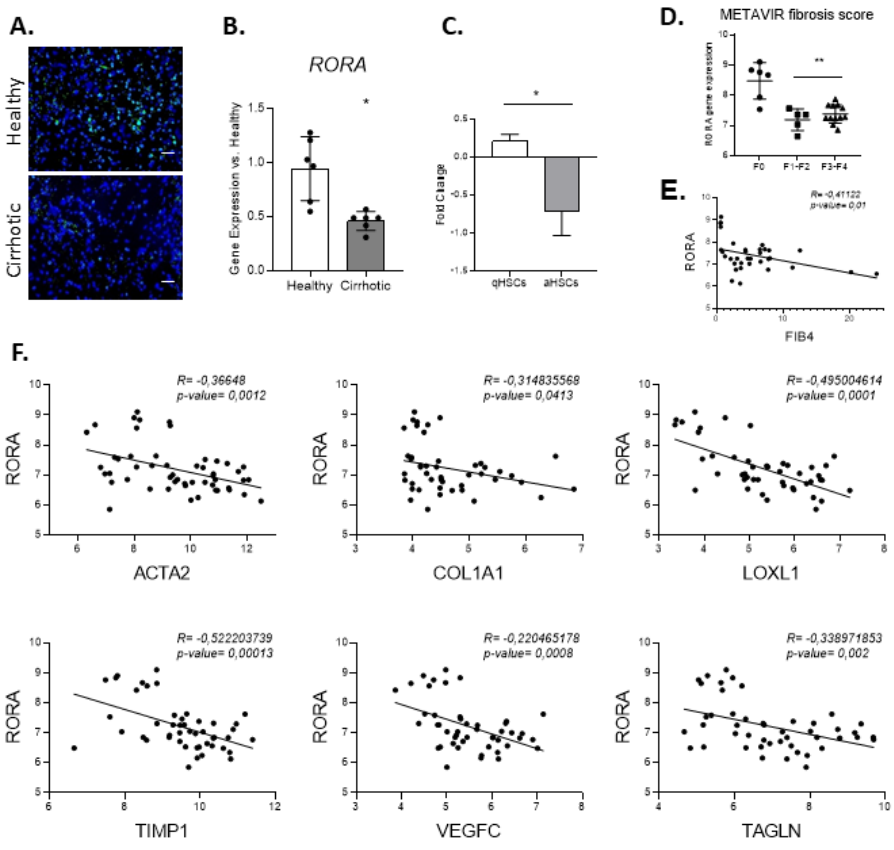

Figure 25. RORA is downregulated in liver disease and inversely correlates with fibrosis severity*. (A) Reduced RORA protein expression in cirrhotic patients compared to healthy controls. Scale bars = 100 µm. (B) Decreased RORA gene expression in cirrhotic livers compared to healthy livers, analyzed by qPCR (n = 6 per group). (C) RORA expression is lower in primary activated hepatic stellate cells (HSCs) compared to quiescent HSCs (data from GSE90525 & GSE67664). (D) RORA expression shows a negative correlation with METAVIR fibrosis score and FIB-4 index in a cohort of liver disease patients. (E) RORA expression negatively correlates with HSC activation markers and fibrosis-related genes (ACTA2, COL1A1, LOXL1, TIMP1, VEGFC, and TAGLN) in liver disease patients. Significant differences are indicated as *p < 0.05.*

In summary, the findings from this second objective underscore the importance of studying disease cell trajectories in vitro, revealing RORA as a key transcriptional regulator of diHSCs differentiation and activation. The modulation of RORA activity has profound effects on cellular metabolism, fibrogenic responses, and overall liver fibrosis. These results not only advance our understanding of HSC biology but also suggest that targeting RORA could be a promising strategy for therapeutic intervention in chronic liver diseases and extrahepatic fibrogenic disorders.
These findings have been published on BioRxiv (135) and are currently under revision for publication.

Objective 3: Define the heterogeneity and differentiation potential of cell populations generated during diHSC differentiation.

The third objective of this PhD thesis is to elucidate the molecular mechanisms underlying distinct cellular states and functional phenotypes along diHSCs differentiation, identify subpopulations of diHSCs and investigate how environmental factors, including endoderm progenitor cells influence the final phenotype of diHSCs into hepatic or pancreatic phenotype. Some of this research was conducted during my internship in Prof. Spagnoli's lab at King's College London (KCL), where it contributed to the submission of a patent related to the tissue specification of the stellate cell phenotype (patent number P26016EP00).

1. **Time affects the heterogeneity of cells during differentiation.**

To capture the transcriptional changes occurring during diHSC differentiation, we sequenced samples at five distinct time points throughout the process. These time points correspond to the stages identified in the timecourse proteome analysis from Objective 2: Day 0 (undifferentiated iPSCs), Day 4 (initial mesoderm commitment), Day

6 (mesenchymal commitment), Day 8 (intermediate stellate cell stage), and Day 12 (mature stellate cells) (Figure 26A).

Our analysis revealed a progressive increase in cell dispersion and heterogeneity across the different time points, indicating that cell heterogeneity grows as differentiation advances. At Day 0, the undifferentiated iPSCs formed a tightly clustered group, representing a homogeneous population with consistent transcriptional profiles. However, as differentiation proceeded, we observed greater dispersion of cells on the UMAP plot, increasing cellular heterogeneity. This dispersion underscores the complex and dynamic nature of cell populations as they transition through differentiation stages. The high reproducibility of our differentiation process was further validated by the consistent clustering of cells across three independent experiments, demonstrating the reliability and robustness of our protocol. (Figure 26A).

We applied batch effect correction using Harmony and performed clustering with the Louvain algorithm. This approach identified 13 distinct clusters, which were annotated based on the expression of specific marker genes, using as reference PanglaoDB and DescatesDB databases (Figure 26B). Notably, we observed co-clustering of cells from different time points, which indicated the presence of overlapping cell populations with shared transcriptional features (Figure 26C).

The composition of dominant cell types varied significantly with time. At Day 0, the population was predominantly composed of iPSCs. By Day 4, we detected a co-existence of iPSCs and mesothelial-like cells, marking the initial stages of differentiation. At Day 6, the predominant populations included mesothelial cells and a subset of stellate cells, reflecting a shift towards more specialized cell types. By Days 8 and 12, the differentiation process led to the emergence of various stellate cell populations, with a single dominant population at each time point (Figure 26D).

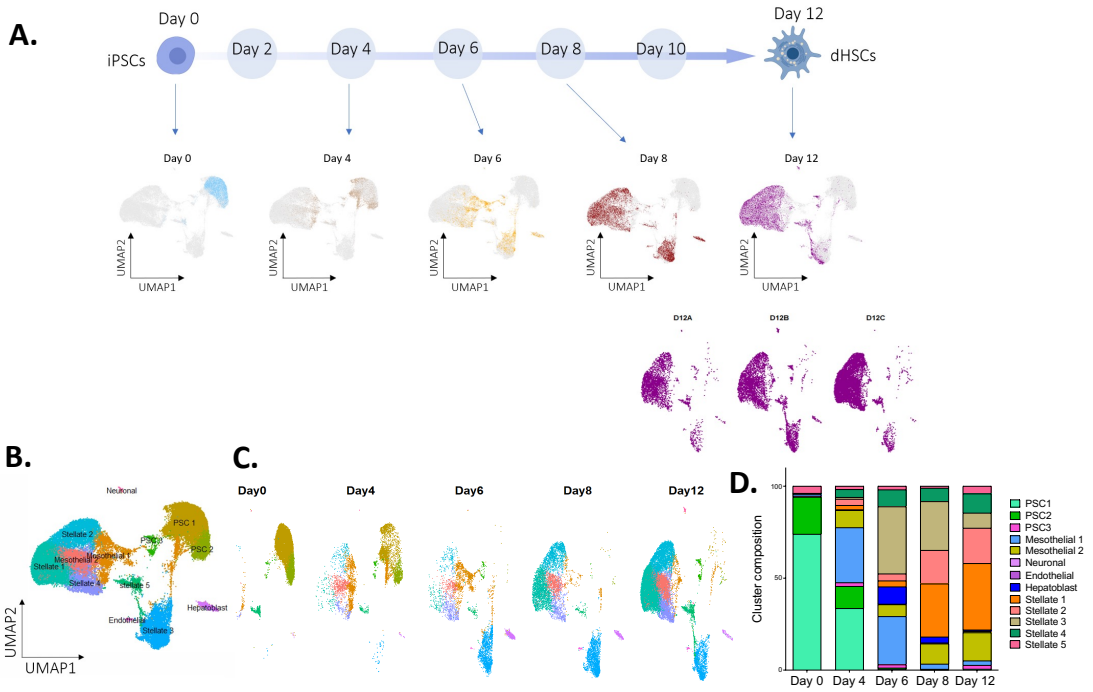

Figure 26. Time-dependent changes in cell heterogeneity during diHSC differentiation*. (A) Schematic representation of the five distinct time points captured during diHSC differentiation: Day 0 (undifferentiated iPSCs), Day 4 (initial mesoderm commitment), Day 6 (mesenchymal commitment), Day 8 (intermediate stellate cell stage), and Day 12 (mature stellate cells). (B) UMAP plot showing the progressive increase in cell dispersion and heterogeneity across time points, with tight clustering at Day 0 and increased dispersion as differentiation advances. Three independent experiments demonstrated high reproducibility and consistent clustering patterns. (C) Cell clustering analysis using Harmony for batch effect correction and the Louvain algorithm identified 13 distinct clusters. Clusters were annotated based on marker gene expression using PanglaoDB and DescatesDB references. The UMAP plot also shows co-clustering of cells from different time points, indicating overlapping cell populations with shared transcriptional features. (D) Proportional composition of dominant cell types at each time point. Day 0 predominantly consisted of iPSCs, while Day 4 showed a mix of iPSCs and mesothelial-like cells. By Day 6, mesothelial cells and a subset of stellate cells became predominant, and by Days 8 and 12, the differentiation process led to various stellate cell populations, with a single dominant population at each time point.*

2. Cell heterogeneity among stellate cell differentiation

Throughout the differentiation process, we identified three distinct pluripotent stem cell (PSC) clusters, each corresponding to specific stages of the differentiation protocol and pluripotency commitment. At Day 0, the predominant cluster, PSC1, is characterized by its maintenance of self-renewal and an undifferentiated state. These cells are marked by key regulators such as *POU5F1*, *TDGF1*, and *ESRG*, which are essential for sustaining pluripotency (Figure 27A). PSC1 cells are not yet primed for premature differentiation and are notably enriched in cell cycle processes, ensuring they remain in a pluripotent and proliferative state.

Also present at Day 0 is the PSC2 cluster, distinguished by markers such as *L1TD1*, *UBE2C*, *TPX2*, and *UCHL1* (Figure 27A). These markers suggest a more active role in cell

cycle regulation, mitotic spindle organization, and protein degradation. PSC2 cells demonstrate potentially higher proliferative activity and represent a more advanced or tightly regulated pluripotent state, with enhanced control over differentiation, proliferation, and chromatin dynamics.

By Day 4 of differentiation, the PSC3 cluster emerges, characterized by markers such as *MUSTN1*, *CDH6*, and *PAX6* (Figure 27A). PSC3 cells display the potential to differentiate into a broad range of cell types and exhibit features related to neural and mesodermal development, cell adhesion, and metabolic functions. This profile marks the transition from a pluripotent state to cells with more specialized potential, highlighting progressive changes in cell identity and function during differentiation.

In addition, two distinct mesothelial cell clusters were observed during the differentiation protocol. Mesothelial 1, present at Day 4, is characterized by the expression of *TUBB2B, ID3, WLS*, and *KRT19*, which are indicative of early developmental stages and pluripotent states (Figure 27A). In contrast, Mesothelial 2, emerging at Day 6 and maintained through Day 8, is associated with ECM dynamics, stress responses, and metabolic functions, as evidenced by the expression of *GPC3, DCN, DSP*, and *MALAT1*, reflecting a more mature or differentiated cell phenotype.

During embryonic development, mesothelial cells give rise to stellate cells. At Day 6 of differentiation, the first cluster of stellate cells, termed Stellate 3, emerges. The Stellate 3 phenotype, characterized by markers such as *HAS2, COL6A3, COL6A1, COL3A1*, and *COL1A2* (Figure 27A), is distinguished by its fibrogenic properties and role in ECM construction (Figure 27B) as depicted by the GO enriched within this cluster, which are crucial for the development and formation of the organ's ECM.

By Day 8, while Stellate 3 remains predominant, new stellate subpopulations also emerge. Stellate 1 is characterized by fibrinolytic properties (Figure 27C), expressing *IGFBP5*, *PTN*, *TGFBI*, and *LGALS3* (Figure 27A). Stellate 2 exhibits proliferative enrichment, as indicated by the expression of *MKI67* and cell cycle genes such as *UBE2C* (Figure 27D). Finally, Stellate 4 displays a contractile-myofibroblastic profile (Figure 27E), marked by the expression of *ACTA2*, *TAGLN*, and *MYL9* (Figure 27A). By Day 12, the Stellate 1 subtype, known for its fibrinolytic properties, becomes the most prevalent. These shifts in stellate cell populations reflect a continuous maturation process during differentiation. This dynamic transition demonstrates the time-dependent nature of

cellular heterogeneity throughout differentiation, providing valuable insights into the complex trajectory of HSC maturation and the evolving nature of cell identity. Finally, the Stellate 5 cluster, which appears at day 12 of the differentiation protocol, shows a significant enrichment in ribosome-related genes (Figure 27A). This suggests that the cells in this cluster are highly active in protein synthesis. The heterogeneity observed in vitro, could partially resemble the heterogeneity observed *in vivo*.

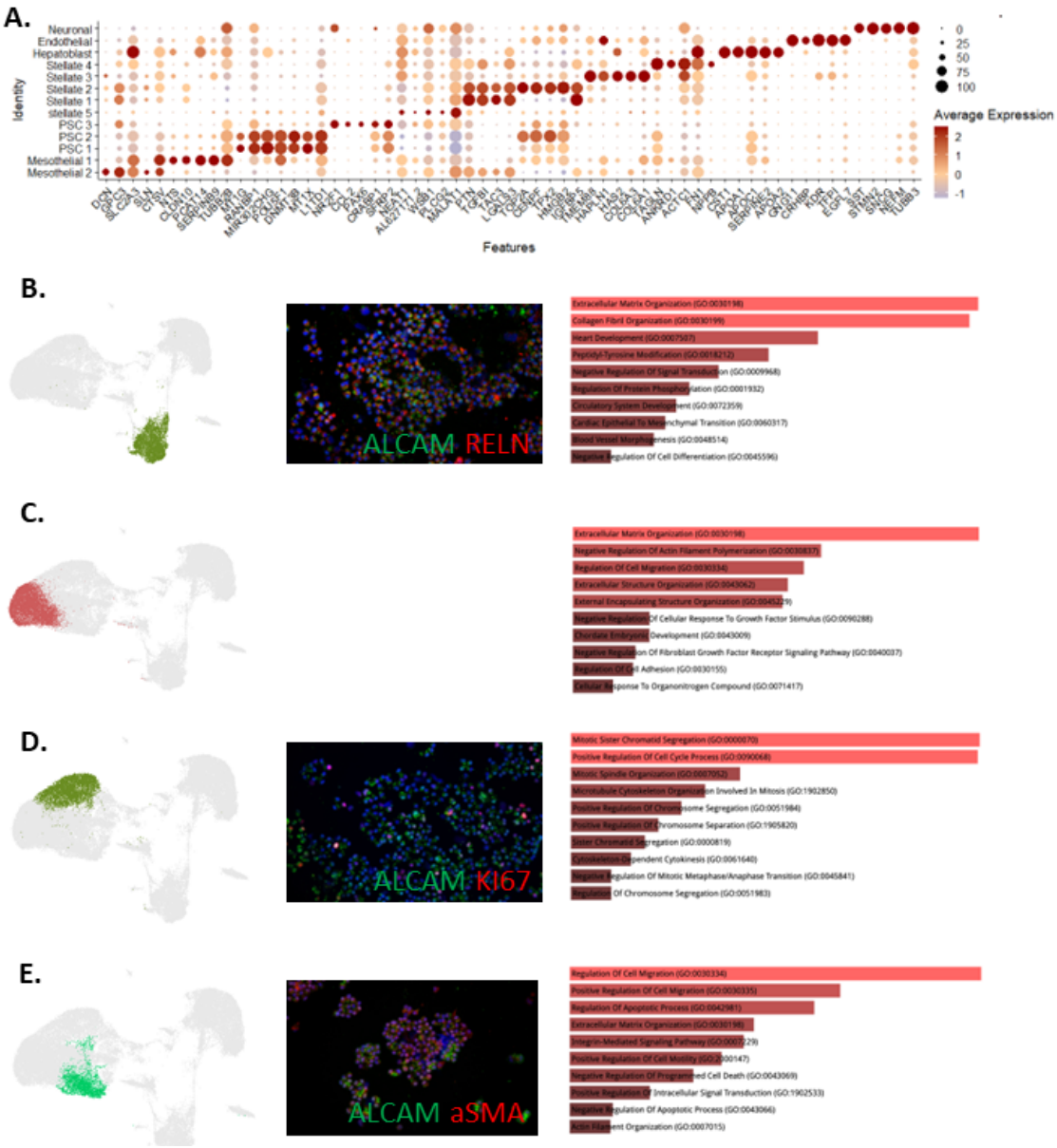

Figure 27. Cell heterogeneity during stellate cell differentiation*. (A) Heatmap of the DEGs (Differential Gene Expression) markers of each identified cluster. (B) UMAP, immunofluorescence of ALCAM and RELN and GO (Gene Ontologies) of the Stellate 3 cluster. (C) UMAP and GO of Stellate 1 cluster. (D) UMAP, immunofluorescence of ALCAM and MKI67 and GO of Stellate 2. (E) UMAP, immunofluorescence of ALCAM and aSMA and GO of Stellate 4. Scale bars of images represent 100μm.*

3. Increased Intercellular Communication During iPSC Differentiation to diHSCs.

As iPSCs progress through various developmental stages, they experience complex changes in cell-to-cell interactions that significantly impact their differentiation pathway. During differentiation, enhanced intercellular communication occurs, potentially facilitating the coordination of signaling pathways essential for the proper development of diHSCs and contributing to the heterogeneity of the final cell population (Figure 28). Consistent with existing literature, there is robust cell-to-cell communication among different stellate cell populations, including in an autocrine manner. Notably, there is strong interaction between the hepatoblast-like population and the early stellate 3 population, indicating that this communication may play a crucial role in ensuring accurate differentiation.

Overall, these findings suggest the importance of cell-cell communication in guiding the differentiation of iPSCs. Understanding these interactions, especially between specific cell populations, could provide valuable insights into the mechanisms that regulate differentiation and contribute to the heterogeneity of the final cell population.

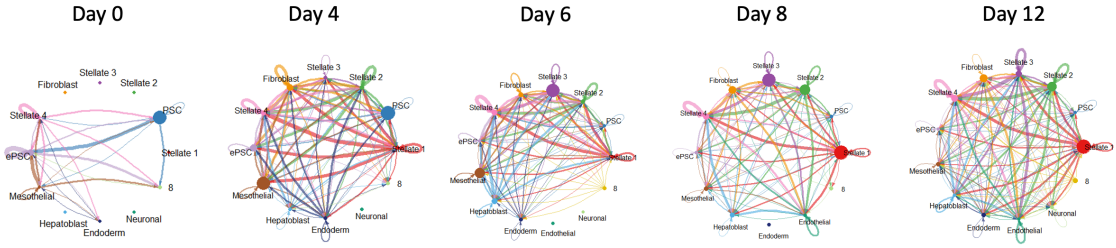

Figure 28. Cell-cell communication intensifies throughout differentiation*. Chord diagram illustrating the cell-to-cell interactions among different populations identified by scRNA-seq over the course of the differentiation process, shown at days 0, 4, 6, 8, and 12.*

4. Pseudotime analysis of differentiation trajectories

We employed the Monocle package to evaluate the pseudotime of our differentiation process. Monocle uses an algorithm to learn the sequence of gene expression changes that each cell undergoes as part of a dynamic biological process(136). By constructing an overall trajectory of gene expression changes, Monocle positions each cell along this trajectory, allowing us to visualize the progression of differentiation.

Cells at the early stages of differentiation exhibit lower pseudotime values and are represented by darker colors on the trajectory map. Given that we initiated our differentiation protocol from undifferentiated iPSCs at Day 0, these cells serve as the

roots of the differentiation process (indicated by white circles) (Figure 29A). As differentiation proceeds, cells diverge into distinct clusters, representing different cell fates (marked by gray circles) (Figure 29A). Branch points within the trajectory correspond to critical cellular decisions and are denoted by black circles. These branches enable us to study the genetic components underlying these differentiation decisions.

Notably, our pseudotime analysis revealed two branched trajectories leading to stellate cell phenotypes. We identified several key genes associated with mesoderm and HSC commitment that exhibited dynamic expression changes as a function of pseudotime such as *EOMES* (Figure 29B). Whether HSCs in embryonic development are differentiated following two molecular trajectories would have to be further investigated.

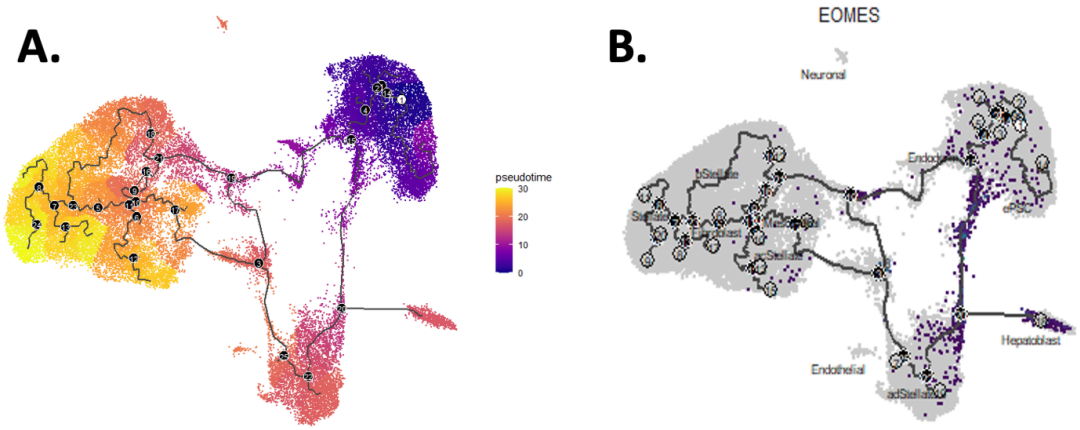

***Figure 29. "Time-resolved analysis reveals two branched trajectories leading to stellate phenotypes**. (A) Pseudotime analysis of diHSC differentiation. (B) Dynamic gene expression of EOMES across pseudotime, showing its changing expression throughout the differentiation process.*

5. **Identification of organ-specific markers in human stellate cells**

When annotating the stellate cell clusters, we observed that the DEGs of these subclusters were also consistent with their pancreatic counterparts. This was particularly evident in Stellate 3, which appears early in the timeline and exhibits fibrogenic properties, suggesting a role in ECM construction during organ development. Based on these findings, we hypothesized that the differentiation protocol could potentially be used to derive pancreatic stellate cells from iPSCs (diPSCs).

To further investigate the differences between hepatic and pancreatic stellate cells, we obtained single-cell RNA sequencing datasets from both embryonic and adult human tissues via public repositories (Table 8).

Table 8. Public single cell RNA sequencing of the liver and pancreas tissues.

Accession number	Repository	Tissue	Age	Reference
E-MTAB-7189	ArrayExpress	Liver	Embryo	Wesley BT et al, Single-cell atlas of human liver development reveals pathways directing hepatic cell fates. Nat Cell Biol. 2022 Oct;24(10):1487-1498. doi: 10.1038/s41556-022-00989-7. Epub 2022 Sep 15. PMID: 36109670.
SE212837	Gene Expression Omnibus	Liver	Adult	Wang S, et al. An autocrine signaling circuit in hepatic stellate cells underlies advanced fibrosis in nonalcoholic steatohepatitis. Sci Transl Med. 2023 Jan 4;15(677):eadd3949. doi: 10.1126/scitranslmed.add3949. Epub 2023 Jan 4. PMID: 36599008; PMCID: PMC10686705.
HRA002757	GSA-Human	Pancreas	Embryo	Ma Z et al, Deciphering early human pancreas development at the single-cell level. Nat Commun. 2023 Sep 2;14(1):5354. doi: 10.1038/s41467-023-40893-8. PMID: 37660175; PMCID: PMC10475098.
EGAS00001004653	European Genome-Phenome Archive	Pancreas	Adult	Tosti L, et al. Single-Nucleus and In Situ RNA-Sequencing Reveal Cell Topographies in the Human Pancreas. Gastroenterology. 2021 Mar;160(4):1330-1344.e11. doi: 10.1053/j.gastro.2020.11.010. Epub 2020 Nov 16. PMID: 33212097.

After preprocessing the data, cells were clustered and annotated based on their DEGs and reference databases to identify stellate cells in both hepatic and pancreatic tissues. Stellate cells from both territories were then subclustered, merged and analyzed together to identify organ-specific markers (Figure 30A). These selected markers were validated at both protein and gene expression levels in tissue samples, resulting in gene signatures for each tissue that were conserved across both embryonic and adult stages (Figure 30B). In human HSCs, markers such as *RELN*, *ROBO2* and *HGF* were enriched, while human pancreatic stellate cells (PSCs) showed enrichment for *SMOC2*, *BACH2*,

IGF1 and *ISL1*. Despite these organ-specific differences, both types of stellate cells shared common markers related to ECM organization and composition, such as *COL6A1*, as well as genes associated with vitamin A metabolism, like *LRAT*, reflecting the unique traits of these mesenchymal cells (Figure 30C).

Given these observations, we hypothesized that the endodermal components of each tissue might influence the acquisition of organ-specific phenotypes in stellate cells. This hypothesis became the focus of my research during an internship in Professor Spagnoli's lab at King's College London. The following results are part of this collaborative study, which ultimately led to the development of a patent for methods involving the co-culture of stellate cell precursors and endoderm progenitors to produce spheroids with tissue-specific mesenchyme (patent number P26016EP00).

6. Endoderm progenitor differentiation towards hepatic and pancreatic lineages

During development, the definitive endoderm gives rise to the posterior foregut endoderm, which can differentiate into hepatoblasts or pancreatic cells depending on the specific signaling cues it receives. In the in vitro experiments, we successfully induced cells to differentiate into definitive endoderm, as indicated by the expression of *FOXA2* on Day 3 of the differentiation protocol (Figure 31A). By Day 7, the cells resembling posterior foregut endoderm were positive for both hepatic markers (HNF4A and AFP) and pancreatic markers (PDX1) at both the protein and gene expression levels (Figure 31B). When exposed to specific differentiation cues, these endoderm progenitors were capable of acquiring organ-specific phenotypes. For pancreatic differentiation, cells showed increased expression of PDX1 and NKX6.1, while hepatic differentiation was marked by elevated levels of ALB (Figure 31C). These findings suggest that the posterior foregut endoderm cells obtained in vitro have a dual differentiation potential, enabling the derivation of both pancreatic and hepatic progenitors from the same differentiation protocol.

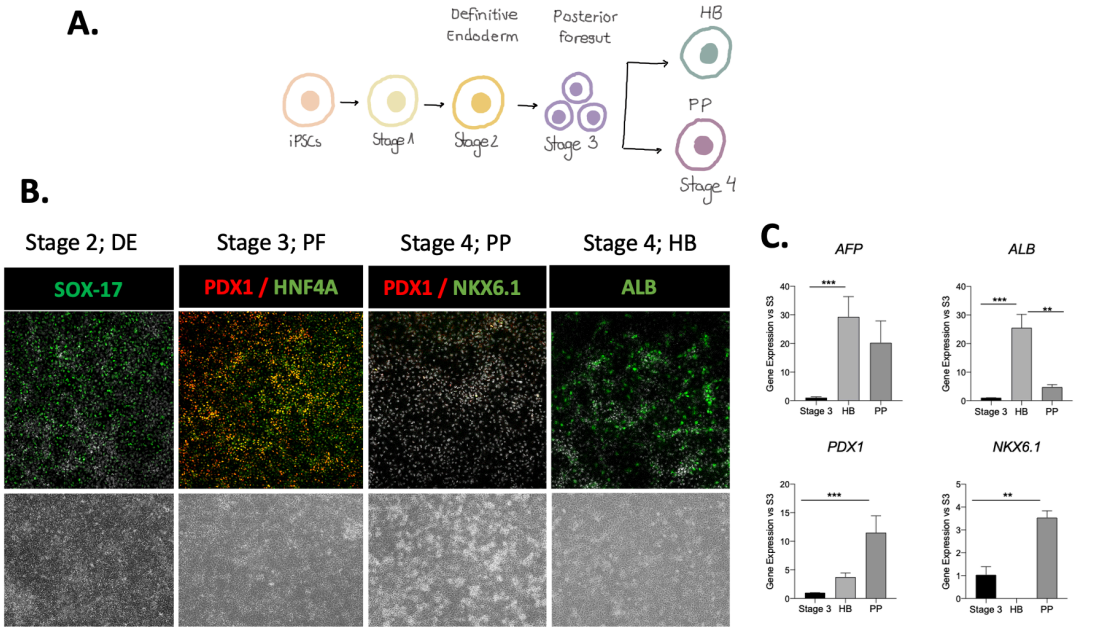

Figure 31. Differentiation of definitive endoderm into posterior foregut endoderm with dual hepatic and pancreatic potential. *(A) Successful induction of definitive endoderm in vitro, as evidenced by FOXA2 expression on Day 3 of the differentiation protocol. (B) By Day 7, posterior foregut endoderm-like cells express both hepatic markers (HNF4A and AFP) and pancreatic marker (PDX1) at the protein and gene expression levels. (C) Exposure of posterior foregut endoderm progenitors to specific differentiation cues leads to organ-specific phenotypes. Pancreatic differentiation is marked by increased expression of PDX1 and NKX6.1, while hepatic differentiation shows elevated ALB and AFP levels. n=3. DE= Definitive Endoderm; PF= Posterior foregut; HB= Hepatoblast; PP = Pancreatic Progenitors.*

7. Co-cultivation of Endoderm Progenitors and Mesenchymal Cells in an Organ-Specific Context

To examine how endoderm progenitors influence stellate cell progenitors, we carried out a preliminary experiment using conditioned media from both hepatic and pancreatic endoderm progenitors. diHSCs, which had reached an immature phenotype by Day 8 of differentiation, were exposed to this conditioned media until finishing the differentiation process at Day 12 (Figure 32A). Exposure to hepatic-conditioned media led to increased expression of *RELN* and *ROBO2*, markers previously identified as enriched in the hepatic phenotype (Figure 32B). In contrast, when the stellate cells were exposed to pancreatic-conditioned media from Day 8 through Day 12, they showed upregulation of *BACH2*, *SMOC2* and *IGF2*, markers associated with pancreatic progenitors (Figure 32C).

Furthermore, there was an upregulation of common markers related to ECM production (*COL6A1*) and retinol storage (*LRAT*), reflecting the influence of the endoderm progenitors on the stellate cell phenotye (Figure 32D).

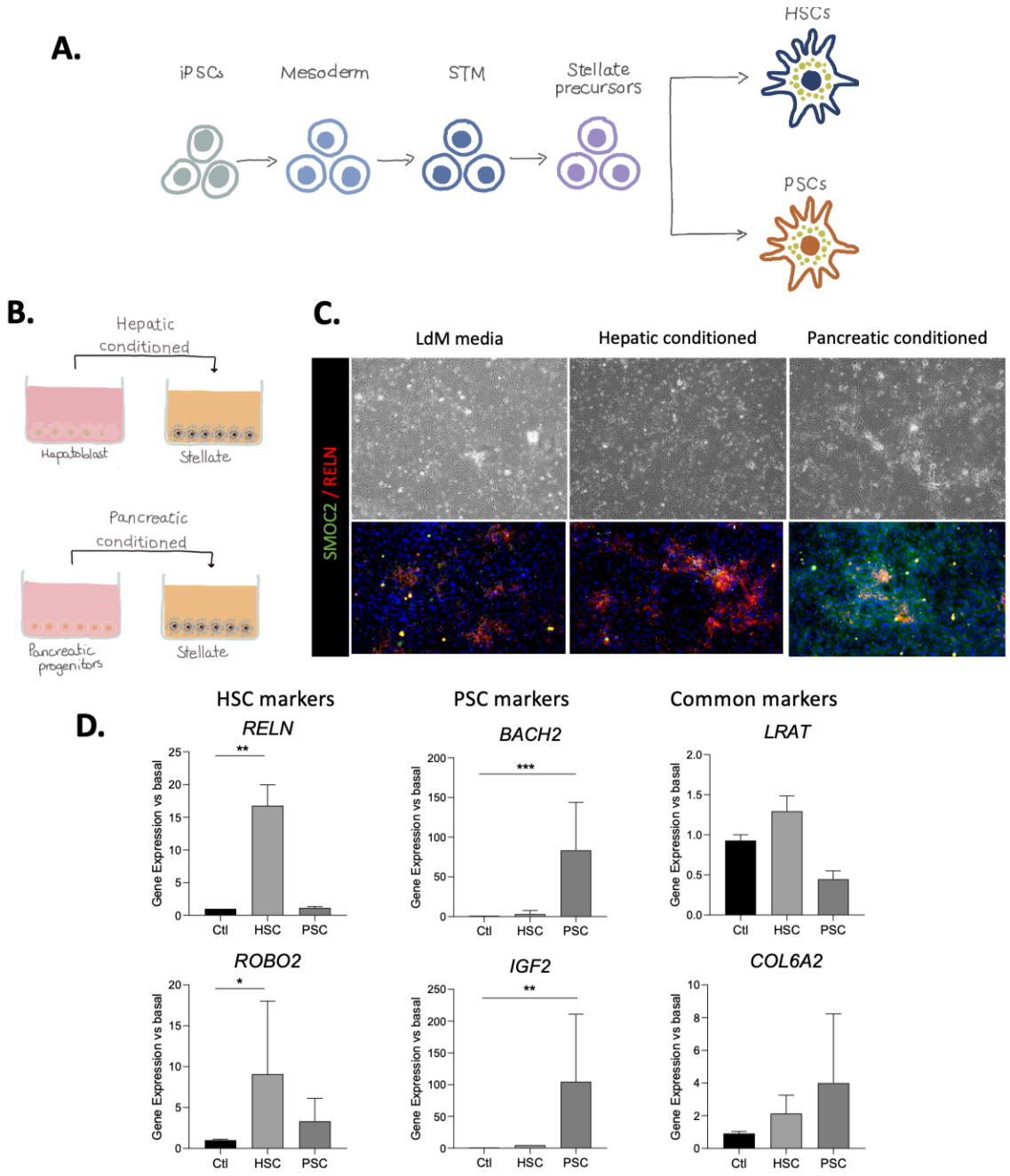

Figure 32. Influence of hepatic and pancreatic endoderm progenitors on stellate cell progenitor differentiation*. (A) Schematic representation of the experimental setup where stellate cells, differentiated until Day 8, were exposed to conditioned media from hepatic or pancreatic endoderm progenitors until Day 12. (B) Exposure to hepatic-conditioned media led to the upregulation of hepatic phenotype-associated markers RELN and ROBO2. (C) In contrast, stellate cells exposed to pancreatic-conditioned media exhibited increased expression of pancreatic progenitor-associated markers BACH2, SMOC2, and IGF2. (D) Both treatments resulted in the upregulation of ECM-related marker COL6A1 and retinol storage marker LRAT, indicating the role of endoderm progenitors in influencing stellate cell functions. n=4 HSC= Hepatic Stellate Cells; PSC= Pancreatic Stellate Cells; Ctl= control with LdM media; Pan = Pancreatic conditioned media; Hep = Hepatic conditioned media.*

We found that direct cell-cell contact between endoderm progenitors and stellate cells significantly enhanced organ-specific phenotypes. We set up a co-culture system where endoderm progenitors were cultured with diHSCs under non-adherent conditions for

four days, until the end of the stellate cell differentiation (Figure 33A). When day 8 stellate progenitor cells were exposed to hepatoblast-like cell contact, there was a notable increase in liver-specific markers such as *RELN*, *ROBO2*, *VIPR1*, and other markers like *HGF* that were not upregulated in the indirect co-culture system (Figure 33B). Similarly, co-culturing stellate progenitors with pancreatic progenitor cells led to an improved pancreatic phenotype, with increased expression of markers including *BACH2*, *SMOC2*, *IGF1*, and *ISL1* (Figure 33C). These findings highlight the essential role of direct epithelial-mesenchymal interactions in specifying organ-specific mesenchymal components, demonstrating that epithelial cells play a crucial role in directing the differentiation of the mesenchymal component of the organ.

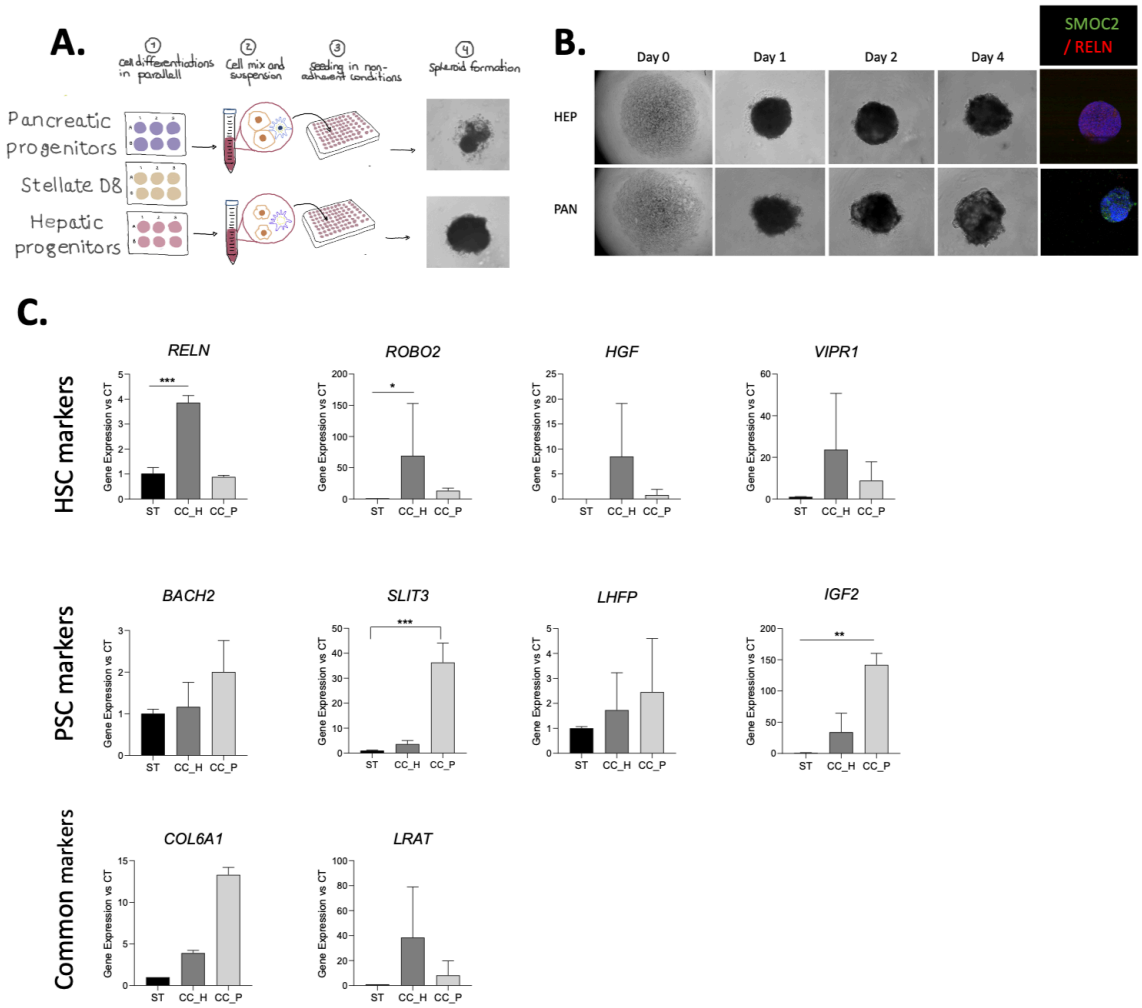

Figure 33. Direct cell-cell contact between endoderm progenitors and stellate cells enhances organ-specific differentiation. *(A) Schematic overview of the co-culture system where endoderm progenitors were cultured with stellate cells under non-adherent conditions for four days, from Day 8 to the end of stellate cell differentiation. (B) Direct contact with hepatoblast-like cells significantly increased the expression of liver-specific markers, including RELN, ROBO2, VIPR1, and HGF, compared to stellate cells alone. (C) Similarly, co-culturing stellate progenitors with pancreatic progenitors led to enhanced expression of pancreatic markers such as BACH2, SMOC2, IGF1, and ISL1, indicating a strengthened pancreatic phenotype.*

8. *In vitro* recapitulation of *in vivo* cellular crosstalk

Single-cell RNA analysis of human tissues using CellChat revealed cell-cell interactions between acinar and stellate cells in the pancreas, and between hepatocytes and stellate cells in the liver (Figure 34A and C). We focused our attention on Notch signaling, that was present in both tissues and play a critical role in exocrine pancreas and hepatocyte development(137,138). We identified specific ligands in the differentiated cells that were also present in *in vivo* analyses. For instance, *DLK1* was found to be enriched in hepatocyte-like cells (Figure 34B), while *JAG1* was prominent in acinar cells (Figure 34D). Notably, DLK1 levels were notably higher in the hepatic co-culture, whereas JAG1 was more abundant in the pancreatic spheroid (Figure 34E). Additionally, NOTCH2 receptor was present in human tissue development analysis and also in differentiated stellate cells (Figure 34E). NOTCH2 decreased in the hepatic spheroid but increased significantly in the pancreatic spheroid (Figure 34E). This pattern suggests that Notch signaling, particularly through *NOTCH2*, may influence the specification of stellate cells to hepatic or pancreatic phenotype.

To explore this, we exposed stellate cell progenitors at Day 8 of differentiation to either a recombinant DLK1 antibody or soluble JAG1 ligand until Day 12. Cells treated with DLK1 showed a reduction in *NOTCH2* expression, coupled with an increase in *RELN* and *ROBO2* (Figure 34F). In contrast, exposure to soluble JAG1 resulted in elevated levels of *NOTCH2* but did not affect markers specific to pancreatic stellate cells (Figure 34F). These findings suggest that Notch signaling may influence the specification of the stellate cell phenotype, warranting further investigation. Additionally, these results underscore the value of the iPSC-based system in mirroring *in vivo* signaling dynamics, highlighting its potential as a model for studying organ-specific cellular interactions and their implications in tissue development and disease.

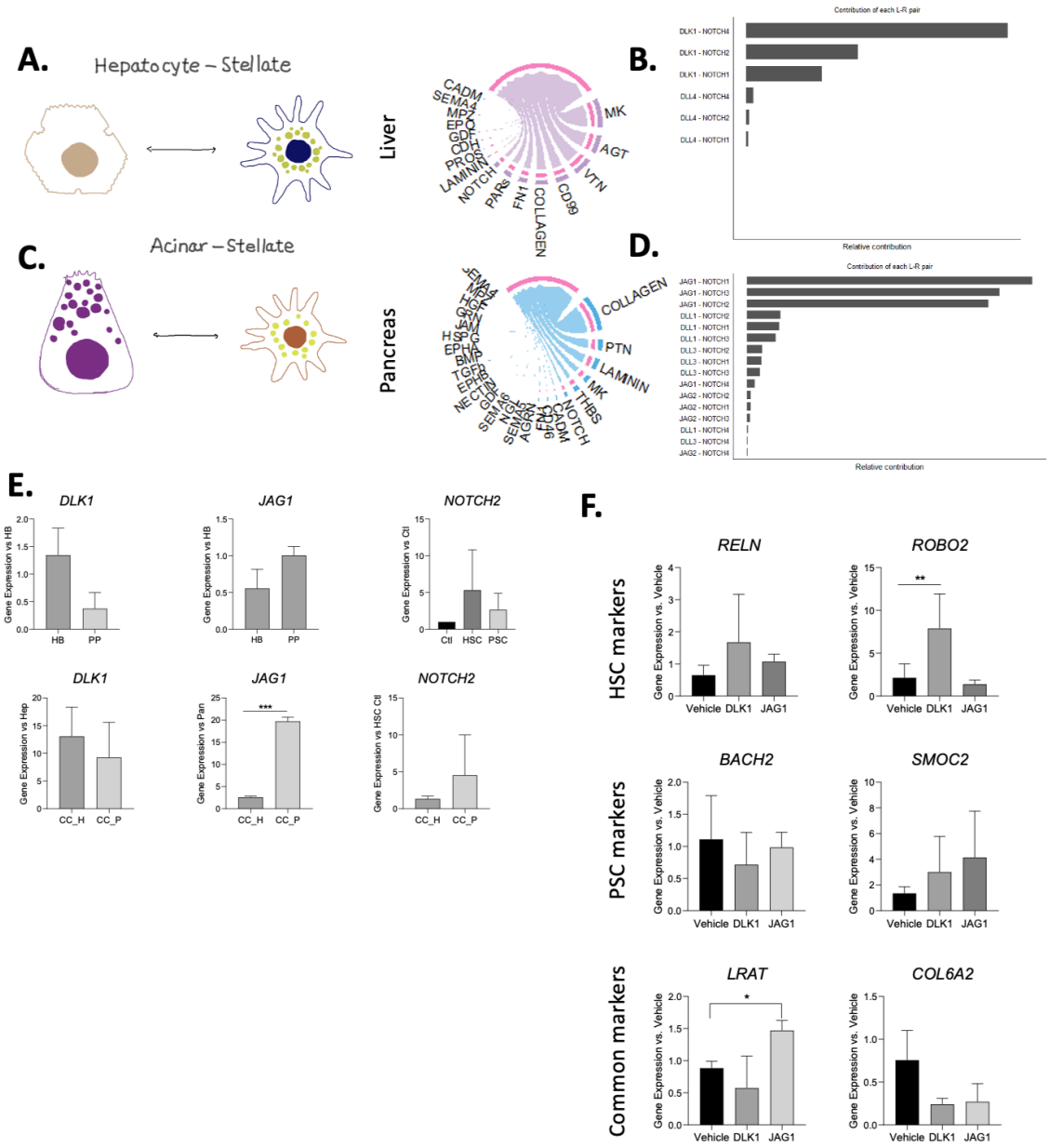

Figure 34. Single-cell RNA analysis reveals cell-cell interactions and Notch signaling dynamics between stellate cells and differentiated cells in human pancreatic and hepatic tissue*s. (A) CellChat analysis of human pancreatic and hepatic tissues identifies conserved cell-cell interactions between acinar and stellate cells in the pancreas and hepatocytes and stellate cells in the liver. (B) Notch signaling was observed in both tissues, with specific ligands reflecting their critical roles: DLK1 was enriched in hepatocyte-like cells, while JAG1 was prominent in pancreatic progenitors. In co-culture models, DLK1 levels were higher in hepatic organoids, and JAG1 was more abundant in pancreatic organoids. Correspondingly, the receptor NOTCH2 was downregulated in hepatic organoids but significantly upregulated in pancreatic organoids, indicating its role in stellate cell specification. (B) Experimental setup where stellate cell progenitors at Day 8 of differentiation were treated with either recombinant DLK1 antibody or soluble JAG1 ligand until Day 12. (C) Cells treated with DLK1 showed reduced NOTCH expression, accompanied by increased RELN and ROBO2, markers associated with hepatic stellate cells. JAG1 exposure led to elevated NOTCH2 expression. Results are from three independent differentiations.*

In summary, we show that cellular heterogeneity significantly evolves over time during differentiation, with single-cell RNA sequencing revealing increased complexity as iPSCs

transition to mature stellate cells. The study identified distinct organ-specific markers for HSCs and PSCs, and co-culture experiments further confirmed that direct interactions between epithelial and mesenchymal cells enhance organ-specific commitment in an *in vitro* system based on iPSCs. Additionally, the differential effects of Notch signaling on hepatic versus pancreatic differentiation underscore its crucial role in specifying stellate cell phenotypes. These findings validate the *in vitro* model's ability to replicate *in vivo* signaling and emphasize its potential for exploring organ-specific cellular interactions, offering a solid basis for future research into tissue development and disease mechanisms.

DISCUSSION

This doctoral thesis has demonstrated the potential of using iPSCs-derived cells to study cell trajectories during differentiation and to model organ physiology and pathophysiology. First, we demonstrated the applications of the diHSCs by standardizing the production, preservation and passage of diHSCs, enhancing reproducibility, reliability and scalability and has led to the publication of a Nature Protocols and a Methods in Molecular Biology as first author (104,105). Our integrated proteomic and transcriptomic analyses further elucidated the dynamics of diHSC differentiation, identifying RORA as a key transcription factor influencing both mesoderm commitment and the quiescent phenotype of diHSCs. These findings stress the importance of mapping sequentially differentiation changes to understand cellular trajectories and cell identities. We have also performed scRNA-seq of different timepoints of the differentiation in order to uncover how cell heterogeneity is defined across the differentiation trajectory. Additionally, our study highlighted the role of environmental factors and interactions with other cell types in influencing the heterogeneity and specification of stellate cell populations, giving rise to both HSCs and PSCs.

The initial objective of this thesis was to scale up the production of diHSCs, which was addressed by transitioning from 12-well plates to 75 cm^2 culture flasks. This change was driven to mitigate the high variability and cell loss observed with smaller culture areas. The larger surface area not only enhanced cell numbers, obtaining up to 8 million cells per flask, but also reduced heterogeneity and improved overall cell viability by providing a more consistent differentiation environment. The successful scaling was validated through comparative analyses, which confirmed that differentiation outcomes and key HSCs markers were consistent across both scales, highlighting the efficacy of the larger culture system in producing homogeneous cell populations. The consistent of the cells differentiated from iPSCs is crucial for both basic research and therapeutic applications, as it ensures the reliable production of the specific cell type. Achieving uniform differentiation is essential to minimize variability in experimental outcomes and to enhance the reproducibility of studies. Inconsistencies in differentiation protocols can lead to heterogeneous cell populations, which may affect the interpretation of results and the efficacy of iPSC-derived treatments (139–141). Furthermore, standardized differentiation methods are vital for scaling up the production of clinical-grade cells,

ensuring that all generated cells meet the safety and functional criteria required for basic research, drug screening testing and therapeutic use(142,143).

Ensuring viability and functionality of diHSCs were other critical aspect addressed in this study. Optimization of the expansion process revealed that maintaining a cell density of 73,000 cells/cm² in Expansion Media was optimal. Additionally, the cryopreservation of diHSCs was effectively managed with various commercial and non-commercial media, with FBS and KoSR emerging as the preferred options due to their cost-effectiveness and superior cell viability. Notably, while cryopreserved and expanded cells showed similar expression profiles of HSC markers compared to freshly differentiated cells, there was an increase in activation markers and a decrease in quiescence markers in passaged and thawed cells. This shift suggests that the passage and thawing processes induce a more activated state in diHSCs, similar to what happens when using primary HSCs(144). Although increasing their activation phenotype, diHSCs showed a reduced activation profile in comparison to pHSCs(145) Also, in order to reduce the activated profile, we tested to cryopreserve them at early stages of the differentiation process. Cryopreserving differentiated cells offers significant advantages, as allows to create a stable and consistent supply of differentiated cells, which can be thawed and used on demand without the need to repeat complex differentiation process (146,147). Moreover, cryopreservation enables long-term storage and the creation of biobanks of differentiated cells, facilitating large-scale studies and collaborations across laboratories. Additionally, the use of cryopreserved cells reduces the risk of batch-to-batch variability, as cells from the same batch can be used for multiple experiments or treatments over time, ensuring consistency in experimental results. The guidelines collected and publicly available(105,148), provide a reliable system for maintain integrity of diHSCs during long-term storage, supporting reproducibility in experimental assays.

Functional assessments of diHSCs, both passaged and cryopreserved, demonstrated their continued response to pro-fibrogenic stimuli such as TGFβ and pro-inflammatory signals like LPS. These cells showed increased expression of fibrogenic markers such as *COL1A1*, *ACTA2*, and *LOX* in response to TGFβ, confirming their utility in fibrogenesis studies. However, the limited response to pro-inflammatory stimuli indicates a need for further optimization to fully use their potential in inflammatory contexts. Moreover,

drug screening assays revealed that diHSCs could effectively evaluate anti-fibrogenic agents. Elafibranor, GS834356, and GLS1 inhibitors showed distinct effects on diHSC markers, with Elafibranor emerging as a robust positive control for anti-fibrogenic activity, opening the possibility to perform high-throughput drug screening assays for antifibrogenic therapies using diHSCs(149,150). Thanks to these optimizations, the distribution of standardized diHSCs was also tested during this PhD. Protocols were established for the preparation, packaging and transportation of diHSCs and stability was confirmed after transportation in collaboration with both researchers and private companies. This has promoted collaborative research projects and will accelerate new discoveries regarding stellate cell biology using diHSCs. Nonetheless, continued refinement of production, cryopreservation and distribution will be essential for high-throughput assays. Also, integration of advanced imaging together with the current omics used and functional assays will enhance our understanding of diHSCs biology.

The ability to generate larger and more consistent populations of diHSCs has allowed us to study their cellular trajectories in detail. While disease-related cell trajectory studies often rely on animal models, translating these findings to human contexts can be complex, and capturing differentiation pathways during human embryonic development remains challenging. By using differentiation protocols with human iPSCs to produce adult-like cells, along with relevant disease models, we have developed valuable tools to explore dynamic cellular pathways involved in differentiation, normal physiology, and disease progression. In this PhD, we constructed a detailed proteomic roadmap of the differentiation trajectory of diHSCs, studying the molecular changes and functional properties at various stages. We identified three distinct differentiation phases: the initial transition from undifferentiated iPSCs to mesoderm-committed cells (stage 1), the progression from mesoderm-like cells to immature stellate cells (stage 2), and the final maturation into mature stellate cells (stage 3). This comprehensive proteomic roadmap reveals the complex molecular dynamics at each stage and serves as a valuable resource for future research on stellate cell plasticity, liver development, and fibrosis. The protein signatures identified in diHSCs closely mirror those of primary HSCs, reflecting markers such as ALCAM, ANXA6, CGN, NES, and DES observed during embryonic HSC development (43,45). However, the lack of detailed understanding of

human HSC development limits our ability to confirm that diHSCs differentiation fully replicates the natural human embryonic development path.

Our analysis also highlighted RORA as a key regulator during the mesodermal phase, with its expression peaking on Day 4 and declining thereafter. This regulation is crucial for the transition to a mesoderm-like state. One of the challenges in achieving proper maturation of iPSC-derived cells is the divergence between primary cell development and iPSC differentiation, which often deviates from the natural developmental path after embryonic stages, delaying full maturation(151). In our study, we identified RORA as a key transcriptional regulator that plays a critical role in the mesodermal and mesenchymal specification of the cells and in maintaining their quiescent phenotype. Furthermore, while RORA genetic deletion disrupts early-stage differentiation, RORA activation by means of the chemical agonist SR1078 enhances the diHSCs phenotype. Our findings support the idea that refining intermediate specification steps in differentiation protocols can be an effective strategy for generating more mature adult cells. Additionally, our analysis of diHSCs trajectories revealed the expression of transcription factors like MEIS1 during differentiation, which are known to regulate HSC biology and activation. Although MEIS1's role in HSC development remains unclear, it has been implicated in HSC activation(152).

The trajectory analysis of diHSCs differentiation identified RORA as a key regulator not only of mesoderm differentiation but also of diHSCs identity and quiescence. In our study, diHSCs derived from iPSC-RORA$^{+/-}$ exhibited an increased activation phenotype, pointing out the RORA's role in maintaining the cells' quiescent state. Furthermore, inducing RORA KO using an inducible iCas9 system at day 4 of differentiation led to a notable increase in activation markers and a decrease in quiescent markers at the endpoint of differentiation.

Although few studies have explored the role of developmental TFs on the regulation of HSC activation, our findings align with previous reports(153–155). For example, Tcf21 and Lhx2 are TFs expressed during the embryonic development of the liver, but their expression in HSCs decreases during activation and fibrosis. Although the exact roles of these TFs at different stages of HSC maturation remain unclear, these observations support the idea that certain TFs may have continuous functions throughout development and disease. This demonstrates the potential of iPSC differentiation

approaches for investigating cell trajectories, offering a powerful tool for understanding the molecular drivers of both differentiation and disease.

Metabolic reprogramming is crucial for both proper embryonic development and cellular adaptations to stress or injury, as it provides cells with the necessary energy at precise moments. For example, during mesoderm differentiation, cells undergo a metabolic switch from glycolysis to increased oxidative phosphorylation (OXPHOS)(19,20). Similarly, activated myofibroblasts, including hepatic stellate cells (HSCs) in the liver, have higher energy demands due to increased proliferation and the secretion of extracellular matrix components, proteases, and cytokines(84). Transcriptomic analysis of activated diHSCs treated with a RORA agonist revealed significant metabolic remodeling: there was a decrease in both lipid beta-oxidation and glycolytic flux. Fatty acid beta-oxidation is critical for HSC activation, as inhibiting mitochondrial fatty acid catabolism can block this process. Additionally, ACC, which regulates both fatty acid beta-oxidation and *de novo* lipogenesis, plays a role in HSC metabolic reprogramming during activation(156). Our data showed that treatment with the RORA agonist reduced ACACA gene expression in diHSCs. Furthermore, activated diHSCs in two *in vitro* models exhibited increased OXPHOS and glycolytic flux, which were downregulated upon RORA treatment, thereby reducing the metabolic demands and preventing activation. At early stages of differentiation, iPSC-RORA$^{+/-}$ cells showed a metabolic profile typical of undifferentiated cells, which was altered by RORA agonist treatment, suggesting that RORA influences metabolic activity during early differentiation and promotes mesoderm differentiation. Moreover, undirected differentiation towards the mesoderm using iPSC-RORA$^{+/-}$ demonstrated a reduced acquisition of the mesodermal phenotype. Lipidomic characterization of activated diHSCs treated with the RORA agonist also revealed a reversion to a quiescent lipidomic profile, consistent with findings described in the literature (132). These results indicate that metabolic plasticity is essential at various stages of the diHSCs trajectory and affects the final cell phenotype. RORA mediates this metabolic regulation and represents a potential target for antifibrogenic therapies, demonstrating that understanding the metabolic adaptations along the diHSCs trajectory could offer as well novel, targeted therapeutic strategies.

Our *in vivo* studies corroborate the in vitro findings, revealing that dysregulation of RORA exacerbates liver fibrosis. sg/sg mice, which lack RORA, showed increased fibrosis, elevated ECM deposition, and impaired liver function compared to wild-type controls. Treatment with the RORA agonist SR1078 in CCl4-induced liver fibrosis models significantly reduced collagen deposition, αSMA staining, and fibrogenic markers such as *Acta2* and *Col1a1*. This beneficial effect was also observed in extrahepatic fibrotic models, including cardiac hypertrophy and kidney fibrosis, where RORA activation similarly decreased fibrogenic markers and collagen accumulation. Further studies using RORA KO mice specific to stellate cells, generated with LRAT Cre drivers, demonstrated increased fibrogenic responses in heterozygous KO mice, reinforcing RORA's role in modulating fibrogenesis. This is supported by human data from a cohort of chronic liver disease patients, where reduced RORA levels were linked to advanced fibrosis. These findings highlight RORA's dual role in HSCs physiology: it regulates diHSCs differentiation and maturation while acting as a critical inhibitor of HSC activation and fibrosis.

RORA, a pleiotropic transcription factor involved in various biological processes, is crucial for the proper differentiation of multiple cell types (157). Fibrosis, an evolutionarily conserved response to chronic injury, becomes pathological when excessive, leading to organ dysfunction, a common feature across many chronic diseases (158). The similarities in fibrotic responses across different organs suggest common core pathways. The results presented in this PhD suggest that diHSCs could serve as a model of pericytes in other tissues, as RORA regulates not only HSC activation but also pericyte function in extrahepatic fibrosis models. This indicates that targeting RORA could be a promising strategy for developing antifibrogenic treatments across various diseases and organs.

The results obtained underscores the importance of examining cell trajectories during differentiation and disease, demonstrating that mechanisms controlling human development and fibrosis can be effectively recapitulated using iPSC differentiation models. The tools and methodologies developed in these studies, such as the differentiation proteomic map, RORA-specific agonists, and *in vivo* models, establish a robust foundation for future investigations. These resources are essential for further exploring RORA's role in various disease contexts and evaluating its potential as a therapeutic target across a range of pathological conditions.

Stellate cell activation is characterized by several key hallmarks, including a transformation into a spindle-like morphology, increased proliferation, loss of retinoids, and the secretion of cytokines, chemoattractants, and ECM proteins. Additionally, activated stellate cells exhibit a dysregulated metabolic profile. However, it remains unclear whether all stellate cells undergo these changes uniformly or if distinct subpopulations of stellate cells perform different functions. With the arrival of scRNA-seq technology, we now understand that there is considerable heterogeneity within the stellate cell population. In this thesis, we also aim to explore this heterogeneity in diHSCs using scRNA-seq, focusing on the molecular mechanisms that drive different cellular states and subpopulations.

We have captured by scRNA-seq analysis the transcriptional evolution of diHSCs at five distinct time points, from undifferentiated iPSCs to mature stellate cells. As differentiation progressed, we observed a progressive increase in cellular dispersion and heterogeneity. Initially, Day 0 iPSCs formed a tightly clustered population, indicative of a homogeneous and undifferentiated state. However, by Day 4, the emergence of mesothelial-like cells marked the beginning of differentiation, and by Days 6, 8, and 12, a clear increase in heterogeneity was evident as the cells transitioned through intermediate and mature stellate stages. As cells undergo differentiation, they exhibit temporal changes in dispersion and diversity, reflecting the transition from a homogeneous state to a more complex and specialized array of cell populations. This process begins with cells displaying broader plasticity, leading to an increasing variability in gene expression profiles as they commit to specific lineages(159). The dynamic nature of this transition is crucial for understanding tissue development and regeneration, as it mirrors the natural progression of cells from undifferentiated progenitors to fully mature, functionally specialized cells(160). The increased heterogeneity of cells during differentiation, evidenced by their transition into distinct clusters, illustrates how cell populations evolve over time, reflecting the increasing complexity and specialization required for proper tissue function.

The capacity to capture these temporal changes manifest the need for advanced in vitro tools to study differentiation as they offer a controlled environment to manipulate and observe these processes in real-time, enabling a more precise understanding of how cells respond to different stimuli and conditions.

Moreover, the variability in dominant cell populations at different time points, from iPSCs to specialized stellate cells, highlights the progressive shift in cell identity and function throughout the differentiation process. The identification of distinct stellate cell subpopulations, such as Stellate 1 through Stellate 5, with unique markers and functional properties, stresses the complexity of stellate cell differentiation and reflects the heterogeneity observed in human tissues (161). For instance, Stellate 1, characterized by its fibrinolytic properties, aligns with the role of HSCs in ECM remodeling and wound healing, as reported by previous studies that highlight their involvement in matrix degradation and tissue repair (Mederacke et al., 2013; Kisseleva et al., 2012). Stellate 2, enriched in cell cycle genes, may correspond to the proliferative phase observed in stellate cells, which is crucial during liver regeneration and fibrogenesis (Schuppan et al., 2013). Stellate 4, which exhibits a contractile-myofibroblastic profile, reflects the myofibroblast-like phenotype of activated stellate cells. This is consistent with literature describing activated HSCs as having contractile properties and contributing to tissue fibrosis through the production of collagen and other ECM components (Friedman, 2008). Moreover, our study identifies Stellate 3 as having early fibrogenic characteristics, similar to findings in other studies where early-stage stellate cells play a key role in ECM deposition during organ development (REF). Stellate 5, which shows enrichment in ribosome-related genes, highlights the high protein synthesis activity typical of fully differentiated stellate cells involved in ECM production and cellular signaling (Bergmann et al., 2017). These findings reflect the maturation of stellate cells and their evolving roles in ECM production and tissue remodeling, corroborating previous research that has demonstrated the functional diversity and plasticity of stellate cells in response to various physiological and pathological cues.

Although unexpected, the appearance of hepatoblast and endothelial-like cells during differentiation was not surprising. During development, these cell types, along with stellate cells, emerge concurrently. Previous research suggests that stellate cells may support the proper differentiation of hepatoblasts and that endothelial and stellate cells might originate from a common progenitor. Therefore, the emergence of endothelial-like cells at mid-stages of differentiation aligns with existing literature(151). This

observation indicates that the differentiation protocol for diHSCs could also be adapted to generate endothelial-like cells, with some modifications.

The appearance of hepatoblast-like cells was particularly interesting, as it suggests that each cell type may establish its own microenvironment, not just epithelial cells but also mesenchymal ones (162,163). This concept is gaining attention, especially in cancer research, where each tumor cell is thought to create its own niche for survival and growth (164). Additionally, the presence of both epithelial and mesenchymal markers in this cluster drew our attention because it may reflect a phenomenon observed in liver development in mice, which is the emergence of an hepatomesenchymal population (165).

The identification of organ-specific markers for hepatic and pancreatic stellate cells such as *RELN* and *ROBO2* for HSCs, and *SMOC2*, *BACH2*, *IGF1*, and *ISL1* for PSCs, supports the notion that each cell type may require its own distinct microenvironment, as we hypothesized that endodermal components influence the acquisition of organ-specific phenotypes by the stellate cells and aligns with existing literature, which suggests that each organ develops its own unique mesenchymal niche (166).

Co-culture experiments have shown that endoderm progenitors significantly enhance the expression of organ-specific markers in stellate cells. This observation underscores the critical role of direct epithelial-mesenchymal interactions in shaping cell phenotypes (166). When stellate cells were cultured with endoderm progenitors, they exhibited a pronounced increase in markers specific to their respective organs, indicating that the presence of endoderm progenitors can actively influence the differentiation and functional specialization of stellate cells. The direct interactions between epithelial and mesenchymal cells within these co-culture systems highlight the importance of the microenvironment in cell development and aligns with the concept that cell phenotypes are not only determined by intrinsic genetic programs but are also affected by the surrounding cellular and molecular environment (167) and reveal that the cellular context provided by endoderm progenitors is crucial for the proper acquisition of organ-specific functions by stellate cells.

In conjunction with these results, the increased expression of hepatocyte, and the predominance of exocrine markers over endocrine markers in the pancreas, suggest that we are accurately replicating the *in vivo* embryonic development of both organs as

anatomically, stellate cells are in close association with hepatocytes in the liver and acinar cells in the pancreas.

Finally, the analysis of Notch signaling in both hepatic and pancreatic contexts revealed differential effects on stellate cell specification. Notch ligands DLK1 and JAG1, and their associated receptors, were found to influence the differentiation of stellate cells in a context-dependent manner. The exposure of stellate progenitors to recombinant Notch ligands demonstrated changes in marker expression consistent with the observed in *in vivo* signaling dynamics, validating the use of our *in vitro* model for studying tissue-specific cellular interactions and their implications for development and disease.

In summary, this doctoral thesis has effectively demonstrated the potential of iPSC-derived cells for studying differentiation trajectories and modeling organ physiology. By standardizing the production, preservation, and scaling of diHSCs, we have significantly improved reproducibility and scalability, leading to significant publications(104,105). Our research identified RORA as a crucial transcription factor in diHSCs differentiation, underscoring the importance of mapping cellular changes to comprehend differentiation and cell identity. This work is currently under review in a high-impact journal due to its clinical relevance (135). We have also refined techniques for maintaining diHSC viability and functionality, including effective cryopreservation strategies, which are vital for both research and clinical applications. Functional assessments validated the use of diHSCs in fibrogenesis studies and drug screening, underscoring their potential for high-throughput applications. Additionally, our investigation regarding organ-specific markers of the stellate cells and their modulation *in vitro*, along with cell interactions, emphasizes the critical role of the microenvironment in cell differentiation. This work has led to a patent (P26016EP00), reflecting the technology's significant potential for industry application. Overall, the research presented in this PhD thesis provides valuable information on the trajectory of diHSCs from the embryonic development to the onset of disease. Moreover, it provides novel tools and methodologies for exploring cellular mechanisms and developing targeted therapies against fibrosis.

CONCLUSIONS

This PhD thesis has provided extensive insights into the differentiation and functionality of diHSCs, addressing key challenges in cell production, characterization, and application. The principal conclusions from this PhD are:

1. The development and optimization of protocols for producing, preserving, and passaging of diHSCs have significantly improved the reproducibility, reliability, and scalability of diHSCs studies.
2. diHSCs after passage and cryopreservation retain responsiveness to pro-fibrogenic stimuli such as TGFβ and pro-inflammatory signals like LPS, making them valuable for studying fibrogenesis and drug screening assays.
3. The diHSCs differentiation process comprises three phases, recapitulating partially the phenotypes of HSCs during embryonic differentiation.
4. Mechanisms controlling human development and fibrosis can be recapitulated using iPSC differentiation models.
5. RORA plays a crucial role in metabolic regulation across various stages of diHSCs differentiation. It is involved in guiding the transition from undifferentiated cells to mesoderm, and in the acquisition and maintenance of the HSC quiescence state.
6. The reduction of RORA expression exacerbates liver fibrosis in human *in vitro* systems and animal models, while RORA agonists treatment reduces fibrogenic content supporting RORA as a target for therapeutic intervention.
7. The *in vitro* differentiation protocol yields an heterogenic diHSCs population resembling partially the HSC heterogeneity observed in liver tissue.
8. Despite their similarities, hepatic and pancreatic stellate cells exhibit distinct tissue-specific markers.
9. Co-education between epithelial and mesenchymal cells during differentiation enhance the acquisition of organ-specific markers in stellate cells, emphasizing the importance of epithelial-mesenchymal interactions in tissue development.
10. The scRNA-seq findings validate the use of the *in vitro* differentiation model for replicating *in vivo* cellular interactions and developmental processes, highlighting NOTCH signaling as important for stellate cell specification.

BIBLIOGRAPHY

1. Cerneckis J, Cai H, Shi Y. Induced pluripotent stem cells (iPSCs): molecular mechanisms of induction and applications. https://doi.org/10.1038/s41392-024-01809-0
2. Takahashi K, Yamanaka S. Induction of Pluripotent Stem Cells from Mouse Embryonic and Adult Fibroblast Cultures by Defined Factors. Cell.126(4):663–76.
3. Takahashi K, Tanabe K, Ohnuki M, Narita M, Ichisaka T, Tomoda K, et al. Induction of Pluripotent Stem Cells from Adult Human Fibroblasts by Defined Factors. Cell. 2007 Nov 30;131(5):861–72.
4. Shi Y, Inoue H, Wu JC, Yamanaka S. Induced pluripotent stem cell technology: a decade of progress. Nature Reviews Drug Discovery 2016 16:2. 2016 Dec 16. 16(2):115–30.
5. Yamanaka S. Pluripotent Stem Cell-Based Cell Therapy—Promise and Challenges. Cell Stem Cell. 2020 Oct 1;27(4):523–31.
6. Takebe T, Wells JM. Organoids by design. Science. 2019 Jun 7;364(6444):956–9.
7. Chang CY, Ting HC, Su HL, Jeng JR. Combining Induced Pluripotent Stem Cells and Genome Editing Technologies for Clinical Applications. Cell Transplant. 2018 Mar 1; 27(3):379.
8. Cerneckis J, Cai H, Shi Y. Induced pluripotent stem cells (iPSCs): molecular mechanisms of induction and applications. Signal Transduction and Targeted Therapy 2024 9:1. 2024 Apr 26;9(1):1–26.
9. Lambert SA, Jolma A, Campitelli LF, Das PK, Yin Y, Albu M, et al. The Human Transcription Factors. Cell. 2018 Feb 8;172(4):650–65.
10. Joung J, Ma S, Tay T, Geiger-Schuller KR, Kirchgatterer PC, Verdine VK, et al. A transcription factor atlas of directed differentiation. Cell. 2023 Jan 5;186(1):209-229.e26.
11. Yamamizu K, Schlessinger D, Ko MSH. SOX9 accelerates ESC differentiation to three germ layer lineages by repressing SOX2 expression through P21 (WAF1/CIP1). 2014;
12. Sharpley MS, Chi F, Hoeve J ten, Banerjee U. Metabolic plasticity drives development during mammalian embryogenesis. Dev Cell. 2021 Aug 23;56(16):2329-2347.e6.
13. Wu J, Ocampo A, Carlos J, Belmonte I. Leading Edge Review Cellular Metabolism and Induced Pluripotency. 2016.
14. Jackson BT, Finley LWS. Metabolic regulation of the hallmarks of stem cell biology. 2024.
15. Du P, Wu J. Hallmarks of totipotent and pluripotent stem cell states. Stem Cell. 2024;31:312–33.
16. Tsogtbaatar E, Landin C, Minter-Dykhouse K, Folmes CDL. Energy Metabolism Regulates Stem Cell Pluripotency. Front Cell Dev Biol. 2020;8. PMC7059177
17. Moussaieff A, Rouleau M, Kitsberg D, Cohen M, Levy G, Barasch D, et al. Glycolysis-Mediated Changes in Acetyl-CoA and Histone Acetylation Control the Early Differentiation of Embryonic Stem Cells. Cell Metab. 2015 Mar 3;21(3):392–402.
18. Lu V, Roy IJ, Teitell MA. Nutrients in the fate of pluripotent stem cells. Cell Metab. 2021;33:2108–21.

19. Cliff TS, Wu T, Boward BR, Glushka JN, Prestegaard JH, Dalton Correspondence S. MYC Controls Human Pluripotent Stem Cell Fate Decisions through Regulation of Metabolic Flux. Stem Cell. 2017;21:502-516.e9.
20. Lu V, Dahan P, Ahsan FM, Patananan AN, Roy IJ, Torres A, et al. Mitochondrial metabolism and glutamine are essential for mesoderm differentiation of human pluripotent stem cells. Cell Research 2019 29:7. 2019 Jun 12;29(7):596–8.
21. Fang Y, Li X. Metabolic and epigenetic regulation of endoderm differentiation. Trends Cell Biol. 2022 Feb 1;32(2):151–64.
22. Zaret KS, Grompe M. Generation and Regeneration of Cells of the Liver and Pancreas. Science. 2008 Dec 5;322(5907):1490–4.
23. Willnow D, Benary U, Margineanu A, Vignola ML, Konrath F, Pongrac IM, et al. Quantitative lineage analysis identifies a hepato-pancreato-biliary progenitor niche. Nature 2021 597:7874. 2021 Aug 25; 597(7874):87–91.
24. Zaret KS. Genetic programming of liver and pancreas progenitors: lessons for stem-cell differentiation. Nature Reviews Genetics 2008 9:5. 2008 May;9(5):329–40.
25. Si-Tayeb K, Lemaigre FP, Duncan SA. Organogenesis and Development of the Liver. Dev Cell. 2010 Feb 16;18(2):175–89.
26. Bastidas-Ponce A, Scheibner K, Lickert H, Bakhti M. Cellular and molecular mechanisms coordinating pancreas development. Development [Internet]. 2017 Aug 15 [cited 2024 Aug 11];144(16):2873–88. Available from: https://dx.doi.org/10.1242/dev.140756
27. Han L, Chaturvedi P, Kishimoto K, Koike H, Nasr T, Iwasawa K, et al. Single cell transcriptomics identifies a signaling network coordinating endoderm and mesoderm diversification during foregut organogenesis. [cited 2024 Aug 11]; Available from: https://doi.org/10.1038/s41467-020-17968-x
28. Kishimoto K, Iwasawa K, Sorel A, Ferran-Heredia C, Han L, Morimoto M, et al. Directed differentiation of human pluripotent stem cells into diverse organ-specific mesenchyme of the digestive and respiratory systems. Nature Protocols 2022 17:11 [Internet]. 2022 Aug 17 [cited 2024 Aug 11];17(11):2699–719. Available from: https://www-nature-com.sire.ub.edu/articles/s41596-022-00733-3
29. Arterbery AS, Bogue CW. Endodermal and mesenchymal cross talk: a crossroad for the maturation of foregut organs. Pediatric Research 2014 75:1 [Internet]. 2013 Nov 5 [cited 2024 Aug 11];75(1):120–6. Available from: https://www.nature.com/articles/pr2013201
30. Takebe T, Sekine K, Enomura M, Koike H, Kimura M, Ogaeri T, et al. Vascularized and functional human liver from an iPSC-derived organ bud transplant. Nature [Internet]. 2013 [cited 2024 Sep 18];499(7459):481–4. Available from: https://pubmed.ncbi.nlm.nih.gov/23823721/
31. Goulart E, De Caires-Junior LC, Telles-Silva KA, Araujo BHS, Kobayashi GS, Musso CM, et al. Adult and iPS-derived non-parenchymal cells regulate liver organoid development through differential modulation of Wnt and TGF-β. Stem Cell Res Ther [Internet]. 2019 Aug 15 [cited 2024 Sep 18];10(1):1–11. Available from: https://stemcellres.biomedcentral.com/articles/10.1186/s13287-019-1367-x
32. Berger DR, Ware BR, Davidson MD, Allsup SR, Khetani SR. Enhancing the functional maturity of induced pluripotent stem cell-derived human hepatocytes

by controlled presentation of cell-cell interactions in vitro. Hepatology [Internet]. 2015 Apr 1 [cited 2024 Sep 18];61(4):1370–81. Available from: https://pubmed.ncbi.nlm.nih.gov/25421237/
33. Raggi C, M'Callum MA, Pham QT, Gaub P, Selleri S, Baratang NV, et al. Leveraging interacting signaling pathways to robustly improve the quality and yield of human pluripotent stem cell-derived hepatoblasts and hepatocytes. Stem Cell Reports. 2022 Mar 8;17(3):584–98.
34. Cozzitorto C, Mueller L, Ruzittu S, Mah N, Willnow D, Darrigrand JF, et al. A Specialized Niche in the Pancreatic Microenvironment Promotes Endocrine Differentiation. Dev Cell [Internet]. 2020 Oct 26 [cited 2024 Sep 18];55(2):150-162.e6. Available from: https://pubmed.ncbi.nlm.nih.gov/32857951/
35. Lotto J, Stephan TL, Hoodless PA. Fetal liver development and implications for liver disease pathogenesis. Nature Reviews Gastroenterology & Hepatology 2023 20:9 [Internet]. 2023 May 19 [cited 2024 Aug 11];20(9):561–81. Available from: https://www.nature.com/articles/s41575-023-00775-2
36. Goessling W, Stainier DY. Endoderm specification and liver development. Methods Cell Biol. 2016 Jan 1;134:463–83.
37. Campbell SA, Stephan TL, Lotto J, Cullum R, Drissler S, Hoodless PA. Signalling pathways and transcriptional regulators orchestrating liver development and cancer. Development (Cambridge) [Internet]. 2021 Sep 1 [cited 2024 Aug 11];148(17). Available from: https://dx.doi.org/10.1242/dev.199814
38. Gérard C, Tys J, Lemaigre FP. Gene regulatory networks in differentiation and direct reprogramming of hepatic cells. Semin Cell Dev Biol. 2017 Jun 1;66:43–50.
39. Wang X, Yang L, Wang YC, Xu ZR, Feng Y, Zhang J, et al. Comparative analysis of cell lineage differentiation during hepatogenesis in humans and mice at the single-cell transcriptome level. Cell Research 2020 30:12 [Internet]. 2020 Jul 20 [cited 2024 Aug 11];30(12):1109–26. Available from: https://www.nature.com/articles/s41422-020-0378-6
40. Gordillo M, Evans T, Gouon-Evans V. Orchestrating liver development. Development [Internet]. 2015 Jun 15 [cited 2024 Aug 11];142(12):2094–108. Available from: https://dx.doi.org/10.1242/dev.114215
41. Ferdek PE, Krzysztofik D, Stopa KB, Kusiak AA, Paw M, Wnuk D, et al. When healing turns into killing – the pathophysiology of pancreatic and hepatic fibrosis. Journal of Physiology. 2022 Jun 1;600(11):2579–612.
42. Asahina K, Tsai SY, Li P, Ishii M, Maxson RE, Sucov HM, et al. Mesenchymal Origin of Hepatic Stellate Cells, Submesothelial Cells, and Perivascular Mesenchymal Cells During Mouse Liver Development. 2009; Available from: www.interscience.wiley.com
43. Asahina K, Zhou B, Pu WT, Tsukamoto H. Septum transversum-derived mesothelium gives rise to hepatic stellate cells and perivascular mesenchymal cells in developing mouse liver. Hepatology. 2011;
44. Asahina K, Zhou B, Pu WT, Tsukamoto H. Septum Transversum-Derived Mesothelium Gives Rise to Hepatic Stellate Cells and Perivascular Mesenchymal Cells in Developing Mouse Liver. 2011;
45. Asahina K, Tsai SY, Li P, Ishii M, Maxson RE, Sucov HM, et al. Mesenchymal Origin of Hepatic Stellate Cells, Submesothelial Cells, and Perivascular

Mesenchymal Cells During Mouse Liver Development. 2009; Available from: www.interscience.wiley.com
46. Yin C, Evason KJ, Asahina K, Stainier DYR. Hepatic stellate cells in liver development, regeneration, and cancer. Journal of Clinical Investigation. 2013 May 1;123(5):1902–10.
47. Kitto LJ, Henderson NC. Hepatic Stellate Cell Regulation of Liver Regeneration and Repair. Hepatol Commun [Internet]. 2021 Mar 1 [cited 2024 Aug 13];5(3):358. Available from: /pmc/articles/PMC7917274/
48. Isaacson A, Spagnoli FM. Pancreatic cell fate specification: insights into developmental mechanisms and their application for lineage reprogramming. Curr Opin Genet Dev. 2021 Oct 1;70:32–9.
49. Cozzitorto C, Mueller L, Ruzittu S, Mah N, Willnow D, Darrigrand JF, et al. A Specialized Niche in the Pancreatic Microenvironment Promotes Endocrine Differentiation. Dev Cell [Internet]. 2020 Oct 26 [cited 2024 Aug 11];55(2):150-162.e6. Available from: http://www.cell.com/article/S1534580720306274/fulltext
50. Ferdek PE, Jakubowska MA. Biology of pancreatic stellate cells-more than just pancreatic cancer. 1968;
51. Loh KM, Ang LT, Zhang J, Kumar V, Ang J, Auyeong JQ, et al. Efficient endoderm induction from human pluripotent stem cells by logically directing signals controlling lineage bifurcations. Cell Stem Cell [Internet]. 2014 Feb 6 [cited 2024 Sep 18];14(2):237–52. Available from: https://pubmed.ncbi.nlm.nih.gov/24412311/
52. Ang LT, Tan AKY, Autio MI, Goh SH, Choo SH, Lee KL, et al. A Roadmap for Human Liver Differentiation from Pluripotent Stem Cells. Cell Rep [Internet]. 2018 Feb 2 [cited 2024 Sep 18];22(8):2190. Available from: /pmc/articles/PMC5854481/
53. Wong YF, Kumar Y, Proks M, Herrera JAR, Rothová MM, Monteiro RS, et al. Expansion of ventral foregut is linked to changes in the enhancer landscape for organ-specific differentiation. Nature Cell Biology 2023 25:3 [Internet]. 2023 Jan 23 [cited 2024 Sep 18];25(3):481–92. Available from: https://www.nature.com/articles/s41556-022-01075-8
54. Barsby T, Ibrahim H, Lithovius V, Montaser H, Balboa D, Vähäkangas E, et al. Differentiating functional human islet-like aggregates from pluripotent stem cells. STAR Protoc [Internet]. 2022 Dec 16 [cited 2024 Sep 12];3(4). Available from: https://pubmed.ncbi.nlm.nih.gov/36136756/
55. Breunig M, Merkle J, Wagner M, Melzer MK, Barth TFE, Engleitner T, et al. Modeling plasticity and dysplasia of pancreatic ductal organoids derived from human pluripotent stem cells. Cell Stem Cell [Internet]. 2021 Jun 3 [cited 2024 Sep 18];28(6):1105-1124.e19. Available from: https://pubmed.ncbi.nlm.nih.gov/33915078/
56. Trefts E, Gannon M, Wasserman DH. The liver. Current Biology [Internet]. 2017 Nov 6 [cited 2024 Aug 11];27(21):R1147–51. Available from: http://www.cell.com/article/S0960982217311831/fulltext
57. Manco R, Itzkovitz S. Liver zonation. J Hepatol [Internet]. 2021 Feb 1 [cited 2024 Aug 11];74(2):466–8. Available from: http://www.journal-of-hepatology.eu/article/S0168827820336138/fulltext

58. Banales JM, Huebert RC, Karlsen T, Strazzabosco M, LaRusso NF, Gores GJ. Cholangiocyte pathobiology. Nature Reviews Gastroenterology & Hepatology 2019 16:5 [Internet]. 2019 Mar 8 [cited 2024 Aug 13];16(5):269–81. Available from: https://www.nature.com/articles/s41575-019-0125-y
59. Natarajan V, Moeun Y, Kidambi S. Exploring interactions between primary hepatocytes and non-parenchymal cells on physiological and pathological liver stiffness. Biology (Basel) [Internet]. 2021 May 1 [cited 2024 Aug 11];10(5):408. Available from: https://www.mdpi.com/2079-7737/10/5/408/htm
60. Basit H, Tan ML, Webster DR. Histology, Kupffer Cell. StatPearls [Internet]. 2022 Dec 30 [cited 2024 Aug 13]; Available from: https://www.ncbi.nlm.nih.gov/books/NBK493226/
61. Kamm DR, McCommis KS. Hepatic stellate cells in physiology and pathology. Journal of Physiology. 2022 Apr 1;600(8):1825–37.
62. Poisson J, Lemoinne S, Boulanger C, Durand F, Moreau R, Valla D, et al. Liver sinusoidal endothelial cells: Physiology and role in liver diseases. J Hepatol. 2017 Jan 1;66(1):212–27.
63. Wells RG. The Portal Fibroblast—Not Just a Poor Man's Stellate Cell. Gastroenterology [Internet]. 2014 [cited 2024 Aug 14];147(1):41. Available from: /pmc/articles/PMC4090086/
64. van Berkel TJC. The role of non-parenchymal cells in liver metabolism. Trends Biochem Sci [Internet]. 1979 Sep 1 [cited 2024 Aug 11];4(9):202–5. Available from: http://www.cell.com/article/096800047990080X/fulltext
65. Malhi H, Gores GJ. Cellular and Molecular Mechanisms of Liver Injury. Gastroenterology. 2008 May 1;134(6):1641–54.
66. Tsuchida T, Friedman SL. Mechanisms of hepatic stellate cell activation. Nature Reviews Gastroenterology & Hepatology 2017 14:7 [Internet]. 2017 May 10 [cited 2024 Aug 13];14(7):397–411. Available from: https://www.nature.com/articles/nrgastro.2017.38
67. Schwabe RF, Tabas I, Pajvani UB. Mechanisms of Fibrosis Development in Nonalcoholic Steatohepatitis. Gastroenterology. 2020 May 1;158(7):1913–28.
68. Carter JK, Friedman SL. Hepatic Stellate Cell-Immune Interactions in NASH. Front Endocrinol (Lausanne). 2022 Jun 9;13.
69. Cogliati B, Yashaswini CN, Wang S, Sia D, Friedman SL. Friend or foe? The elusive role of hepatic stellate cells in liver cancer. Nature Reviews Gastroenterology & Hepatology 2023 20:10 [Internet]. 2023 Aug 7 [cited 2024 Aug 13];20(10):647–61. Available from: https://www.nature.com/articles/s41575-023-00821-z
70. Kisseleva T, Brenner D. Molecular and cellular mechanisms of liver fibrosis and its regression. Nature Reviews Gastroenterology & Hepatology 2020 18:3 [Internet]. 2020 Oct 30 [cited 2024 Aug 13];18(3):151–66. Available from: https://www.nature.com/articles/s41575-020-00372-7
71. Hernandez-Gea V, Friedman SL. Pathogenesis of liver fibrosis. Annual Review of Pathology: Mechanisms of Disease [Internet]. 2011 Feb 28 [cited 2024 Aug 13];6(Volume 6, 2011):425–56. Available from: https://www.annualreviews.org/content/journals/10.1146/annurev-pathol-011110-130246
72. Younossi ZM, Wong G, Anstee QM, Henry L. The Global Burden of Liver Disease. Clinical Gastroenterology and Hepatology [Internet]. 2023 Jul 1 [cited 2024 Aug

13];21(8):1978–91. Available from: http://www.cghjournal.org/article/S1542356523003154/fulltext
73. Lim YS, Kim WR. The Global Impact of Hepatic Fibrosis and End-Stage Liver Disease. Clinics in Liver Disease. 2008.
74. Johnson PJ, Kalyuzhnyy A, Boswell E, Toyoda H. Progression of chronic liver disease to hepatocellular carcinoma: implications for surveillance and management. BJC Reports 2024 2:1 [Internet]. 2024 May 3 [cited 2024 Aug 13];2(1):1–7. Available from: https://www.nature.com/articles/s44276-024-00050-0
75. Zhao M, Wang L, Wang M, Zhou S, Lu Y, Cui H, et al. Targeting fibrosis: mechanisms and clinical trials. [cited 2023 Jul 26]; Available from: https://doi.org/10.1038/s41392-022-01070-3
76. Lee YS, Seki E. In Vivo and In Vitro Models to Study Liver Fibrosis: Mechanisms and Limitations. Cell Mol Gastroenterol Hepatol [Internet]. 2023 [cited 2024 Sep 16];16:355–67. Available from: https://doi.org/10.1016/j.jcmgh.2023.05.010
77. van Grunsven LA. 3D in vitro models of liver fibrosis. Adv Drug Deliv Rev. 2017 Nov 1;121:133–46.
78. Haaker MW, Vaandrager AB, Helms JB. Retinoids in health and disease: A role for hepatic stellate cells in affecting retinoid levels. Biochimica et Biophysica Acta (BBA) - Molecular and Cell Biology of Lipids. 2020 Jun 1;1865(6):158674.
79. Breitkopf K, Godoy P, Ciuclan L, Singer M V., Dooley S. TGF-beta/Smad signaling in the injured liver. Z Gastroenterol [Internet]. 2006 Jan [cited 2024 Aug 13];44(1):57–66. Available from: https://pubmed.ncbi.nlm.nih.gov/16397841/
80. Liu Y, Wen XM, Lui ELH, Friedman SL, Cui W, Ho NPS, et al. Therapeutic targeting of the PDGF and TGF-β-signaling pathways in hepatic stellate cells by PTK787/ZK22258. Laboratory Investigation 2009 89:10 [Internet]. 2009 Aug 10 [cited 2024 Aug 13];89(10):1152–60. Available from: https://www.nature.com/articles/labinvest200977
81. De Smet V, Eysackers N, Merens V, Kazemzadeh Dastjerd M, Halder G, Verhulst S, et al. Initiation of hepatic stellate cell activation extends into chronic liver disease. Cell Death Dis [Internet]. 2021 Dec 1 [cited 2024 Aug 13];12(12). Available from: /pmc/articles/PMC8627507/
82. Kisseleva T, Brenner D. Molecular and cellular mechanisms of liver fibrosis and its regression. Nature Reviews Gastroenterology & Hepatology 2020 18:3 [Internet]. 2020 Oct 30 [cited 2024 Aug 13];18(3):151–66. Available from: https://www.nature.com/articles/s41575-020-00372-7
83. Trivedi P, Wang S, Friedman SL. The Power of Plasticity-Metabolic Regulation of Hepatic Stellate Cells. Cell Metab [Internet]. 2021 Feb 2 [cited 2024 Aug 13];33(2):242–57. Available from: https://pubmed.ncbi.nlm.nih.gov/33232666/
84. Horn P, Tacke F. Metabolic reprogramming in liver fibrosis. Cell Metab [Internet]. 2024 Jul 2 [cited 2024 Aug 13];36(7):1439–55. Available from: http://www.cell.com/article/S1550413124001797/fulltext
85. Domingues R, Pereira C, Cruz MT, Silva A. Therapies for Alzheimer's disease: a metabolic perspective. Mol Genet Metab. 2021 Mar 1;132(3):162–72.
86. Zhou Y, Long D, Zhao Y, Li S, Liang Y, Wan L, et al. Oxidative stress-mediated mitochondrial fission promotes hepatic stellate cell activation via stimulating oxidative phosphorylation. Cell Death & Disease 2022 13:8 [Internet]. 2022 Aug

6 [cited 2024 Aug 13];13(8):1–15. Available from: https://www.nature.com/articles/s41419-022-05088-x
87. Ezhilarasan D. Mitochondria: A critical hub for hepatic stellate cells activation during chronic liver diseases. Hepatobiliary Pancreat Dis Int [Internet]. 2021 Aug 1 [cited 2024 Aug 13];20(4):315–22. Available from: https://pubmed.ncbi.nlm.nih.gov/33975780/
88. Chen Y, Choi SS, Michelotti GA, Chan IS, Swiderska-Syn M, Karaca GF, et al. Hedgehog controls hepatic stellate cell fate by regulating metabolism. Gastroenterology [Internet]. 2012 [cited 2024 Aug 13];143(5). Available from: https://pubmed.ncbi.nlm.nih.gov/22885334/
89. Yoneda A, Sakai-Sawada K, Niitsu Y, Tamura Y. Vitamin A and insulin are required for the maintenance of hepatic stellate cell quiescence. Exp Cell Res. 2016 Feb 1;341(1):8–17.
90. Henderson NC, Rieder F, Wynn TA. Fibrosis: from mechanisms to medicines. Nature 2020 587:7835 [Internet]. 2020 Nov 25 [cited 2024 Sep 25];587(7835):555–66. Available from: https://www.nature.com/articles/s41586-020-2938-9
91. Distler JHW, Györfi AH, Ramanujam M, Whitfield ML, Königshoff M, Lafyatis R. Shared and distinct mechanisms of fibrosis. Nature Reviews Rheumatology 2019 15:12 [Internet]. 2019 Nov 11 [cited 2024 Sep 25];15(12):705–30. Available from: https://www.nature.com/articles/s41584-019-0322-7
92. Zhao X, Kwan JYY, Yip K, Liu PP, Liu FF. Targeting metabolic dysregulation for fibrosis therapy. Nature Reviews Drug Discovery 2019 19:1 [Internet]. 2019 Sep 23 [cited 2024 Sep 25];19(1):57–75. Available from: https://www-nature-com.sire.ub.edu/articles/s41573-019-0040-5
93. Andrews TS, Atif J, Liu JC, Perciani CT, Ma XZ, Thoeni C, et al. Single-Cell, Single-Nucleus, and Spatial RNA Sequencing of the Human Liver Identifies Cholangiocyte and Mesenchymal Heterogeneity. Hepatol Commun. 2022 Apr 1;6(4):821–40.
94. Bogomolova A, Balakrishnan A, Ott M, Deep Sharma A. The Good, the Bad, and the Ugly” - About Diverse Phenotypes of Hepatic Stellate Cells in the Liver. 2024 [cited 2024 Aug 14]; Available from: https://doi.org/10.1016/j.jcmgh.2024.01.002
95. Payen VL, Lavergne A, Alevra Sarika N, Colonval M, Karim L, Deckers M, et al. Single-cell RNA sequencing of human liver reveals hepatic stellate cell heterogeneity. JHEP Reports. 2021 Jun 1;3(3):100278.
96. Ramachandran P, Dobie R, Wilson-Kanamori JR, Dora EF, Henderson BEP, Luu NT, et al. Resolving the fibrotic niche of human liver cirrhosis at single-cell level. Nature [Internet]. 2019 Nov 21 [cited 2024 Aug 14];575(7783):512–8. Available from: https://pubmed.ncbi.nlm.nih.gov/31597160/
97. He W, Huang C, Shi X, Wu M, Li H, Liu Q, et al. Single-cell transcriptomics of hepatic stellate cells uncover crucial pathways and key regulators involved in non-alcoholic steatohepatitis. Endocr Connect [Internet]. 2023 Feb 1 [cited 2024 Aug 14];12(2). Available from: https://ec.bioscientifica.com/view/journals/ec/12/2/EC-22-0502.xml
98. Wang S, Li K, Pickholz E, Dobie R, Matchett KP, Henderson NC, et al. An autocrine signaling circuit in hepatic stellate cells underlies advanced fibrosis in

nonalcoholic steatohepatitis. Sci Transl Med [Internet]. 2023 Jan 4 [cited 2024 Aug 14];15(677). Available from: https://www.science.org/doi/10.1126/scitranslmed.add3949
99. Filliol A, Saito Y, Nair A, Dapito DH, Yu LX, Ravichandra A, et al. Opposing Roles of Hepatic Stellate Cell Subpopulations in Hepatocarcinogenesis. Nature [Internet]. 2022 Oct 13 [cited 2024 Aug 14];610(7931):356. Available from: /pmc/articles/PMC9949942/
100. Senoo H, Mezaki Y, Fujiwara M. The stellate cell system (vitamin A-storing cell system). Anat Sci Int [Internet]. 2017 Sep 1 [cited 2024 Aug 14];92(4):387–455. Available from: https://pubmed.ncbi.nlm.nih.gov/28299597/
101. Ferdek PE, Jakubowska MA. Biology of pancreatic stellate cells—more than just pancreatic cancer. Pflugers Archiv [Internet]. 2017 Sep 1 [cited 2024 Aug 14];469(9):1039. Available from: /pmc/articles/PMC5554282/
102. Di Maggio F, Arumugam P, Delvecchio FR, Batista S, Lechertier T, Hodivala-Dilke K, et al. Pancreatic stellate cells regulate blood vessel density in the stroma of pancreatic ductal adenocarcinoma. Pancreatology [Internet]. 2016 Nov 1 [cited 2024 Aug 17];16(6):995. Available from: /pmc/articles/PMC5123629/
103. Coll M, Perea L, Boon R, Leite SB, Vallverdú J, Mannaerts I, et al. Generation of Hepatic Stellate Cells from Human Pluripotent Stem Cells Enables In Vitro Modeling of Liver Fibrosis. Cell Stem Cell. 2018;
104. Vallverdú J, Martínez RA, De La Torre G, Mannaerts I, Verhulst S, Smout A, et al. Directed differentiation of human induced pluripotent stem cells to hepatic stellate cells. Nat Protoc [Internet]. Available from: https://doi.org/10.1038/s41596-021-00509-1
105. de la Torre RAMG, Sancho-Bru P. Differentiation of Hepatic Stellate Cells from Pluripotent Stem Cells. Methods Mol Biol [Internet]. 2023 [cited 2024 Aug 17];2669:33–42. Available from: https://pubmed.ncbi.nlm.nih.gov/37247052/
106. Richter A, Valdimarsdottir L, Hrafnkelsdottir HE, Runarsson JF, Omarsdottir AR, Oostwaard DW Van, et al. BMP4 promotes EMT and mesodermal commitment in human embryonic stem cells via SLUG and MSX2. Stem Cells [Internet]. 2014 Mar [cited 2024 Aug 17];32(3):636–48. Available from: https://pubmed.ncbi.nlm.nih.gov/24549638/
107. Evseenko D, Zhu Y, Schenke-Layland K, Kuo J, Latour B, Ge S, et al. Mapping the first stages of mesoderm commitment during differentiation of human embryonic stem cells. Proc Natl Acad Sci U S A [Internet]. 2010 Aug 3 [cited 2024 Aug 17];107(31):13742–7. Available from: https://pubmed.ncbi.nlm.nih.gov/20643952/
108. Dorey K, Amaya E. FGF signalling: diverse roles during early vertebrate embryogenesis. Development [Internet]. 2010 Nov 15 [cited 2024 Aug 17];137(22):3731–42. Available from: https://pubmed.ncbi.nlm.nih.gov/20978071/
109. Ijpenberg A, Pérez-Pomares JM, Guadix JA, Carmona R, Portillo-Sánchez V, Macías D, et al. Wt1 and retinoic acid signaling are essential for stellate cell development and liver morphogenesis. Dev Biol. 2007 Dec 1;312(1):157–70.
110. Kumar M, Toprakhisar B, Van Haele M, Antoranz A, Boon R, Chesnais F, et al. A fully defined matrix to support a pluripotent stem cell derived multi-cell-liver

steatohepatitis and fibrosis model. Biomaterials [Internet]. 2021 Sep 1 [cited 2024 Aug 17];276. Available from: https://pubmed.ncbi.nlm.nih.gov/34304139/
111. Lucendo-Villarin B, Meseguer-Ripolles J, Drew J, Fischer L, Ma E, Flint O, et al. Development of a cost-effective automated platform to produce human liver spheroids for basic and applied research. Biofabrication [Internet]. 2020 Dec 1 [cited 2024 Aug 17];13(1). Available from: https://pubmed.ncbi.nlm.nih.gov/33007774/
112. Meseguer-Ripolles J, Kasarinaite A, Lucendo-Villarin B, Hay DC. Protocol for automated production of human stem cell derived liver spheres. STAR Protoc [Internet]. 2021 Jun 18 [cited 2024 Aug 17];2(2):100502. Available from: https://pubmed.ncbi.nlm.nih.gov/33997816/
113. Miyoshi M, Kakinuma S, Kamiya A, Tsunoda T, Tsuchiya J, Sato A, et al. LIM homeobox 2 promotes interaction between human iPS-derived hepatic progenitors and iPS-derived hepatic stellate-like cells. Scientific Reports 2019 9:1 [Internet]. 2019 Feb 14 [cited 2024 Aug 17];9(1):1–13. Available from: https://www.nature.com/articles/s41598-018-37430-9
114. Koui Y, Kido T, Ito T, Oyama H, Chen SW, Katou Y, et al. An In Vitro Human Liver Model by iPSC-Derived Parenchymal and Non-parenchymal Cells. Stem Cell Reports [Internet]. 2017 Aug 8 [cited 2024 Aug 17];9(2):490. Available from: /pmc/articles/PMC5549957/
115. Ouchi R, Togo S, Kimura M, Shinozawa T, Koido M, Koike H, et al. Modeling Steatohepatitis in Humans with Pluripotent Stem Cell-Derived Organoids. Cell Metab. 2019 Aug 6;30(2):374-384.e6.
116. Friedman SL, Pinzani M. Hepatic fibrosis 2022: Unmet needs and a blueprint for the future. Hepatology [Internet]. 2022 Feb 1 [cited 2024 Sep 18];75(2):473–88. Available from: https://pubmed.ncbi.nlm.nih.gov/34923653/
117. Tan Z, Sun H, Xue T, Gan C, Liu H, Xie Y, et al. Liver Fibrosis: Therapeutic Targets and Advances in Drug Therapy. Front Cell Dev Biol [Internet]. 2021 Sep 21 [cited 2024 Sep 16];9:730176. Available from: www.frontiersin.org
118. Rajapaksha IG, Gunarathne LS, Angus PW, Herath CB. Update on New Aspects of the Renin-Angiotensin System in Hepatic Fibrosis and Portal Hypertension: Implications for Novel Therapeutic Options. J Clin Med [Internet]. 2021 Feb 2 [cited 2024 Sep 16];10(4):1–20. Available from: /pmc/articles/PMC7916881/
119. Gong L, Wei F, Gonzalez FJ, Li G. Hepatic fibrosis: Targeting peroxisome proliferator-activated receptor alpha from mechanism to medicines. Hepatology [Internet]. 2023 Nov 1 [cited 2024 Sep 16];78(5):1625–53. Available from: https://pubmed.ncbi.nlm.nih.gov/36626642/
120. Ratziu V, Harrison SA, Francque S, Bedossa P, Lehert P, Serfaty L, et al. CLINICAL-LIVER Elafibranor, an Agonist of the Peroxisome ProliferatorLActivated ReceptorLa and Ld, Induces Resolution of Nonalcoholic Steatohepatitis Without Fibrosis Worsening. 2016 [cited 2024 Sep 16]; Available from: http://dx.doi.org/10.1053/j.gastro.2016.01.038
121. Bates J, Vijayakumar A, Ghoshal S, Marchand B, Yi S, Kornyeyev D, et al. Acetyl-CoA carboxylase inhibition disrupts metabolic reprogramming during hepatic stellate cell activation. J Hepatol [Internet]. 2020 Oct 1 [cited 2024 Sep 18];73(4):896–905. Available from: http://www.journal-of-hepatology.eu/article/S0168827820302816/fulltext

122. Simon J, Nuñez-García M, Fernández-Tussy P, Barbier-Torres L, Fernández-Ramos D, Gómez-Santos B, et al. Targeting hepatic Glutaminase 1 ameliorates Non-Alcoholic Steatohepatitis by restoring Very-Low Density Lipoproteins triglyceride assembly. Cell Metab [Internet]. 2020 Mar 3 [cited 2024 Sep 18];31(3):605. Available from: /pmc/articles/PMC7259377/
123. Peng D, Fu M, Wang M, Wei Y, Wei X. Targeting TGF-β signal transduction for fibrosis and cancer therapy. Molecular Cancer 2022 21:1 [Internet]. 2022 Apr 23 [cited 2024 Sep 16];21(1):1–20. Available from: https://molecular-cancer.biomedcentral.com/articles/10.1186/s12943-022-01569-x
124. Chen L, Ren F, Zhang H, Wen T, Piao Z, Zhou L, et al. Inhibition of glycogen synthase kinase 3β ameliorates D-GalN/LPS-induced liver injury by reducing endoplasmic reticulum stress-triggered apoptosis. PLoS One [Internet]. 2012 Sep 28 [cited 2024 Sep 18];7(9). Available from: https://pubmed.ncbi.nlm.nih.gov/23028846/
125. Shi Z, Ren M, Rockey DC. Myocardin and myocardin-related transcription factor-A synergistically mediate actin cytoskeletal-dependent inhibition of liver fibrogenesis. Am J Physiol Gastrointest Liver Physiol [Internet]. 2020 [cited 2024 Sep 18];318(3):G504–17. Available from: https://pubmed.ncbi.nlm.nih.gov/31928221/
126. Sakai N, Kamimura K, Miyamoto H, Ko M, Nagoya T, Setsu T, et al. Letrozole ameliorates liver fibrosis through the inhibition of the CTGF pathway and 17β-hydroxysteroid dehydrogenase 13 expression. J Gastroenterol [Internet]. 2023 Jan 1 [cited 2024 Sep 18];58(1):53–68. Available from: https://pubmed.ncbi.nlm.nih.gov/36301364/
127. Pantazis CB, Yang A, Lara E, McDonough JA, Blauwendraat C, Peng L, et al. A reference human induced pluripotent stem cell line for large-scale collaborative studies Graphical abstract. Stem Cell [Internet]. 2022 [cited 2024 Aug 13];29:1685-1702.e22. Available from: https://doi.org/10.1016/j.stem.2022.11.004
128. Castaño J, Bueno C, Jiménez-Delgado S, Roca-Ho H, Fraga MF, Fernandez AF, et al. Generation and characterization of a human iPSC cell line expressing inducible Cas9 in the “safe harbor” AAVS1 locus. Stem Cell Res [Internet]. 2017 May 1 [cited 2024 Sep 18];21:137. Available from: /pmc/articles/PMC5446316/
129. Ölander M, Wiśniewski JR, Artursson P. Cell-type-resolved proteomic analysis of the human liver. Liver Int [Internet]. 2020 Jul 1 [cited 2024 Sep 18];40(7):1770–80. Available from: https://pubmed.ncbi.nlm.nih.gov/32243721/
130. Zhang DY, Goossens N, Guo J, Tsai MC, Chou HI, Altunkaynak C, et al. A hepatic stellate cell gene expression signature associated with outcomes in hepatitis C cirrhosis and hepatocellular carcinoma after curative resection. Gut [Internet]. 2016 Oct 1 [cited 2024 Sep 18];65(10):1754–64. Available from: https://pubmed.ncbi.nlm.nih.gov/26045137/
131. Boukhtouche F, Mariani J, Tedgui A. The “CholesteROR” Protective Pathway in the Vascular System. Arterioscler Thromb Vasc Biol [Internet]. 2004 Apr 1 [cited 2024 Sep 18];24(4):637–43. Available from: https://www.ahajournals.org/doi/10.1161/01.ATV.0000119355.56036.de
132. Molenaar MR, Haaker MW, Vaandrager AB, Houweling M, Helms JB. Lipidomic profiling of rat hepatic stellate cells during activation reveals a two-stage

process accompanied by increased levels of lysosomal lipids. Journal of Biological Chemistry [Internet]. 2023 Apr 1 [cited 2024 Aug 24];299(4). Available from: http://www.jbc.org/article/S0021925823001746/fulltext
133. Mederacke I, Hsu CC, Troeger JS, Huebener P, Mu X, Dapito DH, et al. Fate-tracing reveals hepatic stellate cells as dominant contributors to liver fibrosis independent of its etiology. Nat Commun [Internet]. 2013 [cited 2024 Sep 18];4:2823. Available from: /pmc/articles/PMC4059406/
134. Graupera I, Isus L, Coll M, Pose E, Díaz A, Vallverdú J, et al. Molecular characterization of chronic liver disease dynamics: From liver fibrosis to acute-on-chronic liver failure. JHEP Reports [Internet]. 2022 Jun 1 [cited 2024 Aug 24];4(6). Available from: /pmc/articles/PMC9079303/
135. Martínez RA, De La Torre G, Vallverdú J, Xu Q, Ariño S, Aguilar-Bravo B, et al. Trajectory Analysis of Hepatic Stellate Cell Differentiation Reveals Metabolic Regulation of Cell Commitment and Fibrosis. bioRxiv [Internet]. 2024 Feb 17 [cited 2024 Aug 24];2024.02.15.577777. Available from: https://www.biorxiv.org/content/10.1101/2024.02.15.577777v1
136. Trapnell C, Cacchiarelli D, Grimsby J, Pokharel P, Li S, Morse M, et al. Pseudo-temporal ordering of individual cells reveals dynamics and regulators of cell fate decisions. Nat Biotechnol [Internet]. 2014 [cited 2024 Aug 26];32(4):381. Available from: /pmc/articles/PMC4122333/
137. Li XY, Zhai WJ, Teng CB. Notch Signaling in Pancreatic Development. Int J Mol Sci [Internet]. 2016 Jan 1 [cited 2024 Sep 18];17(1). Available from: /pmc/articles/PMC4730293/
138. Adams JM, Jafar-Nejad H. The Roles of Notch Signaling in Liver Development and Disease. Biomolecules [Internet]. 2019 Oct 1 [cited 2024 Sep 18];9(10). Available from: /pmc/articles/PMC6843177/
139. Jung Y, Bauer G, Nolta JA. Concise Review: Induced Pluripotent Stem Cell-Derived Mesenchymal Stem Cells: Progress Toward Safe Clinical Products. Stem Cells [Internet]. 2012 Jan [cited 2024 Aug 28];30(1):42. Available from: /pmc/articles/PMC3784250/
140. Madrid M, Lakshmipathy U, Zhang X, Bharti K, Wall DM, Sato Y, et al. Considerations for the development of iPSC-derived cell therapies: a review of key challenges by the JSRM-ISCT iPSC Committee. Cytotherapy. 2024 Jun 12;
141. Chen CXQ, Abdian N, Maussion G, Thomas RA, Demirova I, Cai E, et al. Standardized Quality Control Workflow to Evaluate the Reproducibility and Differentiation Potential of Human iPSCs into Neurons. SSRN Electronic Journal [Internet]. 2021 Mar 18 [cited 2024 Aug 28]; Available from: https://papers.ssrn.com/abstract=3804839
142. Pang L. Toxicity testing in the era of induced pluripotent stem cells: A perspective regarding the use of patient-specific induced pluripotent stem cell–derived cardiomyocytes for cardiac safety evaluation. Curr Opin Toxicol. 2020 Oct 1;23–24:50–5.
143. Ellis J, Bhatia M. iPSC Technology: Platform for Drug Discovery. Clin Pharmacol Ther [Internet]. 2011 May 1 [cited 2024 Aug 28];89(5):639–41. Available from: https://onlinelibrary.wiley.com/doi/full/10.1038/clpt.2011.22
144. Perea L, Coll M, Sancho-Bru P. Assessment of Liver Fibrotic Insults In Vitro. Methods in Molecular Biology [Internet]. 2015 Jan 1 [cited 2024 Aug

28];1250:391–401. Available from: https://link.springer.com/protocol/10.1007/978-1-4939-2074-7_30
145. Coll M, Perea L, Boon R, Leite SB, Vallverdú J, Mannaerts I, et al. Generation of Hepatic Stellate Cells from Human Pluripotent Stem Cells Enables In Vitro Modeling of Liver Fibrosis. Cell Stem Cell [Internet]. 2018 Jul 5 [cited 2023 Mar 14];23(1):101-113.e7. Available from: https://pubmed.ncbi.nlm.nih.gov/30049452/
146. Hiramatsu S, Morizane A, Kikuchi T, Doi D, Yoshida K, Takahashi J. Cryopreservation of Induced Pluripotent Stem Cell-Derived Dopaminergic Neurospheres for Clinical Application. J Parkinsons Dis [Internet]. 2022 [cited 2024 Aug 28];12(3):871. Available from: /pmc/articles/PMC9108593/
147. Zhang JZ, Belbachir N, Zhang T, Liu Y, Shrestha R, Wu JC. Effects of Cryopreservation on Human Induced Pluripotent Stem Cell-Derived Cardiomyocytes for Assessing Drug Safety Response Profiles. Stem Cell Reports. 2021 Jan 12;16(1):168–81.
148. Vallverdú J, Martínez García de la Torre RA, Mannaerts I, Verhulst S, Smout A, Coll M, et al. Directed differentiation of human induced pluripotent stem cells to hepatic stellate cells. Nature Protocols 2021 16:5 [Internet]. 2021 Apr 16 [cited 2023 Mar 14];16(5):2542–63. Available from: https://www-nature-com.sire.ub.edu/articles/s41596-021-00509-1
149. Nakano Y, Saijou E, Itoh T, Tanaka M, Miyajima A, Kido T. Development of a high throughput system to screen compounds that revert the activated hepatic stellate cells to a quiescent-like state. Scientific Reports 2024 14:1 [Internet]. 2024 Apr 12 [cited 2024 Aug 28];14(1):1–9. Available from: https://www.nature.com/articles/s41598-024-58989-6
150. Morimoto S, Takahashi S, Ito D, Daté Y, Okada K, Kato C, et al. Phase 1/2a clinical trial in ALS with ropinirole, a drug candidate identified by iPSC drug discovery. Cell Stem Cell [Internet]. 2023 Jun 1 [cited 2024 Aug 28];30(6):766-780.e9. Available from: http://www.cell.com/article/S1934590923001352/fulltext
151. Wesley BT, Ross ADB, Muraro D, Miao Z, Saxton S, Tomaz RA, et al. Single-cell atlas of human liver development reveals pathways directing hepatic cell fates. Nat Cell Biol [Internet]. 2022 Oct 1 [cited 2024 Aug 28];24(10):1487–98. Available from: https://pubmed.ncbi.nlm.nih.gov/36109670/
152. Yang W, He H, Wang T, Su N, Zhang F, Jiang K, et al. Single-Cell Transcriptomic Analysis Reveals a Hepatic Stellate Cell-Activation Roadmap and Myofibroblast Origin During Liver Fibrosis in Mice. Hepatology [Internet]. 2021 Nov 1 [cited 2024 Aug 28];74(5):2774–90. Available from: https://pubmed.ncbi.nlm.nih.gov/34089528/
153. Wandzioch E, Kolterud A, Jacobsson M, Friedman SL, Carlsson L. Lhx2 / mice develop liver fibrosis. 2004 [cited 2023 Mar 1]; Available from: www.pnas.orgcgidoi10.1073pnas.0404678101
154. Arroyo N, Villamayor L, Díaz I, Carmona R, Ramos-Rodríguez M, Muñoz-Chápuli R, et al. GATA4 induces liver fibrosis regression by deactivating hepatic stellate cells. 2021 [cited 2023 Mar 1]; Available from: https://doi.org/10.1172/jci.
155. Nakano Y, Kamiya A, Sumiyoshi H, Tsuruya K, Kagawa T, Inagaki Y. A Deactivation Factor of Fibrogenic Hepatic Stellate Cells Induces Regression of

Liver Fibrosis in Mice. Hepatology [Internet]. 2020 Apr 1 [cited 2023 Mar 1];71(4):1437–52. Available from: https://pubmed.ncbi.nlm.nih.gov/31549421/
156. Bates J, Vijayakumar A, Ghoshal S, Marchand B, Yi S, Kornyeyev D, et al. Acetyl-CoA carboxylase inhibition disrupts metabolic reprogramming during hepatic stellate cell activation. J Hepatol. 2020 Oct 1;73(4):896–905.
157. Boukhtouche F, Mariani J, Tedgui A. The "CholesteROR" protective pathway in the vascular system. Arterioscler Thromb Vasc Biol [Internet]. 2004 Apr [cited 2024 Aug 28];24(4):637–43. Available from: https://pubmed.ncbi.nlm.nih.gov/14751813/
158. Zhao M, Wang L, Wang M, Zhou S, Lu Y, Cui H, et al. Targeting fibrosis: mechanisms and clinical trials. Signal Transduction and Targeted Therapy 2022 7:1 [Internet]. 2022 Jun 30 [cited 2024 Aug 28];7(1):1–21. Available from: https://www.nature.com/articles/s41392-022-01070-3
159. Goldman SL, MacKay M, Afshinnekoo E, Melnick AM, Wu S, Mason CE. The impact of heterogeneity on single-cell sequencing. Front Genet [Internet]. 2019 [cited 2024 Aug 28];10(MAR). Available from: /pmc/articles/PMC6405636/
160. Tani S, Okada H, Onodera S, Chijimatsu R, Seki M, Suzuki Y, et al. Stem cell-based modeling and single-cell multiomics reveal gene-regulatory mechanisms underlying human skeletal development. Cell Rep [Internet]. 2023 Apr 25 [cited 2024 Aug 28];42(4). Available from: https://pubmed.ncbi.nlm.nih.gov/36965484/
161. Bogomolova A, Balakrishnan A, Ott M, Sharma AD. "The Good, the Bad, and the Ugly" – About Diverse Phenotypes of Hepatic Stellate Cells in the Liver. Cell Mol Gastroenterol Hepatol. 2024 Jan 1;17(4):607–22.
162. Fuchs E, Blau HM. Tissue Stem Cells: Architects of Their Niches. Cell Stem Cell [Internet]. 2020 Oct 10 [cited 2024 Aug 28];27(4):532. Available from: /pmc/articles/PMC7861346/
163. Zhang Y, Guo A, Lyu C, Bi R, Wu Z, Li W, et al. Synthetic liver fibrotic niche extracts achieve in vitro hepatoblasts phenotype enhancement and expansion. iScience [Internet]. 2021 Nov 19 [cited 2024 Aug 28];24(11):103303. Available from: http://www.cell.com/article/S2589004221012724/fulltext
164. Grockowiak E, Korn C, Rak J, Lysenko V, Hallou A, Panvini FM, et al. Different niches for stem cells carrying the same oncogenic driver affect pathogenesis and therapy response in myeloproliferative neoplasms. Nature Cancer 2023 4:8 [Internet]. 2023 Aug 7 [cited 2024 Aug 28];4(8):1193–209. Available from: https://www.nature.com/articles/s43018-023-00607-x
165. Lotto J, Drissler S, Cullum R, Wei W, Setty M, Bell EM, et al. Single-Cell Transcriptomics Reveals Early Emergence of Liver Parenchymal and Non-parenchymal Cell Lineages. Cell [Internet]. 2020 Oct 29 [cited 2024 Aug 28];183(3):702-716.e14. Available from: https://pubmed.ncbi.nlm.nih.gov/33125890/
166. Han L, Chaturvedi P, Kishimoto K, Koike H, Nasr T, Iwasawa K, et al. Single cell transcriptomics identifies a signaling network coordinating endoderm and mesoderm diversification during foregut organogenesis. Nature Communications 2020 11:1 [Internet]. 2020 Aug 27 [cited 2024 Aug 28];11(1):1–16. Available from: https://www.nature.com/articles/s41467-020-17968-x

167. Huang S. Non-genetic heterogeneity of cells in development: more than just noise. Development [Internet]. 2009 Dec 12 [cited 2024 Aug 28];136(23):3853. Available from: /pmc/articles/PMC2778736/

nature protocols

PROTOCOL

https://doi.org/10.1038/s41596-021-00509-1

Check for updates

Directed differentiation of human induced pluripotent stem cells to hepatic stellate cells

Julia Vallverdú[1,5], Raquel A. Martínez García de la Torre[1,5], Inge Mannaerts[2], Stefaan Verhulst[2], Ayla Smout[2], Mar Coll[1,3], Silvia Ariño[1], Teresa Rubio-Tomás[1], Beatriz Aguilar-Bravo[1], Celia Martínez-Sánchez[1], Delia Blaya[1], Catherine M. Verfaillie[4,6]✉, Leo A. van Grunsven[2,6]✉ and Pau Sancho-Bru[1,3,6]✉

Hepatic stellate cells (HSCs) are nonparenchymal liver cells responsible for extracellular matrix homeostasis and are the main cells involved in the development of liver fibrosis following injury. The lack of reliable sources of HSCs has hence limited the development of complex in vitro systems to model liver diseases and toxicity. Here we describe a protocol to differentiate human induced pluripotent stem cells (iPSCs) into hepatic stellate cells (iPSC-HSCs). The protocol is based on the addition of several growth factors important for liver development sequentially over 12 d. iPSC-HSCs present phenotypic and functional characteristics of primary HSCs and can be expanded or frozen and used to perform high-throughput in vitro studies. We also describe how to coculture iPSC-HSCs with hepatocytes, which self-assemble into three-dimensional (3D) hepatic spheroids. This protocol enables the generation of HSC-like cells for in vitro modeling and drug screening studies.

Introduction

The liver is a complex organ containing not only hepatocytes—parenchymal cells that are the main cell type of the organ—but also nonparenchymal cells, including hepatic stellate cells (HSCs), Kupffer cells (liver macrophages) and liver sinusoidal endothelial cells (LSECs). Although hepatocytes exert the main metabolic and synthetic functions of the liver, nonparenchymal cells are essential for maintaining the structure, homeostasis and function of the organ, as well as enabling adequate response to tissue injury and inflammation[1].

HSCs are located in the space of Disse among hepatocytes and LSECs. In healthy liver, HSCs are in a quiescent state, which is characterized by low proliferative and metabolic activity. In the quiescent state, they participate in the homeostasis of the extracellular matrix (ECM) and store retinyl esters in their cytoplasmic lipid droplets[2]. When the liver is injured, HSCs become activated, acquire a myofibroblast phenotype and participate in the wound-healing response of the tissue[1,3]. If damage is acute or limited, the phenotype of HSCs can revert to a quiescent state, or they die by apoptosis or by natural killer cell activity[4]. However, when damage persists, activated HSCs become proliferative and contractile, secrete proinflammatory and profibrogenic cytokines and increase the production of ECM components, thus becoming the main cell type responsible for the development of liver fibrosis[3].

The need for nonparenchymal cells in biomedical and biotechnological applications is increasing with the development of new complex in vitro systems to study liver toxicity and disease modeling, as well as the generation of liver devices containing parenchymal and nonparenchymal cells[5,6]. Currently, the most reliable source of human HSCs is primary HSCs, which can be obtained from human liver resections. Shortcomings, however, include the complexity of the isolation process, the shortage of healthy livers and the high variability among donors. Moreover, the use of primary HSCs is hampered by their limited proliferative capacity and rapid activation when seeded in culture plates, far beyond the activation state of HSCs in fibrotic livers[7,8]. As an alternative to primary cultures, cell

[1]Institut d'Investigacions Biomèdiques August Pi i Sunyer (IDIBAPS), Barcelona, Spain. [2]Liver Cell Biology research group, Faculty of Medicine and Pharmacy, Vrije Universiteit Brussel (VUB), Brussels, Belgium. [3]Centro de Investigación Biomédica en Red de Enfermedades Hepáticas y Digestivas (CIBERehd), Barcelona, Spain. [4]Stem Cell Institute Leuven, Leuven, Belgium. [5]These authors contributed equally: Julia Vallverdú, Raquel A. Martínez García de la Torre. [6]These authors jointly supervised this work: Catherine M. Verfaillie, Leo A. van Grunsven, Pau Sancho-Bru.
✉e-mail: catherine.verfaillie@kuleuven.be; lvgrunsv@vub.be; psancho@clinic.cat

lines such as LX-2 have been used to study liver fibrosis in vitro, but they have an intrinsic activated phenotype, and their genetic profiles differ from those of primary HSCs[9,10].

Recently, several papers have described the differentiation of induced pluripotent stem cells (iPSCs) to hepatocyte- and cholangiocyte-like cells[11–13]; however, these did not produce non-parenchymal cells. We recently generated HSC-like cells from human iPSCs (iPSC-HSCs) and used this method to produce 2D and 3D culture models of fibrosis and drug toxicity[14]. In this protocol, we provide additional details of how to differentiate human iPSC to HSC-like cells and coculture these cells with hepatocytes to generate hepatic spheroids.

Development of the protocol

While little is known about the embryonic development of HSCs in humans, studies in animal models have provided important information regarding the origin of fetal HSCs. On day E9.5 of mouse embryogenesis, mesenchymal cells derived from mesoderm, which are situated in the septum transversum mesenchyme, differentiate to mesothelial cells. At day E11.5, these cells migrate to the liver surface, generating fetal HSCs and perivascular mesenchymal cells[15,16]. However, the cytokines and factors implicated in the differentiation of HSCs are not well defined. We developed a differentiation protocol based on the addition of several growth factors that have been described to play an important role during embryonic and fetal liver development. Bone morphogenetic proteins (BMPs), which belong to the transforming growth factor-beta (TGFβ) family, induce differentiation of embryonic stem cells to a mesodermal state[17]. In the early stages of mouse embryogenesis (day E9.5), a member of the TGFβ family, BMP4, is highly expressed in the septum transversum mesenchyme. Evseenko et al. demonstrated that BMP4 is required for the generation of a multipotent mesoderm progenitor population from human ESCs[18]. We therefore stimulated iPSCs with BMP4 to start our differentiation protocol, to induce the development of a mesodermal precursor state.

Other factors, such as fibroblast growth factor (FGF) family members, are involved in mesoderm induction. The presence of FGFs induces differentiation of iPSCs to hepatic progenitor cells, and FGFs have been shown to be involved in the proliferation and expansion of mesenchymal stem cells[19,20]. In mouse models, FGF1 plays an important role during gastrulation, showing that homozygous mutant embryos for the FGF1 receptor develop an aberrant mesodermal pattern during gastrulation[21]. Other authors demonstrated that FGF3 is also necessary during the first stages of early mesoderm induction[22,23]. Therefore, we added FGF1 and FGF3 at day 4 of culture to further enhance mesoderm formation.

As a final stage, we cultured cells with palmitic acid and retinol to promote HSC differentiation, maturation and retinyl ester accumulation, an important characteristic of primary HSCs[24,25]. As described by Asahina et al., activated leukocyte cell adhesion molecule-positive ($ALCAM^+$) cells were able to differentiate to HSCs when treated with retinol and palmitic acid[16]. The important role of retinol for HSC development was also described by Ijpenberg et al., who demonstrated that depletion of Raldh2, a factor related to retinol metabolism, impaired the differentiation of HSCs in mice[26].

Comparison with other methods

The main sources of HSCs that are currently used are primary cells obtained from human liver resections and commercial cell lines (LX-2). However, they present some limitations, such as the difficulty of isolation and expansion of primary HSCs and, for cell lines, an overactivated phenotype[7–10]. The use of HSCs derived from iPSCs has several advantages. The main advantage is that iPSCs can be expanded extensively, allowing the generation of large numbers of progeny for high-throughput in vitro assays. Moreover, obtaining HSCs from multiple different patient-specific iPSCs can enable their use in personalized medicine strategies[27].

Alternative approaches have also been reported to generate HSC-like cells from iPSCs. Koui et al. described the generation of $ALCAM^+$ progenitor HSCs from human iPSCs. These progenitor HSCs were able to sustain hepatic progenitor cell maturation in a coculture system[28]. Moreover, $ALCAM^+$ progenitor HSC-like cells could be expanded and further differentiated to mature HSC-like cells following inhibition of the Rho signaling pathway. Miyoshy et al. obtained HSC-like cells that stored vitamin A following 6 d of differentiation. When exposed to fibrogenic stimuli, the resulting HSC-like cells developed an activated phenotype. The maturation of the HSC progeny could be enhanced by coculturing with iPSC-derived hepatic progenitor cells[29]. Cells obtained following these strategies also promoted hepatocyte maturation in coculture studies, and thus, alternative approaches can be used to model liver physiology and diseases[30,31].

Following a different experimental approach, Ouchi et al. generated HSC-like cells by codifferentiating parenchymal and nonparenchymal cells from PSCs. These complex organoids were composed of hepatocytes, HSCs and Kupffer cells coderived from human PSCs. The differentiation protocol recapitulates liver bud formation, and 31% of the resulting cells express HSC markers. This approach allows direct generation of liver organoids without the need to optimize the coculture and results in the production of a multicellular liver model fully derived from PSCs[32].

As in the first two studies[28,29], our approach[14] is based on a directed differentiation protocol to obtain a HSC-like cell population. Although the other studies used similar factors, such as BMP4 or FGFs, to induce differentiation, timing and culture conditions are different, and the extent of characterization of the resulting cells varies between them. In our protocol, the option to passage and cryopreserve iPSC-HSCs adds flexibility to downstream experimental designs. Thus, direct comparison of the methodologies is challenging, and it cannot yet be determined whether a particular methodology is better. Direct side-by-side comparison and better characterization of the phenotype and function of the final population of cells are required to determine the best procedure to obtain HSC-like cells from iPSCs.

Applications of HSCs derived from iPSCs

iPSC-HSCs have the potential to be used in multiple applications. They represent a new source of HSC-like cells that can be used to evaluate the role of HSCs in wound healing, and in fibrogenic and inflammatory responses. The differentiated cells can be aggregated with hepatocyte cell lines, and thus, cell–cell interactions can be modeled that might facilitate the understanding of liver physiology and enable the development of in vitro models of chronic liver diseases. In addition, iPSC-HSCs can be used for toxicity assays, drug screening and discovery in both 2D and 3D systems. Additionally, this differentiation protocol could be adapted to facilitate the generation of pericytes from other organs. Finally, the differentiation part of the protocol may facilitate the study of human embryonic development of HSCs. Since iPSCs can be genetically modified, iPSC-HSCs can also be used to study the role of specific genes in human liver development and disease[30,31].

Limitations of our protocol

Although mesenchymal and mesothelial markers are expressed progressively during the differentiation of iPSCs[14], greater knowledge of the process might enable the protocol to be further optimized and better determine whether the differentiation is similar to the development of human HSCs that occurs in the embryo. Despite the fact that iPSC-HSCs present a similar phenotype and functionality to primary HSCs, at the end of the protocol we obtain a mix of cells with different degrees of platelet-derived growth factor receptor beta (PDGFRβ) expression.

Although differentiated cells are transcriptionally less activated than cultured primary HSCs, they show higher expression of activation markers than do quiescent primary HSCs, indicating that iPSC-HSCs have to some extent an activated phenotype[14]. Moreover, passaging or thawing iPSC-HSCs enhances their activation phenotype. For these reasons, the iPSC-HSCs generated via this protocol are not suitable as a model of completely quiescent HSCs. Therefore, further studies that modify or provide an alternative protocol are required if less activated iPSC-HSCs are needed, particularly for passage and cryopreserved cells.

Experimental design

We have optimized the concentration of cytokines and reagents, as well as the timing of the procedure, to obtain HSC-like cells derived from human iPSCs. The procedure begins by describing the thaw and maintenance of iPSCs (Steps 1–8). The preparation of iPSCs for induction of differentiation is described in Steps 9–17. Induction of iPSCs differentiation toward HSC-like cells, which takes 12 d, is described in Steps 18–25. At the end of the differentiation, iPSC-HSCs can be expanded, cryopreserved, stimulated, or cocultured with hepatocytes to form spheroids (described from Step 26 onward).

iPSCs are seeded at 15,000 cells per cm^2 in a 12-well plate coated with growth-factor reduced matrigel (Matrigel) and are maintained in Essential 8 Medium (E8 medium). Once iPSCs achieve 70% confluence, the liver differentiation medium (LdM) together with the different sequential growth factors is added to induce differentiation, according to Table 1.

Mesodermal induction is initiated by adding BMP4 until day 4 of differentiation. This is associated with a decreased expression of pluripotency markers such as octamer-binding transcription factor 4

Table 1 | Scheme of the differentiation protocol indicating all the medium changes

Day	Treatment	Analysis
0	LdM + 2 µL of BMP4 per mL of LdM	Collect one well for qPCR analysis, two for PDGFRβ FACS analysis and one for vitamin A FACS analysis
2	LdM + 2 µL of BMP4 per mL of LdM	NA
4	LdM + 2 µL of BMP4 + 2 µL of FGF1 + 2 µL of FGF3 per mL of LdM	Collect one well for qPCR analysis
6	LdM + 2 µL of FGF1 + 2 µL of FGF3 + 1 µL retinol + 1 µL palmitic acid per mL of LdM	NA
8	LdM + 1 µL retinol + 1 µL palmitic acid per mL of LdM	Collect one well for qPCR analysis, two for PDGFRβ FACS analysis and one for vitamin A FACS analysis
10	LdM + 1 µL retinol + 1 µL palmitic acid per mL of LdM	Collect one well for qPCR
12	LdM + 1 µL retinol + 1 µL palmitic acid per mL of LdM	Collect one well for qPCR analysis, two for PDGFRβ FACS analysis and one for vitamin A FACS analysis

At each medium change, cells should first be washed with DPBS (−/−).

(*OCT4*)[14]. On day 4 of differentiation, FGF1 and FGF3 are added together with BMP4. On day 6, BMP4 is removed and cells are cultured in retinol and palmitic acid medium, also containing FGF1 and FGF3, to promote a mesenchymal and mesothelial phenotype, which is characterized by the expression of platelet-derived growth factor receptor alpha (*PDGFRα*), ecto-5′-nucleotidase (*CD73*) and neurotrophin receptor p75 (*P75NTR*)[14,33,34]. On day 8, FGF1 and FGF3 are removed and the culture is maintained in medium containing only retinol and palmitic acid until day 12 to promote expression of HSCs markers, such as *PDGFRβ*, protocadherin 7 (*PCHD7*) and collagen type 1, alpha 1 (*COL1α1*) among others[14]. A schematic representation of the differentiation protocol and representative images of cell confluence and morphology changes are shown in Fig. 1a. As shown by Coll et al., transcriptomic, phenotypic and functional characterization of iPSC-HSCs demonstrated that HSCs derived from iPSCs mimic the primary cell phenotype and properties[14].

We recommend monitoring differentiation efficiency by flow cytometry (FACS) analysis of PDGFRβ expression and vitamin A incorporation (described in Box 1) at various time points during differentiation (Fig. 2a). We suggest evaluating the expression of the main HSC markers by quantitative polymerase chain reaction (qPCR) and immunofluorescence, as shown in Fig. 1b and Fig. 2c, respectively. Appropriate markers to compare derived cells with hepatocytes, quiescent and fibrogenic HSCs, are detailed in Table 2. Details of the methods, primers and antibodies we used can be found in Tables 3 and 4. For further technical details, see the manufacturer's instructions.

At the end of differentiation, 500,000–600,000 iPSC-HSCs are usually present in each well of a 12-well plate. Differentiated cells can be expanded, cryopreserved, stimulated, or cocultured with hepatocytes to model liver fibrosis in vitro following the schemes shown in Fig. 3a. Additional assays, such as inflammatory stimulation and toxicity studies that have been successfully undertaken using the cells generated, are described in Coll et al.[14]. Two different human iPSCs lines, BJ1 (made in house and used in this study) and from Sigma, have been successfully differentiated in two different laboratories, and both showed similar gene expression patterns[35]. This differentiation protocol can also be used in embryonic cell lines such as H9, demonstrating the robustness of the protocol[14,35]. It is also inexpensive and has a shorter differentiation time (only 12 d) than that for the differentiation protocols of other hepatic cell types, such as hepatocytes or cholangiocytes[11–13].

Procedure

FACS analysis of PDGFRβ

▲ **CRITICAL** Program the centrifuge at 4 °C. Warm trypsin-EDTA 0.25% and medium containing 10% FBS before starting.

1 Detach cells from two wells as described in Step 26A(i–iii).

2 Resuspend cells in 3 mL of cold DMEM Glutamax, and place 1 mL in each of three FACS tubes for analysis of autofluorescence, isotype and PDGFRβ.

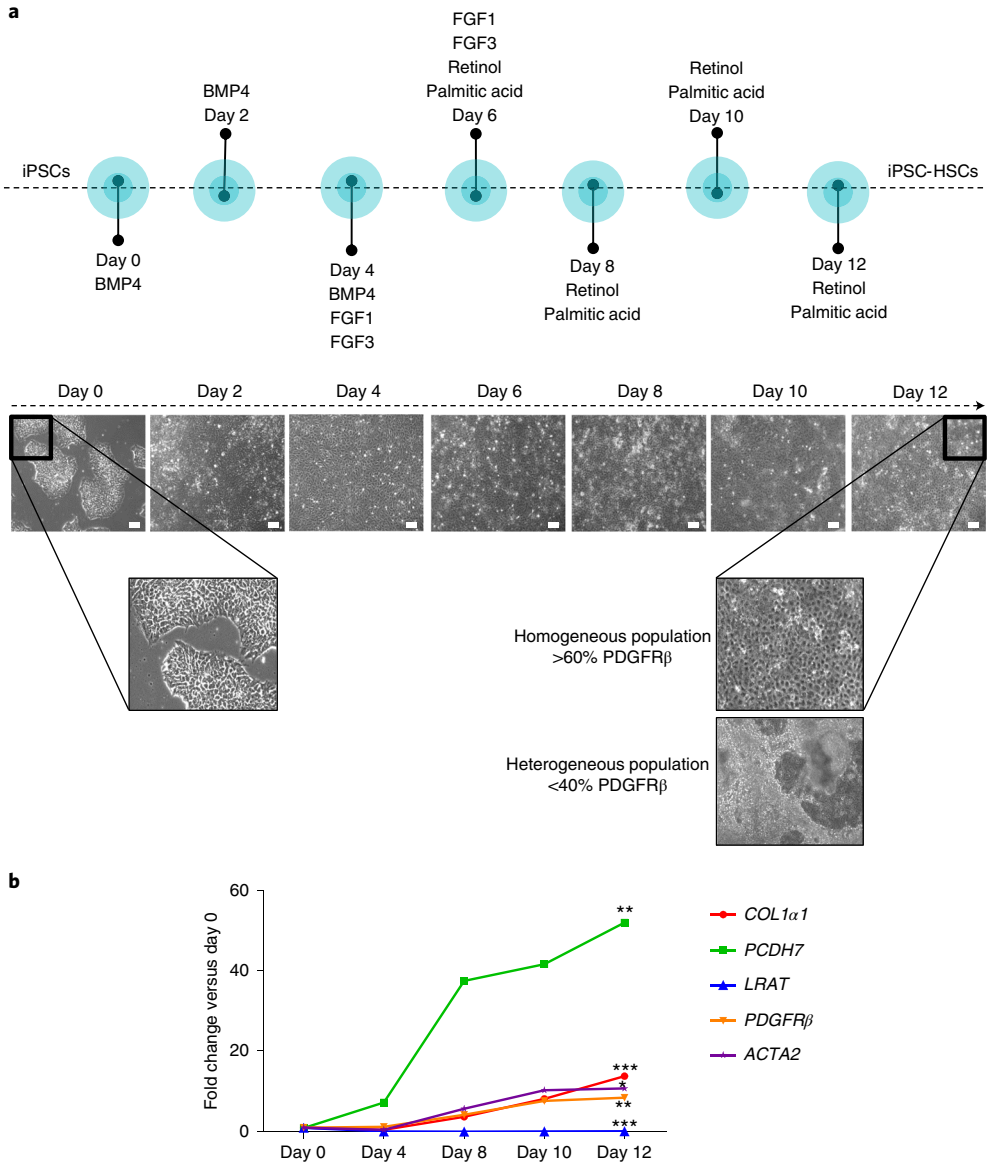

Fig. 1 | Time course of the 12-d differentiation protocol. a, Schematic representation indicating which growth factors and cytokines (BMP4, FGF1, FGF3, retinol and palmitic acid) are included at different timepoints. Microscopy images show the changes in cell morphology observed during differentiation. Scale bars, 100 μm. Homogeneous and heterogeneous final populations are shown as representative images of good and poor differentiation. **b**, Gene expression of *COL1α1*, *PCDH7*, *LRAT*, *PDGFRβ* and *ACTA2* assayed by qPCR in samples taken on days 0, 4, 8, 10, and 12 of the differentiation protocol. qPCR was undertaken following the manufacturer's instructions and using the materials and reagents detailed in Table 3. Experiment performed in five independent differentiations. $^*P < 0.05$ compared with day 0 by *t*-test.

3 Add DPBS (–/–) to the top of each tube to wash the cells.
4 Centrifuge at 300*g* for 5 min at 4 °C.
5 Discard the supernatant and add 100μL of cold FACS buffer to each tube. Resuspend cells and, in dark conditions, add 1 μL of each antibody to isotype and PDGFRβ tubes.
▲ **CRITICAL STEP** The final volume of antibodies will depend on the cell concentration. For this analysis, we optimized two wells of a 12-well plate at the end of differentiation (~340,000 cells) and found the best dilution to be 1:100.
6 Incubate for 30 min at RT under photoprotected conditions. At the end of the incubation, add DPBS (–/–) to the top of the tube to wash the cells.
7 Centrifuge at 300*g* for 5 min at 4 °C.

Box 1 | Flow cytometry analysis of PDGFRβ and vitamin A across differentiation ● Timing 1 h 30 min

Additional materials required for flow cytometry

Antibodies and reagents

- PE mouse anti-human CD140b clone 28D4 (BD PharMingen, cat. no. 558821 RRID: AB_397132)
- PE mouse IgG2a, κ isotype control clone MOPC-173 (Biolegend, cat. no. 400214 RRID: AB_326460)
- FACs tubes (BD Biosciences, cat. no. 352052)
- Sodium azide Natriumazid (Sigma, cat. no. S2002)
- MACS SmartStrainer (100μm) (Milteny Biotec, cat. no. 130-098-463)
- FACS buffer: 2% FBS, 1% sodium azide and DPBS (−/−). Filter the solution with a 0.22 μm filter. Once prepared, keep it at 4 °C for up to 2 months.

Equipment

- FACSCanto II cytometer and GACSDiva software (BD Biosciences)
- BD FACSDiva software (BD PharMingen, http://www.bdbiosciences.com/us/home)

8 Discard the supernatant and resuspend cells in 200 μL of FACS buffer and perform FACS analysis. Follow the gate strategy described in Fig. 2a to analyze the percentage of PDGFRβ-positive cell population.
▲ **CRITICAL STEP** When detaching cells, Matrigel can also be released. Filter the final solution with a cell strainer of 100 μm to avoid Matrigel obstructing the cytometer.

Flow Cytometry analysis of vitamin A

▲ **CRITICAL** Warm trypsin-EDTA 0.25% and medium containing 10% FBS before starting.

1 Detach one well of cells as described in Step 26A(i–iii).
2 After centrifugation at 300*g* for 5 min at 4 °C, remove and discard the supernatant.
3 Add DPBS (–/–) to the top of the tube to wash cells.
4 Centrifuge at 300*g* for 5 min at 4 °C.
5 Discard the supernatant and resuspend cells in 200 μL of FACS buffer. Transfer cell suspension to a FACS tube.
6 As for PDGFRβ FACS analysis, select the singlet population by SSC-A and FSC-A. Detect vitamin A storage positive cells by assessing cells that are autofluorescent at 350–450/50-A, as autofluorescence at this wavelength is an indication that cells contain vitamin A. Figure 2b shows the percentage of vitamin A storage positive cells typically obtained on days 0, 8 and 12 of the differentiation. iPSCs cells can be run as a negative control for autofluorescence.

Expertise needed to implement this protocol

Any student or postdoctoral fellow with iPSCs culture experience can use this protocol. All equipment is standard to most cell culture facilities, and reagents can be purchased from standard scientific companies.

Materials

Reagents

Biological reagents

iPSC

We have successfully used the human BJ1 iPSC line that was generated in the laboratory of Catherine Verfaillie, from human fibroblast (ATCC CRL-252228; RRID: CVCL_3653). The results shown here are from that line[36].

Differentiated HepaRG cells

We use HPR116215-TA08 purchased from Biopredic (RRID: CVCL_9720) **! CAUTION** The cell lines used should be regularly checked to ensure they are authentic and are not infected with mycoplasma. We authenticate iPSC by evaluating pluripotency markers by gene expression, FACS and immunofluorescence, formation of embryoid bodies and single-nucleotide polymorphism profiling. **! CAUTION** iPSCs research should always be conducted in accordance with all relevant governmental and institutional guidelines and regulations, depending on each country.

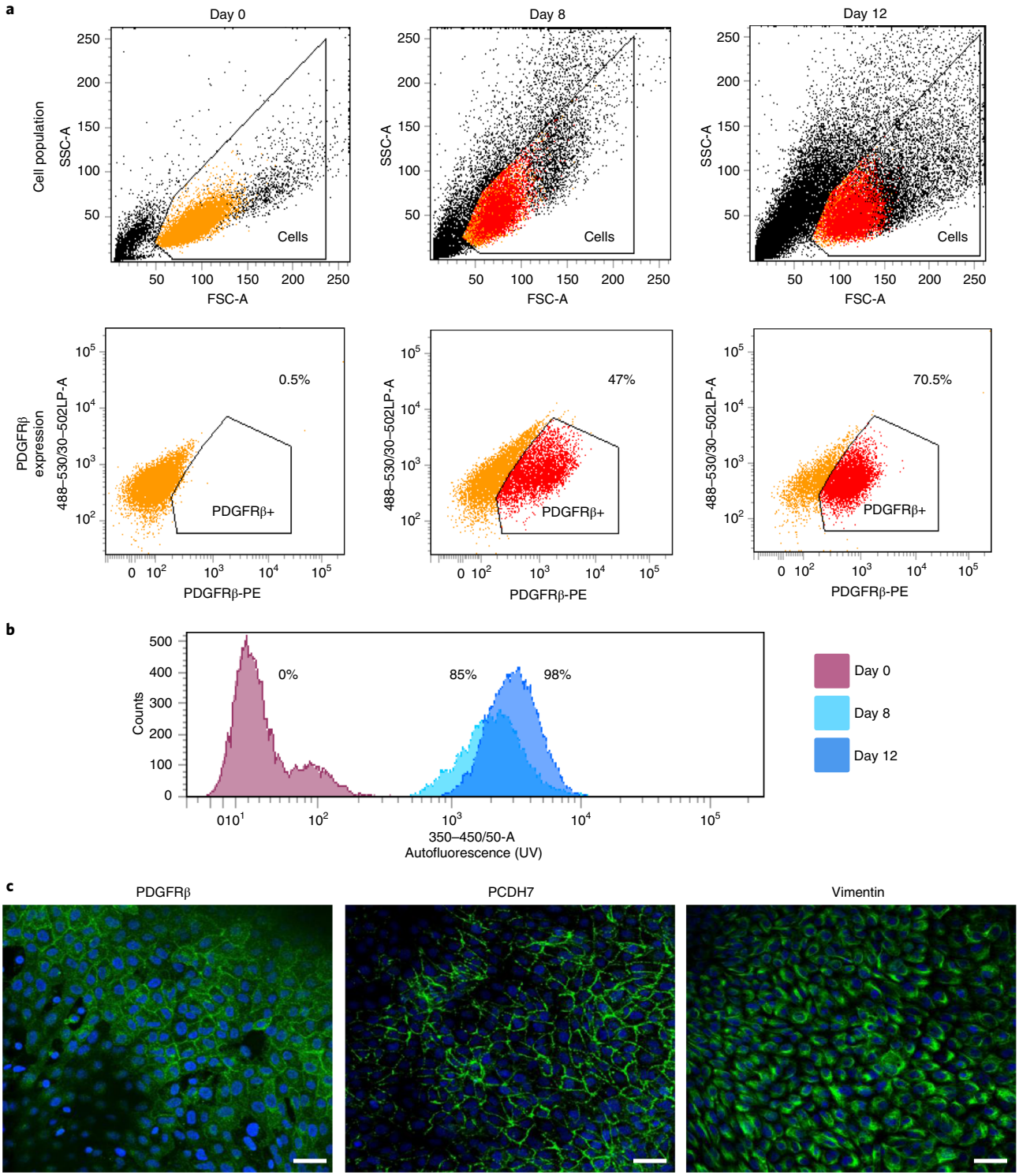

Fig. 2 | Characterization of iPSCs differentiation to HSC-like cells. a, Representative flow cytometry plots of total cell population and PDGFRβ-positive cells on days 0, 8 and 12 of the differentiation. PDGFRβ antibody and isotype antibody were used in a 1:100 dilution as indicated in Box 1. **b**, Representative histogram of flow cytometry analysis of the expression of vitamin A at days 0, 8 and 12 as indicated in Box 1. **c**, Representative immunofluorescence confocal images of PDGFRβ, PCDH7 and vimentin in iPSC-HSCs at day 12. Details of the antibodies used are given in Table 4. PDGFRβ antibody was used at a 1:50 dilution, PCDH7 antibody was used at a 1:100 dilution, vimentin antibody was used at a 1:100 dilution, and Hoechst (blue) was used at a 1:2000 dilution. Secondary antibodies (goat anti-mouse and donkey anti-rabbit) were used at a final dilution of 1:500. Scale bars, 100 μm.

Table 2 | Main hepatocytes, quiescent and fibrogenic HSC markers used for gene expression analysis

Hepatocytes	Quiescent HSCs	Fibrogenic HSCs
Albumin	*LRAT*	*LOXL2*
CYP3A4	*PPARγ*	*COL1α1*
GSTA1	*SPARCL*	*COL3α1*
SLCO1B1		*ACTA2*
	PDGFRβ	*PDGFRβ*
	PCDH7	*PCDH7*

Table 3 | Additional materials we use for qPCR analysis

Oligonucleotides	Reference	Company
GAPDH	Hs99999905_m1	Thermo Fisher Scientific
PCDH7	Hs00941345_m1	Thermo Fisher Scientific
LRAT	Hs00428109_m1	Thermo Fisher Scientific
SMAD7	Hs00178696_m1	Thermo Fisher Scientific
LOX	Hs00184700_m1	Thermo Fisher Scientific
ACTA2	Hs00909449_m1	Thermo Fisher Scientific
COL1α1	Hs00164004_m1	Thermo Fisher Scientific
PDGFRβ	Hs00182163_m1	Thermo Fisher Scientific
P75NTR	Hs00609976_m1	Thermo Fisher Scientific
Other reagents		
RNeasy Micro Kit	Cat. no. 74004	QIAGEN
High-capacity cDNA reverse transcription kit	Cat. no. 4368813	Applied Biosystems
TaqMan Fast Advanced Master Mix	Cat. no. 4444556	Thermo Fisher Scientific
TaqMan gene expression assay	Cat. no. 4351372	Thermo Fisher Scientific
Equipment		
PTC-100 programmable thermal controller	Cat. no. 78299-1	MJ Research, INC
Applied Biosystems 7900HT fast real-time PCR system	Cat. no. 4329001	Applied Biosystems

Coating reagents

- Vitronectin (VTN-N) recombinant human protein, truncated (Thermo Fisher Scientific, cat. no. A14700)
- Corning Matrigel Growth Factor Reduced (GFR) basement membrane matrix, LDEV-free (Cultek, cat. no. 356230)

Cell culture medium

- Essential 8 Medium (E8 medium; Thermo Fisher Scientific, cat. no. A1517001)
- Dulbecco's modified Eagle's medium (DMEM), low glucose, pyruvate (Thermo Fisher Scientific, cat. no. 31885)
- DMEM, high glucose, GlutaMAX supplement, pyruvate (Thermo Fisher Scientific, cat. no. 31966)
- MCDB 201 medium (Sigma, cat. no. M66770)
- L-Ascorbic acid 2-phosphate sesquimagnesium salt hydrate (L-ascorbic acid) (Sigma, cat. no. A8960)
- Insulin-transferrin-selenium 100× (ITS-G; Invitrogen, cat. no. 41400045)
- Linoleic acid-albumin from bovine serum albumin (LA-BSA; Sigma, cat. no. L9530)
- 2-Mercaptoethanol (50 mM) (Invitrogen, cat. no. 31350)
- Dexamethasone (Sigma, cat. no. D1756)
- Penicillin–streptomycin mixture (P/S; LONZA, cat. no. 17-603E)

Table 4 | Additional materials we use for immunofluorescence analysis

Antibodies	Reference	Company
Recombinant Anti-PDGFR beta antibody [Y92] - C-terminal	Cat. no. ab32570 (RRID: AB_777165)	Abcam
Anti-PCDH7 antibody [OTI2G6]	Cat. no. ab139274 (RRID: AB_2868608)	Abcam
Novocastra Liquid Mouse Monoclonal Antibody Vimentin	Cat. no. NCL-VIM-V9 (RRID: AB_442141)	Leica Biosystems
Goat anti-Mouse IgG (H+L) Cross-Adsorbed Secondary Antibody, Alexa Fluor 488	Cat. no. A-11001 (RRID: AB_2534088)	Thermo Fisher Scientific
Alexa Fluor 488 AffiniPure Donkey Anti-Rabbit IgG (H+L)	Cat. no. 711-545-152 (RRID: AB_2313584)	Jackson Immuno Research
Hoechst 33342, trihydrochloride, trihydrate – 10 mg mL^{-1}	Cat. no. H3570 (RRID: AB_2868610)	Thermo Fisher Scientific
Other reagents		
Formaldehyde solution 4%, buffered, pH 6.9	Cat. no. 100496	Millipore Corporation
Equipment		
Laser scanning confocal spectral high-speed multiphoton microscope	TCS SP8 MP	Leica
Fiji ImageJ	https://imagej.net/Using_Fiji	Fiji

- HepaRG thawing medium supplement (HTM; Biopredic, cat. no. ADD670049)
- HepaRG serum-free induction medium supplement (HFM; Biopredic, cat. no. ADD650036)
- Gibco fetal bovine serum, qualified, One Shot format (FBS; Life Technologies, cat. no. A3160802)

Cytokines

- Bone morphogenic protein (BMP4; R&D, cat. no. 314-BP-010)
- Fibroblast growth factor 1 (FGF1; R&D, cat. no. 232-FA-025)
- Fibroblast growth factor 3 (FGF3; R&D, cat. no. 1206-F3-025)
- Retinol (Sigma, cat. no. R7632-100MG)
- Palmitic acid (Sigma, cat. no. P0500)

Other reagents

- UltraPure 0.5 M EDTA (Life Technologies, cat. no. 15575-020)
- Dulbecco's phosphate-buffered saline (DPBS) without calcium/magnesium; DPBS (–/–) (LONZA, no. BE17-515F)
- Trypsin-EDTA (0.25%), phenol red (trypsin; Thermo Fisher Scientific, cat. no. 25200056)
- TGF-beta 1 human recombinant (TGFβ; Peprotech, cat. no. AF-100-21C)
- Dimethyl sulfoxide (DMSO; Sigma, cat. no. 5879-100mL)
- 10× PBS buffer 4 L OmniPur (Calbiochem-Merck, cat. no. 6505-OP)
- Absolute ethanol for molecular biology (Panreac Quimica, cat. no. A8075.1000)
- 2-Propanol (Panreac Química, cat. no. 8710901212)
- Chloridric acid 35% (AGROVIN, cat. no. 141019)
- Bovine serum albumin (BSA; Sigma, cat. no. A8806)
- Citric acid 99% (Sigma, cat. no. C0759)

Equipment

- Orbital cell shaker suited for use in cell culture incubator (Infors Celltron benchtop shaker for CO_2 incubator Ø 25 mm, cat. no. INF69222)
- Integra Viaflo assist base unit (Integra, cat. no. 4500)
- Corning LSE vortex mixer with standard tube head, 230V, EU Plug (Corning, cat. no. 6776)
- Milli-Q water purification system (Millipore, cat. no. 7003/7005)
- Pipetboy Acu Classic (Cultek, cat. no. 39155000)
- Serologic tips pipettes of 5 mL, 10 mL and 25 mL (Cultek, cat. no. 4487, cat. no. 4488 and cat. no. 4489)
- Pipette tips: 10 µL, 100 µL, 200 µL and 1,000 µL (Eppendorf, cat. nos. 0030078500, 0030078543, 0030078837 and 0030077571)

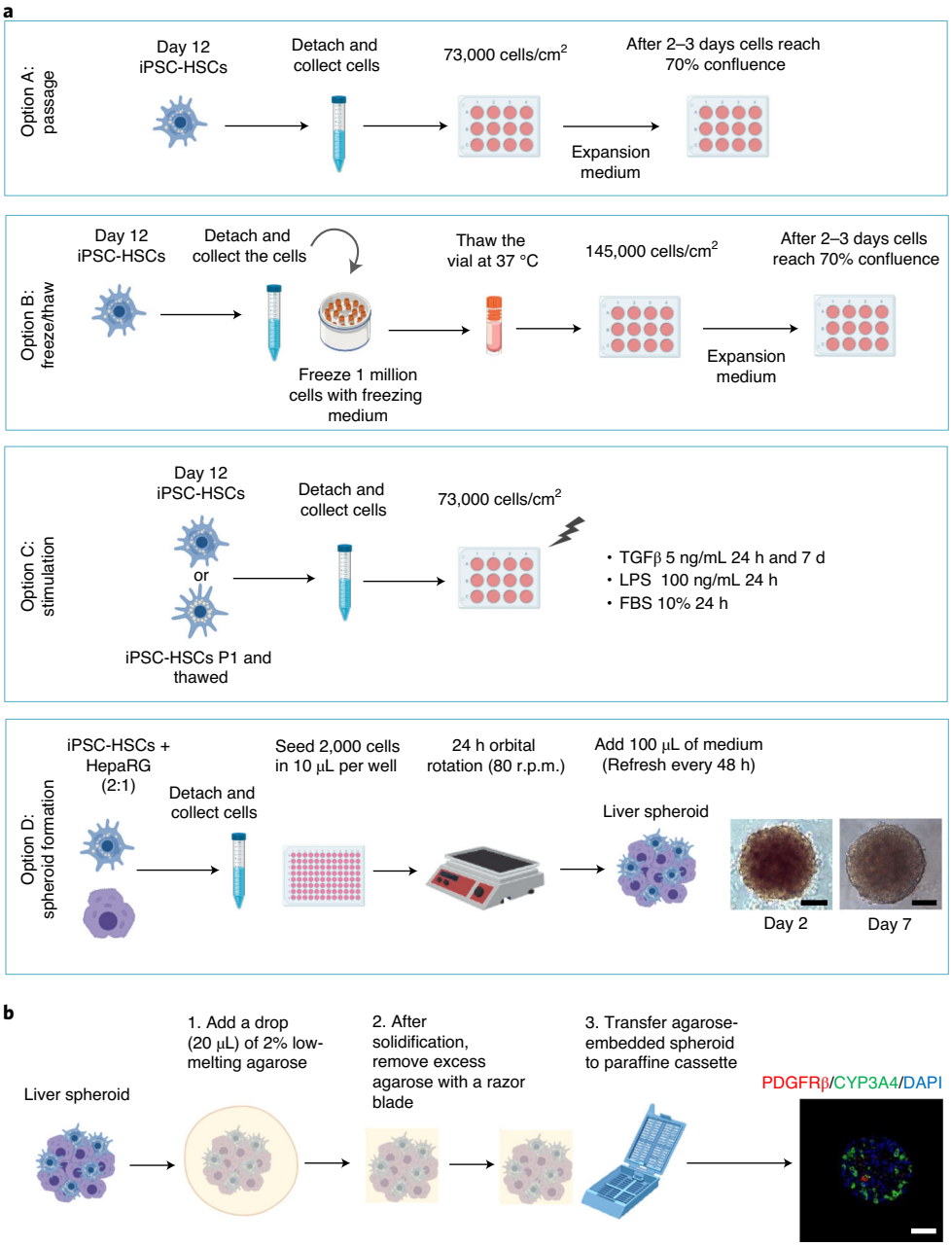

Fig. 3 | Scheme of the downstream assays with iPSC-HSCs. a, Schematic representations of the different downstream assays that can be undertaken at the end of the differentiation (Step 26). Option A: subculture and expansion of iPSC-HSCs. Option B: freezing and thawing iPSC-HSCs. Option C: stimulation of iPSC-HSCs. Option D: spheroid formation. Scale bar, 100 µm. **b**, Schematic process of spheroid embedding used for immunofluorescence analysis of spheroids for PDGFRβ antibody used in a 1:50 dilution, CYP3A4 antibody used in a 1:100 dilution and DAPI (mounted DAPI containing medium) staining. Scale bar, 100 µm. For more technical information, see Box 2.

- 10 µL graduated filter tip (sterile) (StarLab, cat. no. S1121-3810)
- CLEARLine filter tips racked sterile 100 µL (DDBiolab, cat. no. 036060CL)
- 200 µL and 1,000 µL filter tips (Labclinics, cat. nos. LAB200ULFNL and LAB1000ULFNL)
- 8-channel INTEGRA Viaflo electronic pipettes 10–300 µL and 50–1,250 µL (Integracat. no. 4623, cat. no. 4624)
- Tissue culture test plates 6 wells (TPP_Reactiva, cat. no. 92006)
- Tissue culture test plates 12 wells (TPP_Reactiva, cat. no. 92012)
- Microplate 96 well, ps, clear, sterile, u-bottom, cell-repellent surface (Greiner-Bio, cat. no. 650970)

- Stericup and Steritop vacuum-driven sterile filters (Merck, cat. no. SCGVU05RE)
- Falcon 15 mL and 50 mL tubes (Corning, cat. nos. 15430791 and 10604551)
- Eppendorf tubes 1.5 mL pyrogen free, RNase free (STARLAB, cat. no. S1615-5510)
- Acrodisc syringe filters with supor membrane 0.2 µm (Pall Life Sciences, cat. no. PN4612)
- BD Plastipak syringe Luer 20 mL 300613 (BD Plastipack, cat. no. 300613)
- Mr. Frosty freezing container (Thermo Fisher Scientific, cat. no. 5100-0001)
- Cryogenic vials (Greiner CRYOS.S, cat. no. 121263)

Software

- ZEN Lite from ZEISS Microscopy (ZEISS, https://www.zeiss.com/microscopy/us/products/microscope-software/zen-lite.html)
- GraphPad Prism 5 (GraphPad Software, http://www.graphpad.com/)

Reagent setup

Vitronectin-coated six-well plates

To coat a six-well plate, thaw a 60 µL aliquot and dilute it in 6 mL of sterile DPBS without calcium and magnesium DBPS (–/–) to give a final concentration of vitronectin of 1% (vol/vol). Resuspend, add 1 mL to each well, move the plate gently to spread the solution evenly across the well and incubate the plate at room temperature (RT; 20 °C) for 1 h or at 37 °C for 20–30 min before seeding the cells. Coated plates can alternatively be stored wrapped in parafilm at 4 °C for a maximum of 1 week. Before use, aspirate and discard excess vitronectin solution and wash the wells once with DPBS (–/–).

Matrigel-coated 12-well plates

To coat a 12-well plate, resuspend a 120 µL Matrigel aliquot in 6 mL ice-cold DMEM, low glucose, pyruvate (DMEM), to give a final Matrigel concentration of 2% (vol/vol). Add 500 µL of the solution to each well, move the plate gently to spread the solution evenly across the well and incubate the plate at RT for 1 h or at 37 °C for 20–30 min before seeding the cells. Alternatively, coated plates can be stored wrapped in parafilm at 4 °C for a maximum of 1 week. Before use, aspirate and discard excess Matrigel solution and wash the wells once with DPBS (–/–). ▲ **CRITICAL** Matrigel should be kept under cold conditions (on ice) during the whole process to avoid spontaneous polymerization.

Essential 8 Medium (E8 medium)

To prepare 500 mL of complete E8 medium, add 10 mL of Essential 8 Supplement (50×) to 490 mL of E8 medium. E8 medium supplemented medium can be stored at 2–8 °C for up to 2 weeks, according to the manufacturer's instructions.

0.5 mM EDTA

Dissolve 50 µL of UltraPure 0.5 M EDTA, pH 8, in 50 mL of DPBS (–/–) and filter with a 0.22 µm filter. EDTA should be stored at RT. Diluted EDTA can be stored at 2–8 °C for up to 6 months.

MCDB

Dissolve 8.85 g of MCDB in 500 mL of MilliQ water. Stir with magnetic bar for 10–20 min, and adjust the pH to 7.2. Filter the solution with a 0.22 µm filter. Store the dry powder medium at 2–8 °C. Once the solution is made, store it at 2–8 °C for up to 1 month.

Dexamethasone

Dissolve 5 mg in 1 mL of pure ethanol to obtain a 5,000 ng μL^{-1} stock solution. Dilute the stock dexamethasone solution to a final working concentration of 98 ng μL^{-1} in MilliQ water. Filter the solution with a 0.22 µm filter. Stock solution should be stored at –20 °C. The working solution is stable at 4 °C for up to 1 month, according to the manufacturer's instructions.

BMP4

Reconstitute the vial (10 µg) in 1 mL of 4 mM HCl containing 0.1% (wt/vol) BSA to obtain a final concentration of 10 ng μL^{-1}. Powdered cytokine can be stored for up to 12 months at –20 °C to –70 °C. After reconstitution, it can be stored for 1 month at 2–8 °C and for longer storage (3 months) at –70 °C, according to the manufacturer's instructions.

FGF1
Reconstitute the vial (25 µg) in 2.5 mL of DPBS (–/–) containing 0.1% (wt/vol) BSA to obtain a final concentration of 10 ng μL^{-1}. Powdered cytokine can be stored for up to 12 months at –20 °C to –70 °C. After reconstitution, it can be stored for 1 month at 2–8 °C and for longer storage (3 months) at – 70°C, according to the manufacturer's instructions.

FGF3
Reconstitute the vial (25 µg) in 2.5 mL of DPBS (–/–) containing 0.1% (wt/vol) BSA to obtain a final concentration of 10 ng μL^{-1}. Powder cytokine can be stored for up to 12 months at –20 °C to –70 °C. After reconstitution, it can be stored for 1 month at 2–8 °C and for longer storage (3 months) at –70 °C, according to the manufacturer's instructions.

Retinol
Reconstitute the vial (100 mg) in 0.348 mL of pure ethanol to obtain a stock solution of 1 M under dark conditions. Filter the solution with a 0.22 µm filter. Dilute it in pure ethanol to a final working concentration of 5 mM. Retinol is stable for up to 1 year at –20 °C. Once diluted, it should be stored in dark conditions at –70 °C, according to the manufacturer's instructions.

Palmitic acid
Dissolve 25.643 mg of palmitic acid in 1 mL of pure ethanol to obtain a final concentration of 0.1 M. Filter the solution with a 0.22 µm filter. Vortex the solution vigorously to dissolve it. Powder palmitic acid should be stored at RT. Working solution should be stored at –20 °C to –70 °C for up to 1 month.

TGF-β
Resuspend the vial (2 µg) in 1 mL of 10 mM citric acid at pH 3, filter the solution using a 0.22 µm filter and prepare aliquots at a final concentration of 2,000 ng mL^{-1}. Store TGF-β at –20 °C and after reconstitution at –70 °C for 3 months.

l-Ascorbic acid
Dissolve 1.45 g of L-ascorbic acid in 500 mL PBS 1× to obtain a 10 mM solution. Stir with magnetic bar for 10–20 min in dark conditions and filter with a 0.22 µm filter. L-Ascorbic acid should be stored at –20 °C for up to 2 years, according to the manufacturer's instructions.

LdM
To prepare a final volume of 500 mL, add 285 mL DMEM low glucose (can be stored at 2–8 °C for up to 12 months from date of manufacture), 200 mL of MCDB, 5 mL of P/S (store at –10 °C to –20 °C up to the expiry date according to the manufacturer's instructions), 5 mL of L-ascorbic acid, 1.25 mL of ITS-G (store at 2–8 °C for up to 2 years), 1.25 mL of LA-BSA (can be stored at 2–8 °C for up to 2 years), 0.5 mL of 2-mercaptoethanol (can be stored at 2–8 °C for up to the expiry date according to the manufacturer's instructions) and 2 mL of dexamethasone (working solution). Filter the solution with a 0.22 µm filter. This prepared medium can be maintained at 4 °C for 1 month.

Freezing medium
80% FBS (can be stored at 2–8 °C up to the expiry date) and 20% DMSO (store at RT). Filter the solution with a 0.22 µm filter.

Expansion medium
DMEM Glutamax (can be stored at 2–8 °C for up to 12 months from date of manufacture), 10% FBS and 1% P/S. Filter the solution with a 0.22 µm filter.

Low FBS medium
DMEM Glutamax, 1% FBS and 1% P/S. Filter the solution with a 0.22 µm filter.

Thawing differentiated HepaRG cells ● Timing 20 min
▲ **CRITICAL** Prewarm the HepaRG thawing medium supplement (HTM) in a 37 °C water bath.
1 Pipette 9 mL of prewarmed HTM into a sterile tube.
2 Under the laminar flow hood, briefly twist the cap of the cryovial a quarter turn (do not open it completely) to release the internal pressure and then close it again.

3 Quickly transfer the cryovial to a water bath set at 37 °C. Do not submerge it completely, and be careful not to allow water to penetrate the cap.
4 Aseptically transfer the 'semi'-thawed HepaRG cell suspension into the tube containing 9 mL of the prewarmed HTM.
5 Rinse out the cryovial once with ~1 mL of HTM, and return the resulting suspension to the tube.
6 Centrifuge the differentiated HepaRG cell suspension for 3 min at 500*g* at RT.
7 Aspirate the supernatant, and resuspend the differentiated HepaRG cell pellet gently with HTM in 5 mL. ▲ **CRITICAL STEP** Do not try to dissociate any large clusters of cells.

Procedure

Maintenance of human iPSCs ● Timing 3–4 d (15 min for plating cells)

▲ **CRITICAL** E8 medium should be warmed at RT prior to thawing the cells. Keep the vitronectin-coated plate inside the incubator for a minimum of 20 min before seeding the cells. Ensure that the water bath is at 37 °C before starting the procedure.

1 Thaw the cells at 37 °C by swirling the cryovial in a water bath. When only a small ice crystal remains, which is usually after 1–2 min, take the cryovial out of the water bath.
2 Spray the cryovial with ethanol and place it in the laminar flow hood.
3 Add 0.5 mL of warmed E8 medium in the cryovial, and transfer the cells into a 15 mL conical tube containing 9.5 mL of E8 medium.
4 Centrifuge cell suspension at 300*g* for 5 min at RT.
5 Meanwhile, wash the vitronectin-coated six-well plate with DPBS (–/–).
6 Remove the supernatant, and resuspend cells in 2 mL of E8 medium. Pipette carefully as it is important to maintain cell clusters. Transfer the cell suspension to one well.
? TROUBLESHOOTING
7 Incubate cells at 37 °C and replace medium daily with fresh E8 medium.
? TROUBLESHOOTING
8 When cells reach 70% confluence, move to next step to disaggregate the colonies.
? TROUBLESHOOTING

Preparation of human iPSCs for HSC differentiation ● Timing 1–3 d (15 min for plating cells)

▲ **CRITICAL** One well of undifferentiated iPSCs must be expanded into a full 6-well plate to have enough cells to start a 12-well plate differentiation. To expand iPSCs, cells have to be detached following Steps 9–12.

▲ **CRITICAL** Coat 12-well plate with Matrigel before starting iPSC differentiation. Incubate the plate at 37 °C for at least 20 min before seeding the cells. Also, warm E8 medium and EDTA solution at RT.

9 Remove E8 medium from cells and rinse the wells with DPBS (–/–) to wash them.
10 Remove DPBS (–/–) and add 1 mL of EDTA 0.5 mM to each well. Wait 1–2 min at 37 °C or 2–3 min at RT.
11 Check the cell colonies under the microscope. Colonies should start to detach.
12 Aspirate and discard EDTA. Add 1 mL of E8 medium to each well, and disrupt the cell colonies by gently pipetting the medium several times using a 1 mL pipette. Collect the cell suspension in a 15 mL tube.
13 Wash the Matrigel-coated plate with DPBS (–/–).
14 Count the cells collected in the 15 mL tube. Plate cells at a density of 15,000 cells per cm^2 in E8 medium.
▲ **CRITICAL** 720,000 iPSCs are usually obtained from 1.5 wells of a six-well plate at 70% confluence but can differ between iPSC cell lines.
? TROUBLESHOOTING
15 Move the plate to distribute the cells homogeneously.
16 Keep the cells in the incubator.
17 Change the medium daily to fresh E8 medium until the culture reaches 70% confluency (this usually takes 1–2 d). Then go on to the next step to start the differentiation protocol.
? TROUBLESHOOTING

iPSC differentiation to HSCs ● Timing 12 d for complete the differentiation (10 min for medium change)

▲ CRITICAL STEP Prepare the corresponding media to the day of differentiation before starting culture work and warm it up at RT or 37 °C. Medium changes should be performed every 48 h as detailed in Table 1.

18 Remove and discard E8 medium, and wash cells once with DPBS (–/–).
▲ CRITICAL STEP Washing is important to remove any remaining E8 medium.

19 Add LdM supplemented with 2 μL per mL of medium of BMP4 stock solution (10 ng μL^{-1}). This is considered day 0 of differentiation. To characterize the cells at the start of differentiation, we recommend you follow the analyses described in Box 1 for flow cytometry analysis and Table 3 for qPCR. Use one well for qPCR analysis, two wells for flow cytometry analysis of PDGFRβ, and one well for flow cytometry analysis of vitamin A.

20 On day 2, remove and discard medium, wash cells with DPBS (–/–) and add LdM supplemented with 2 μL of BMP4 stock solution (10 ng μL^{-1}) per mL of LdM.

21 On day 4, remove and discard medium, wash the cells with DPBS (–/–) and add LdM supplemented with 2 μL of BMP4, 2 μL of FGF1 and 2 μL of FGF3 stock solutions (10 ng μL^{-1}) per mL of LdM. We recommend you use one well of cells for qPCR analysis (Table 3).
▲ CRITICAL On day 4, the wells should be completely confluent.

22 On day 6, remove and discard medium, wash cells with DPBS (–/–) and add LdM containing 2 μL of FGF1 and 2μL of FGF3 stock solutions (10 ng μL^{-1}), 1 μL of retinol working solution (5 mM) and 1 μL of palmitic acid stock solution (0.1 M) per mL of LdM.
▲ CRITICAL Palmitic acid is difficult to dilute, and therefore, the stock solution might precipitate. Vortex the solution before use.

23 On day 8, remove and discard the medium, wash cells with DPBS (–/–) and add LdM supplemented with 1 μL of retinol working solution (5 mM) and 1 μL of palmitic acid stock solution (0.1 M) per mL of LdM. We recommend you use one well for qPCR analysis (Table 3) and another three wells for FACS analysis to check the expression of PDGFRβ and presence of vitamin A as described in Box 1.
▲ CRITICAL STEP Around 50% and 90% of cells should express PDGFRβ and contain vitamin A, respectively. If the expression of PDGFRβ is less than 25%, do not continue with the differentiation.

24 On day 10, remove and discard the medium, wash cells with DPBS (–/–) and add LdM supplemented with 1 μL of retinol working solution (5 mM) and 1 μL of palmitic acid stock solution (0.1 M) per mL of LdM. We recommend you process one well for qPCR analysis (Table 3).
▲ CRITICAL The cell population should have a more homogeneous morphology compared with previous days, and lipid droplets should be visible by viewing the culture under the microscope using a 10× objective.

25 On day 12, iPSC-HSCs should have been obtained and can be used in downstream assays, as described in the next step. We also recommend one well of cells be used for qPCR analysis (Table 3) and two for PDGFRβ FACS analysis and one for vitamin A analysis as described in Box 1. At day 12, supernatant can be collected to perform ELISA analysis if required.
▲ CRITICAL STEP Around 60% of iPSC-HSCs should be positive for PDGFRβ. Close to 100% of cells should contain vitamin A.
▲ CRITICAL At the end of the differentiation, each well should contain 500,000–600,000 cells.
▲ CRITICAL Gene expression assays and immunofluorescence procedures for further characterization of the differentiation are explained in Tables 3 and 4. For more information about technical details, see the manufacturer's instructions.
▲ CRITICAL Be aware that iPSC-HSCs are not quiescent and show some degree of activation, and therefore their activation state could potentially limit downstream applications.
■ PAUSE POINT iPSC-HSCs can be incubated in the same plate until day 14 without further changes. However, we recommend to use them on day 12. Cells maintained in the same plate for more than 14 d start to detach and die.
? TROUBLESHOOTING

Downstream assays that can be undertaken with iPSC-HSCs

26 The iPSC-HSCs can now be used in a variety of ways. Follow Option A to subculture and expand iPSC-HSCs. Follow Option B to freeze and subsequently thaw iPSC-HSCs. Follow Option C to stimulate iPSC-HSCs. Follow Option D to coculture with hepatocytes and form spheroids.

(A) **Subculture and expansion of iPSC-HSCs ● Timing 2–3 d (10 min for cell passage)**

▲ **CRITICAL** A new 12-well plate coated with Matrigel should be used to expand iPSC-HSCs. Depending on the experiments to be performed, other plate types can be used. Incubate it at 37 °C for a minimum of 20 min before seeding cells. Warm the expansion medium and trypsin-EDTA 0.25% at 37 °C or RT before use.

(i) Remove and discard medium, incubate iPSC-HSCs with DPBS (–/–) for 1 min at RT, remove, and add 0.5 mL of trypsin-EDTA 0.25% to each well. Incubate cells at 37 °C for 2–3 min to detach.

▲ **CRITICAL STEP** Differentiated iPSC-HSCs are strongly attached to the Matrigel-coated plate as they secrete ECM proteins. Therefore, dissociation with trypsin might take longer than is usual for iPSCs. If cells are detached before day 8 or 10 of differentiation, dissociation times tend to be shorter (1–2 min at 37 °C). If the percentage of PDGFRβ-positive cells is less than 60%, dissociation might take longer.

(ii) Check the cells under a microscope and, when cells start detaching, add 0.5 mL per well of medium containing 10% FBS to stop the reaction. Collect the cells by gently pipetting the medium.

▲ **CRITICAL STEP** When detaching cells, Matrigel can also be released. If so, carefully remove it.

? TROUBLESHOOTING

(iii) Centrifuge at 300*g* for 5 min at RT.

(iv) During the centrifugation, wash the Matrigel precoated 12-well plate with DPBS (–/–).

(v) After centrifugation, aspirate the supernatant and add an appropriate volume of expansion medium. Usually, a cell split ratio of 1:2 for the first passage in a 12-well plate enables seeding of 73,000 cells per cm^2. The split ratio should be adapted according to the plate type and the number of wells being used.

(vi) Seed the cell suspension in the Matrigel-coated plate, move the plate to distribute cells homogeneously and place it in the incubator.

(vii) Discard and replace the medium the day after seeding and subsequently every other day with fresh expansion medium.

? TROUBLESHOOTING

(viii) After 2–3 d the wells should be ~70% confluent. They can be used for in vitro studies or expanded and passaged for a total of three passages.

▲ **CRITICAL** Passaging iPSC-HSCs promote cell activation, which could potentially limit downstream applications.

▲ **CRITICAL STEP** Passaged iPSC-HSCs can be seeded without a Matrigel coating for in vitro studies of HSC activation.

(B) **Freezing and thawing iPSC-HSCs ● Timing 2–3 d to obtain a confluent culture postthaw (30 min to freeze and 20 min to thaw)**

▲ **CRITICAL** Prepare the freezing medium and store it at 4 °C. It should be cold when added to the cell suspension. Warm trypsin-EDTA 0.25% and medium containing FBS at RT or 37 °C. Program the centrifuge at 4 °C.

(i) **Freezing**: remove and discard medium, incubate iPSC-HSCs with DPBS (–/–) for 1 min at RT, remove, and add 0.5 mL of trypsin-EDTA 0.25% to each well. Incubate cells at 37 °C for 2–3 min to detach.

▲ **CRITICAL STEP** Differentiated iPSC-HSCs are strongly attached to the Matrigel-coated plate as they secrete ECM proteins. Therefore, dissociation with trypsin might take longer than is usual for iPSCs.

(ii) Check the cells under a microscope and, when cells start detaching, add 0.5 mL per well of medium containing 10% FBS to stop the reaction. Collect the cells by gently pipetting the medium.

▲ **CRITICAL STEP** When detaching cells, Matrigel can also be released. If so, carefully remove it.

(iii) Count the collected cells.

▲ **CRITICAL STEP** Two wells of the 12-well plate should contain 1 million iPSC-HSCs, which is usually sufficient for one cryovial.

(iv) Centrifuge the cells at 300*g* for 5 min at 4 °C.

(v) Discard the supernatant and resuspend the cells with the corresponding volume of freezing medium to give a final concentration of 1 million iPSC-HSCs per mL of medium. Add 1 mL cell suspension per cryovial.

(vi) Place the cryovials rapidly into a cryofreezing container, and keep overnight at −80 °C.

(vii) After 24 h, transfer the cryovial to a liquid nitrogen tank for long-term storage.

PAUSE POINT Cells can be stored in liquid nitrogen.

(viii) **Thawing:** incubate plate precoated with Matrigel at 37 °C for at least 20 min, and also warm the expansion medium. Ensure the water bath is at 37 °C before moving to the next step. Thaw a cryovial of cells in the 37 °C water bath. When only an ice crystal remains, take the cryovial out of the bath and spray it with ethanol before placing it into the hood.

(ix) Add 0.5 mL warmed expansion medium to the cryovial, and transfer the cells to a 15 mL tube containing 9.5 mL of the same medium.

CRITICAL After thawing, cell viability should be ~70%.

(x) Centrifuge cells at 300*g* for 5 min at RT.

(xi) Meanwhile, wash the Matrigel-coated plate with DPBS (−/−).

(xii) After centrifugation, aspirate the supernatant, resuspend cells with the corresponding volume of expansion medium to plate 145,000 cells per cm^2. (As one million cells were frozen per cryovial, approximately, one cryovial should be split across two wells of a 12-well plate.) Move the plate gently to distribute cells homogeneously.

(xiii) Incubate the cells at 37 °C.

(xiv) After 24 h, discard and replace with expansion medium.

? TROUBLESHOOTING

(xv) Replace medium every 48 h until cells reach 70% confluence (this usually occurs after 2–3 d). Cells are now ready to be used for further studies.

(C) **Stimulation of iPSC-HSCs ● Timing 24 h or 7 d of stimulation (15 min for medium change)**

CRITICAL Passaged or thawed iPSC-HSCs at 70% confluence can be used.

CRITICAL Low FBS medium should be warmed before use.

(i) Remove medium, and replace it with Low FBS medium.

(ii) After 24 h incubation in Low FBS medium, aspirate and discard the medium and incubate with Low FBS medium containing TGFβ at 2.5 µL of the stock solution per mL (final concentration of 5 ng mL^{-1}).

CRITICAL Inflammatory assays can be performed by lipopolysaccharide (LPS) stimulation instead of TGFβ stimuli. Incubate the cells for 24 h with a final LPS concentration of 100 ng mL^{-1} as described in Coll et al.[14].

(iii) After 24 h or 7 d of stimulation, remove medium and harvest RNA from iPSC-HSCs for activation analysis (Table 3).

CRITICAL For chronic TGFβ stimulation, change medium every other day.

CRITICAL As a positive control for the activation of iPSC-HSCs, cells can be compared with primary HSCs. Also, passaged cells can be used as a positive control for the activation.

(D) **Spheroid formation ● Timing 21 d for the complete formation and stabilization of the culture (1 h for seeding cells and 10 min for medium refreshment every 48 h)**

CRITICAL Differentiated HepaRG cells are also required, thawed immediately prior to starting this section following the procedure described in the Materials section (Thawing differentiated HepaRG cells). For iPSC-HSCs detachment, warm up trypsin-EDTA 0.25% and medium containing FBS at RT or 37 °C.

(i) **Spheroid formation:** fill the outer wells of a cell-repellent 96-well microplate with 100 µL of DPBS (−/−) supplemented with P/S, to prevent medium evaporation during culture.

(ii) Remove and discard medium, incubate iPSC-HSCs with DPBS (−/−) for 1 min at RT, remove, and add 0.5 mL of trypsin-EDTA 0.25% to each well. Incubate cells at 37 °C for 2–3 min to detach.

CRITICAL STEP Differentiated iPSC-HSCs are strongly attached to the Matrigel-coated plate as they secret ECM proteins. Therefore, dissociation with the trypsin might take longer than is usual for iPSCs. If cells are detached before day 8 or 10 of differentiation, dissociation times tend to be shorter (1–2 min at 37 °C).

(iii) Check the cells under a microscope and, when cells start detaching, add 0.5 mL per well of medium containing 10% FBS to stop the reaction. Collect the cells by gently pipetting the medium.

CRITICAL STEP When detaching cells, Matrigel can also be released, if so, carefully remove it.

Box 2 | Immunostaining of the liver spheroids ● Timing 2 h

Procedure

Fixing spheroids

1 Remove medium (keep for ELISA analysis if desired) from the wells, and wash spheroids twice with DPBS (-/-).
2 Add 100 µL of 4% formaldehyde solution (formalin) to fix spheroids, and incubate 8 min at RT.
3 Dispose of formalin waste according to institutional disposal instructions, and wash spheroids three times with PBS 1×.
▲ **CRITICAL STEP** Fixed spheroids can be stored in PBS 1× at 4 °C for several weeks. Spheroids can be used for whole spheroid staining (conditions need to be optimized for each antibody) or can be further processed for paraffin embedding and sectioning as described in the next step.
? TROUBLESHOOTING

Embed spheroids in paraffin

4 Transfer three to six fixed spheroids per condition to a microscope slide, placing them close together. Remove as much PBS 1× as possible.
5 Carefully add a drop of ~20 µL of 2% low-melting-point agarose on top of the spheroids and leave to solidify. This should not take more than 1 min.
▲ **CRITICAL** Aim to keep the spheroids in one plane. This will allow staining, imaging and quantification of the spheroids at the same time.
6 Use a razor blade to remove excess agarose and cut into a square shape. Gently slide the agarose cube with spheroids into a paraffin embedding cassette.
7 Use a benchtop tissue processor to embed the spheroids in paraffin. Cut paraffin sections of 3–7 µm with a microtome according to Fig. 3b.

(iv) Centrifuge at 300*g* for 5 min at RT.
(v) Mix HepaRG and iPSC-HSCs in a 1:2 ratio to give a volume of 2,000 cells total per 10 µL HFM medium. Allow an extra ~10% cell mix to compensate for loss of cells and medium when using a multichannel pipette for seeding.
(vi) Carefully seed 10 µL of cell suspension mix in the center of each well of the microplate. The hydrophobic properties of the plate ensure that drop integrity is maintained during seeding and after starting the shaker in Step viii.
▲ **CRITICAL** The use of an electronic multichannel pipette is recommended to obtain uniform spheroids.
(vii) Incubate the plate for 15–30 min in a cell culture incubator to allow cells to settle at the bottom of the wells.
(viii) Place the plates on an orbital shaker suited for use in a cell culture incubator at 80 r.p.m. for 24 h.
(ix) The day after, most cells should be aggregated, forming spheroids.
▲ **CRITICAL STEP** If a large volume of cells was seeded in Step vi, more time will be needed for cells to form aggregates. Add 100 µL of HepaRG serum-free induction medium supplement (HFM) culture medium, and place the plates back on the orbital shaker inside the incubator.
? TROUBLESHOOTING
(x) Replace 90% of the HFM medium after 24 h. Subsequently replace 90% of the medium in the culture every 48 h. Follow Box 2 if you wish to fix and stain the coculture at any point during the culture.
▲ **CRITICAL STEP** Medium refreshing must be done with precision to avoid aspiration and loss of samples. Ideally, medium change is done using an electronic multichannel 1,000 µL pipette. The medium is removed by placing the pipette tip at the medium–air interface at low aspiration speed, and fresh medium is added at the lowest dispensing speed to the side of the well.
▲ **CRITICAL** After 7–14 d in culture, there should be increased hepatocyte activity due to the presence of the iPSC-HSCs[14]. From this time point onward, fibrosis or toxicity studies can be started as shown in Coll et al.[14]. Cultures can be maintained for at least 21 d with both cell types present and functional. For longer culture periods, replenish the DPBS (–/–) with P/S in the outer wells to minimize evaporation of the medium in outer wells containing spheroids.
▲ **CRITICAL** Guidance on how to carry out analysis of gene expression or immunofluorescence of liver spheroids can be found in refs. [14] and [37], Tables 2–4, Fig. 3b and Box 2.
? TROUBLESHOOTING

Troubleshooting

See Table 5 for troubleshooting guidance. Figure 1a shows examples of the morphology of cells on day 12 following successful and poor differentiations.

Table 5 | Troubleshooting table

Step	Problem	Possible reasons	Solutions
6	Cells stay as single cells or colonies do not grow	The growth rate of different cell lines can vary, as can the growth rate following cryopreservation	Incubate iPSCs for an additional day and/or adjust initial seeding density. Ensure that cell pipetting is done carefully so cell clusters are maintained. Be sure to thaw cells correctly, and do not overheat the cryovial
7	iPSCs die	Cell contamination might be impacting iPSC culture. Also, the number of cells plated or the number of colonies that have been plated can affect cell growth	Check the incubator and the reagents used. E8 medium can be supplemented with antibiotics such as P/S at a 1:1000 dilution without affecting cell growth
8	Colonies become elongated instead of rounded	The cells might be starting to differentiate and lose pluripotent characteristics	A new cryovial of iPSCs should be thawed. Note that this can happen with the addition of cold E8 medium, which can induce cell stress
14	Cells do not attach to the Matrigel-coated plate	Matrigel concentration might not be correct. Matrigel might not have been prepared in cold conditions. Plate was prepared more than 5 d ago	Check the Matrigel concentration and expiry date, and prepare the coating in cold conditions. It is also critical to ensure uniform Matrigel distribution. Ensure the correct number of iPSCs are plated and that they are viable
17	Cells do not grow sufficiently at 1–2 d of culture	Low concentration of plated cells or quality of the iPSCs. Sometimes this occurs because the Matrigel coating was not prepared correctly	Check plating cell number, quality of iPSCs and the concentration, lot and expiration of reagents. Ensure that the Matrigel-coated plate is correctly prepared and Matrigel evenly distributed across the plate
25	iPSC-HSCs differentiate suboptimally	The confluence of the cells was not ~60–70% at the start of differentiation. The Matrigel coating was not prepared correctly	Check the quality of iPSCs and the confluence as well as the distribution of the cells when starting the differentiation. It is important to move the plate after cell seeding to avoid cell accumulation in the center of the well. Growth factors and cytokines should not be stored at 4 °C for more than 1 week
26A(ii)	Differentiated cells do not detach from the culture plate	The differentiated cells might produce more ECM proteins, which can impact detaching efficiency	Check the quality of the trypsin used. Increase the time of exposure if there is a lot of ECM in the well, and be sure to pipette the medium several times across the entire well to collect the maximum number of cells. It is important to wash the cells with DPBS (−/−) for 1 min before the addition of trypsin
26A(vii)	Cells do not attach or do not grow	PDGFRβ expression is lower than 60%. Matrigel coating was not prepared correctly. Cells were incubated for more than 5 min with trypsin	Ensure medium is warmed before plating cells. Check the number of cells plated, and check cells are expressing PDGFRβ
26B(xiv)	Thawed cells do not grow well	The quality of the differentiation can affect the thawing process. Low viability before freezing the cells can affect the thawing efficiency. Also, exposure to DMSO at RT for too long can affect cell viability	Before freezing cells, check the quality of the differentiation by assessing the percentage of PDGFRβ-positive cells. Check cell viability when freezing and thawing cells. Count the number of frozen cells. Transfer the cryovials from the −80 °C freezer to a liquid nitrogen tank 24 h after freezing. After freezing, ensure a sufficient number of cells is plated. We recommend plating one vial in two wells of a 12-well plate
26D(ix)	Less than 90% of cells are integrated in a round spheroid after 24 h in culture	The quality of the differentiation can affect the capacity to form spheroids. Also, check the viability before seeding cells	If the cells do not form spheroids after 24 h in culture, the culture should be abandoned
26D(x)	Spheroids are absent	Small spheroids can be aspirated when changing medium	Carefully perform 50% medium changes, and check the pipette when aspirating. Add fresh medium carefully to the wall of the wells
Box 2	Spheroid staining is heterogeneous	Staining intensity depends on the depth of the spheroid and can vary among spheroids	Multiple spheroids need to be analyzed per condition and, preferentially, multiple sections per condition need to be stained

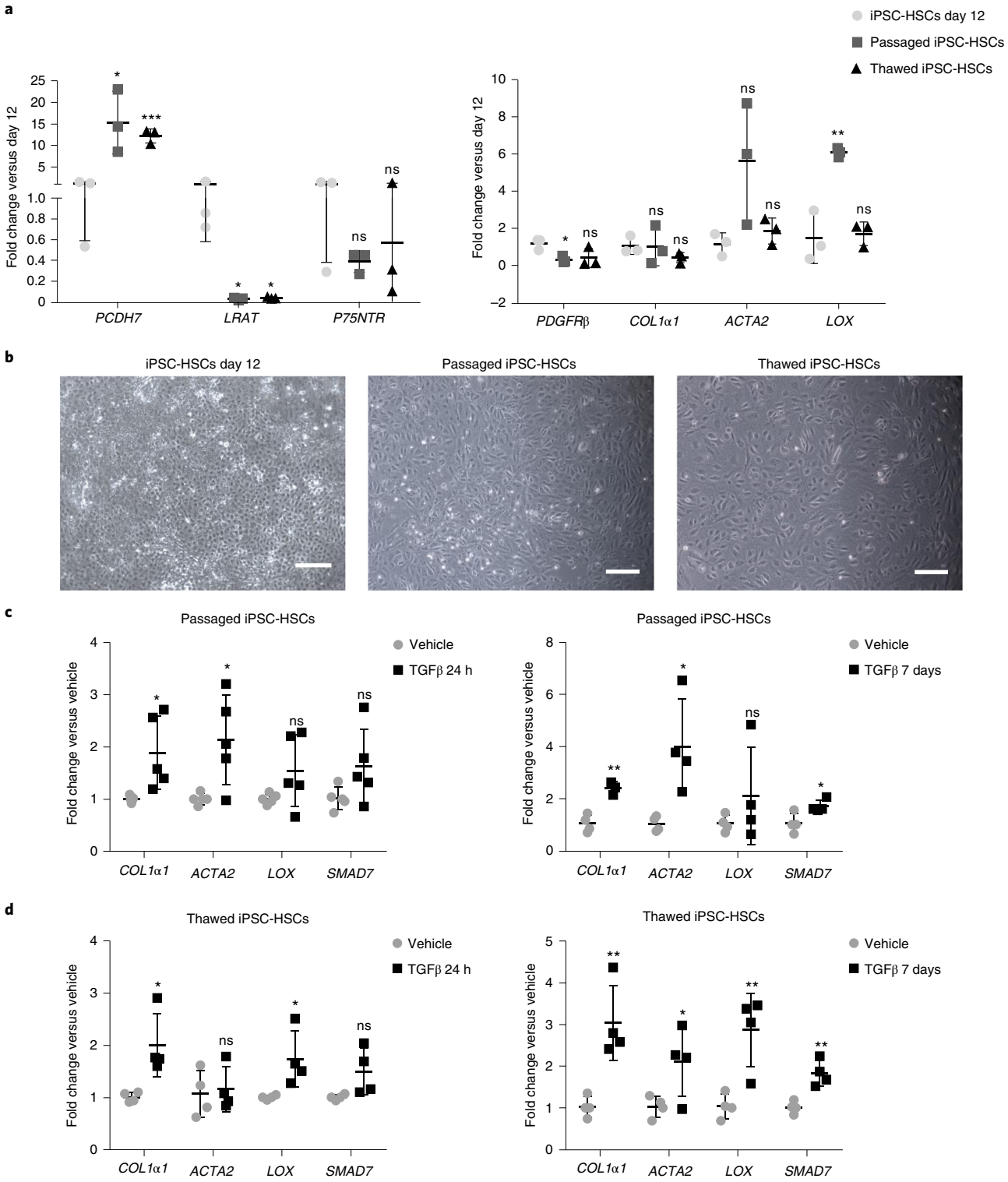

Fig. 4 | Passage and thawed iPSC-HSCs characterization and stimulation. a, Gene expression of *PCHD7*, *LRAT*, *P75NTR*, *PDGFRβ*, *COL1α1*, *ACTA2* and *LOX* in iPSC-HSCs passage 1 and thawed iPSC-HSCs compared with cells at day 12. qPCR was undertaken following the manufacturer's instructions and using the materials and reagents detailed in Table 3. Experiments were performed using three independent differentiations. *$P < 0.05$ compared with iPSC-HSCs at day 12 by *t*-test. **b**, Bright-field microscopy images of iPSC-HSCs morphology at day 12, passage 1 and thawed cells. Scale bar, 100 µm. **c**, Gene expression analysis of *COL1α1*, *ACTA2*, *LOX* and *SMAD7* in passaged iPSC-HSCs after 24 h or 7 d of TGFβ stimuli (5 ng mL^{-1}), as detailed in Step 26C(ii). qPCR was undertaken following the manufacturer's instructions and using the materials and reagents detailed in Table 3. Experiments were performed using five and four independent differentiations. *$P < 0.05$ compared with vehicle by *t*-test. **d**, Gene expression analysis of *COL1α1*, *ACTA2*, *LOX* and *SMAD7* in thawed iPSC-HSCs after 24 h or 7 d of TGFβ stimuli (5 ng mL^{-1}). qPCR was undertaken following the manufacturer's instructions and using the materials and reagents detailed in Table 3. Experiment were performed using four independent differentiations. *$P < 0.05$ compared with vehicle by *t*-test.

Anticipated results

Differentiation can be started when iPSCs plated on Matrigel-coated 12-well plate reach 70% confluence. After ~4 d of differentiation, cells should be 100% confluent (Fig. 1a).

At day 12, the percentage of PDGFRβ should be ~60–70%, while in undifferentiated cells (day 0) less than 1% of cells are PDGFRβ positive and ~50% of cells are PDGFRβ positive at day 8 (Fig. 2a). The majority (98%) of the day 12 progeny contain vitamin A, detected by autofluorescence measurement, again consistent with the acquisition of an HSC-like cell phenotype (Fig. 2b). The presence of vitamin A can also be detected in more than 85% of cells at day 8, whereas at day 0 autofluorescence is not seen. Lipid droplets should be visible under a 10× magnification microscope. In addition, the gene expression of HSC markers such as *COL1α1*, *PCDH7*, *PDGFRβ*, and actin alpha 2 smooth muscle (*ACTA2*) increases during differentiation, whereas lecithin retinol acyltransferase (*LRAT*) expression is maintained, indicative of acquisition of an HSC phenotype (Fig. 1b and Table 3). Consistent with the gene expression, day 12 iPSC-HSCs stain positive for PDGFRβ, PCDH7 and vimentin, detected by immunofluorescence using the antibodies listed in Table 4 (Fig. 2c).

iPSC-HSCs can be split and cultured with expansion medium, seeding 73,000 cells per cm^2. In addition, iPSC-HSCs progeny can be cryopreserved by freezing 1 million cells and thawing afterward in expansion medium, seeding 145,000 cells per cm^2. Once cells are 70% confluent, they can then be used for further assays. Although there are differences in the expression of some activation markers, passaged iPSC-HSCs and thawed iPSC-HSCs maintain an HSC-like morphology and the expression of constitutive markers such as PCDH7 (Fig. 4a,b). Be aware that passaged and thawed cells differ from the final population of the differentiation and are more activated. It is important to take into account the activation state of iPSC-HSCs when designing the studies, particularly those aiming at evaluating quiescent HSCs function.

As shown in Fig. 4c,d, passaged and thawed iPSC-HSCs stimulated with TGFβ for 24 h become activated, with significantly increased expression of activation markers, such as *COL1α1*, *ACTA2* and lysyl oxidase (*LOX*) and nonsignificantly SMAD family member 7 (*SMAD7*). Although modest, the induction of activation and fibrogenic genes is comparable to the differentiated cells at day 12 and primary HSCs[14]. However, when they are exposed to TGFβ for a longer period of time (7 d), expression of HSC activation markers further increases, indicating their potential use for chronic injury modeling. In addition, differentiated cells express proinflammatory genes in response to mediators such as LPS[14]. For qPCR analysis, reference Table 3.

Differentiated cells can also be cocultured at a ratio of 2:1 (iPSC-HSCs:HepaRG) with hepatocyte cell lines to generate multicellular spheroids. As shown in Fig. 3a, complete cell aggregation occurs on days 2–3, and the spheroids can be maintained 21 d for long-term in vitro studies. Under this condition, iPSC-HSCs present a reduced activation phenotype and hepatocytes maintain their metabolic profile during, at least, 21 d of culture. Further data can be found in Coll et al.[14], which describes how treatment of iPSC-HSCs-HepaRG spheroids with TGFβ, thioacetamide and acetaminophen induced expression of HSC activation markers and secretion of procollagen type I.

Altogether, these results indicate that the protocol presented here is efficient, as a large fraction of iPSC-HSCs express PDGFRβ, contain vitamin A and express the main markers of HSCs, quite closely mimicking cultured primary HSCs. Moreover, they represent a source of iPSC-HSCs to perform in vitro fibrogenic, inflammation and toxicity assays, under acute and chronic insults. In addition, the possibility of culturing iPSC-HSCs in 3D cocultures allows the generation of complex in vitro systems and the study of cell–cell interactions in liver spheroids.

Reporting Summary

Further information on research design is available in the Nature Research Reporting Summary linked to this article.

Data availability

The authors declare that all data supporting the findings of this study are available within the paper. Source data are provided with this paper.

References

1. Hernandez-Gea, V. & Friedman, S. L. Pathogenesis of liver fibrosis. *Annu. Rev. Pathol.* https://doi.org/10.1146/annurev-pathol-011110-130246 (2011).
2. Friedman, S. L. Hepatic stellate cells: protean, multifunctional, and enigmatic cells of the liver. *Physiol. Rev.* https://doi.org/10.1152/physrev.00013.2007 (2008).
3. Mederacke, I. et al. Fate tracing reveals hepatic stellate cells as dominant contributors to liver fibrosis independent of its aetiology. *Nat. Commun.* https://doi.org/10.1038/ncomms3823 (2013).
4. Issa, R. et al. Apoptosis of hepatic stellate cells: involvement in resolution of biliary fibrosis and regulation by soluble growth factors. *Gut* https://doi.org/10.1136/gut.48.4.548 (2001).
5. van Grunsven, L. A. 3D in vitro models of liver fibrosis. *Adv. Drug Deliv. Rev.* https://doi.org/10.1016/j.addr.2017.07.004 (2017).
6. Lauschke, V. M. et al. Novel 3D culture systems for studies of human liver function and assessments of the hepatotoxicity of drugs and drug candidates. *Chem. Res. Toxicol.* https://doi.org/10.1021/acs.chemrestox.6b00150 (2016).
7. Sancho-Bru, P. et al. Genomic and functional characterization of stellate cells isolated from human cirrhotic livers. *J. Hepatol.* https://doi.org/10.1016/j.jhep.2005.02.035 (2005).
8. Perea, L., Coll, M. & Sancho-Bru, P. Assessment of liver fibrotic insults in vitro. in *Protocols in In Vitro Hepatocyte Research* (eds. Vinken, M. & Rogiers, V.) 391–401 (Springer, 2015). https://doi.org/10.1007/978-1-4939-2074-7_30
9. Xu, L. et al. Human hepatic stellate cell lines, LX-1 and LX-2: new tools for analysis of hepatic fibrosis. *Gut* https://doi.org/10.1136/gut.2004.042127 (2005).
10. Herrmann, J., Gressner, A. M. & Weiskirchen, R. Immortal hepatic stellate cell lines: useful tools to study hepatic stellate cell biology and function? *J. Cell. Mol. Med.* https://doi.org/10.1111/j.1582-4934.2007.00060.x (2007).
11. Nishio, M. et al. Feeder-free and serum-free production of hepatocytes, cholangiocytes, and their proliferating progenitors from human pluripotent stem cells: application to liver-specific functional and cytotoxic assays. *Cell. Rep.* https://doi.org/10.1089/cell.2011.0064 (2018).
12. Takebe, T. et al. Vascularized and functional human liver from an iPSC-derived organ bud transplant. *Nature* https://doi.org/10.1038/nature12271 (2013).
13. Sancho-Bru, P. et al. Directed differentiation of murine-induced pluripotent stem cells to functional hepatocyte-like cells. *J. Hepatol.* https://doi.org/10.1016/j.jhep.2010.06.014 (2011).
14. Coll, M. et al. Generation of hepatic stellate cells from human pluripotent stem cells enables in vitro modeling of liver fibrosis. *Cell Stem Cell* https://doi.org/10.1016/j.stem.2018.05.027 (2018).
15. Asahina, K., Zhou, B., Pu, W. T. & Tsukamoto, H. Septum transversum-derived mesothelium gives rise to hepatic stellate cells and perivascular mesenchymal cells in developing mouse liver. *Hepatology* https://doi.org/10.1002/hep.24119 (2011).
16. Asahina, K. et al. Mesenchymal origin of hepatic stellate cells, submesothelial cells, and perivascular mesenchymal cells during mouse liver development. *Hepatology* https://doi.org/10.1002/hep.24119 (2009).
17. Richter, A. et al. BMP4 promotes EMT and mesodermal commitment in human embryonic stem cells via SLUG and MSX2. *Stem Cells* https://doi.org/10.1002/stem.1592 (2014).
18. Evseenko, D. et al. Mapping the first stages of mesoderm commitment during differentiation of human embryonic stem cells. *Proc. Natl Acad. Sci. USA* https://doi.org/10.1073/pnas.1002077107 (2010).
19. Ng, F. et al. PDGF, TGF-β, and FGF signaling is important for differentiation and growth of mesenchymal stem cells (MSCs): transcriptional profiling can identify markers and signaling pathways important in differentiation of MSCs into adipogenic, chondrogenic, and osteogenic lineages. *Blood* https://doi.org/10.1182/blood-2007-07-103697 (2008).
20. Wang, Y., Yu, X., Chen, E. & Li, L. Liver-derived human mesenchymal stem cells: A novel therapeutic source for liver diseases. *Stem Cell Res. Ther.* https://doi.org/10.1186/s13287-016-0330-3 (2016).
21. Yamaguchi, T. P., Harpal, K., Henkemeyer, M. & Rossant, J. fgfr-1 is required for embryonic growth and mesodermal patterning during mouse gastrulation. *Genes Dev.* https://doi.org/10.1101/gad.8.24.3032 (1994).
22. Dorey, K. & Amaya, E. FGF signalling: diverse roles during early vertebrate embryogenesis. *Development* https://doi.org/10.1242/dev.037689 (2010).
23. Schuldiner, M., Yanuka, O., Itskovitz-Eldor, J., Melton, D. & Benvenisty, N. Effects of eight growth factors on the differentiation of cells derived from human embryonic stem cells. *Proc. Natl Acad. Sci. USA* https://doi.org/10.1073/pnas.97.21.11307 (2000).
24. El Taghdouini, A. et al. In vitro reversion of activated primary human hepatic stellate cells. *Fibrogenesis Tissue Repair* https://doi.org/10.1186/s13069-015-0031-z (2015).
25. Senoo, H. et al. Hepatic stellate cell (vitamin A–storing cell) and its relative—past, present and future. *Cell Biol. Int.* https://doi.org/10.1042/Cbi20100321 (2010).
26. Ijpenberg, A. et al. Wt1 and retinoic acid signaling are essential for stellate cell development and liver morphogenesis. *Dev. Biol.* https://doi.org/10.1016/j.ydbio.2007.09.014 (2007).
27. Chun, Y. S., Byun, K. & Lee, B. Induced pluripotent stem cells and personalized medicine: current progress and future perspectives. *Anat. Cell Biol.* https://doi.org/10.5115/acb.2011.44.4.245 (2011).
28. Koui, Y. et al. An in vitro human liver model by iPSC-derived parenchymal and non-parenchymal cells. *Stem Cell Rep.* https://doi.org/10.1016/j.stemcr.2017.06.010 (2017).

29. Miyoshi, M. et al. LIM homeobox 2 promotes interaction between human iPS-derived hepatic progenitors and iPS-derived hepatic stellate-like cells. *Sci. Rep*. https://doi.org/10.1038/s41598-018-37430-9 (2019).
30. Lee, U. E. & Friedman, S. L. Mechanisms of hepatic fibrogenesis. *Best Pract. Res. Clin. Gastroenterol*. https://doi.org/10.1016/j.bpg.2011.02.005 (2011).
31. Dongiovanni, P., Anstee, Q. & Valenti, L. Genetic predisposition in NAFLD and NASH: impact on severity of liver disease and response to treatment. *Curr. Pharm. Des*. https://doi.org/10.2174/13816128113199990381 (2013).
32. Ouchi, R. et al. Modeling steatohepatitis in humans with pluripotent stem cell-derived organoids. *Cell Metab*. https://doi.org/10.1016/j.cmet.2019.05.007 (2019).
33. Farahani, R. M. & Xaymardan, M. Platelet-derived growth factor receptor alpha as a marker of mesenchymal stem cells in development and stem cell biology. *Stem Cells Int*. https://doi.org/10.1155/2015/362753 (2015).
34. Ullah, I., Subbarao, R. B. & Rho, G. J. Human mesenchymal stem cells—current trends and future prospective. *Biosci. Rep*. https://doi.org/10.1042/BSR20150025 (2015).
35. Kumar, M. et al. A fully defined pluripotent stem cell derived multi-liver-cell model for steatohepatitis and fibrosis. Preprint at *bioRxiv* https://doi.org/10.1101/2020.09.03.280883 (2020).
36. Ordovás, L. et al. Efficient recombinase-mediated cassette exchange in hPSCs to study the hepatocyte lineage reveals AAVS1 locus-mediated transgene inhibition. *Stem Cell Rep*. https://doi.org/10.1016/j.stemcr.2015.09.004 (2015).
37. Leite, S. B. et al. Novel human hepatic organoid model enables testing of drug-induced liver fibrosis in vitro. *Biomaterials* https://doi.org/10.1016/j.biomaterials.2015.11.026 (2016).

Acknowledgements

This work was performed in Center Esther Koplowitz and Vrije Universiteit Brussel. We thank the Advanced Optical Microscopy Unit from the Scientific and Technological Centers of the University of Barcelona for their support with the confocal image technique. We are indebted to the Cytomics Unit of the Institut d'Investigacions Biomèdiques August Pi i Sunyer (IDIBAPS) for flow cytometry analysis. Figures were created using BioRender.com. P.S.-B. is supported by the Fondo de Investigación Sanitaria Carlos III, cofinanced by the Fondo Europeo de Desarrollo Regional (FEDER), Unión Europea, 'Una manera de hacer Europa' (FIS PI20/00765, PI17/00673), DTS18/00088, COST Action H2020 PRO-EURO-DILI-NET CA17112 and Miguel Servet (CPII16/00041) to P.S.-B., PFIS (FI18/00215) to R.M. and APIF to J.V. MC FIS (PI18/00862). I.M. is supported by an FWO–V post-doctoral fellowship (12N5419 N) and S.V. is supported by an FWO–V postdoctoral fellowship (1243121N). L.A.v.G is supported by FWO projects G042719N, FWO-SBO-S001121 'iPSC-LiMiC' and a 'Wetenschappelijk Fonds Willy Gepts' grant from the Vrije Universiteit Brussel. C.M.V. is supported by FWO-G0D9917N; IWT-140045, HILIM-3D; FWO-SBO-S001121, iPSC-LiMiC and the European Union's Horizon 2020 research and innovation program under grant agreement 681002 (EU-ToxRisk).

Author contributions

J.V. and R.A.M. equally contributed to the optimization of expansion and freezing processes, characterization of the cells and drafting the manuscript. I.M. and A.S. performed the 3D spheroid experiments, and S.V. and. A.S. carried out parallel iPSC differentiations using a different iPSC line (not included in the manuscript). M.C. participated in the differentiation protocol design and reviewed the manuscript. S.A., T.R.-T., B.A.-B., C.M.-S. and D.B., participated in the differentiation protocol process. C.M.V. contributed to the design of the IPSCs differentiation protocol and reviewed the manuscript. L.A.v.G. guided the iPSC and spheroid studies in Brussels and critically reviewed the manuscript. P.S.-B. designed and supervised the study and critically reviewed the manuscript.

Competing interests

M.C., C.M.V. and P.S.-B. have a patent application PCT/EP2016/079464, and L.A.v.G. has a patent application PCT/EP2015/062551.

Additional information

Supplementary information The online version contains supplementary material available at https://doi.org/10.1038/s41596-021-00509-1.

Correspondence and requests for materials should be addressed to C.M.V., L.A.v.G. or P.S.-B.

Peer review information *Nature Protocols* thanks the anonymous reviewers for their contribution to the peer review of this work.

Reprints and permissions information is available at www.nature.com/reprints.

Publisher's note Springer Nature remains neutral with regard to jurisdictional claims in published maps and institutional affiliations.

Received: 8 April 2020; Accepted: 21 January 2021;
Published online: 16 April 2021

Related links
Key reference using this protocol
Coll, M. et al. *Cell Stem Cell* **23**, 101–113.e7 (2018): https://doi.org/10.1016/j.stem.2018.05.027

nature research

Corresponding author(s): Pau Sancho-Bru

Last updated by author(s): 10th December 2020

Reporting Summary

Nature Research wishes to improve the reproducibility of the work that we publish. This form provides structure for consistency and transparency in reporting. For further information on Nature Research policies, see our Editorial Policies and the Editorial Policy Checklist.

Statistics

For all statistical analyses, confirm that the following items are present in the figure legend, table legend, main text, or Methods section.

n/a	Confirmed	
☐	☒	The exact sample size (*n*) for each experimental group/condition, given as a discrete number and unit of measurement
☐	☒	A statement on whether measurements were taken from distinct samples or whether the same sample was measured repeatedly
☐	☒	The statistical test(s) used AND whether they are one- or two-sided *Only common tests should be described solely by name; describe more complex techniques in the Methods section.*
☒	☐	A description of all covariates tested
☒	☐	A description of any assumptions or corrections, such as tests of normality and adjustment for multiple comparisons
☐	☒	A full description of the statistical parameters including central tendency (e.g. means) or other basic estimates (e.g. regression coefficient) AND variation (e.g. standard deviation) or associated estimates of uncertainty (e.g. confidence intervals)
☐	☒	For null hypothesis testing, the test statistic (e.g. *F*, *t*, *r*) with confidence intervals, effect sizes, degrees of freedom and *P* value noted *Give P values as exact values whenever suitable.*
☒	☐	For Bayesian analysis, information on the choice of priors and Markov chain Monte Carlo settings
☒	☐	For hierarchical and complex designs, identification of the appropriate level for tests and full reporting of outcomes
☒	☐	Estimates of effect sizes (e.g. Cohen's *d*, Pearson's *r*), indicating how they were calculated

Our web collection on statistics for biologists contains articles on many of the points above.

Software and code

Policy information about availability of computer code

Data collection	N/A
Data analysis	N/A

For manuscripts utilizing custom algorithms or software that are central to the research but not yet described in published literature, software must be made available to editors and reviewers. We strongly encourage code deposition in a community repository (e.g. GitHub). See the Nature Research guidelines for submitting code & software for further information.

Data

Policy information about availability of data

All manuscripts must include a data availability statement. This statement should provide the following information, where applicable:

- Accession codes, unique identifiers, or web links for publicly available datasets
- A list of figures that have associated raw data
- A description of any restrictions on data availability

The authors declare that all data supporting the findings of this study are available within the paper.

Field-specific reporting

Please select the one below that is the best fit for your research. If you are not sure, read the appropriate sections before making your selection.

☒ Life sciences ☐ Behavioural & social sciences ☐ Ecological, evolutionary & environmental sciences

For a reference copy of the document with all sections, see nature.com/documents/nr-reporting-summary-flat.pdf

Life sciences study design

All studies must disclose on these points even when the disclosure is negative.

Sample size	No sample size calculation was performed and three or more independent differentiations were used.
Data exclusions	No data were excluded for the analysis.
Replication	All attemps of replication were successful and for each differentiation we have replicates.
Randomization	N/A
Blinding	N/A

Reporting for specific materials, systems and methods

We require information from authors about some types of materials, experimental systems and methods used in many studies. Here, indicate whether each material, system or method listed is relevant to your study. If you are not sure if a list item applies to your research, read the appropriate section before selecting a response.

Materials & experimental systems

n/a	Involved in the study
☐	☒ Antibodies
☐	☒ Eukaryotic cell lines
☒	☐ Palaeontology and archaeology
☒	☐ Animals and other organisms
☒	☐ Human research participants
☒	☐ Clinical data
☒	☐ Dual use research of concern

Methods

n/a	Involved in the study
☒	☐ ChIP-seq
☐	☒ Flow cytometry
☒	☐ MRI-based neuroimaging

Antibodies

Antibodies used

PE Mouse Anti-Human CD140b Clone 28D4 (BD PharMingen, Cat#558821). RRID: AB_397132
PE Mouse IgG2a, Isotype Control Clone MOPC-173 (Biolegend, Cat#400214). RRID: AB_ 326460
Recombinant Anti-PDGFR beta antibody [Y92] - C-terminal (Abcam, Cat#ab32570). RRID: AB_777165
Anti-PCDH7 antibody [OTI2G6] (Abcam, Cat#ab139274). RRID: AB_2868608
Goat anti-Mouse IgG (H+L) Cross-Adsorbed Secondary Antibody, Alexa Fluor 488 (Invitrogen, Cat#A-11001). RRID: AB_2534088
Alexa Fluor® 488 AffiniPure Donkey Anti-Rabbit IgG (H+L) (Jackson Immuno Research, Cat#711-545-152). RRID: AB_2313584

Validation

PE Mouse Anti-Human CD140b Clone 28D4 Human (QC Testing) Application Flow cytometry (Routinely Tested) provided by the manufacturer website.
In addition, iPSC-HSCs can be co-cultured with hepatocyte cell lines, such as HepaRGs, obtaining complex 3D spheroids14. Here in this protocol a ratio of 2:1 (iPSC-HSCs-HepaRG) was used to form liver spheroids following Leite et al (2016) and Figure 3A. This ratio allows to maintain iPSC-HSCs in a less activated state. A different cell ratio may be reacquired according to the final objective of the investigators. Spheroids can be characterized by immunostaining and gene expression analysis of both cell types (Table 5 and 6) and, as discussed in the Anticipated Results section can be used in assays looking at liver fibrosis, inflammation and toxicity (Table 3).
PE Mouse IgG2a, Isotype Control Clone MOPC-173 Mouse conjugated with PE, Flow Cytometry (Quality tested) provided by the manufacturer website.
Recombinant Anti-PDGFR beta antibody [Y92] - C-terminal (Human, host in rabbit) suitable for IHC-Fr, Flow Cyt, IHC-FoFr, WB, IHC-P, ICC/IF, IP, IHC-FrFl applicaitons provided by manufacturer website.
Anti-PCDH7 antibody [OTI2G6] (Human, host in mouse) suitable for WB, IHC-P and ICC/IF provided by manufacturer website.
Goat anti-Mouse IgG (H+L) Cross-Adsorbed Secondary Antibody, Alexa Fluor 488 (target mouse, host in goat) suitable for Flow Cytometry, ICC, IF, IHC F, IHC P, WB and IHC provided by manufacturer website.
Alexa Fluor® 488 AffiniPure Donkey Anti-Rabbit IgG (H+L) (target rabbit, host in donkey) polyclonal antibody suitable for ELISA, FACS, IFIHC and WB provided by manufacturer website.

Eukaryotic cell lines

Policy information about cell lines

Cell line source(s)	Human BJ1 iPSCs line: The BJ1 line is generated in Catherine Verfaillie's Lab, from fibroblast cell line (ATCC® CRL-2522™, 28). Made in house cell line. Details on how to generate this cell line is described in Ordovas L et al (2015). Differentiated HepaRG cells: HPR116215-TA08 purchased from Biopredic.
Authentication	Human BJ1 iPSCs line was authenticated following the stablished stem cells characterization procedures (evaluate pluripotency markers by gene expression, FACS and IF, formation of EBs, SNP profiling). HepaRG were pruchased and no authentication procedure was performed.
Mycoplasma contamination	iPSC Cell line tested negatively for mycoplasma contatmination.
Commonly misidentified lines (See ICLAC register)	N/A

Flow Cytometry

Plots

Confirm that:

☒ The axis labels state the marker and fluorochrome used (e.g. CD4-FITC).

☒ The axis scales are clearly visible. Include numbers along axes only for bottom left plot of group (a 'group' is an analysis of identical markers).

☒ All plots are contour plots with outliers or pseudocolor plots.

☒ A numerical value for number of cells or percentage (with statistics) is provided.

Methodology

Sample preparation	Once the differentiation is finished, wash iPSC-HSCs with DPBS (-/-) for 1min, remove it and add 0.5mL of Trypsin-EDTA 0.25% to each well. Incubate cells at 37ºC during 2-3min in order to detach them. Check the cells under microscopy and when cells start detaching, add an equal amount of medium containing 10% Fetal Bovine Serum (FBS) as trypsin solution in order to stop the reaction. Collect the cells by gently pipetting the medium. Centrifuge at 300g for 5min at RT. After centrifugation, resuspend cells in 3mL of cold DMEM Glutamax and distribute them in 3 FACS tubes: Autofluorescence, Isotype and PDGFRb. Add DPBS (-/-) to each tube in order to wash the cells. Centrifuge at 300g for 5min at 4ºC. Discard the supernatant and add 100uL of cold FACS Buffer to each tube. Resuspend cells and add 1uL of each antibody to Isotype and PDGFRb tubes. Incubate for 30min at RT under photo-protected conditions. At the end of the incubation add DPBS (-/-) to wash the cells. Centrifuge at 300g for 5min at 4ºC. Discard the supernatant and resuspend cells in 200uL of FACS Buffer and perform FACS analysis.
Instrument	FACSCanto II Cytometer
Software	BD FACS DIVA
Cell population abundance	After the differentiation, 60% of the cells are positive for PDGFRb.
Gating strategy	Comparison between SSCA vs FSCA to find our interest population. Use 488-530/30-502LP-A vs PDGFRb-PE to locate the positive fraction of the population.

☒ Tick this box to confirm that a figure exemplifying the gating strategy is provided in the Supplementary Information.